Molecular cloud dynamics and star formation

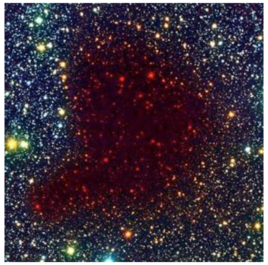
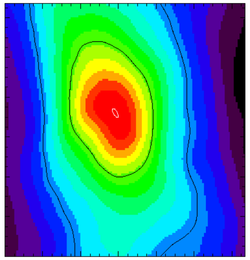

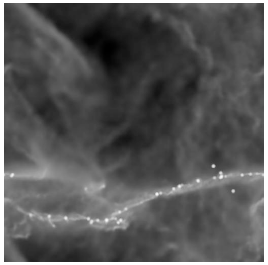

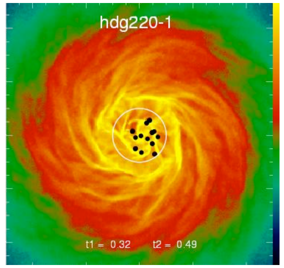

Ralf Klessen

Zentrum für Astronomie der Universität Heidelberg
Institut für Theoretische Astrophysik

thanks to ...

... the organizers for making this school happen!

... people in the group in Heidelberg:

Robi Banerjee, Paul Clark, Gustavo Dopcke, Philipp Girichidis, Simon Glover, Christoph Federrath, Milica Milosavljevic, Faviola Molina, Thomas Peters, Stefan Schmeja, Daniel Seifried, Rahul Shetty, Rowan Smith, Sharanya Sur, Hsiang-Hsu Wang

... many collaborators abroad!

Deutsche Forschungsgemeinschaft DFG

Emmy Noether-Programm

ASTRONET

LANDESSTIFTUNG Baden-Württemberg

HGSFP

IMPRS

- Structured PhD program
  - HGSFP: Heidelberg Graduate School for Fundamental Physics
    ----> http://www.fundamental-physics.uni-hd.de/

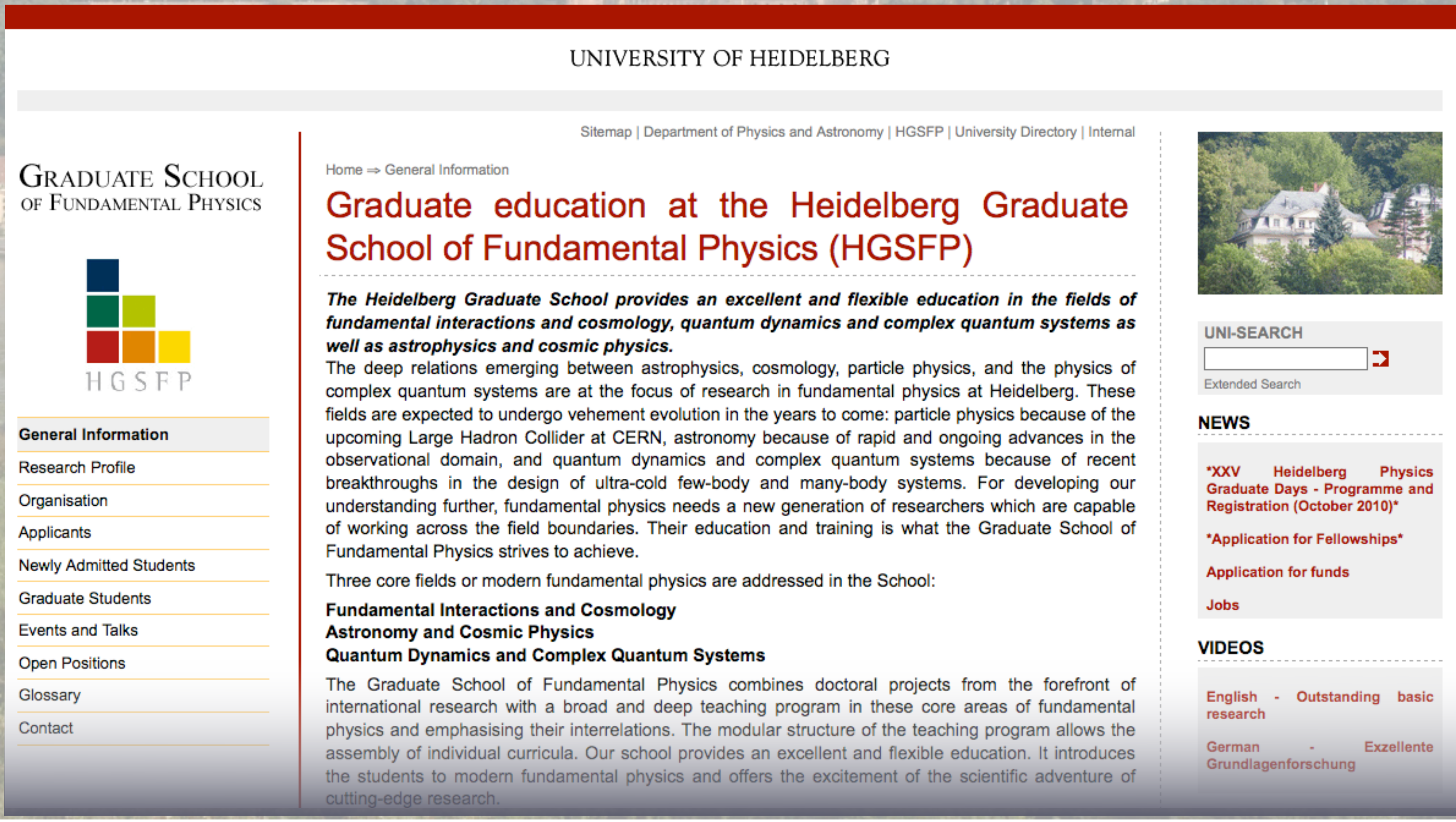

UNIVERSITY OF HEIDELBERG

Sitemap | Department of Physics and Astronomy | HGSFP | University Directory | Internal

GRADUATE SCHOOL OF FUNDAMENTAL PHYSICS

HGSFP

- General Information
- Research Profile
- Organisation
- Applicants
- Newly Admitted Students
- Graduate Students
- Events and Talks
- Open Positions
- Glossary
- Contact

Home ⇒ General Information

Graduate education at the Heidelberg Graduate School of Fundamental Physics (HGSFP)

The Heidelberg Graduate School provides an excellent and flexible education in the fields of fundamental interactions and cosmology, quantum dynamics and complex quantum systems as well as astrophysics and cosmic physics.

The deep relations emerging between astrophysics, cosmology, particle physics, and the physics of complex quantum systems are at the focus of research in fundamental physics at Heidelberg. These fields are expected to undergo vehement evolution in the years to come: particle physics because of the upcoming Large Hadron Collider at CERN, astronomy because of rapid and ongoing advances in the observational domain, and quantum dynamics and complex quantum systems because of recent breakthroughs in the design of ultra-cold few-body and many-body systems. For developing our understanding further, fundamental physics needs a new generation of researchers which are capable of working across the field boundaries. Their education and training is what the Graduate School of Fundamental Physics strives to achieve.

Three core fields or modern fundamental physics are addressed in the School:

Fundamental Interactions and Cosmology
Astronomy and Cosmic Physics
Quantum Dynamics and Complex Quantum Systems

The Graduate School of Fundamental Physics combines doctoral projects from the forefront of international research with a broad and deep teaching program in these core areas of fundamental physics and emphasising their interrelations. The modular structure of the teaching program allows the assembly of individual curricula. Our school provides an excellent and flexible education. It introduces the students to modern fundamental physics and offers the excitement of the scientific adventure of cutting-edge research.

UNI-SEARCH

Extended Search

NEWS

XXV Heidelberg Physics Graduate Days - Programme and Registration (October 2010)

Application for Fellowships

Application for funds

Jobs

VIDEOS

English - Outstanding basic research

German - Exzellente Grundlagenforschung

- Structured PhD program
  - IMPRS-HD: International Max Planck Research School for Astronomy and Cosmic Physics at the University of Heidelberg ---> http://www.mpia-hd.mpg.de/imprs-hd/

Disclaimer

- I try to cover the field as broadly as possible, however, there will clearly be a bias towards my personal interests and many examples will be from my own work.

Structure

Schedule

Formation of molecular clouds

Origin and statistical characteristics of ISM turbulence

Star (cluster) formation in molecular clouds

Stellar initial mass function

Literature

- Books
  - Stahler, S., & Palla, F., 2004, "The Formation of Stars" (Weinheim: Wiley-VCH)
  - Osterbrock, D., & Farland, G., 2006, "Astrophysics of Gaseous Nebulae & Active Galactic Nuclei, 2nd ed. (Sausalito: Univ. Science Books)
  - Lada, C. F., & Kylafis, N. D. 1999, "The Origin of Stars and Planetary Systems", NATO ASI Series 540 (Kluwer Academic Publisher)
  - Reipurth et al. 2007, "Protostars and Planets V" (University of Arizona Press)

Literature

- Review Articles
  - Mac Low, M.-M., Klessen, R.S., 2004, "The control of star formation by supersonic turbulence", Rev. Mod. Phys., 76, 125 - 194
  - Zinnecker, H., Yorke, McKee, C.F., Ostriker, E.C., 2008, "Toward Understanding Massive Star Formation", ARA&A, 45, 481 - 563
  - McKee, C.F., Ostriker, E.C., 2008, "Theory of Star Formation", ARA&A, 45, 565 - 687
  - Bromm, V., Larson, R.B., 2004, "The first stars", ARA&A, 42, 79 - 118

Lecture 1+2: ISM dynamics

- phases of the ISM
- how to observe the ISM
- formation of molecular clouds in convergent flows
  - chemistry
  - dynamics
- origin of ISM turbulence

inventory of Galactic disc component

- **stellar disc**
  - thin disc (80% of mass): stars of all ages 0-12Gyr
  - thick disc (5% of mass): older stars with lower metallicity
- **interstellar medium (ISM)**
  - gas (15% of mass): hot, warm, and cool component (atomic and molecular)
  - dust (<1% of gas mass): well mixed with the cool gas
  - cosmic rays: relativistic particles
  - magnetic fields: frozen to the gas (field lines are co-moving with the gas); energy density comparable to the kinetic energy of gas

Interstellar Matter: ISM

Abundances, scaled to 1.000.000 H atoms

element		atomic number	abundance
hydrogen	H	1	1.000.000
deuterium	$_1H^2$	1	16
helium	He	2	68.000
carbon	C	6	420
nitrogen	N	7	90
oxygen	O	8	700
neon	Ne	10	100
sodium	Na	11	2
magnesium	Mg	12	40
aluminium	Al	13	3
silicium	Si	14	38
sulfur	S	16	20
calcium	Ca	20	2
iron	Fe	26	34
nickel	Ni	28	2

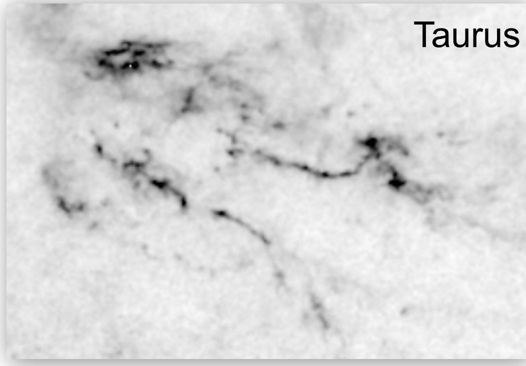

hydrogen is by far the most abundant element (more than 90% in number).

Phases of the ISM

Because hydrogen is the dominating element, the classification scheme is based on its chemical state:

ionized atomic hydrogeN	*HII (H^+)*	ionization
neutraler atomic hydrogen	*HI (H)*	
molecular hydrogen	*H_2*	dissociation

different regions consist of almost 100% of the appropriate phase, the transition regions between HII, H and H_2 are very thin.

star formation always takes place in dense and cold molecular clouds.

Phases of the ISM

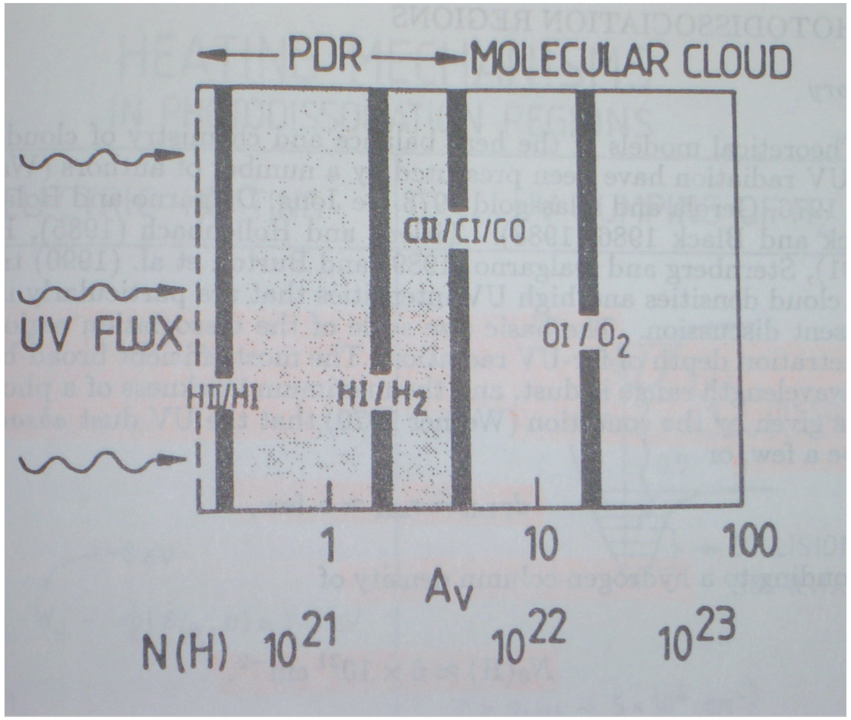

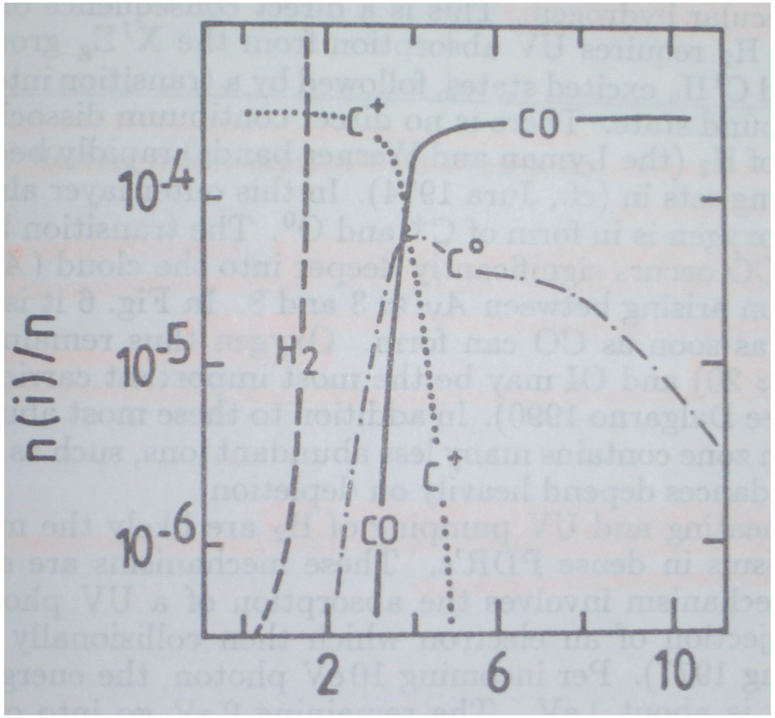

A_V

A_V denotes the extinction, the attenuation of radiation due to absorption (mostly on dust grains)

Life-cycle of ISM

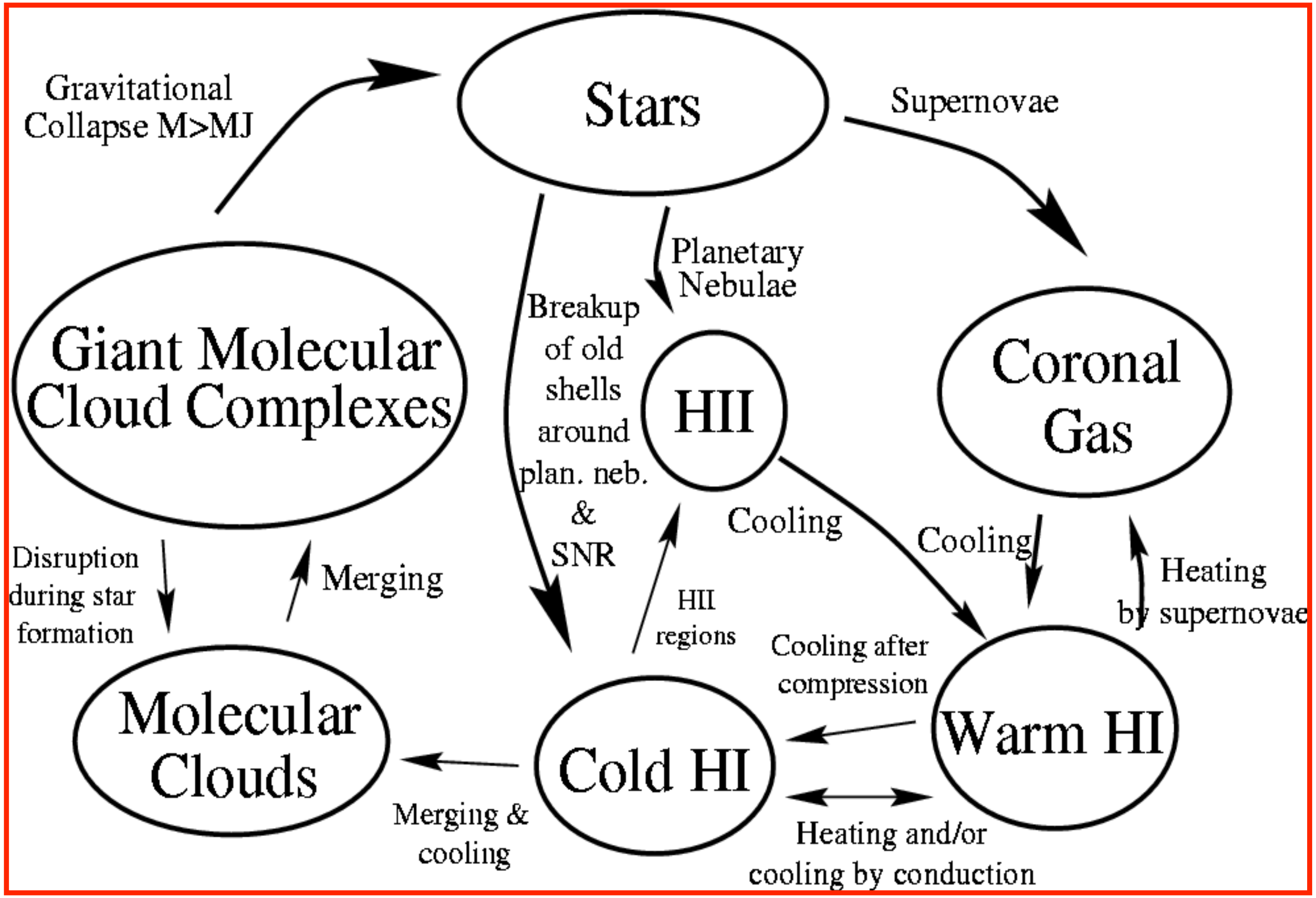

Life-cycle of ISM

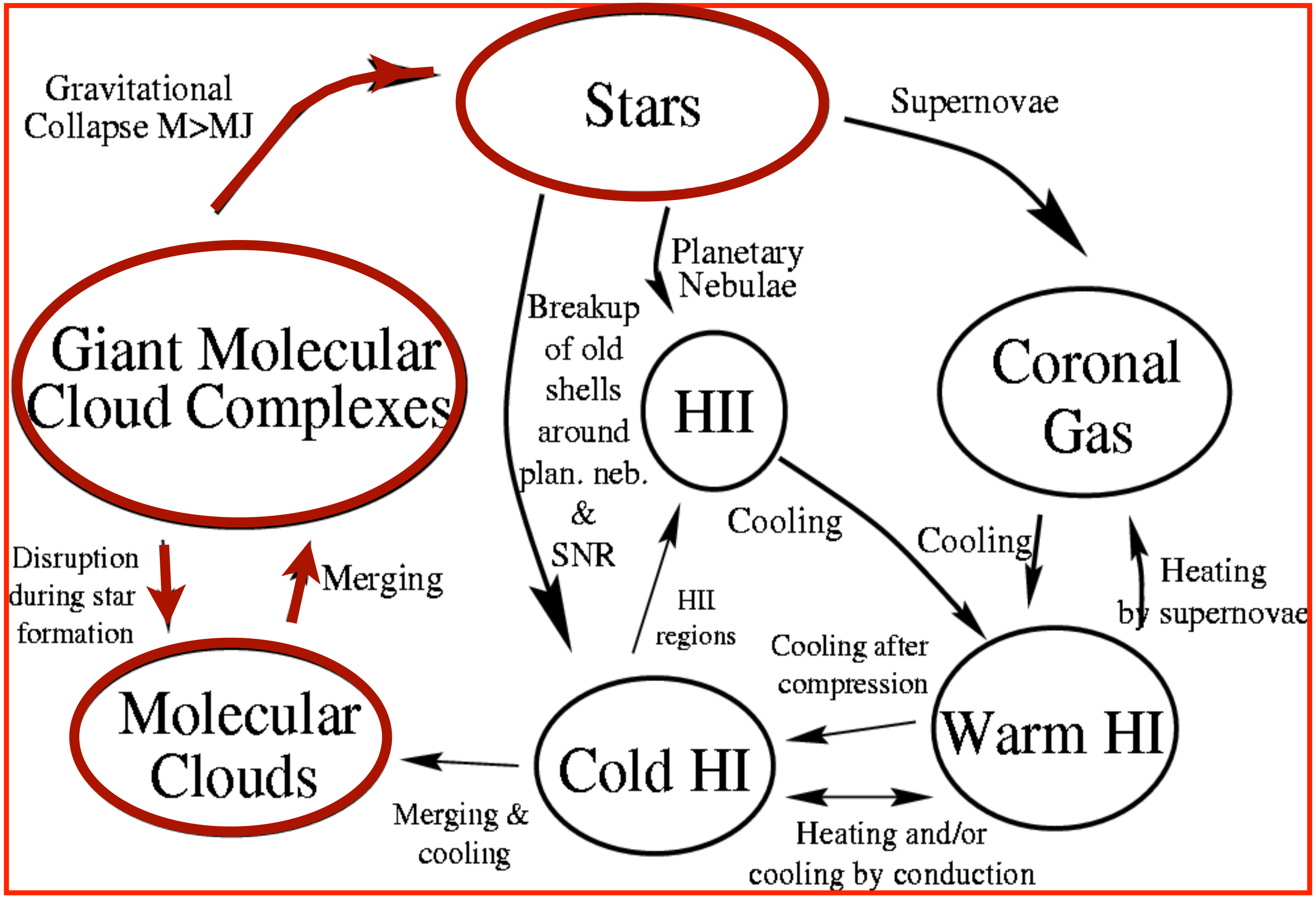

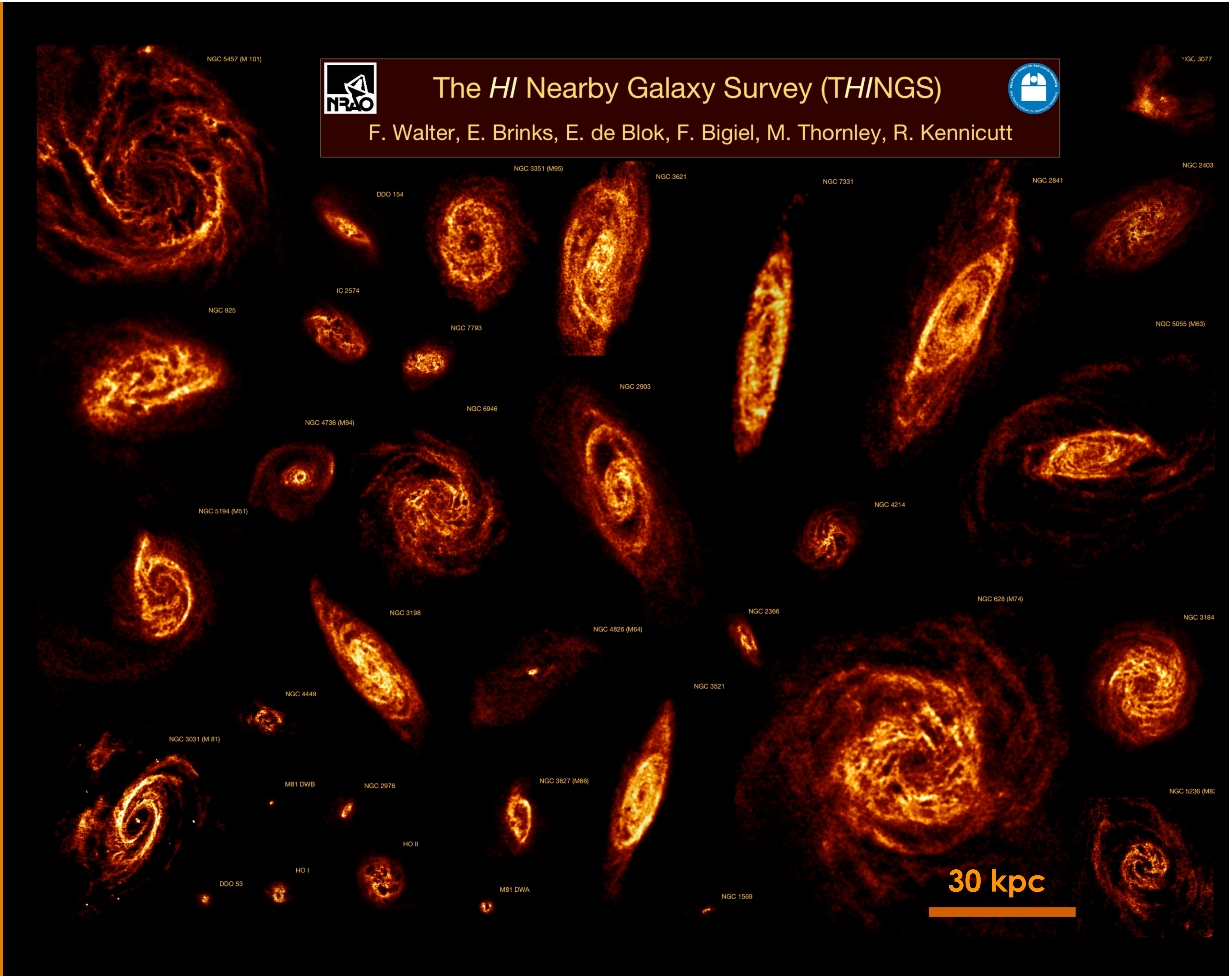

EveryTHINGS

HI Maps

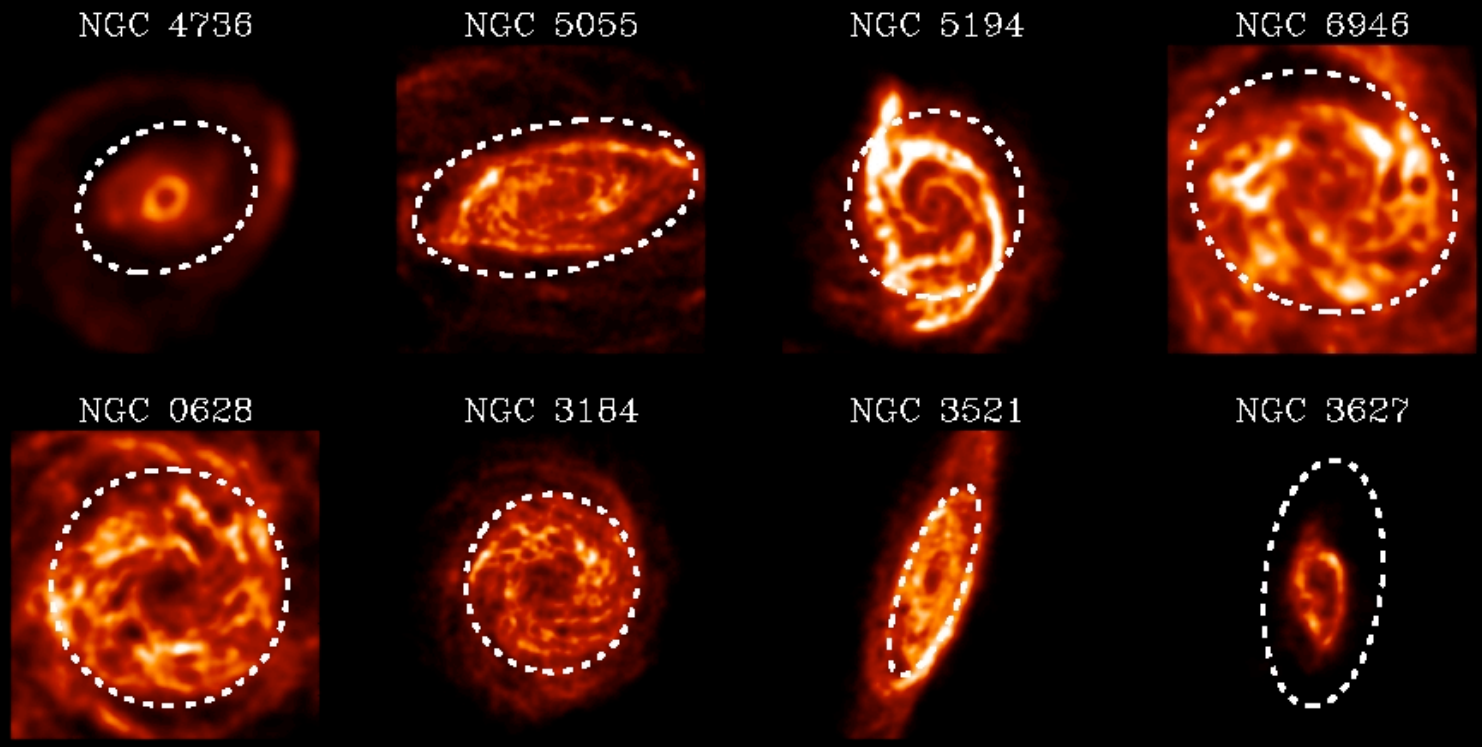

work by Frank Bigiel (now Berkeley)

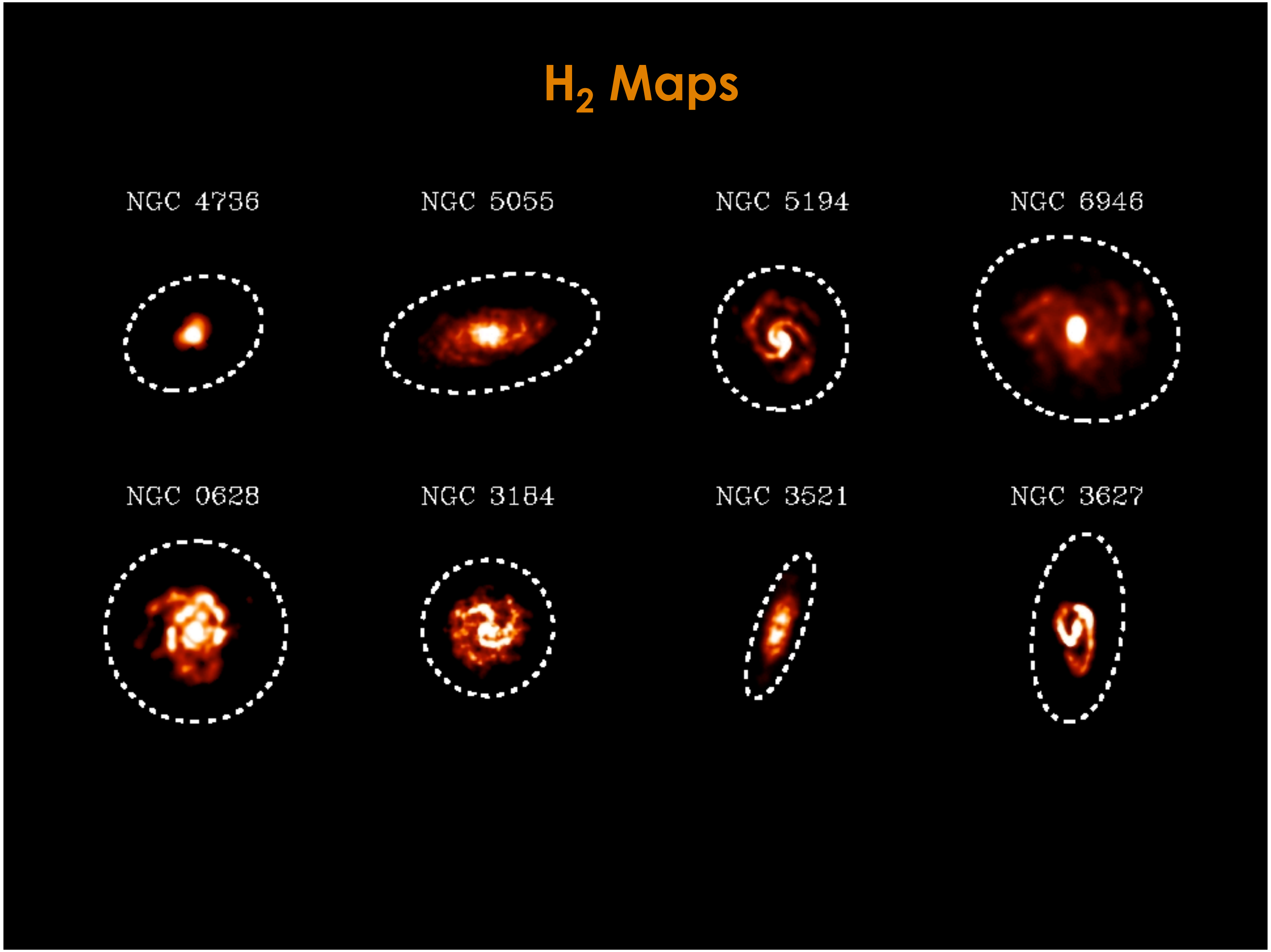

work by Frank Bigiel (now Berkeley)

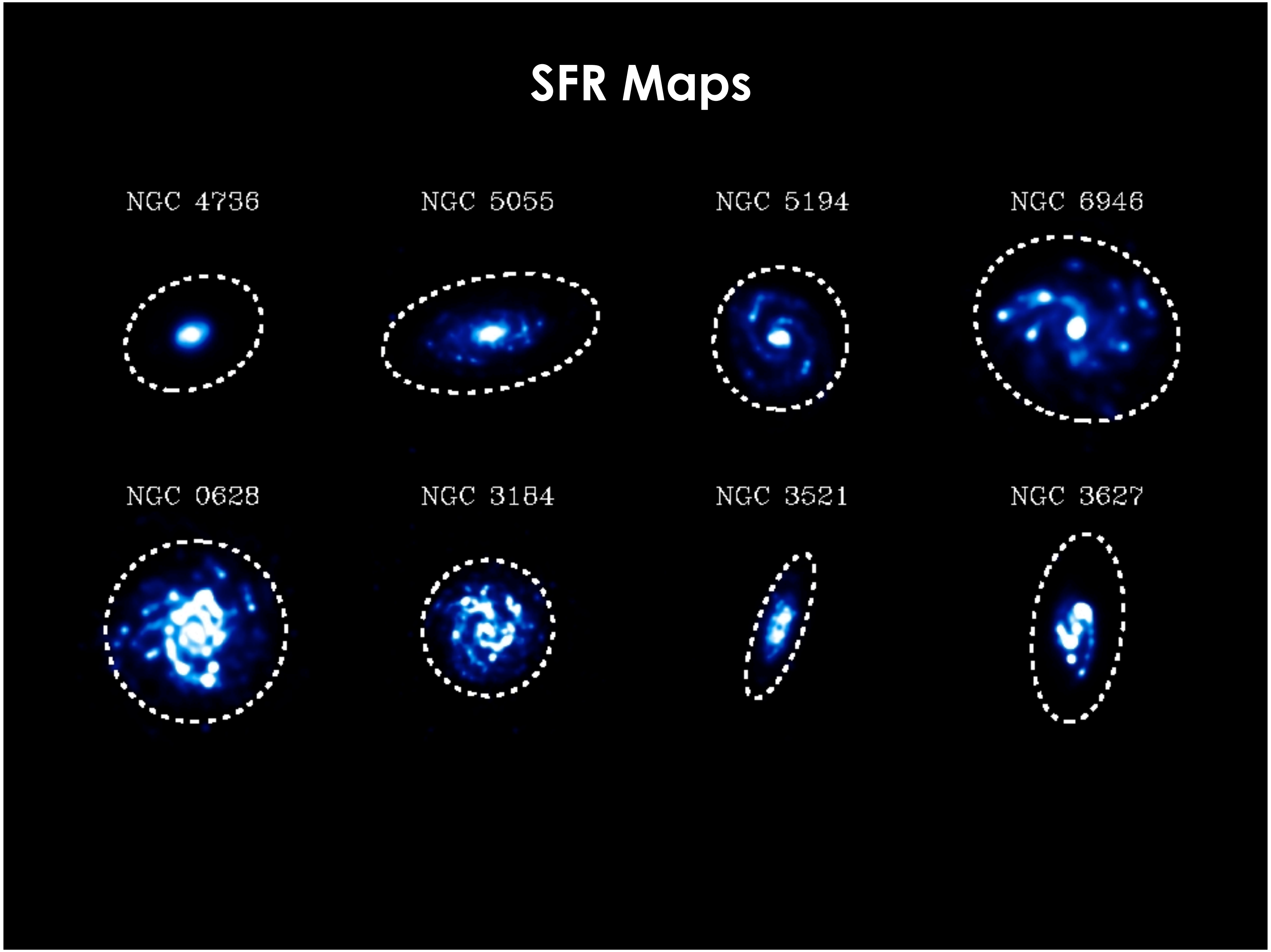

work by Frank Bigiel (now Berkeley)

Correlation between H_2 and HI

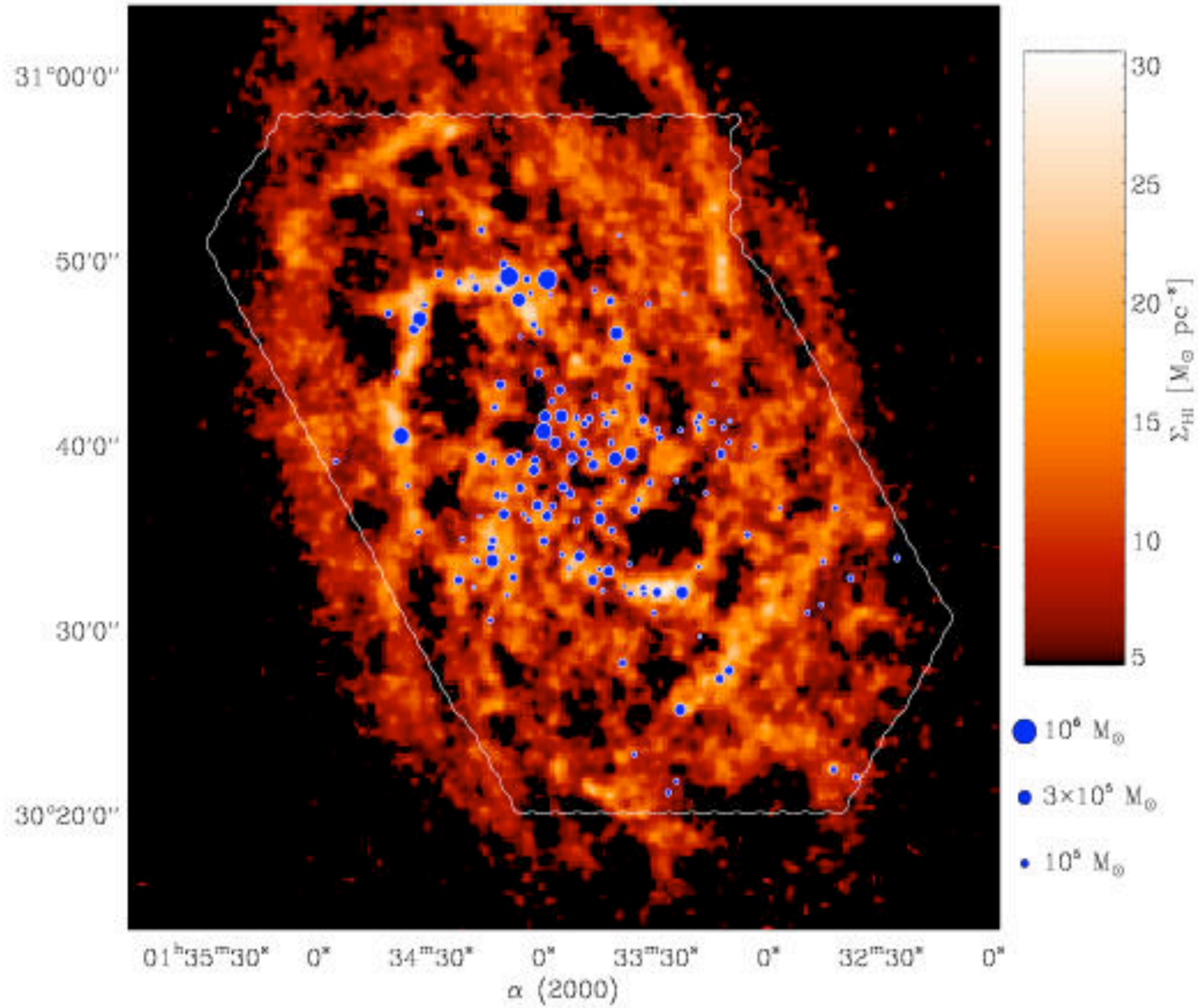

Compare H_2 - HI in M33:

- H_2: BIMA-SONG Survey, see Blitz et al.
- HI: Observations with Westerbork Radio T.

H_2 clouds are seen in regions of high HI density
(in spiral arms and filaments)

(Deul & van der Hulst 1987, Blitz et al. 2004)

Radial Distribution in Spirals

- HI versus H_2:
  - H_2 is restricted to the optical disk
  - while the HI extends 2 - 4 x optical radius
- HI hole or depression in the centers, sometimes compensated by H_2
- often H_2 is exponential like stars, HI does *not* follow in most cases

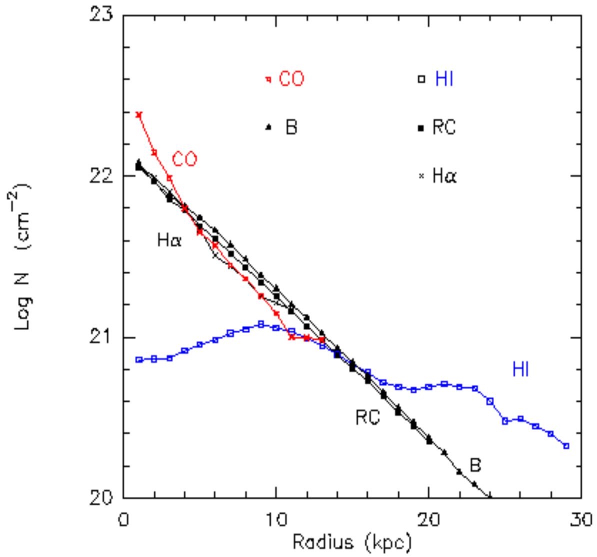

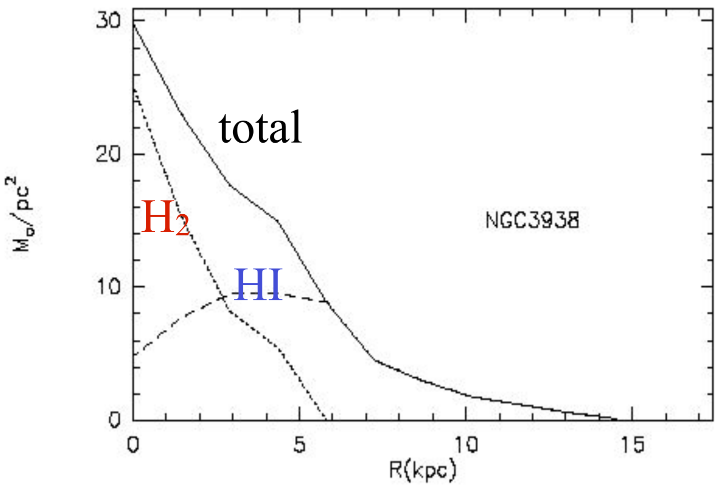

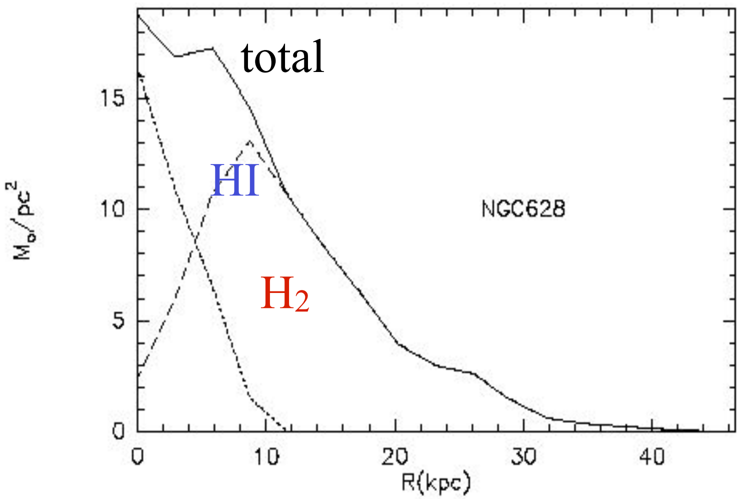

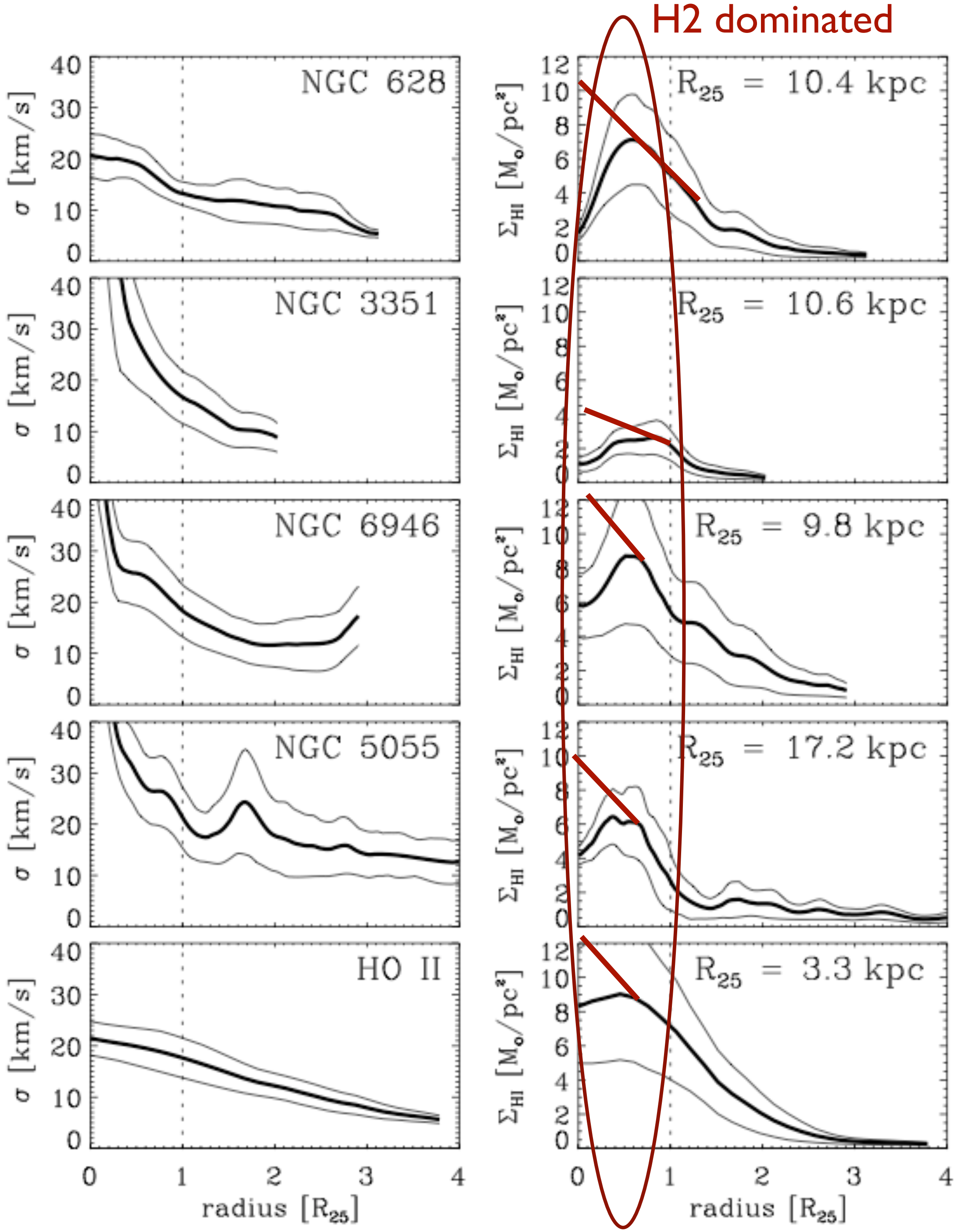

H2 dominated
NGC 628
R25 = 10.4 kpc
NGC 3351
R25 = 10.6 kpc
NGC 6946
R25 = 9.8 kpc
NGC 5055
R25 = 17.2 kpc
HO II
R25 = 3.3 kpc
σ [km/s]
ΣHI [Mo/pc²]
radius [R25]

some important trends

- typically comparable amounts of H_2 and HI gas in the Galaxy
- in Milky Way $M(H_2) \sim 2 \times 10^9\ M_\odot$ and $M(H_2) \sim 6 \times 10^9\ M_\odot$
- But: Very different radial distribution
  - H_2 is centrally concentrated, and in a molecular ring at 4-8kpc (seen in our Galaxy, and in external ones)
  - HI depleted in the center and more radially extended
- H_2 is clumped in clouds and superclouds
- Velocity dispersion falls of slowly from σ_g= 20 km/s to 5 km/s (and this holds more or less for all spiral galaxies)

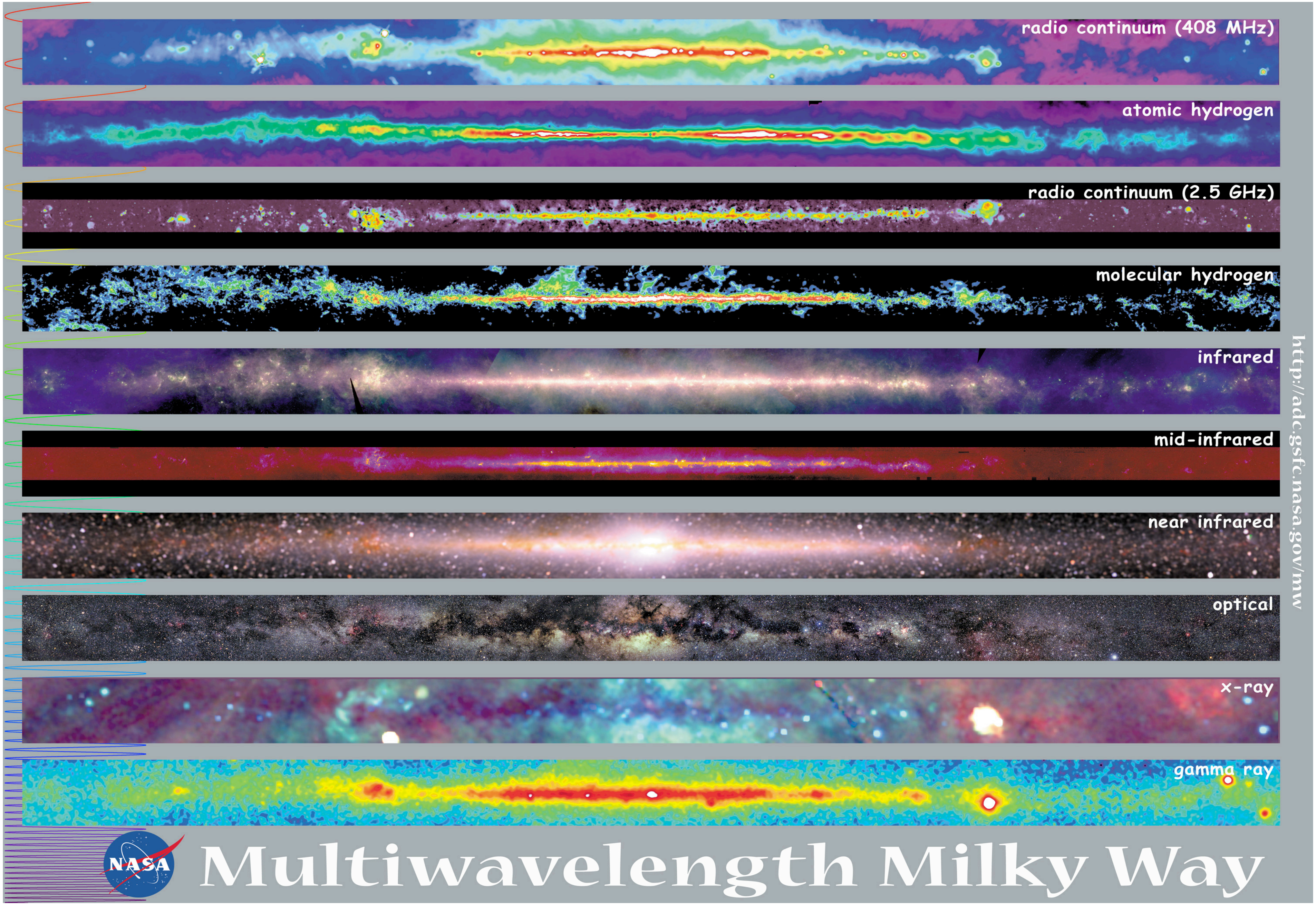
radio continuum (408 MHz)
atomic hydrogen
radio continuum (2.5 GHz)
molecular hydrogen
infrared
mid-infrared
near infrared
optical
x-ray
gamma ray
http://adc.gsfc.nasa.gov/mw
NASA
Multiwavelength Milky Way

Multi-wavelength observations

different wavelengths provide different information.

→astronomer use the full electromagnetic spectrum

- radio: interstellar gas (line emission -> velocity information)
- sub-mm range: dust (thermal emission)
- infrared & optical: stars
- x-rays: stars (coronae), supernovae remnants (very hot gas)
- γ-rays: supernovae remnants (radioactive decay, e.g. ^{26}Al), compact objects, merging of neutron stars (γ-ray burst)

dust

ingredients of the ISM

- interstellar dust
- smoothly distributed with HI
- and in dark (molecular) clouds

- rough distance of clouds by star counts: Wolf diagram
- mean absolute brightness M_1 and m_1 -> distance
- from m_1-m_2 -> depth
- clouds are typically at a distance of a few 100pc with an extinction of Δm=1-3mag
- clouds sharply concentrated to the galactic plane

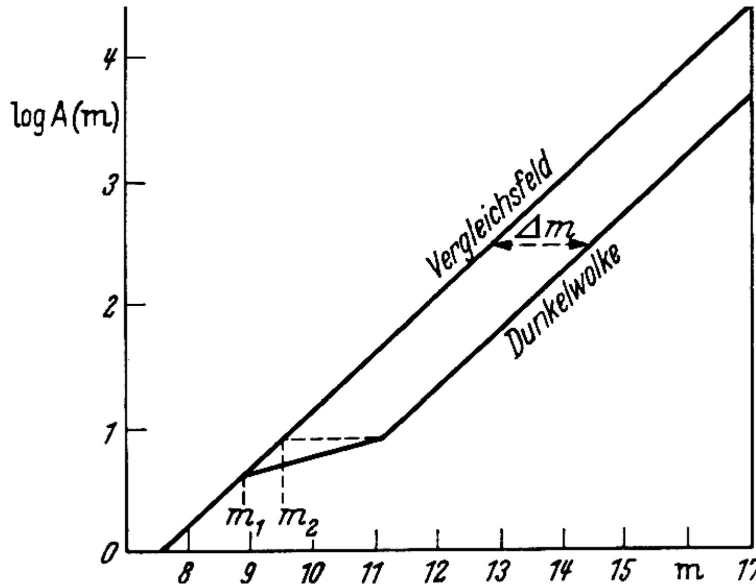

Src.: New Cosmos

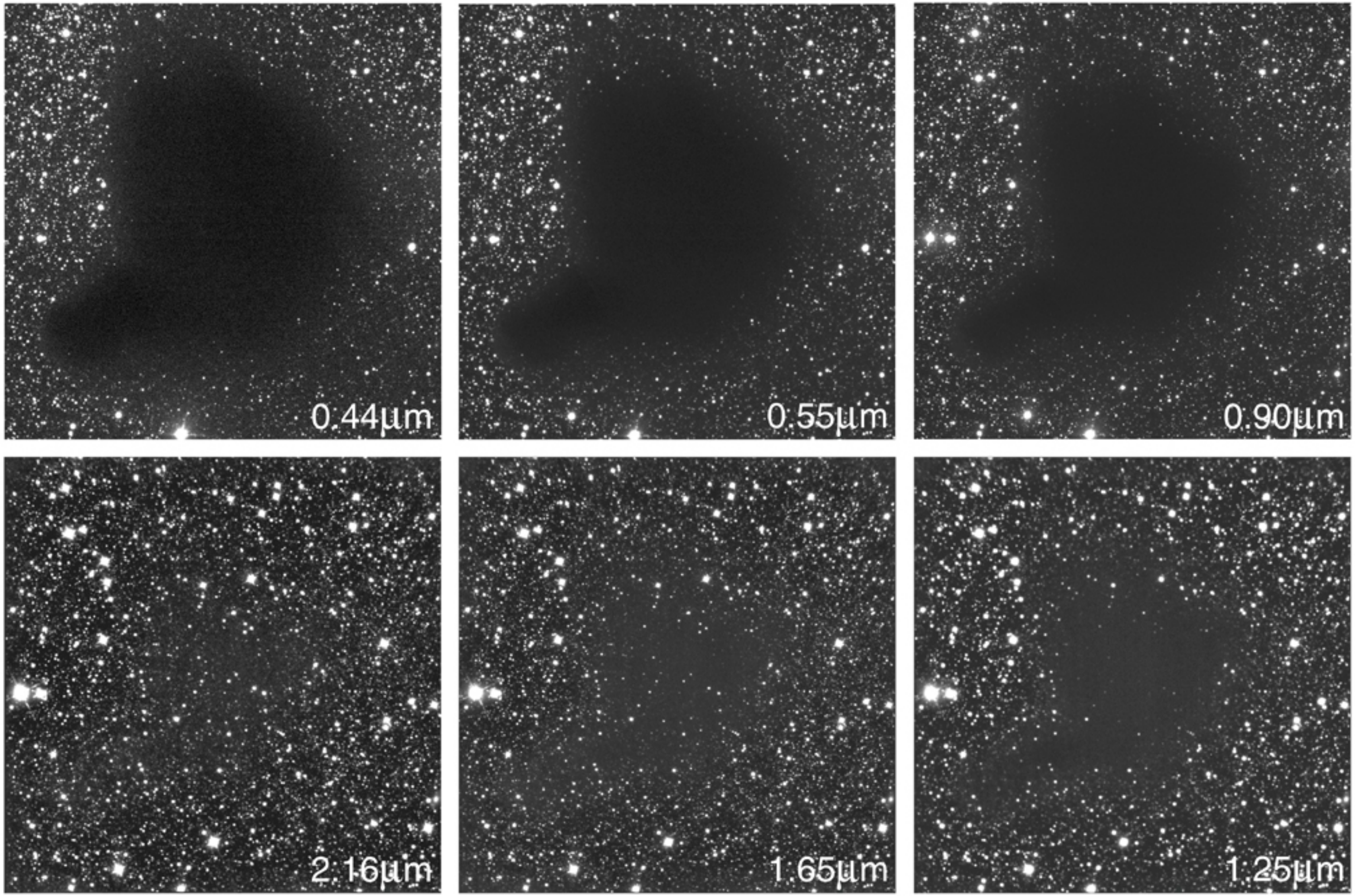

The Dark Cloud B68 at Different Wavelengths (NTT + SOFI)

ESO PR Photo 29b/99 (2 July 1999)

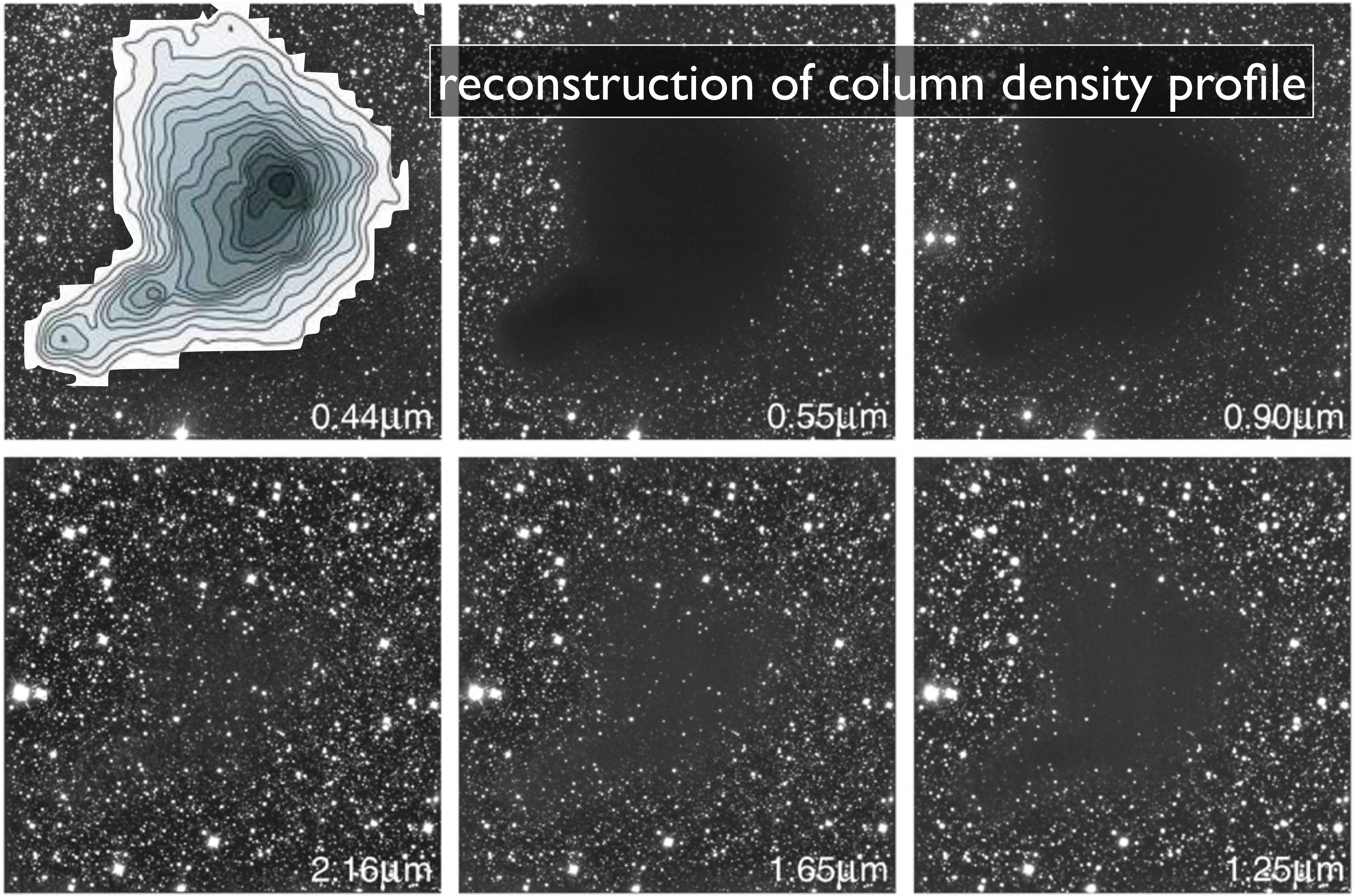

The Dark Cloud B68 at Different Wavelengths (NTT + SOFI)

ESO PR Photo 29b/99 (2 July 1999)

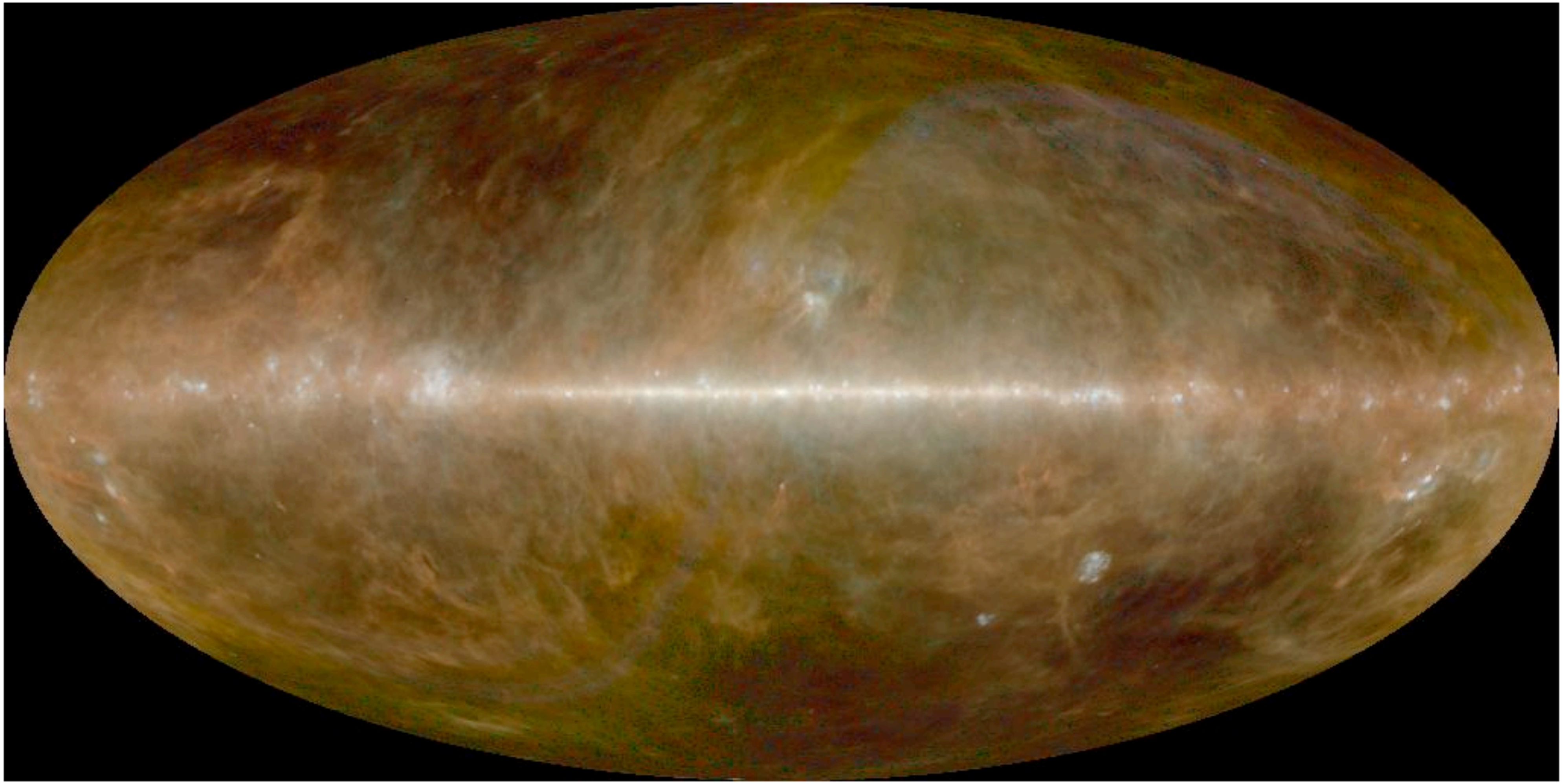

COBE Dirby results: Galactic foreground

DIRBE: Diffuse Infrared Background Experiment

atomic gas

Phases of interstellar matter

HI regions

Detection with 21cm line (1420 MHz, 6×10^{-6} eV))

Parallel spin (higher energy level)   antiparallel spins (lower energy level)

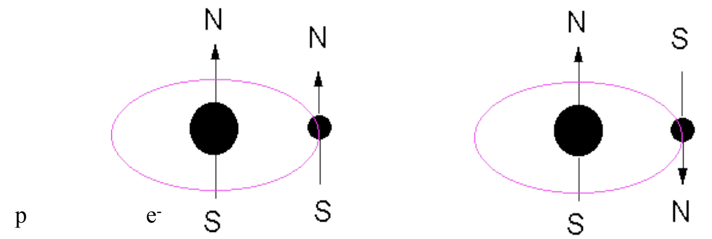

- Excitation by collisions (t_c ~ 500 yr)
- Deexcitation by radiation (t_r ~ 1×10^7 yr)
- (hyperfine structure transition)

Properties of HI gas

Galactic plane — mean density $n \sim 1\ cm^{-3}$ ($\sim1{,}7\times10^{-18}$ g/cm³)

envelope of MC's, cold clouds in disk — $n \sim 10 \ldots 100\ cm^{-3}$, $T_k > 100$ K

matter between clouds — $n \sim 0{,}05 \ldots 0{,}2\ cm^{-3}$, $T_k > 1000$ K

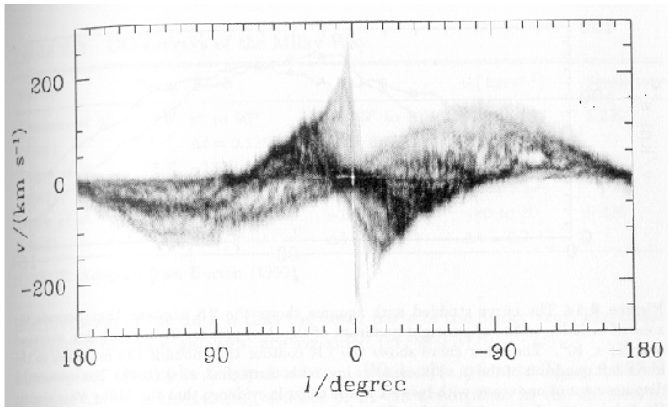

Radial velocity of 21cm radiation as function of galactic longitute (Leiden/Dwingeloo Survey)

- forbidden transition
- $n\sim1cm^{-3}$, $l\sim1pc\sim3\times10^{18}cm$, ¾ of atoms are excited
  → 10^{18} atoms cm^{-2} → $t=10^{14}s$ → 10^4 transitions $s^{-1}cm^{-2}pc^{-1}$
- optically thin: $I_\nu=B_\nu\tau\sim$const. $\kappa_\nu\sim5.5\times10^{-14}\ N_\nu/T$ & $B\sim T$
- T dependence cancels → directly get cm^{-2} column Nl

observing molecules

molecular Gas

H_2, CO, ...

transitions of two-atomic molecules

a) rotational transitions (needs dipole moment)

b) ro-vibrational transitions

c) electronic ro-vibrational transitions

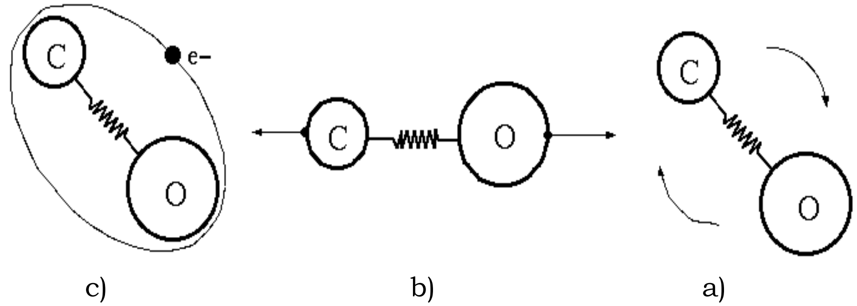

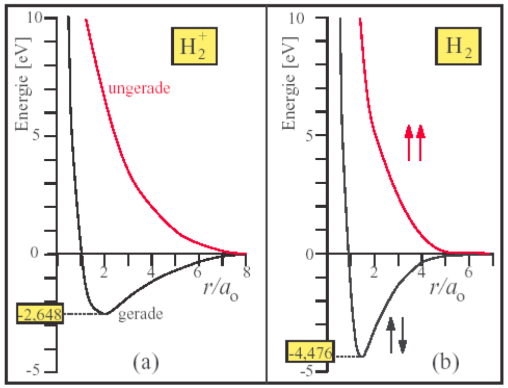

Abbildung 7.2: Energie von (a) H_2^+ (b) H_2 als Funktion des Abstands r der Kerne relativ zum Bohrschen Radius a_o.

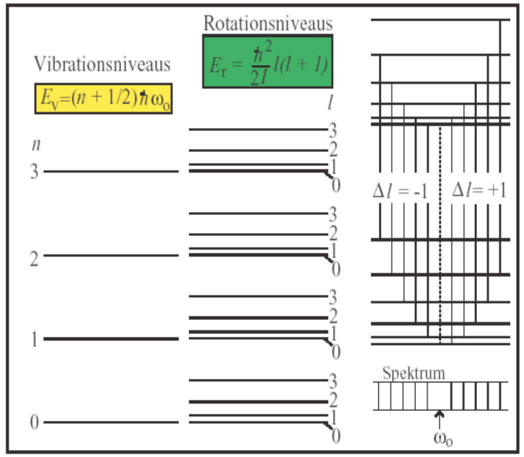

Abbildung 7.3: Rotations- und Vibrationsniveaus eines zweiatomigen Moleküls mit den nach den Auswahlregeln möglichen Übergängen.

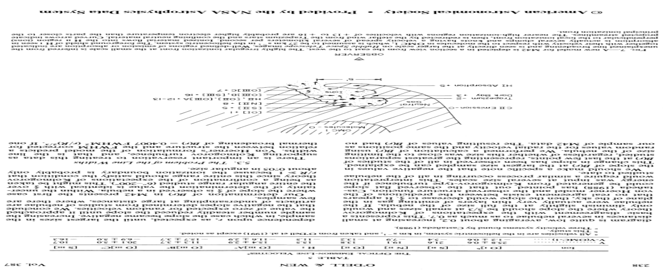

Niedrigste Rotations- und Schwingungsübergänge

	J = 1 – 0			n = 1 - 0		
	Frequenz	Wellenlänge	T	Frequenz	Wellenlänge	T
H_2	3,87 THz	77 µm	185 K	131 THz	2,28 µm	6300 K
^{12}CO	115 GHz	2,6 mm	5,5 K	64 THz	4,63 µm	3100 K

Phases of interstellar matter

Molecular Gas

Global properties of molecular clouds

	Temperature	Density	Radius	Mass	velocity gradient	E_{rot}/E_{pot}
diffuse molecular clouds (10 ... 50% of total H_2 mass)	T = 40 ... 80 K	n = 100 cm^{-3}				
Dark clouds/globules	T = 20 ... 40 K	n = 10^3 ... 10^4 cm^{-3}	R = 0,1 ... 5 pc	1 ... 10 $M_\odot$	0,5 ... 4 km/s/pc	10^{-3}... 0.3
Giant molecular clouds	T = 10 ... 50 K	n = 10^4 ... 10^6 cm^{-3}	R = 10 ... 100 pc	10^3 ... 10^6 $M_\odot$	0,1 ... 0,2 km/s/pc	10^{-4}... 0.1
Hot cores in MCs	T = 100 ... 300 K	n > 10^7 cm^{-3}	R < 0,1 pc	10 ... 100 $M_\odot$		

Giant molecular clouds are strongly concentrated in the galactic plane and towards the center of the Galaxy (similar holds for external galaxies)

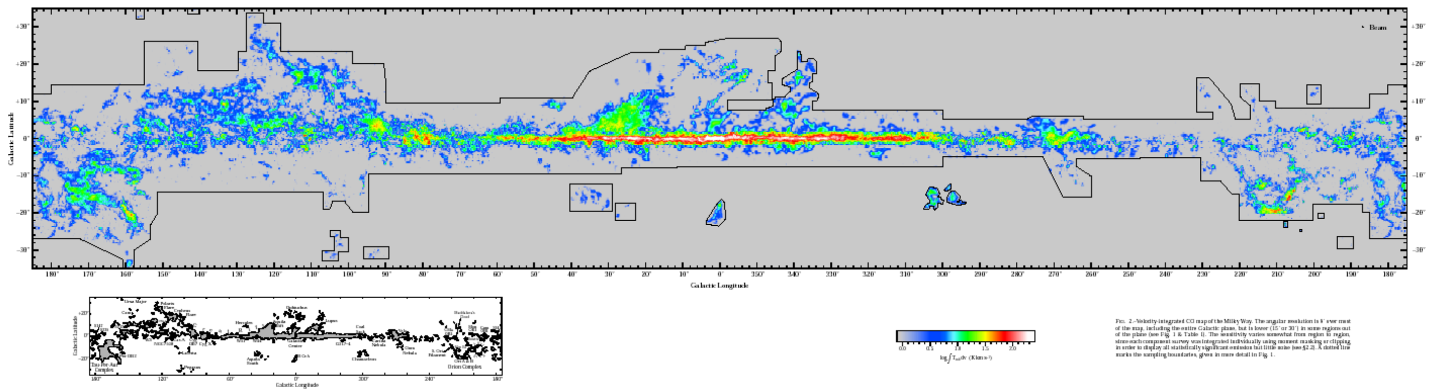

CO Survey of Milky Way
(Dame et al. 2001)

Data from Thomas Dame, CfA Harvard

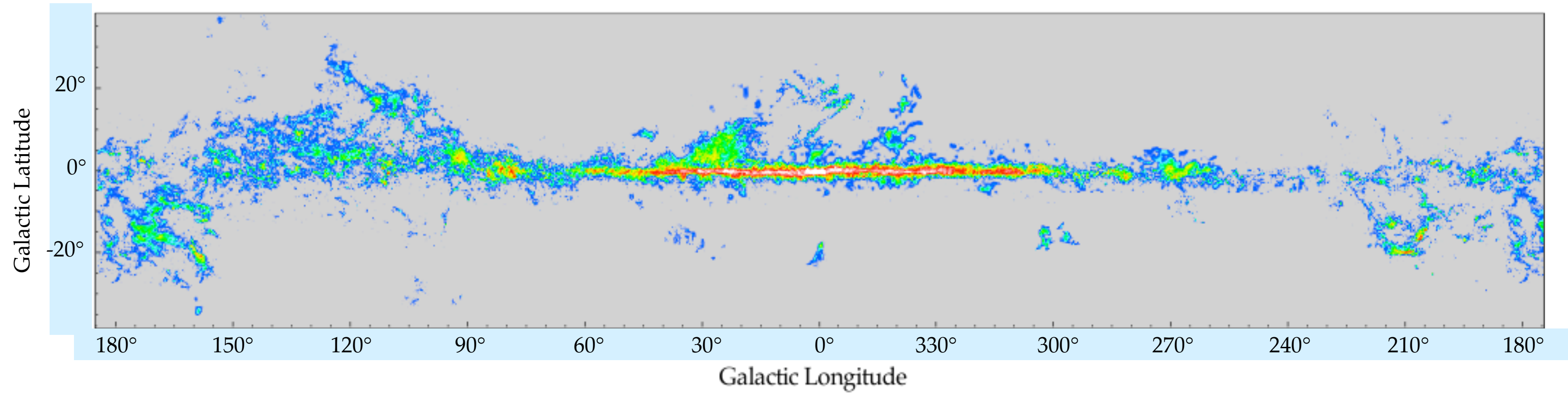

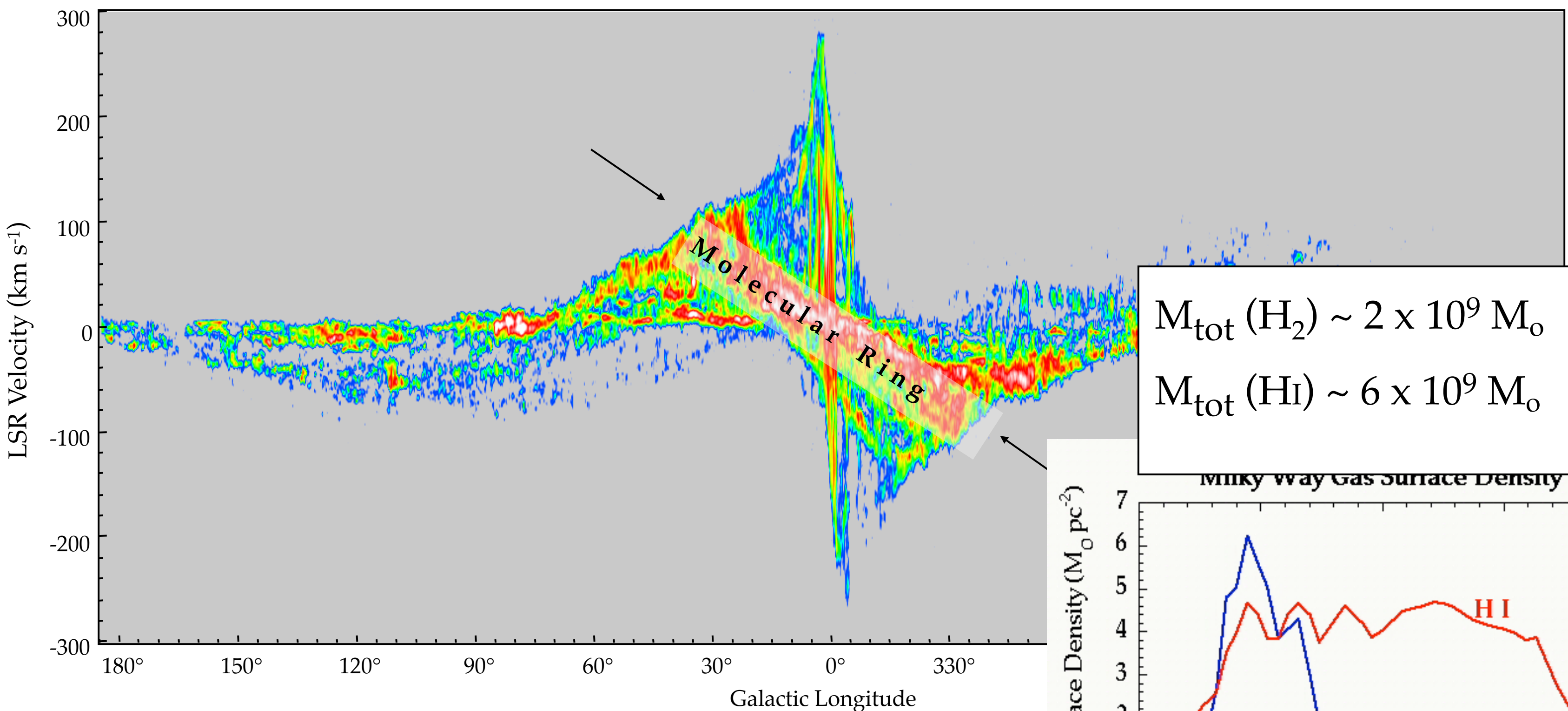

M_{tot} (H_2) ~ 2 x 10^9 M_o

M_{tot} (HI) ~ 6 x 10^9 M_o

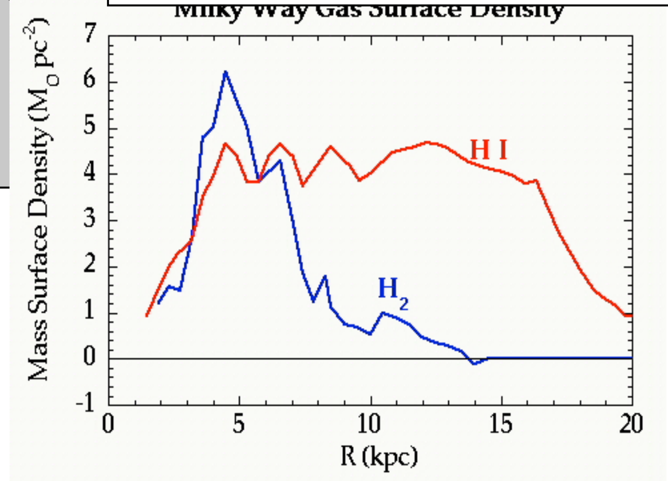

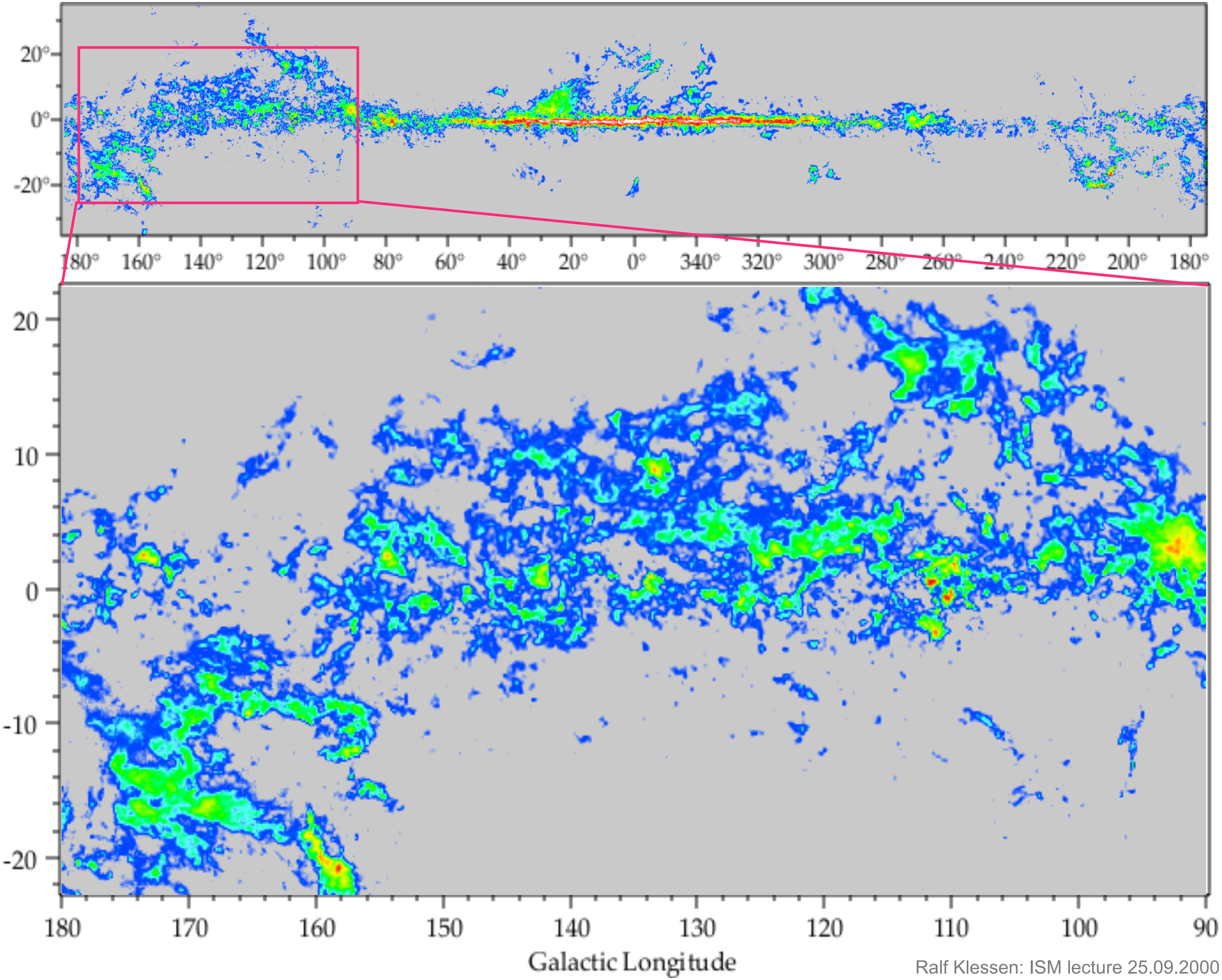

ata from Thomas Dame, CfA Harvard

Ralf Klessen: ISM lecture 25.09.2000

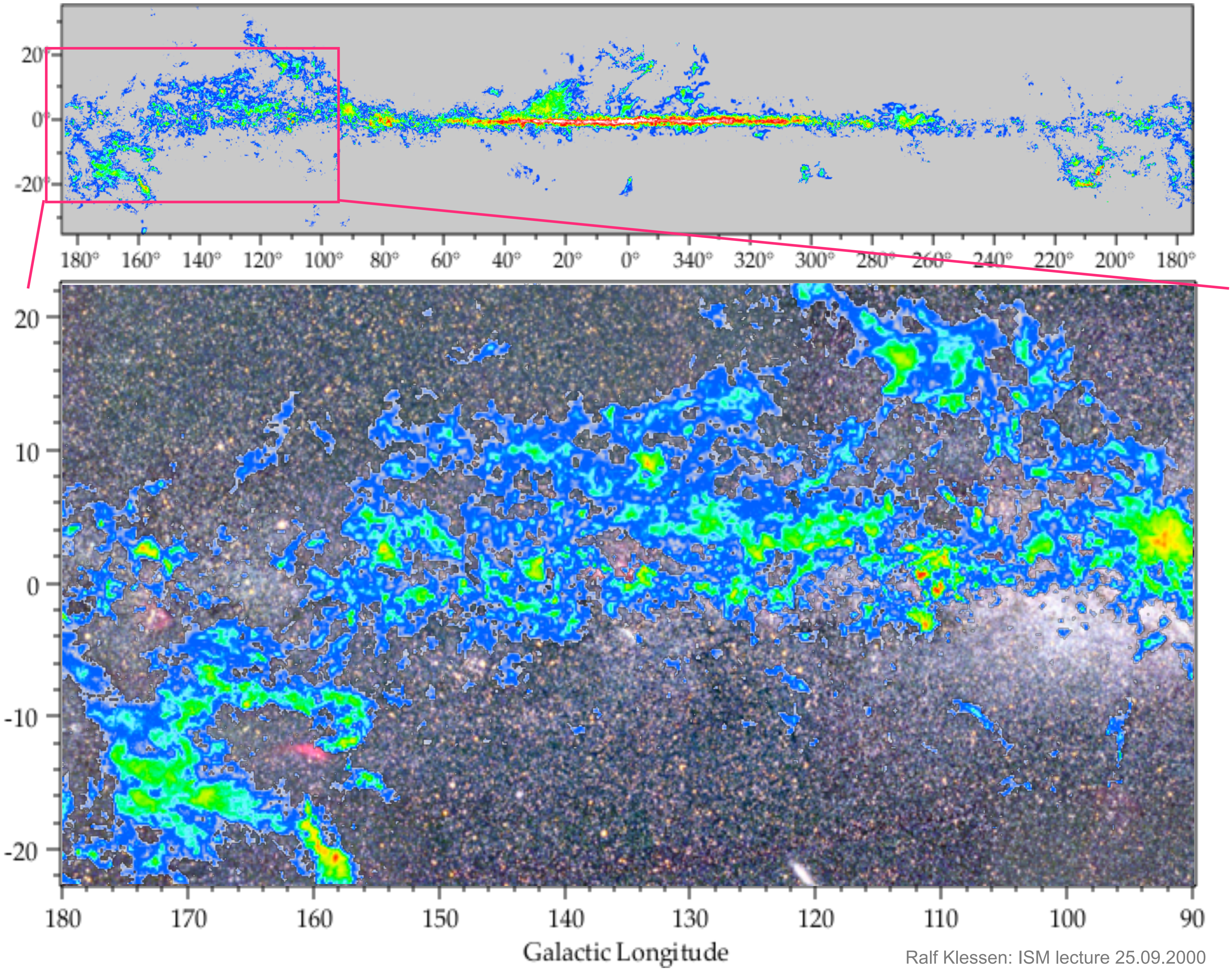

ata from Thomas Dame, CfA Harvard

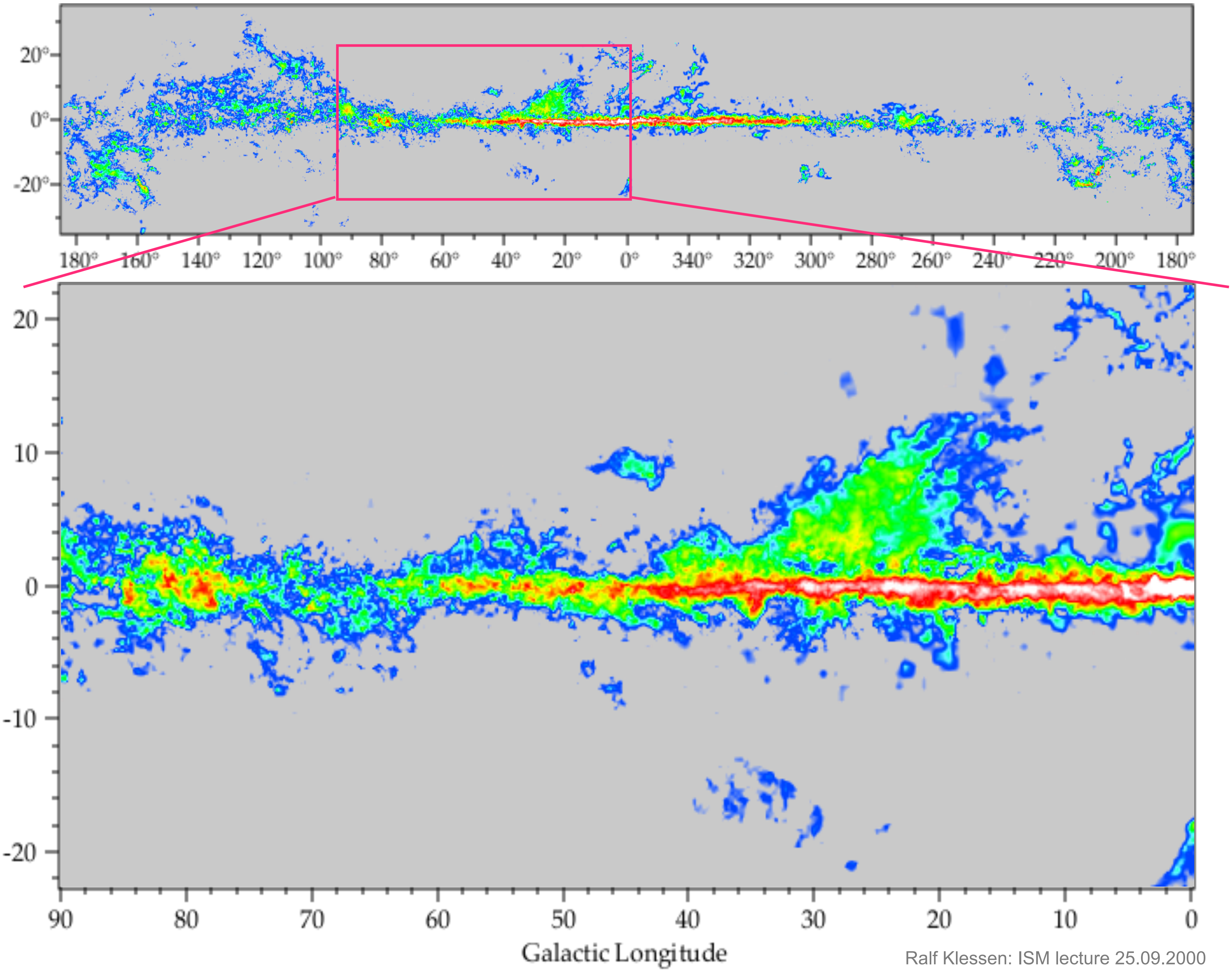

data from Thomas Dame, CfA Harvard

ata from Thomas Dame, CfA Harvard

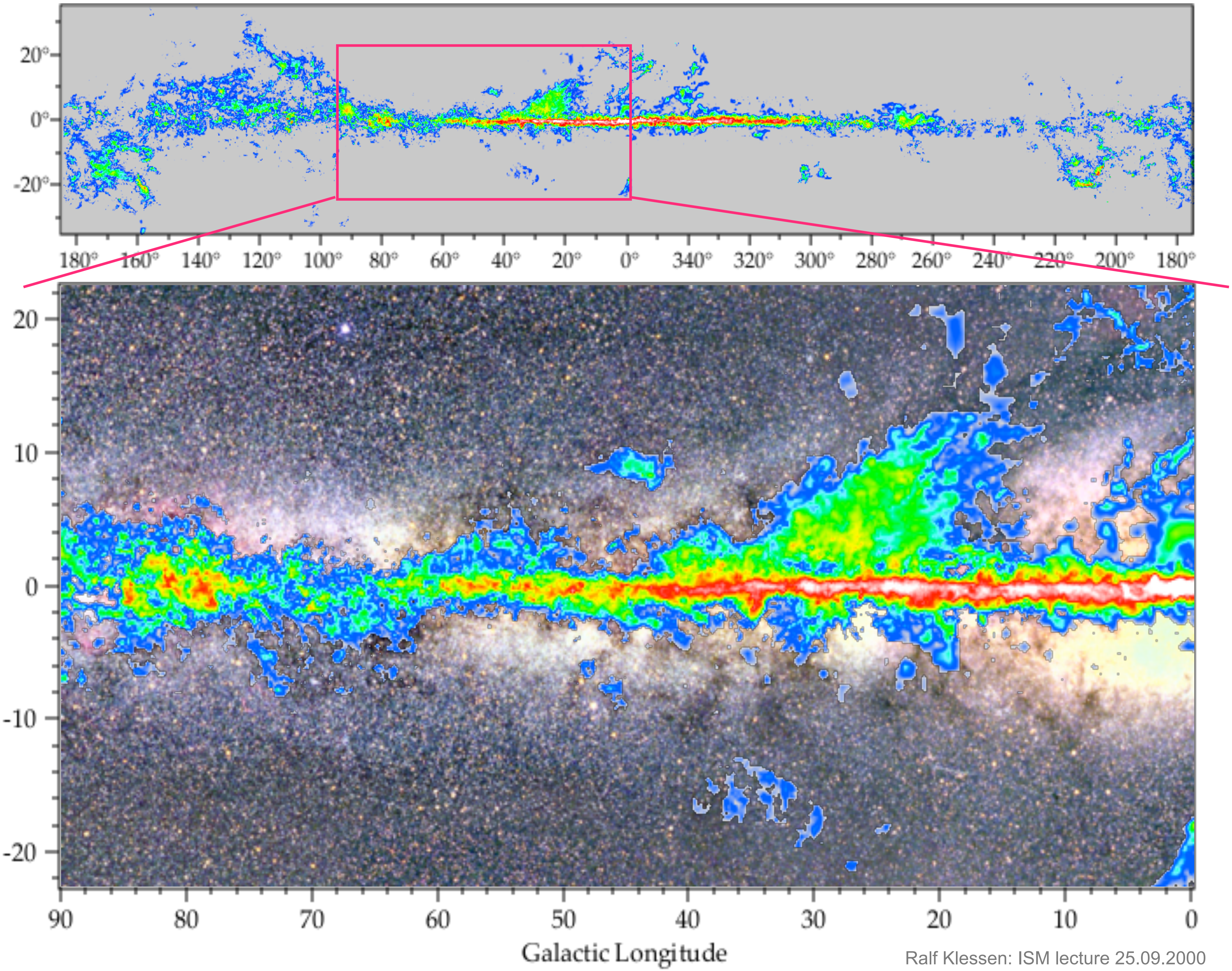

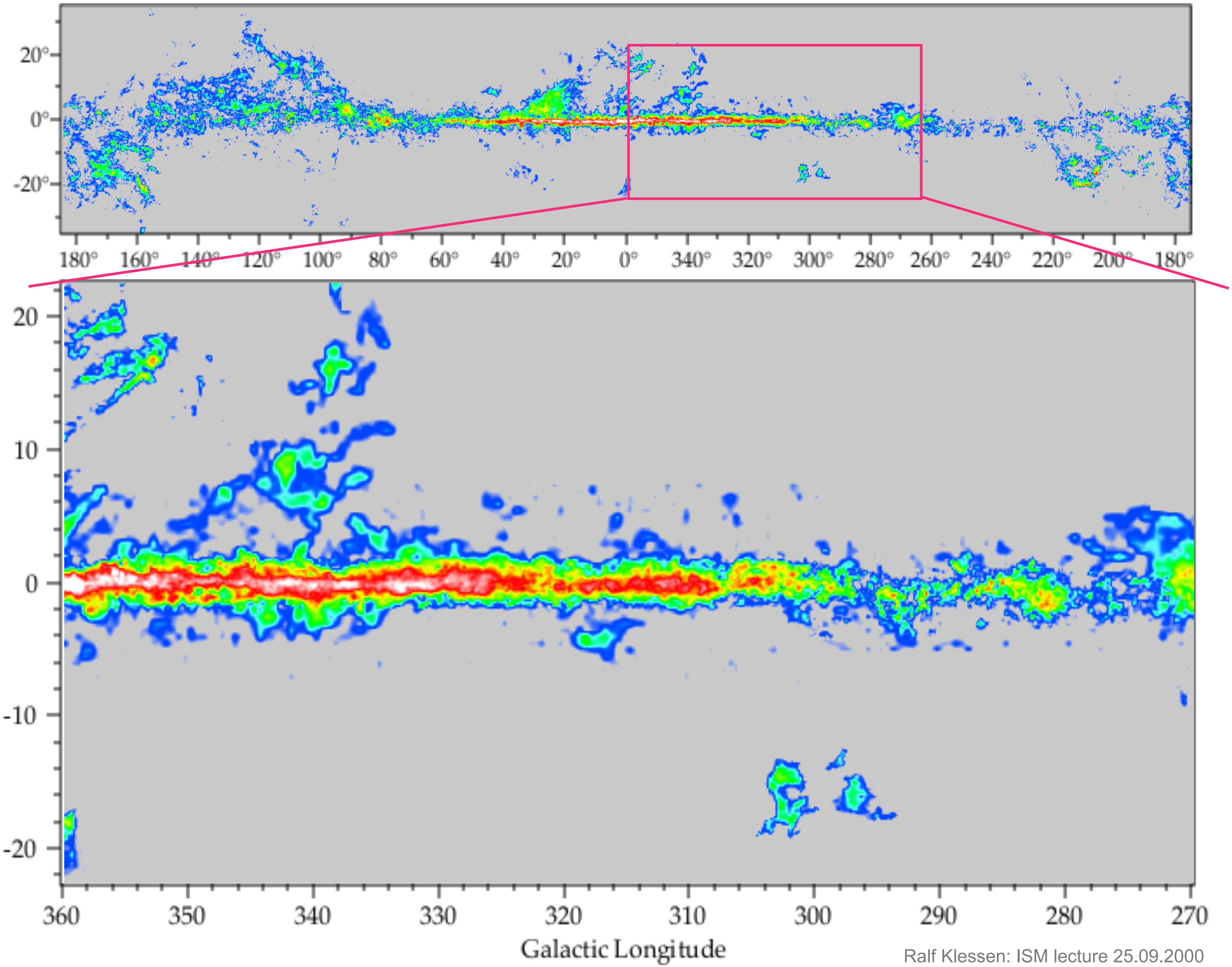

ata from Thomas Dame, CfA Harvard

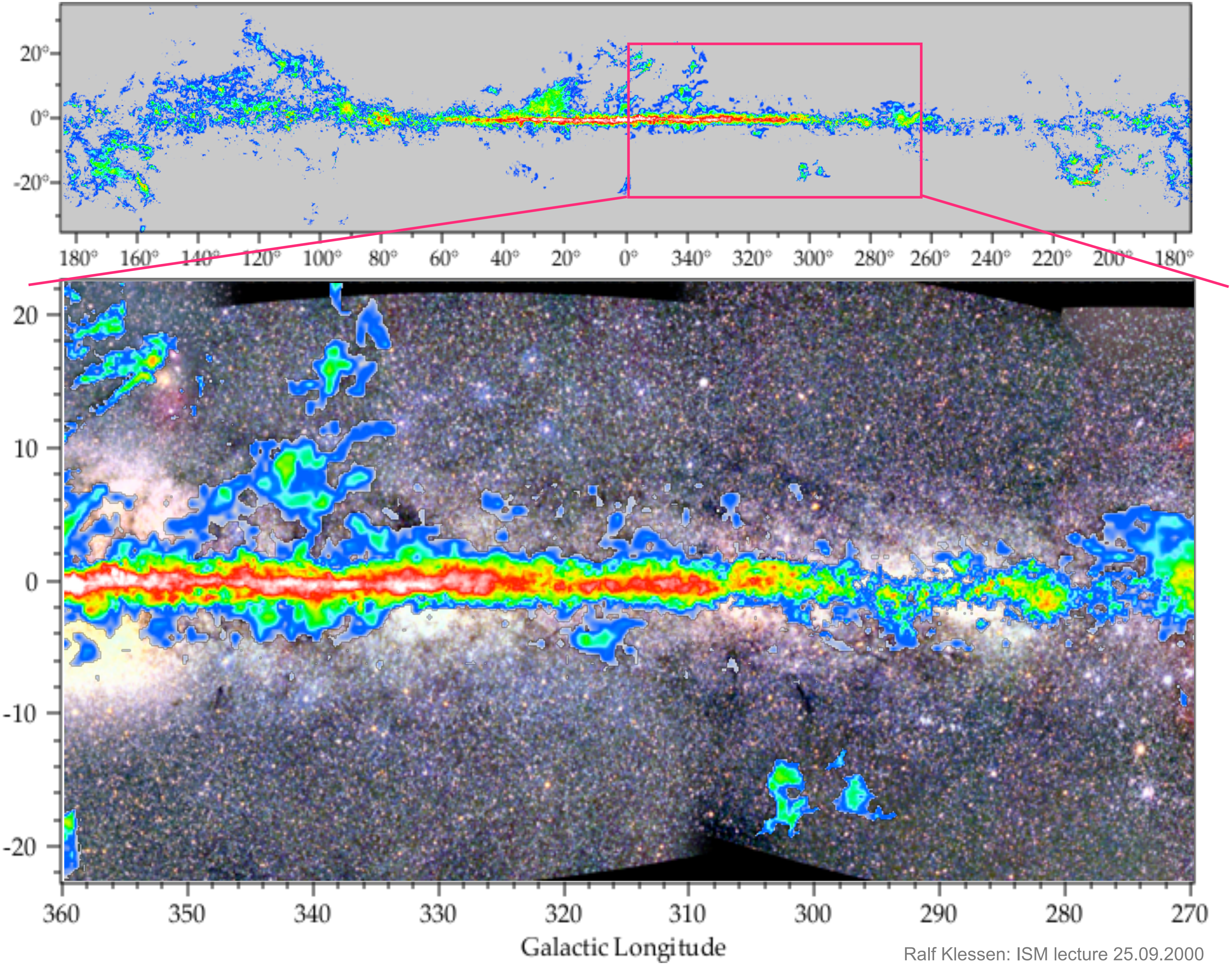

ata from Thomas Dame, CfA Harvard

Ralf Klessen: ISM lecture 25.09.2000

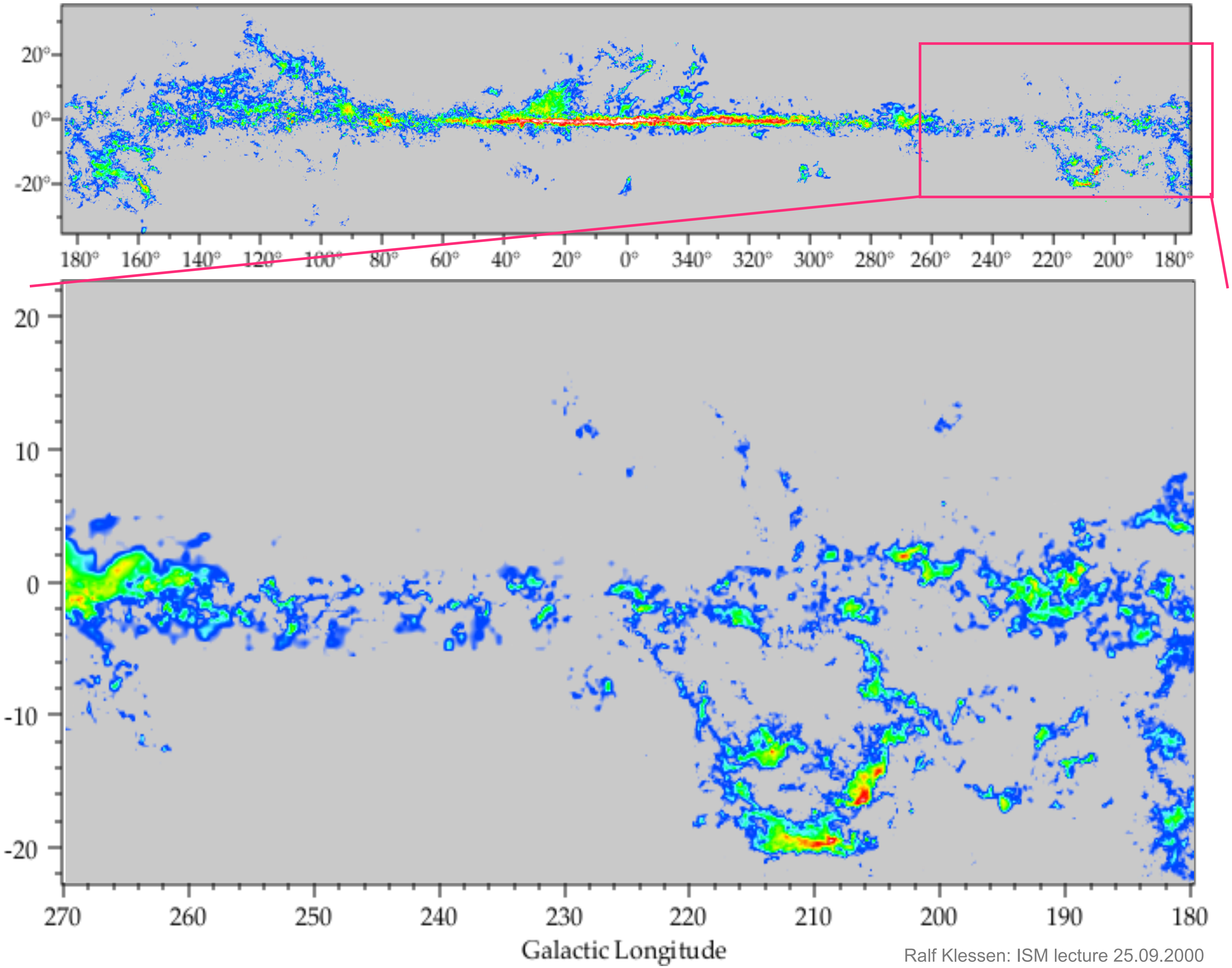

ata from Thomas Dame, CfA Harvard

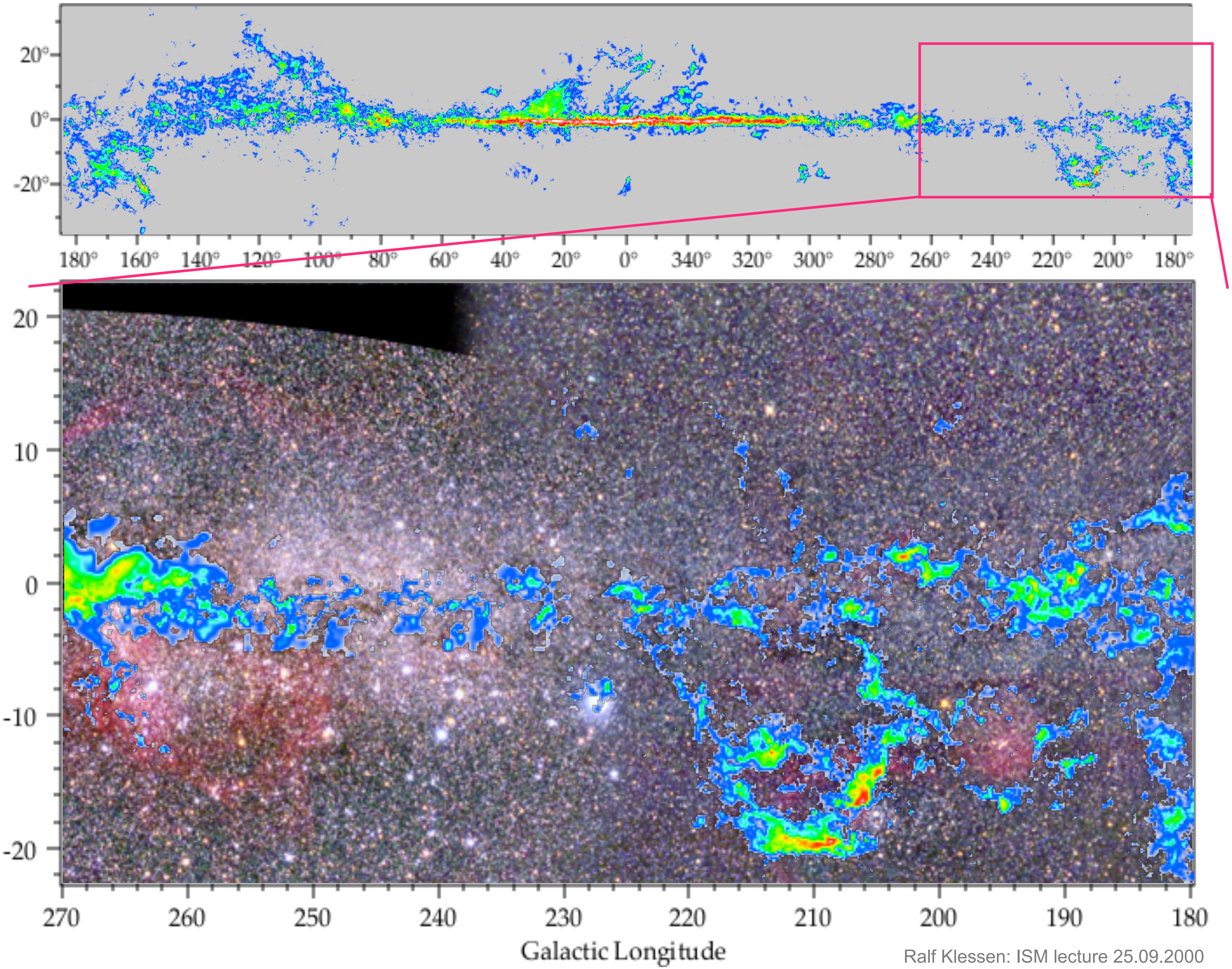

ata from Thomas Dame, CfA Harvard

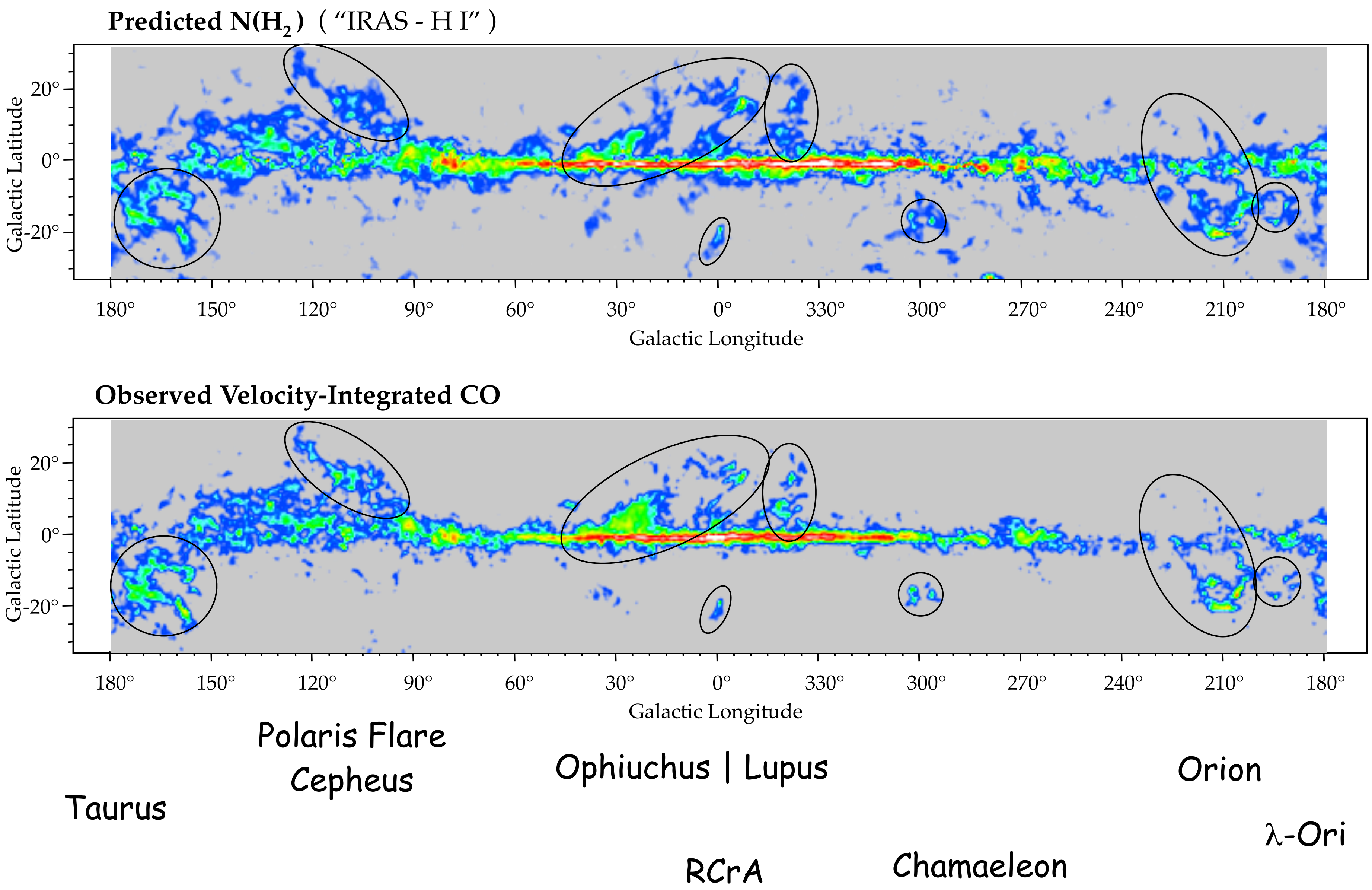

ata from Thomas Dame, CfA Harvard

nearby molecular clouds

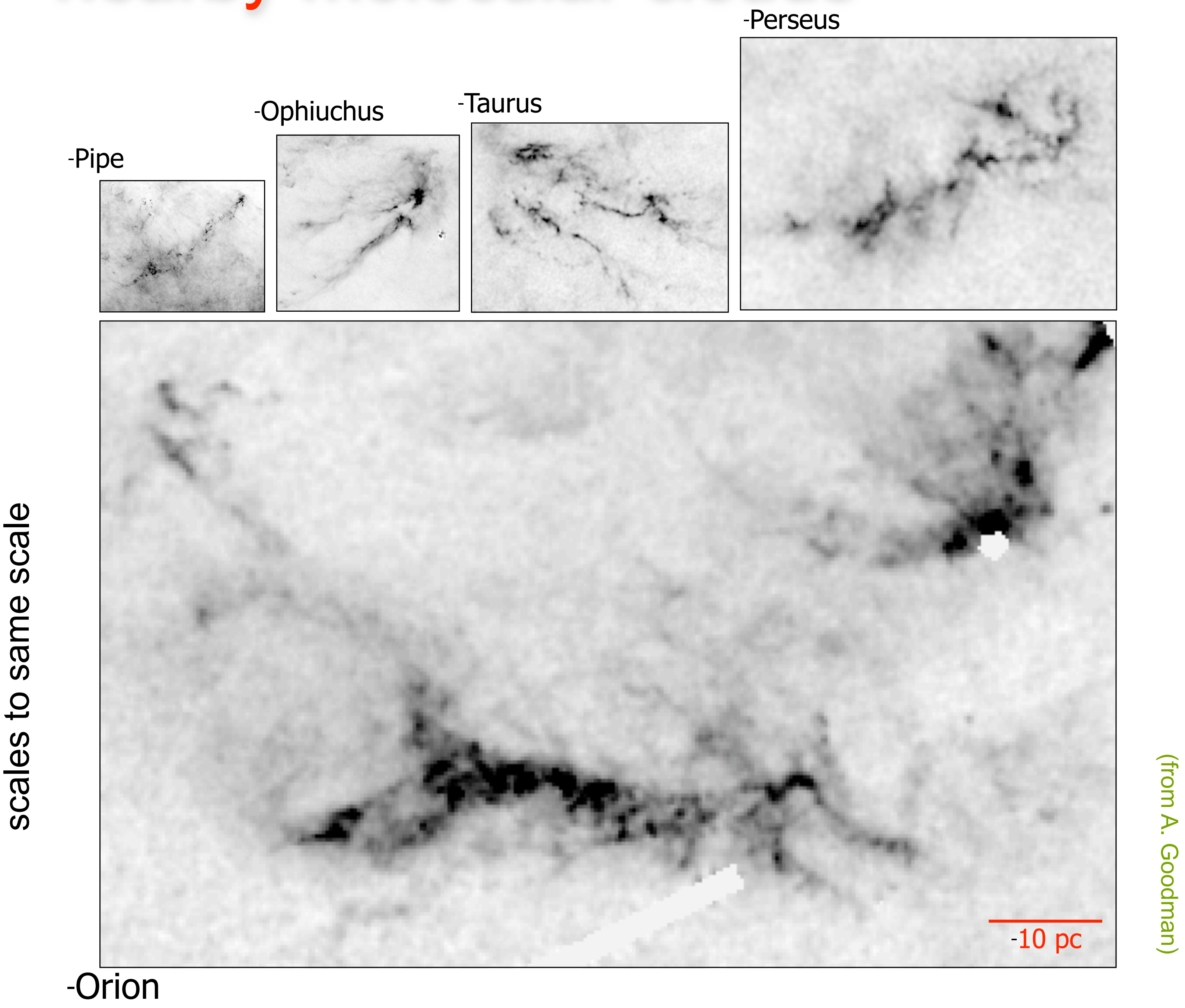

nearby molecular clouds

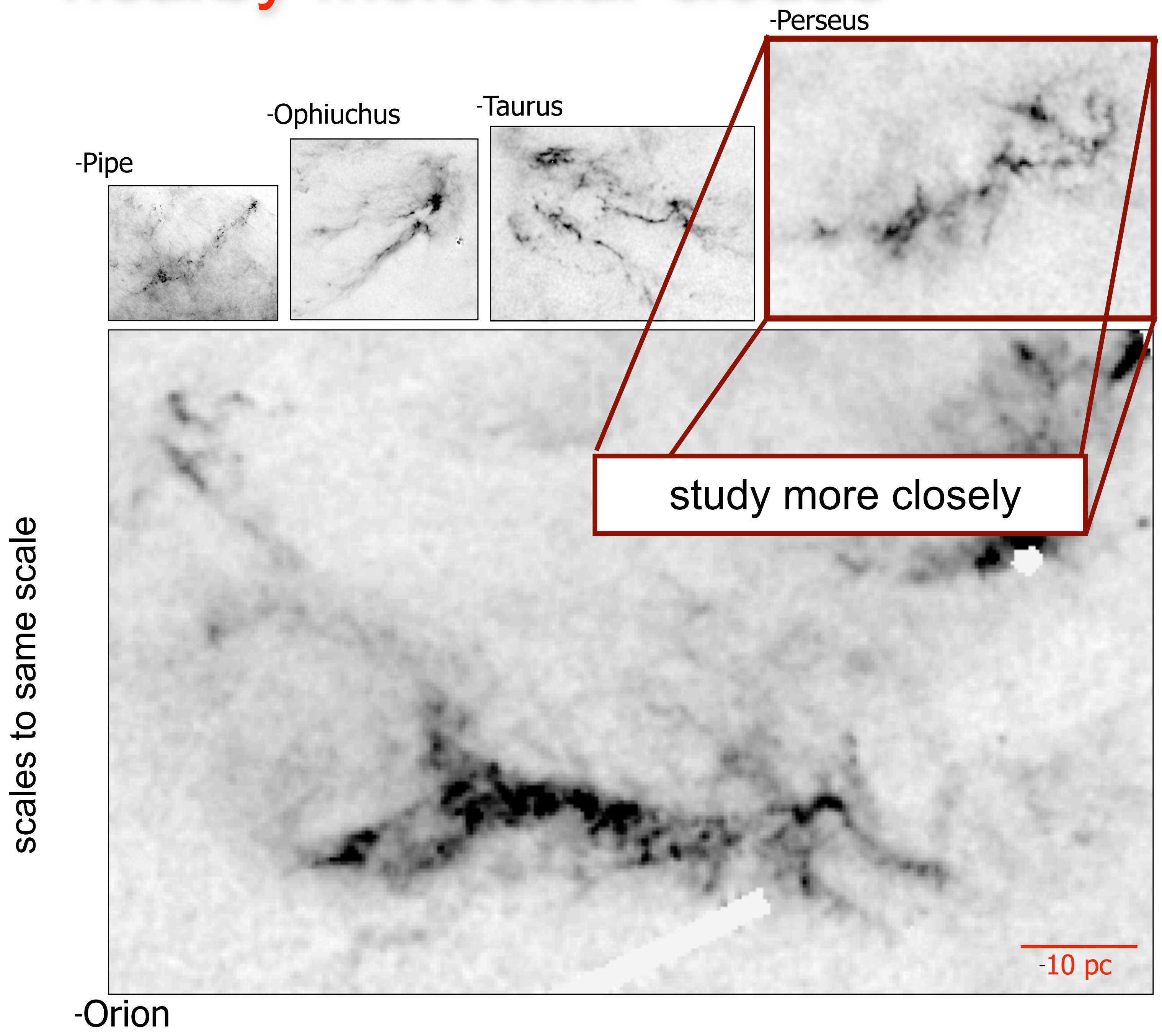

(from A. Goodman)

COMPLETE = **CO**ordinated **M**olecular **P**robe **L**ine **E**xtinction **T**hermal **E**mission Survey of Star-Forming Regions

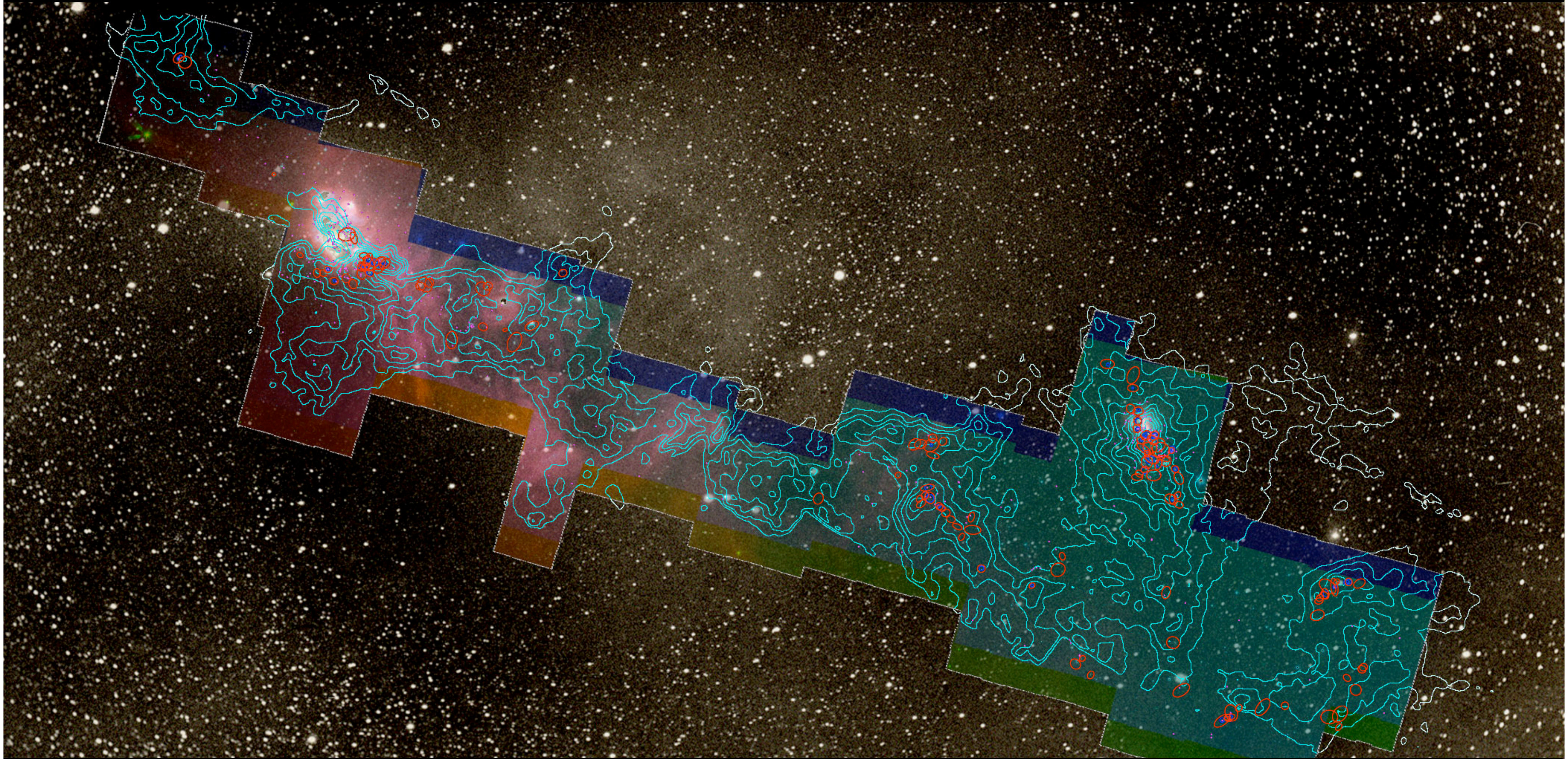

COMPLETE Collaborators, Summer 2008:

Alyssa A. Goodman (CfA/IIC)

João Alves (Calar Alto, Spain)

Héctor Arce (Yale)

Michelle Borkin (IIC)

Paola Caselli (Leeds, UK)

James DiFrancesco (HIA, Canada)

Jonathan Foster (CfA, PhD Student)

Katherine Guenthner (CfA/Leipzig)

Mark Heyer (UMASS/FCRAO)

Doug Johnstone (HIA, Canada)

Jens Kauffmann (CfA/IIC)

Helen Kirk (HIA, Canada)

Di Li (JPL)

Jaime Pineda (CfA, PhD Student)

Erik Rosolowsky (UBC Okanagan)

Rahul Shetty (CfA)

Scott Schnee (Caltech)

Mario Tafalla (OAN, Spain)

molecular clouds

- high-density regions in the ISM
- consist mostly of H_2
- cold
- extremely complex velocity and density structure (turbulence, fractal dimension?)
- all stars form in molecular clouds
- mass spectrum $dN/dM \sim M^{-2}$

molecular cloud formation

molecular cloud formation

- star formation on galactic scales
  → requires understanding of
  formation of molecular clouds
- questions
  - *where* and *when* do molecular clouds form?
  - *what* are their properties?
  - *how* do stars form in their interior?
  - global correlations? → *Schmidt law*

molecular cloud formation

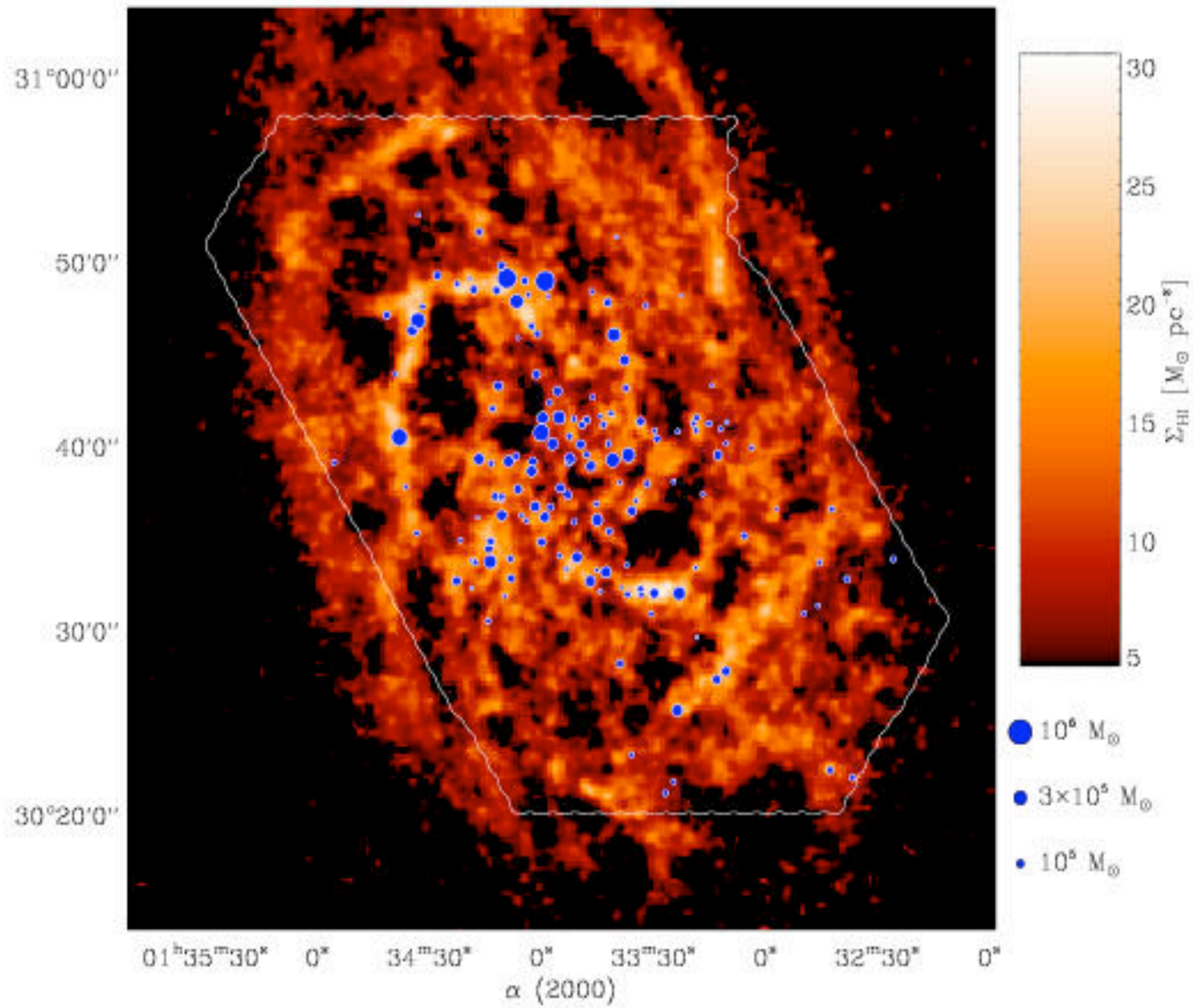

Thesis:

Molecular clouds form at *stagnation points* of large-scale convergent flows, mostly triggered by global (or external) perturbations.

(Deul & van der Hulst 1987, Blitz et al. 2004)

correlation with large-scale perturbations

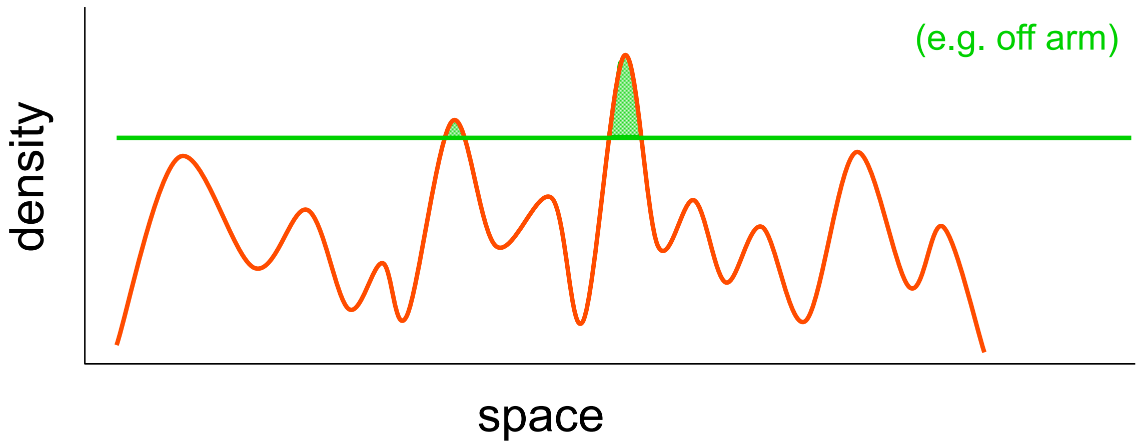

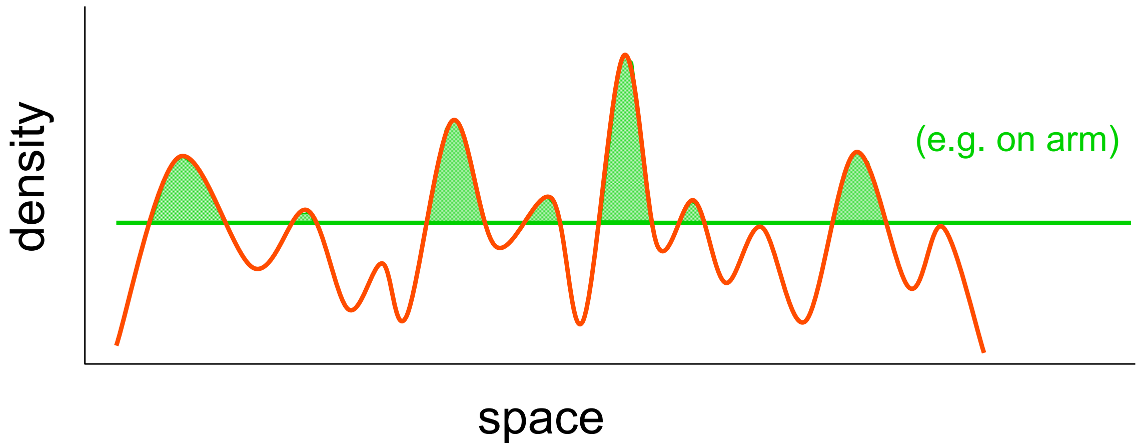

density/temperature fluctuations in warm atomar ISM are caused by *thermal/ gravitational instability* and/ or *supersonic turbulence*

some fluctuations are *dense* enough to *form H_2* within "*reasonable time*"

→ *molecular cloud*

external perturbuations (i.e. potential changes) *increase* likelihood

star formation on *global* scales

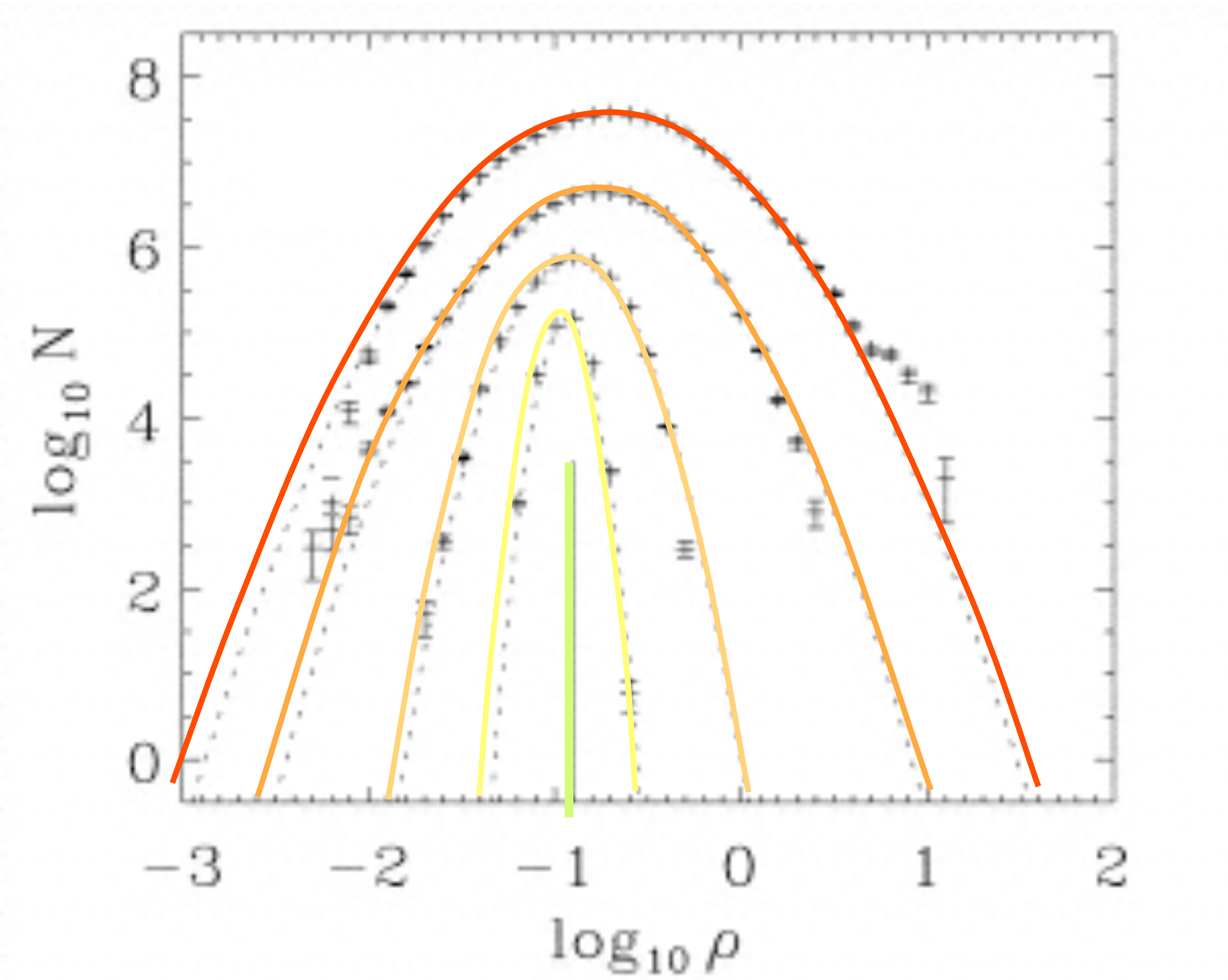

probability distribution function of the density *(ρ-pdf)*

varying rms Mach numbers:

M1 > M2 > M3 > M4 > 0

mass weighted ρ-pdf, each shifted by ΔlogN=1

(from Klessen, 2001; also Gazol et al. 2005, Krumholz & McKee 2005, Glover & Mac Low 2007ab)

star formation on *global* scales

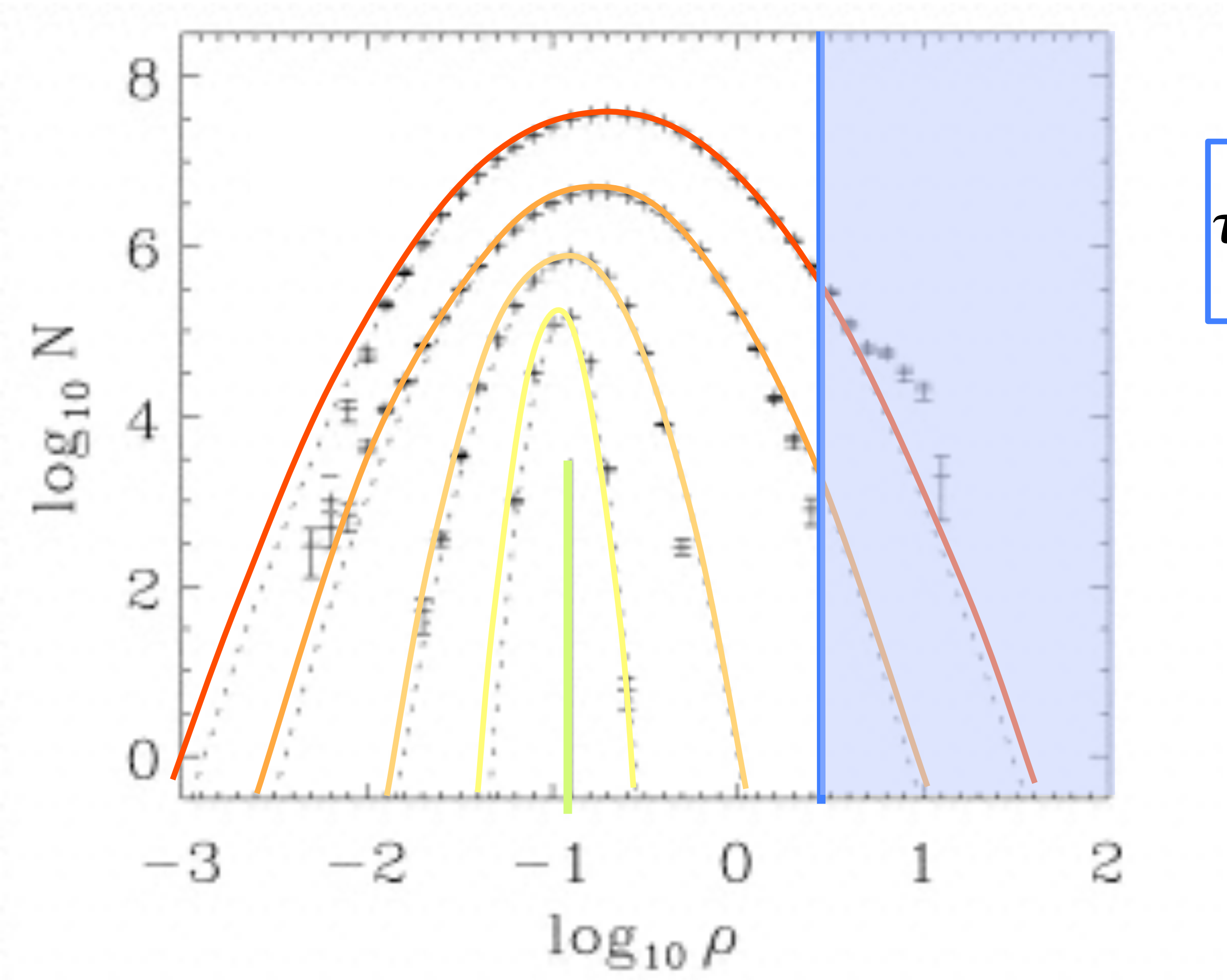

mass weighted ρ-pdf, each shifted by ΔlogN=1

(rate from Hollenback, Werner, & Salpeter 1971)

H_2 formation rate:

$$\tau_{H_2} \approx \frac{1.5\,\text{Gyr}}{n_H / 1\text{cm}^{-3}}$$

for $n_H \geq 100$ cm^{-3}, H_2 forms within 10 Myr, this is about the lifetime of typical MC's.

in turbulent gas, the H_2 fraction can become very high on short timescale

(for models with coupling between cloud dynamics and time-dependent chemistry, see Glover & Mac Low 2007a,b)

star formation on *global* scales

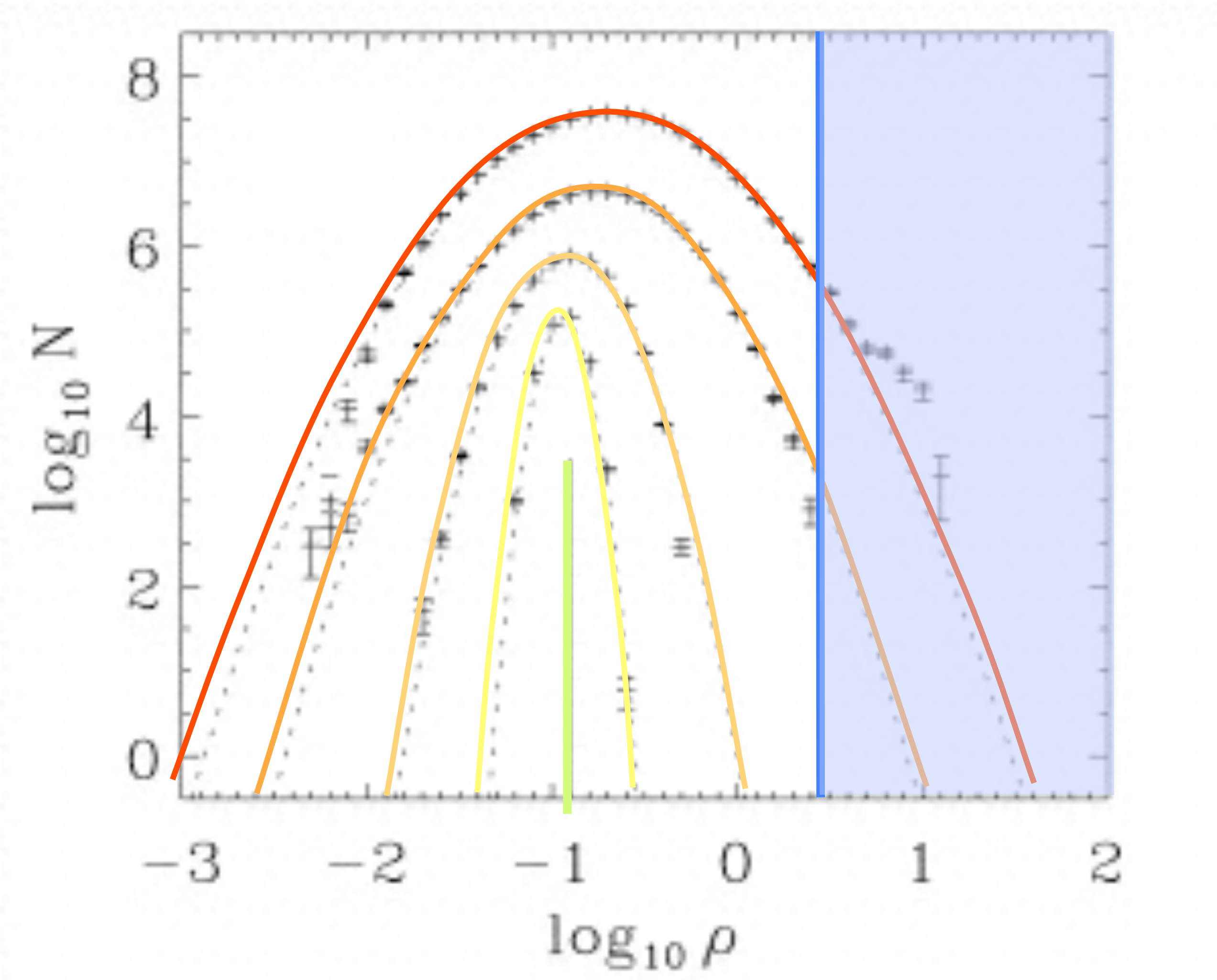

mass weighted ρ-pdf, each shifted by $\Delta\log N=1$

(rate from Hollenback, Werner, & Salpeter 1971)

BUT: *it doesn't work*
(at least not so easy):

Chemistry has a memory effect!

H2 forms more quickly in high-density regions as it gets destroyed in low-density parts.

(for models with coupling between cloud dynamics and time-dependent chemistry, see Glover & Mac Low 2007a,b)

modeling galactic SF

SPH calculations of self-gravitating disks of stars and (isothermal) gas in dark-matter potential, sink particles measure local collapse --> star formation

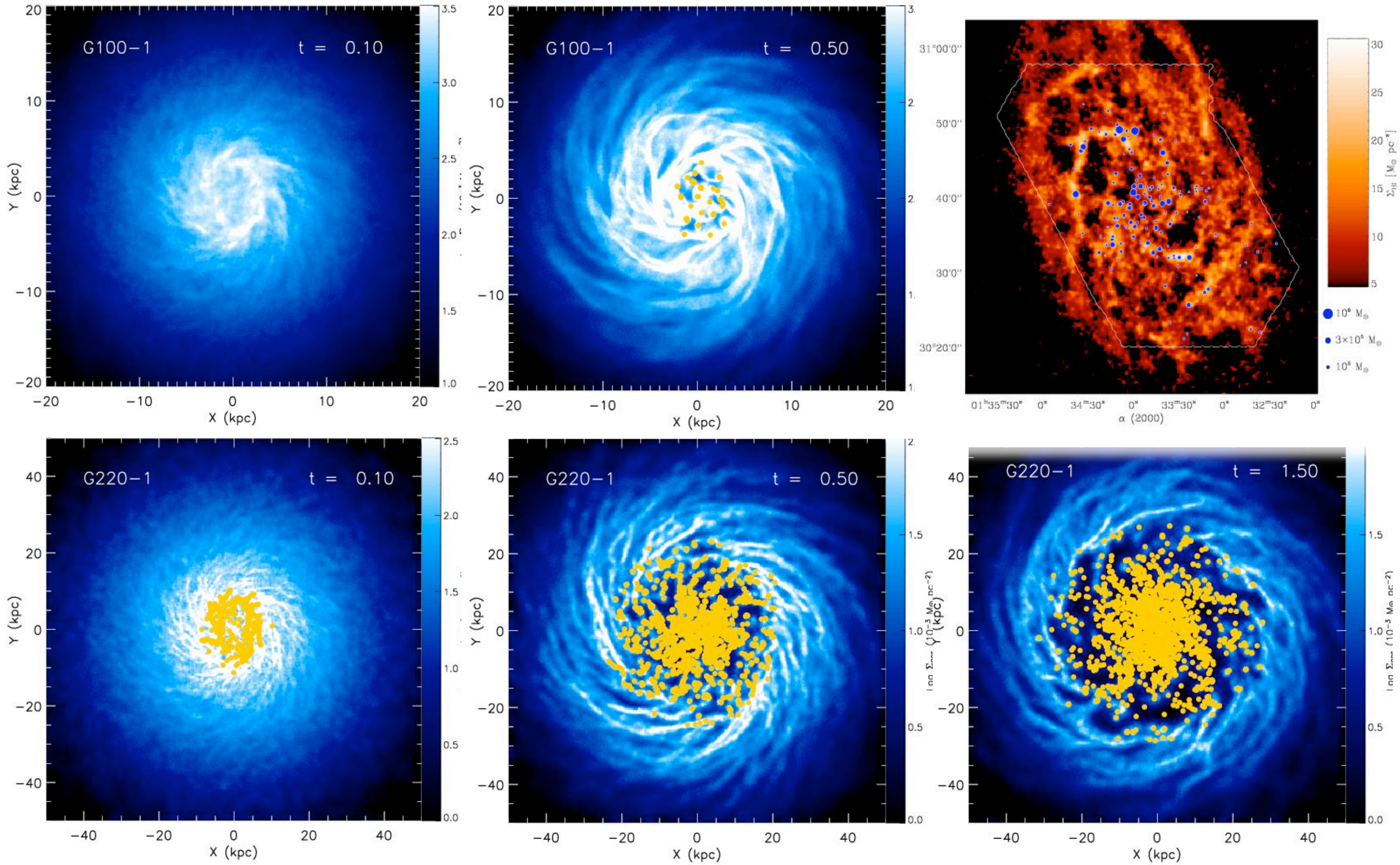

(Li, Mac Low, & Klessen, 2005, ApJ, 620,L19 - L22)

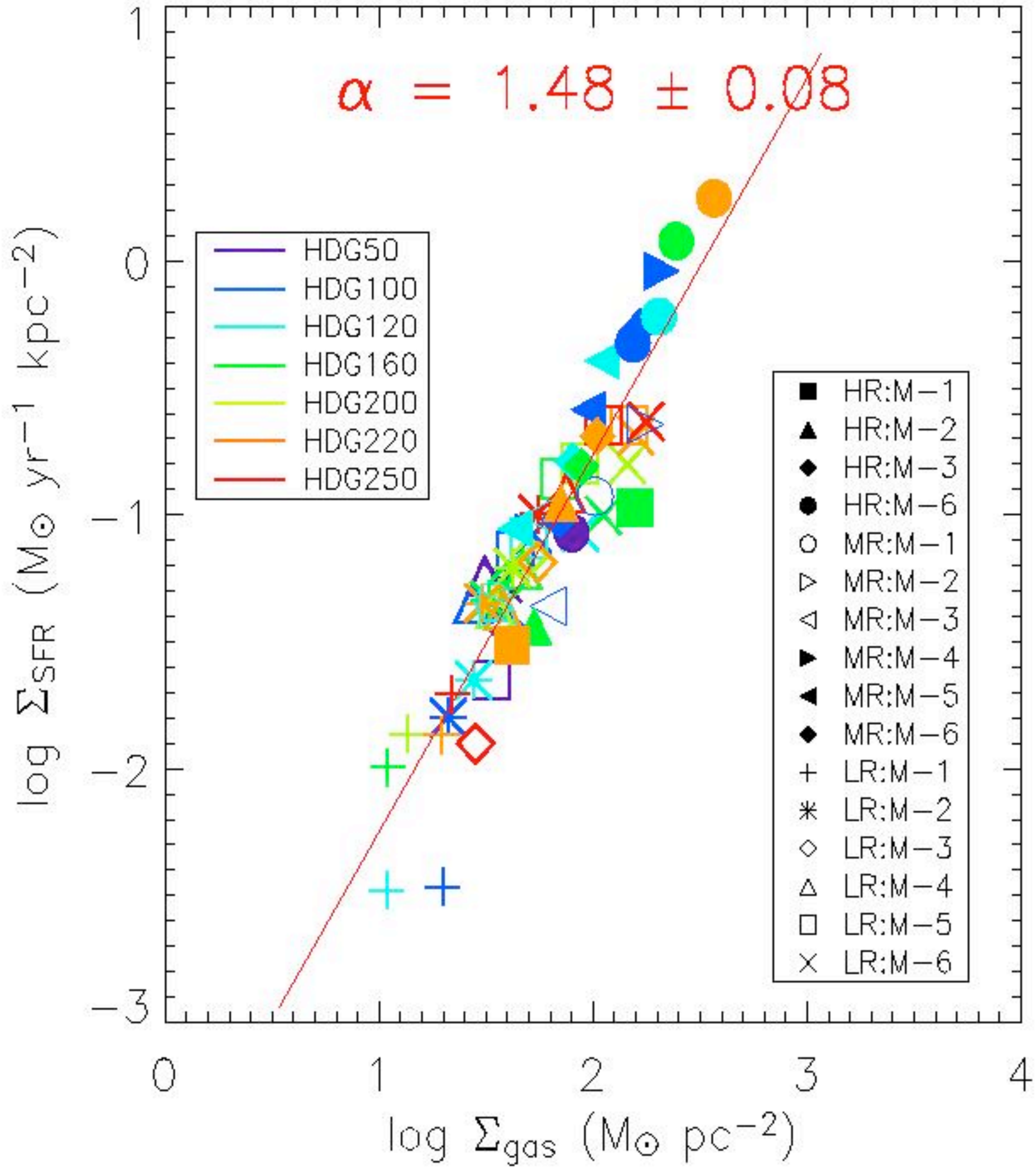

(Li, Mac Low, & Klessen, 2005, ApJ, 620, L19 - L22)

We find correlation between *star formation rate* and *gas surface density:*

$$\boxed{\Sigma_{SFR} \propto \Sigma_{gas}^{1.5}}$$

global Schmidt law

observed Schmidt law

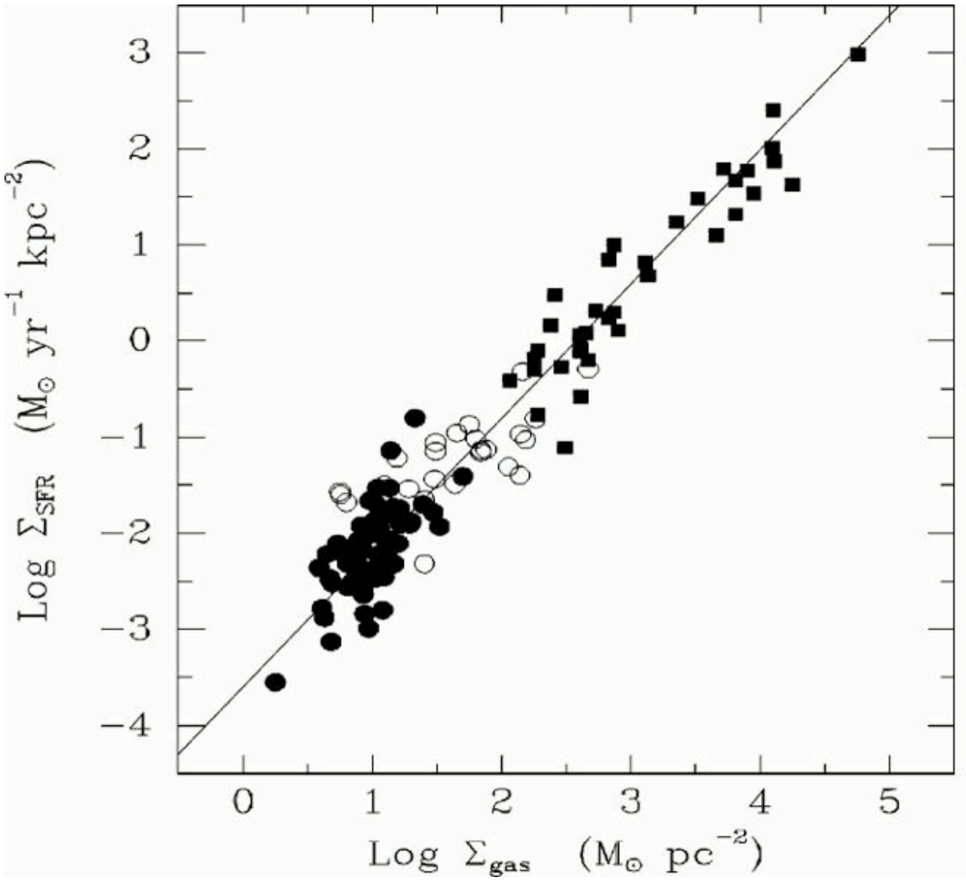

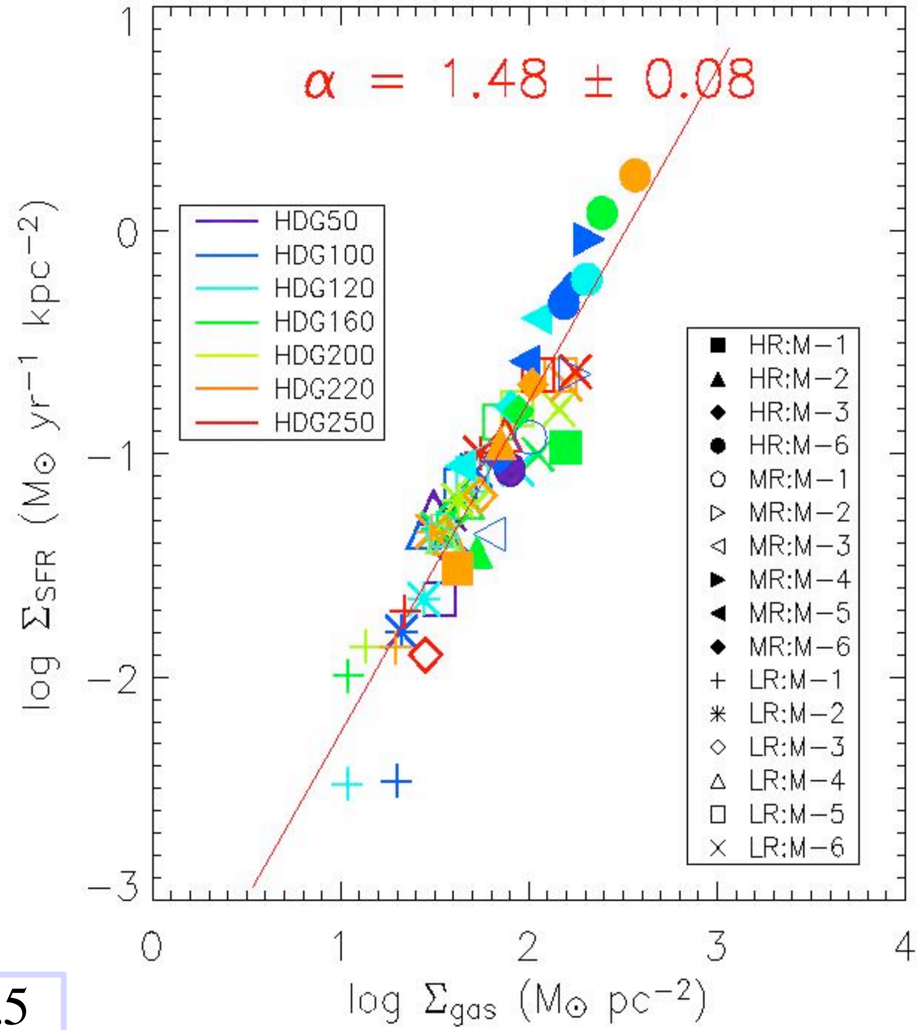

in both cases: $\boxed{\Sigma_{SFR} \propto \Sigma_{gas}^{1.5}}$

(from Kennicutt 1998)

local Schmidt law

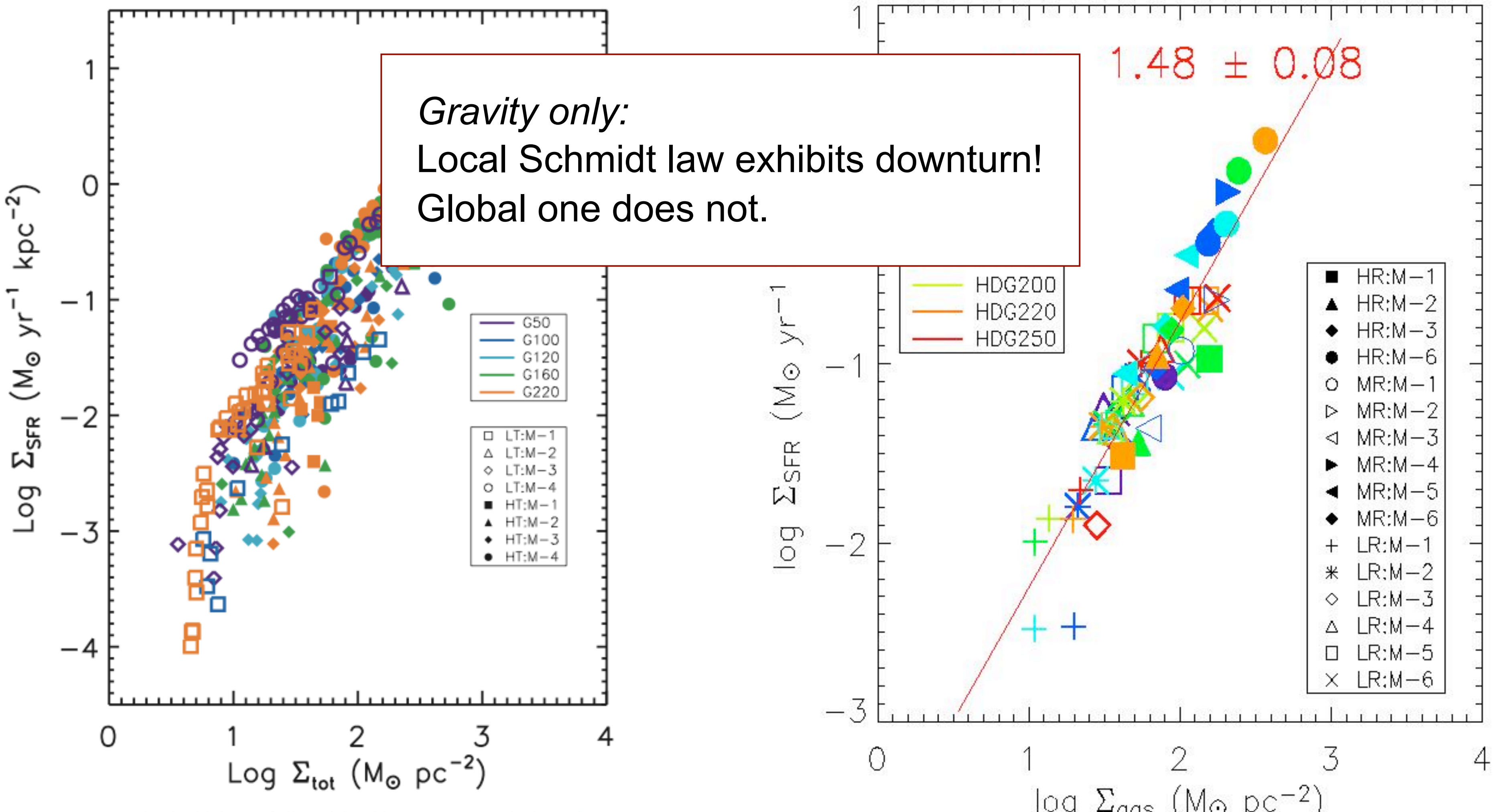

FIG. 11.—Local Schmidt laws of all models with $\tau_{SF} < 3$ Gyr. The legends are the same as in Fig. 5: the color of the symbol indicates the rotational velocity for each model as given in Table 1, the shape indicates the submodel classified by gas fraction, and open and filled symbols represent low- and high-T models, respectively.

(Li et al. 2006)

molecular cloud formation

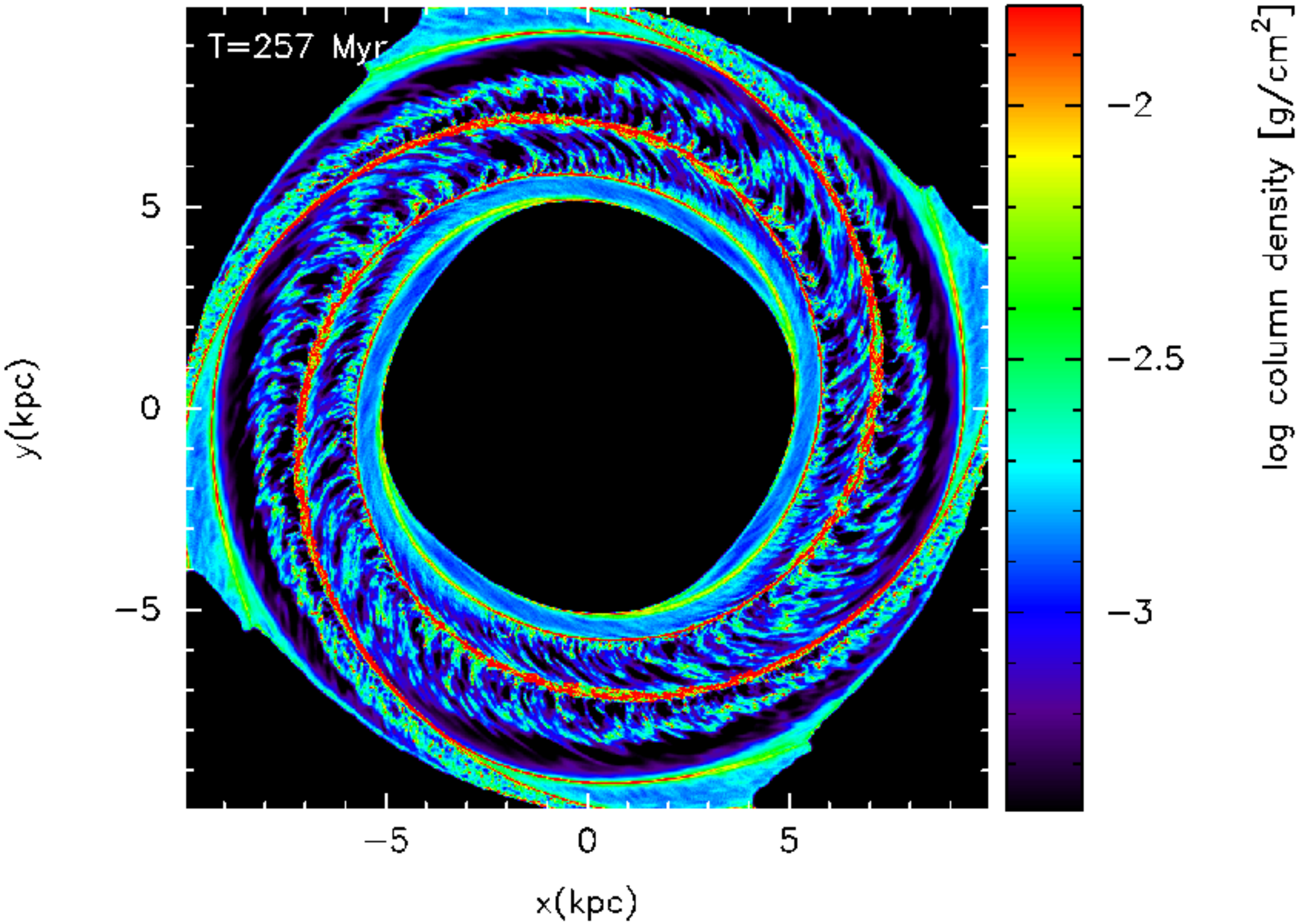

(from Dobbs et al. 2008)

molecular cloud formation

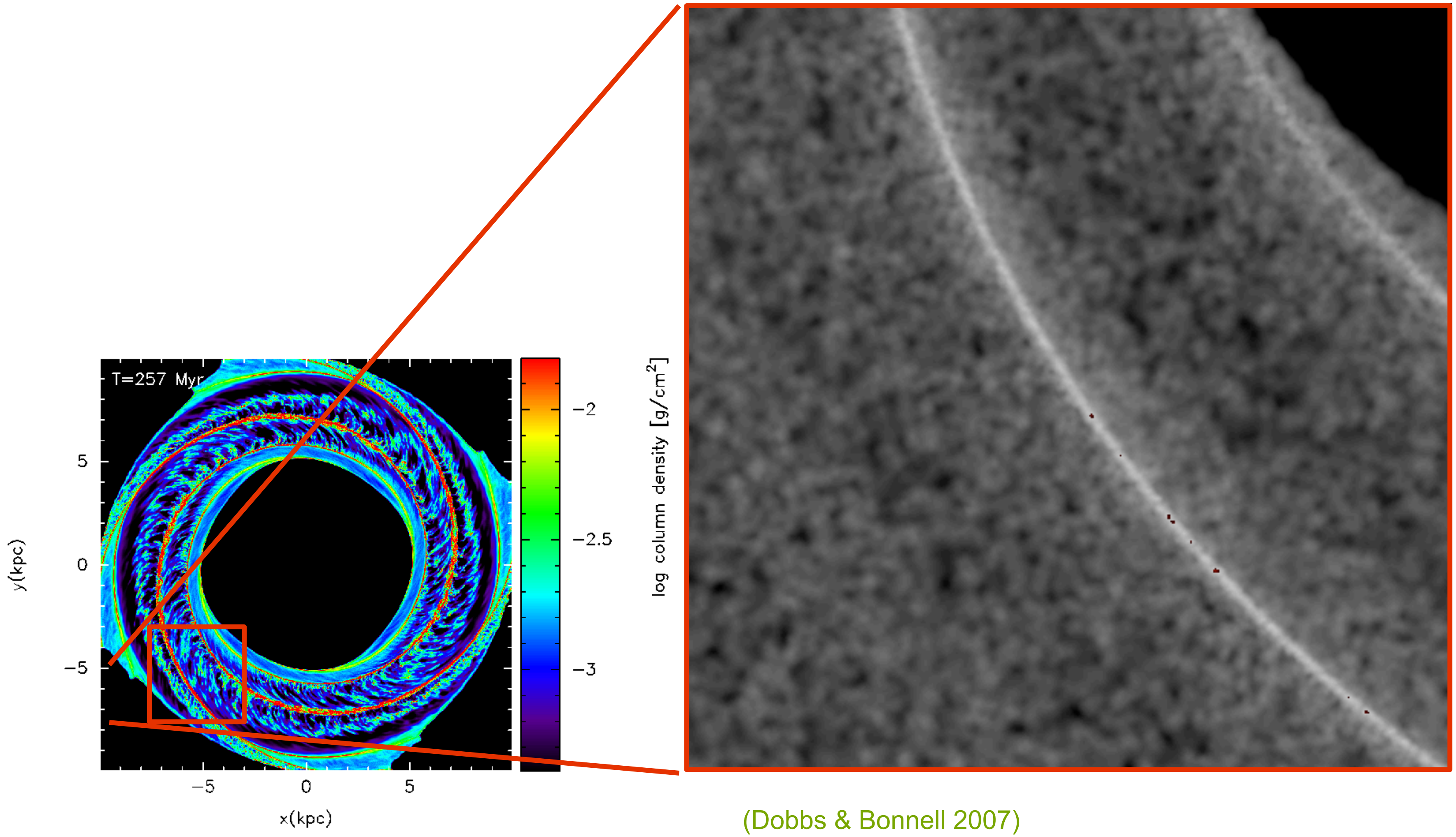

(Dobbs & Bonnell 2007)

molecular cloud formation

molecular gas fraction as function of time

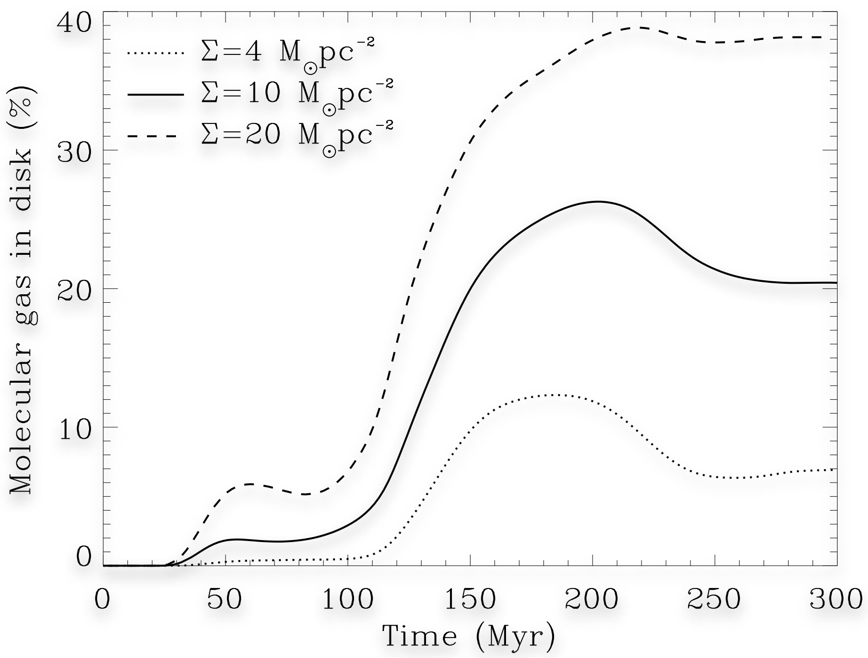

molecular gas fraction as function of density

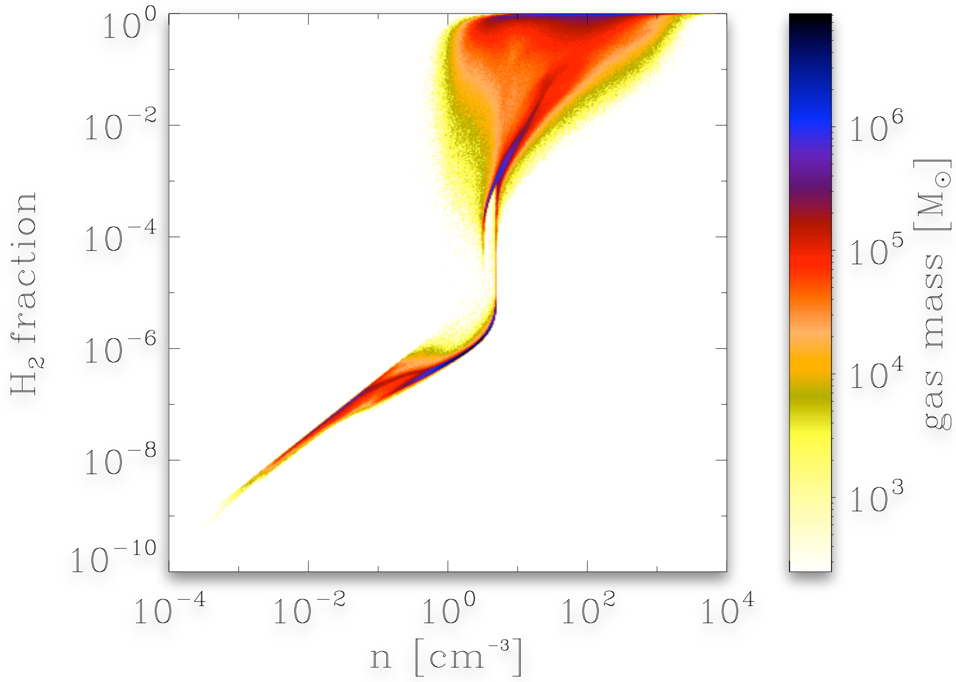

(Dobbs et al. 2008)

molecular cloud formation

molecular gas fraction of fluid element as function of time

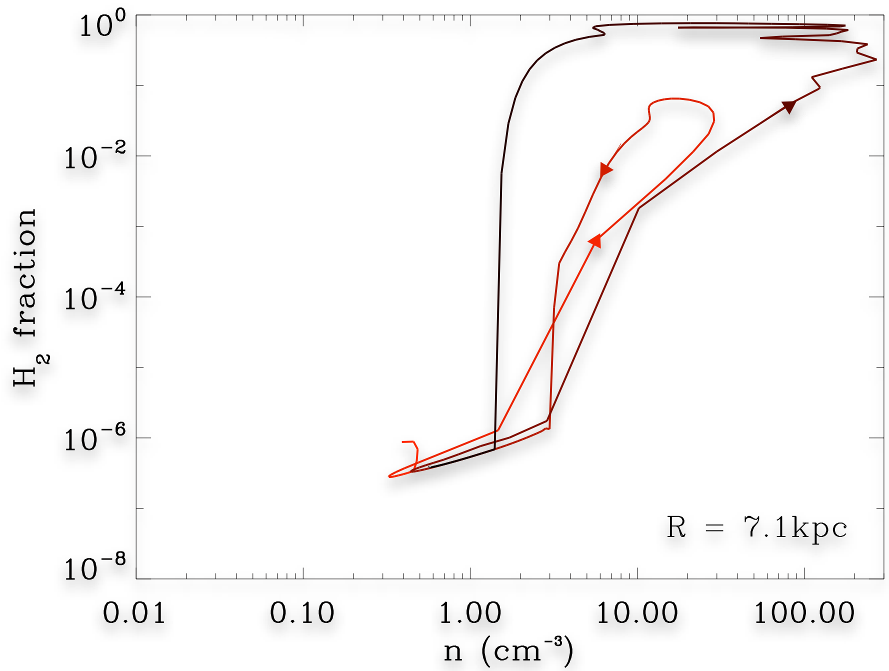

molecular gas fraction as function of density

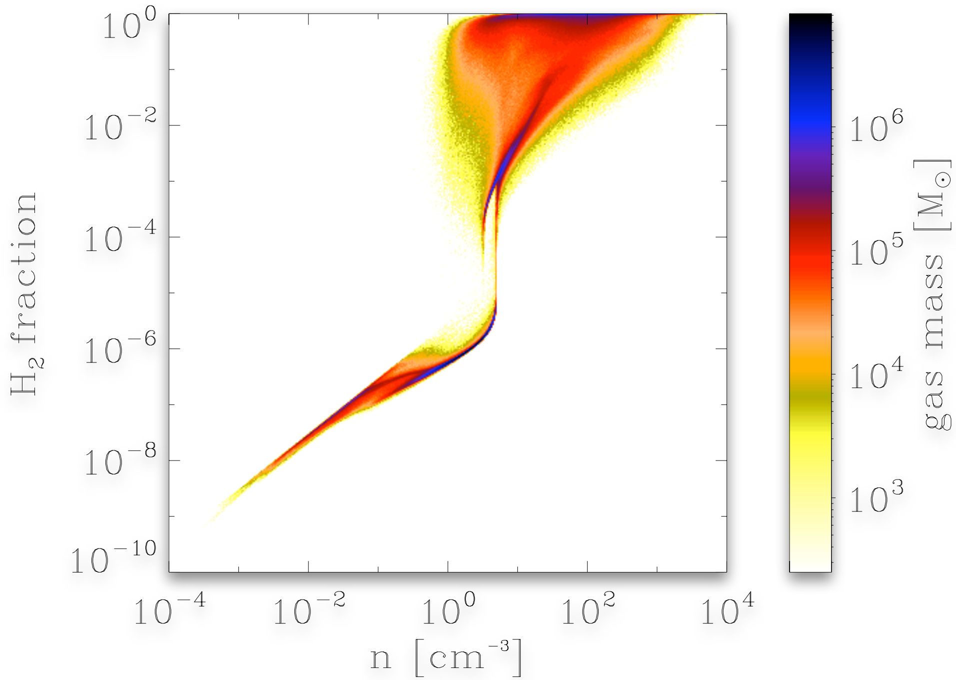

(Dobbs et al. 2008)

observed timescales

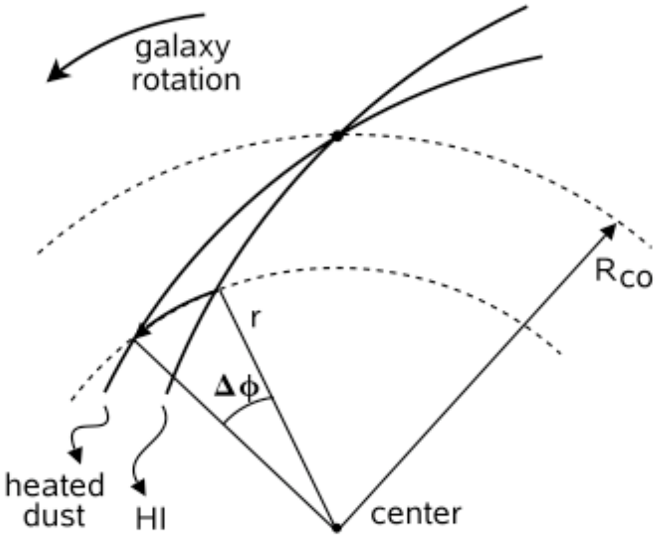

Tamburro et al. (2008)

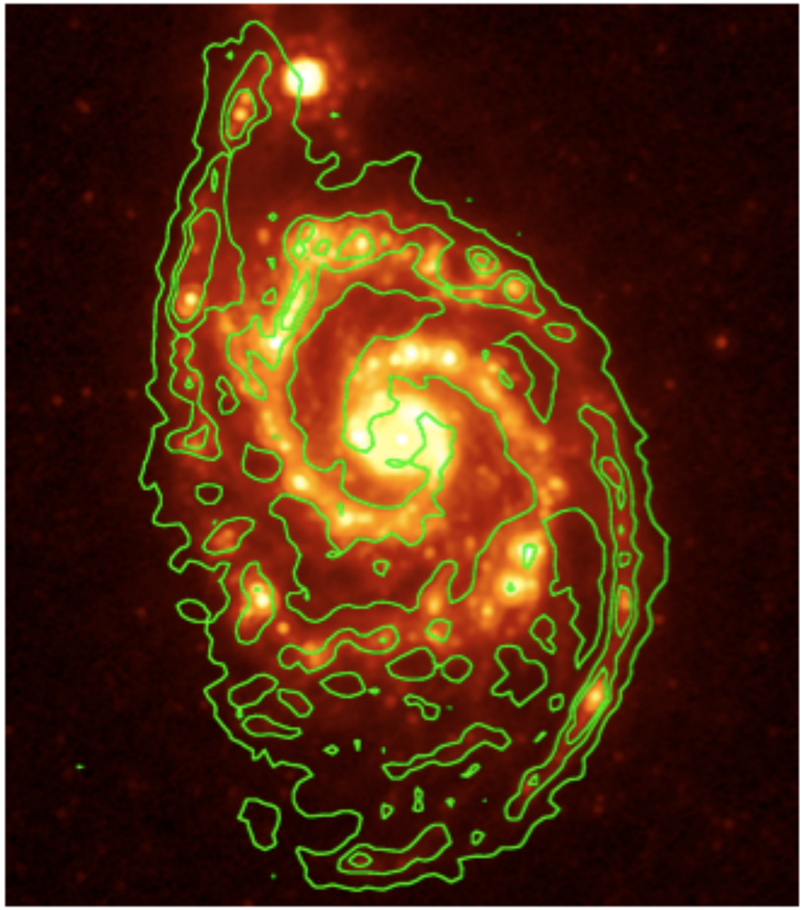

Fig. 1.— NGC 5194: the 24 μm band image is plotted in color scale; the H I emission map is overlayed with green contours.

observed timescales

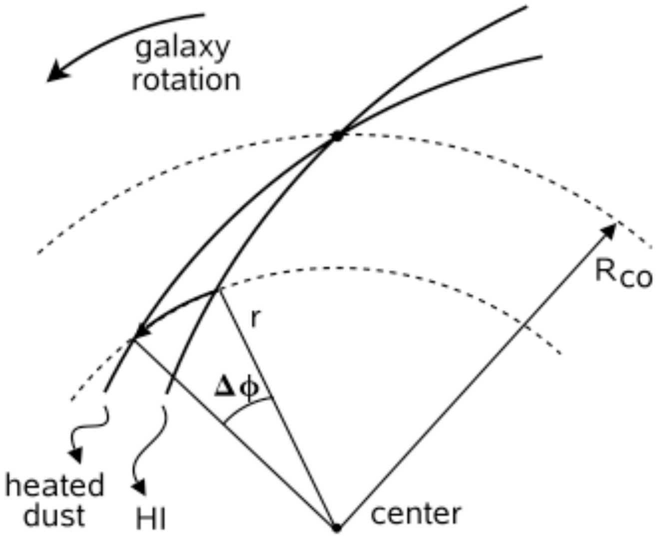

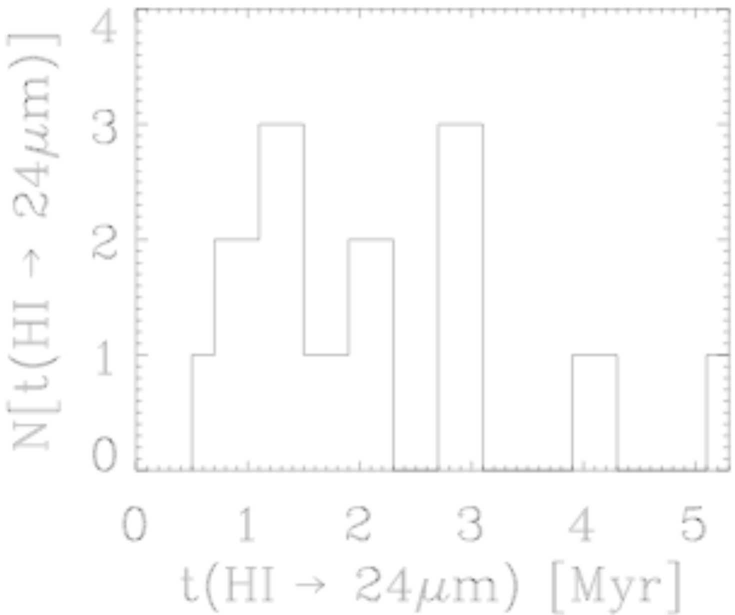

Fig. 5.— Histogram of the time scales $t_{\mathrm{HI}\mapsto 24\,\mu\mathrm{m}}$ derived from the fits in Figure 4 and listed in Table. 2 for the 14 sample galaxies listed in Table. 1. The timescales range between 1 and 4 Myr for almost all galaxies.

Tamburro et al. (2008)

calculated timescales

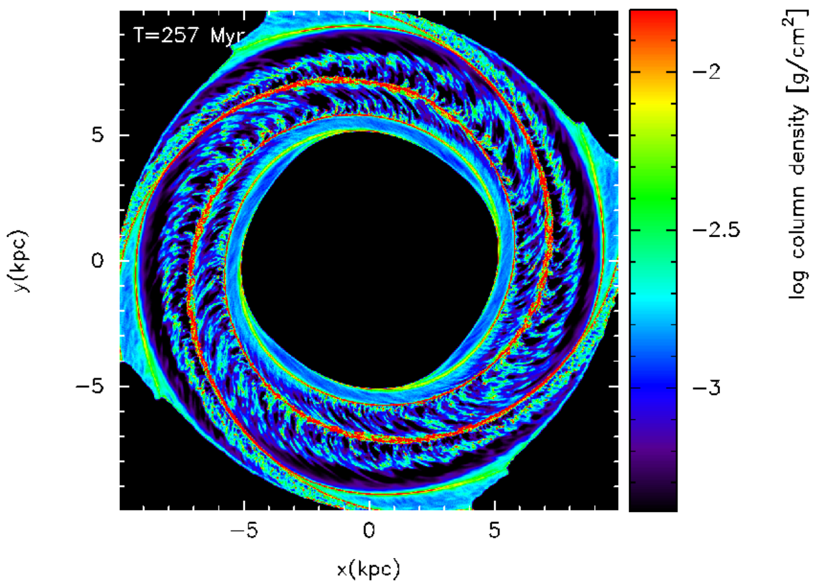

Dobbs et al. (2008)

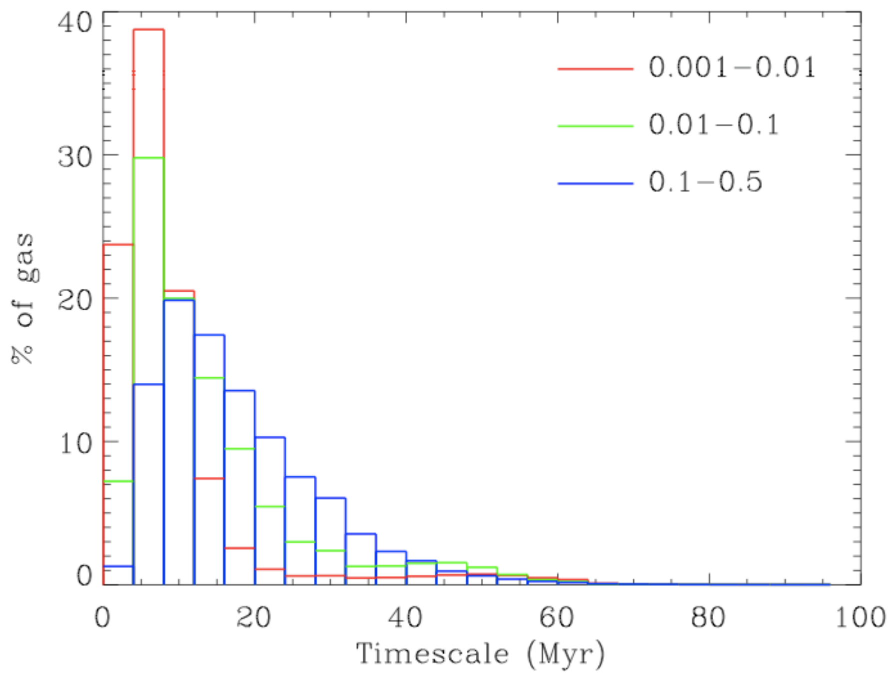

Figure 16. This histogram gives the distribution of timescales over which the gas reaches certain molecular gas fractions. The timescales denote the time for the H_2 fraction of a particle to increase from 0.001 to 0.01, 0.01 to 0.1 and 0.1 to 0.5, as indicated.

models with B-fields

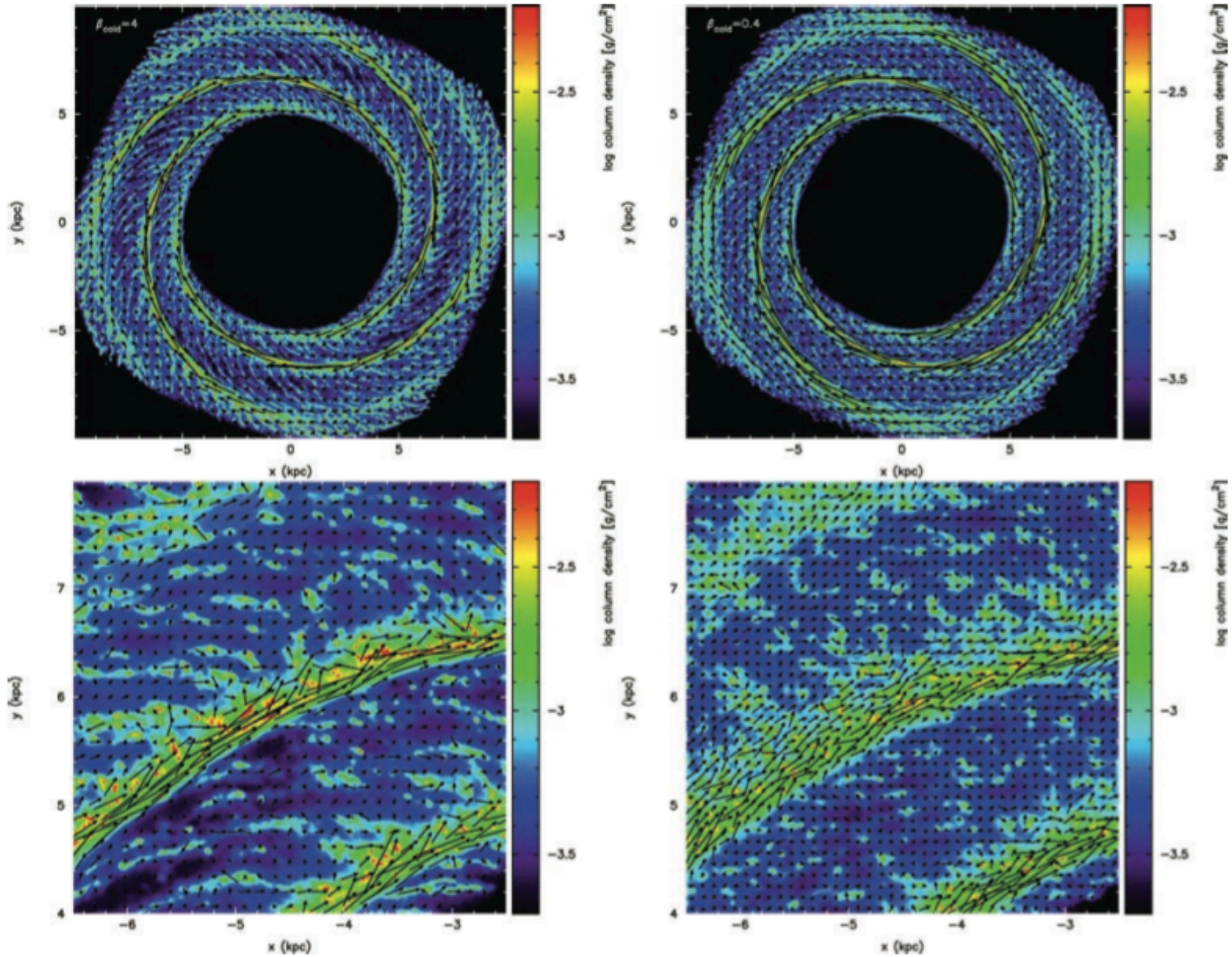

Figure 9. The column density is shown for the two-phase simulations after 250 Myr, for the whole disc (top panel) and a 4 × 4 kpc subsection (bottom panel). The left-hand panels show the case where $\beta_{\rm cold} = 4$ and the right-hand panels where $\beta_{\rm cold} = 0.4$. Both the cold and warm phases are shown in the plots, but we show them separately for the case where $\beta_{\rm cold} = 4$ in Fig. 12. There is more structure in the cold gas when the magnetic field is weaker ($\beta_{\rm cold} = 4$). The vectors show the magnetic field smoothed over a particular grid size. There is more detailed structure on smaller scales, particularly in the spiral arms which are better resolved.

obbs & Price (2008), Shetty & Ostriker (2007, 2008) modeling

chemistry

experimental set-up

6 ray approximation to
external radiation field

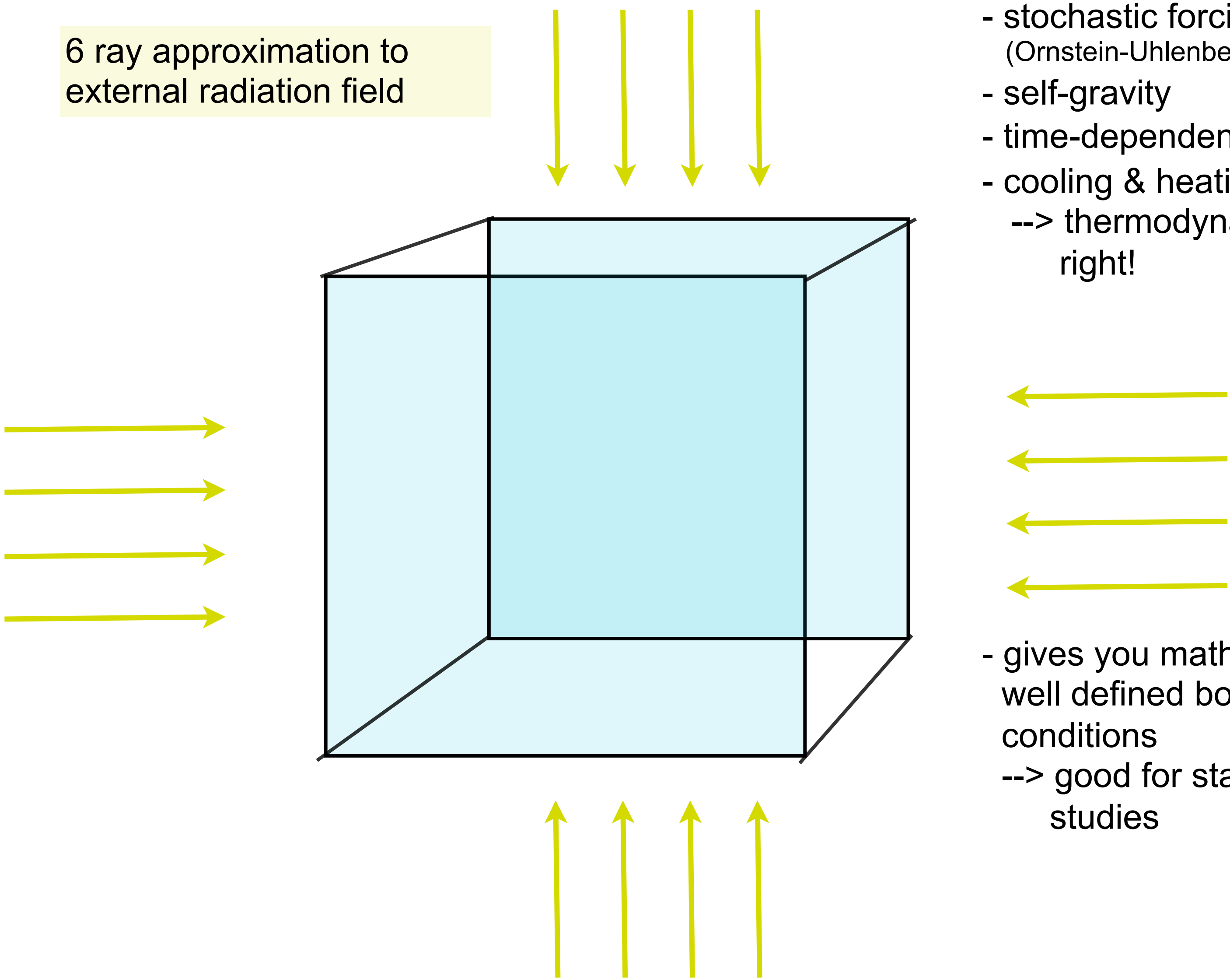

- AMR MHD (B = 2 muG)
- stochastic forcing
  (Ornstein-Uhlenbeck)
- self-gravity
- time-dependent chemistry
- cooling & heating processes
  --> thermodynamics done right!

- gives you mathematically well defined boundary conditions
  --> good for statistical studies

chemical model 0

- 32 chemical species
  - 17 in instantaneous equilibrium:

H^-, H_2^+, H_3^+, CH^+, CH_2^+, OH^+, H_2O^+, H_3O^+, CO^+, HOC^+, O^-, C^- and O_2^+

  - 19 full non-equilibrium evolution

e^-, H^+, H, H_2, He, He^+, C, C^+, O, O^+, OH, H_2O, CO,

C_2, O_2, HCO^+, CH, CH_2 and CH_3^+

- 218 reactions
- various heating and cooling processes

(Glover, Federrath, Mac Low, Klessen, 2010, MNRS, 404, 2)

chemical model 1

Process	Reference(s)
Cooling:	
C fine structure lines	Atomic data – Silva & Viegas (2002)
	Collisional rates (H) – Abrahamsson, Krems & Dalgarno (2007)
	Collisional rates (H_2) – Schroder et al. (1991)
	Collisional rates (e^-) – Johnson et al. (1987)
	Collisional rates (H^+) – Roueff & Le Bourlot (1990)
C^+ fine structure lines	Atomic data – Silva & Viegas (2002)
	Collisional rates (H_2) – Flower & Launay (1977)
	Collisional rates (H, $T < 2000$ K) – Hollenbach & McKee (1989)
	Collisional rates (H, $T > 2000$ K) – Keenan et al. (1986)
	Collisional rates (e^-) – Wilson & Bell (2002)
O fine structure lines	Atomic data – Silva & Viegas (2002)
	Collisional rates (H) – Abrahamsson, Krems & Dalgarno (2007)
	Collisional rates (H_2) – see Glover & Jappsen (2007)
	Collisional rates (e^-) – Bell, Berrington & Thomas (1998)
	Collisional rates (H^+) – Pequignot (1990, 1996)
H_2 rovibrational lines	Le Bourlot, Pineau des Forêts & Flower (1999)
CO and H_2O rovibrational lines	Neufeld & Kaufman (1993); Neufeld, Lepp & Melnick (1995)
OH rotational lines	Pavlovski et al. (2002)
Gas-grain energy transfer	Hollenbach & McKee (1989)
Recombination on grains	Wolfire et al. (2003)
Atomic resonance lines	Sutherland & Dopita (1993)
H collisional ionization	Abel et al. (1997)
H_2 collisional dissociation	See Table B1
Compton cooling	Cen (1992)
Heating:	
Photoelectric effect	Bakes & Tielens (1994); Wolfire et al. (2003)
H_2 photodissociation	Black & Dalgarno (1977)
UV pumping of H_2	Burton, Hollenbach & Tielens (1990)
H_2 formation on dust grains	Hollenbach & McKee (1989)
Cosmic ray ionization	Goldsmith & Langer (1978)

(Glover, Federrath, Mac Low, Klessen, 2010, MNRS, 404, 2)

chemical model 2

Table B1. List of collisional gas-phase reactions included in our chemical model

No.	Reaction	Rate coefficient (cm^3 s^{-1})	Notes	Ref.
1	$H + e^- \rightarrow H^- + \gamma$	$k_1 = \mathrm{dex}[-17.845 + 0.762 \log T + 0.1523(\log T)^2 - 0.03274(\log T)^3]$	$T \leqslant 6000$ K	1
		$= \mathrm{dex}[-16.420 + 0.1998(\log T)^2 - 5.447 \times 10^{-3}(\log T)^4 + 4.0415 \times 10^{-5}(\log T)^6]$	$T > 6000$ K	
2	$H^- + H \rightarrow H_2 + e^-$	$k_2 = 1.5 \times 10^{-9}$	$T \leqslant 300$ K	2
		$= 4.0 \times 10^{-9} T^{-0.17}$	$T > 300$ K	
3	$H + H^+ \rightarrow H_2^+ + \gamma$	$k_3 = \mathrm{dex}[-19.38 - 1.523 \log T + 1.118(\log T)^2 - 0.1269(\log T)^3]$		3
4	$H + H_2^+ \rightarrow H_2 + H^+$	$k_4 = 6.4 \times 10^{-10}$		4
5	$H^- + H^+ \rightarrow H + H$	$k_5 = 2.4 \times 10^{-6} T^{-1/2}(1.0 + T/20000)$		5
6	$H_2^+ + e^- \rightarrow H + H$	$k_6 = 1.0 \times 10^{-8}$	$T \leqslant 617$ K	6
		$= 1.32 \times 10^{-6} T^{-0.76}$	$T > 617$ K	
7	$H_2 + H^+ \rightarrow H_2^+ + H$	$k_7 = [-3.3232183 \times 10^{-7} + 3.3735382 \times 10^{-7} \ln T - 1.4491368 \times 10^{-7}(\ln T)^2 + 3.4172805 \times 10^{-8}(\ln T)^3 - 4.7813720 \times 10^{-9}(\ln T)^4 + 3.9731542 \times 10^{-10}(\ln T)^5 - 1.8171411 \times 10^{-11}(\ln T)^6 + 3.5311932 \times 10^{-13}(\ln T)^7] \times \exp\left(\frac{-21237.15}{T}\right)$		7
8	$H_2 + e^- \rightarrow H + H + e^-$	$k_8 = 3.73 \times 10^{-9} T^{0.1121} \exp\left(\frac{-99430}{T}\right)$		8
9	$H_2 + H \rightarrow H + H + H$	$k_{9,l} = 6.67 \times 10^{-12} T^{1/2} \exp\left[-(1 + \frac{63590}{T})\right]$		9
		$k_{9,h} = 3.52 \times 10^{-9} \exp\left(-\frac{43900}{T}\right)$		10
		$n_{cr,H} = \mathrm{dex}\left[3.0 - 0.416 \log\left(\frac{T}{10000}\right) - 0.327\left\{\log\left(\frac{T}{10000}\right)\right\}^2\right]$		10
10	$H_2 + H_2 \rightarrow H_2 + H + H$	$k_{10,l} = \frac{5.996 \times 10^{-30} T^{4.1881}}{(1.0 + 6.761 \times 10^{-6} T)^{5.6881}} \exp\left(-\frac{54657.4}{T}\right)$		11
		$k_{10,h} = 1.3 \times 10^{-9} \exp\left(-\frac{53300}{T}\right)$		12
		$n_{cr,H_2} = \mathrm{dex}\left[4.845 - 1.3 \log\left(\frac{T}{10000}\right) + 1.62\left\{\log\left(\frac{T}{10000}\right)\right\}^2\right]$		12
11	$H + e^- \rightarrow H^+ + e^- + e^-$	$k_{11} = \exp[-3.271396786 \times 10^1 + 1.35365560 \times 10^1 \ln T_e - 5.73932875 \times 10^0(\ln T_e)^2 + 1.56315498 \times 10^0(\ln T_e)^3 - 2.87705600 \times 10^{-1}(\ln T_e)^4 + 3.48255977 \times 10^{-2}(\ln T_e)^5 - 2.63197617 \times 10^{-3}(\ln T_e)^6 + 1.11954395 \times 10^{-4}(\ln T_e)^7 - 2.03914985 \times 10^{-6}(\ln T_e)^8]$		13
12	$H^+ + e^- \rightarrow H + \gamma$	$k_{12,A} = 1.269 \times 10^{-13}\left(\frac{315614}{T}\right)^{1.503} \times \left[1.0 + \left(\frac{604625}{T}\right)^{0.470}\right]^{-1.923}$	Case A	14
		$k_{12,B} = 2.753 \times 10^{-14}\left(\frac{315614}{T}\right)^{1.500} \times \left[1.0 + \left(\frac{115188}{T}\right)^{0.407}\right]^{-2.242}$	Case B	14
13	$H^- + e^- \rightarrow H + e^- + e^-$	$k_{13} = \exp[-1.801849334 \times 10^1 + 2.36085220 \times 10^0 \ln T_e - 2.82744300 \times 10^{-1}(\ln T_e)^2 + 1.62331664 \times 10^{-2}(\ln T_e)^3 - 3.36501203 \times 10^{-2}(\ln T_e)^4 + 1.17832978 \times 10^{-2}(\ln T_e)^5 - 1.65619470 \times 10^{-3}(\ln T_e)^6 + 1.06827520 \times 10^{-4}(\ln T_e)^7 - 2.63128581 \times 10^{-6}(\ln T_e)^8]$		13

(Glover, Federrath, Mac Low, Klessen, 2010, MNRS, 404, 2)

chemical model 2

(Glover, Federrath, Mac Low, Klessen, 2010, MNRS, 404, 2)

Table B1. I

No.	Rea
1	H +
2	H^-
3	H +
4	H +
5	H^-
6	H_2^+
7	H_2
8	H_2
9	H_2
10	H_2
11	H +
12	H^+
13	H^-

14	$H^- + H \rightarrow H + H + e^-$	$k_{14} = 2.5634 \times 10^{-9} T_e^{1.78186}$ $= \exp[-2.0372609 \times 10^1$ $+ 1.13944933 \times 10^0 \ln T_e$ $- 1.4210135 \times 10^{-1} (\ln T_e)^2$ $+ 8.4644554 \times 10^{-3} (\ln T_e)^3$ $- 1.$[illegible]$7641 \times 10^{-3} (\ln T_e)^4$ $+ 2.$[illegible]$ \times 10^{-4} (\ln T_e)^5$ $+ 8.6639632 \times 10^{-5} (\ln T_e)^6$ $- 2.5850097 \times 10^{-5} (\ln T_e)^7$ $+ 2.4555012 \times 10^{-6} (\ln T_e)^8$ $- 8.0683825 \times 10^{-8} (\ln T_e)^9]$	$T_e \leqslant 0.1$ eV $T_e > 0.1$ eV	13
15	$H^- + H^+ \rightarrow H_2^+ + e^-$	$k_{15} = 6.9 \times 10^{-9} T^{-0.35}$ $= 9.6 \times 10^{-7} T^{-0.90}$	$T \leqslant 8000$ K $T > 8000$ K	15
16	$He + e^- \rightarrow He^+ + e^- + e^-$	$k_{16} = \exp[-4.409864886 \times 10^1$ $+ 2.391596563 \times 10^1 \ln T_e$ $- 1.07532302 \times 10^1 (\ln T_e)^2$ $+ 3.05803875 \times 10^0 (\ln T_e)^3$ $- 5.6851189 \times 10^{-1} (\ln T_e)^4$ $+ 6.79539123 \times 10^{-2} (\ln T_e)^5$ $- 5.0090561 \times 10^{-3} (\ln T_e)^6$ $+ 2.06723616 \times 10^{-4} (\ln T_e)^7$ $- 3.64916141 \times 10^{-6} (\ln T_e)^8]$		13
17	$He^+ + e^- \rightarrow He + \gamma$	$k_{17,\mathrm{rr,A}} = 10^{-11} T^{-0.5} [12.72 - 1.615 \log T$ $- 0.3162 (\log T)^2 + 0.0493 (\log T)^3]$ $k_{17,\mathrm{rr,B}} = 10^{-11} T^{-0.5} [11.19 - 1.676 \log T$ $- 0.2852 (\log T)^2 + 0.04433 (\log T)^3]$ $k_{17,\mathrm{di}} = 1.9 \times 10^{-3} T^{-1.5} \exp\left(-\frac{473421}{T}\right)$ $\times \left[1.0 + 0.3 \exp\left(-\frac{94684}{T}\right)\right]$	Case A Case B	16 16 17
18	$He^+ + H \rightarrow He + H^+$	$k_{18} = 1.25 \times 10^{-15} \left(\frac{T}{300}\right)^{0.25}$		18
19	$He + H^+ \rightarrow He^+ + H$	$k_{19} = 1.26 \times 10^{-9} T^{-0.75} \exp\left(-\frac{127500}{T}\right)$ $= 4.0 \times 10^{-37} T^{4.74}$	$T \leqslant 10000$ K $T > 10000$ K	19
20	$C^+ + e^- \rightarrow C + \gamma$	$k_{20} = 4.67 \times 10^{-12} \left(\frac{T}{300}\right)^{-0.6}$ $= 1.23 \times 10^{-17} \left(\frac{T}{300}\right)^{2.49} \exp\left(\frac{21845.6}{T}\right)$ $= 9.62 \times 10^{-8} \left(\frac{T}{300}\right)^{-1.37} \exp\left(\frac{-115786.2}{T}\right)$	$T \leqslant 7950$ K $7950\ \mathrm{K} < T \leqslant 21140$ K $T > 21140$ K	20
21	$O^+ + e^- \rightarrow O + \gamma$	$k_{21} = 1.30 \times 10^{-10} T^{-0.64}$ $= 1.41 \times 10^{-10} T^{-0.66} + 7.4 \times 10^{-4} T^{-1.5}$ $\times \exp\left(-\frac{175000}{T}\right) [1.0 + 0.062 \times \exp\left(-\frac{145000}{T}\right)]$	$T \leqslant 400$ K $T > 400$ K	21
22	$C + e^- \rightarrow C^+ + e^- + e^-$	$k_{22} = 6.85 \times 10^{-8} (0.193 + u)^{-1} u^{0.25} e^{-u}$	$u = 11.26/T_e$	22
23	$O + e^- \rightarrow O^+ + e^- + e^-$	$k_{23} = 3.59 \times 10^{-8} (0.073 + u)^{-1} u^{0.34} e^{-u}$	$u = 13.6/T_e$	22
24	$O^+ + H \rightarrow O + H^+$	$k_{24} = 4.99 \times 10^{-11} T^{0.405} + 7.54 \times 10^{-10} T^{-0.458}$		23
25	$O + H^+ \rightarrow O^+ + H$	$k_{25} = [1.08 \times 10^{-11} T^{0.517}$ $+ 4.00 \times 10^{-10} T^{0.00669}] \exp\left(-\frac{227}{T}\right)$		24
26	$O + He^+ \rightarrow O^+ + He$	$k_{26} = 4.991 \times 10^{-15} \left(\frac{T}{10000}\right)^{0.3794} \exp\left(-\frac{T}{1121000}\right)$ $+ 2.780 \times 10^{-15} \left(\frac{T}{10000}\right)^{-0.2163} \exp\left(\frac{T}{815800}\right)$		25
27	$C + H^+ \rightarrow C^+ + H$	$k_{27} = 3.9 \times 10^{-16} T^{0.213}$		24
28	$C^+ + H \rightarrow C + H^+$	$k_{28} = 6.08 \times 10^{-14} \left(\frac{T}{10000}\right)^{1.96} \exp\left(-\frac{170000}{T}\right)$		24
29	$C + He^+ \rightarrow C^+ + He$	$k_{29} = 8.58 \times 10^{-17} T^{0.757}$ $= 3.25 \times 10^{-17} T^{0.968}$ $= 2.77 \times 10^{-19} T^{1.597}$	$T \leqslant 200$ K $200 < T \leqslant 2000$ K $T > 2000$ K	26
30	$H_2 + He \rightarrow H + H + He$	$k_{30,\mathrm{l}} = \mathrm{dex}[-27.029 + 3.801 \log(T) - 29487/T]$ $k_{30,\mathrm{h}} = \mathrm{dex}[-2.729 - 1.75 \log(T) - 23474/T]$ $n_{\mathrm{cr,He}} = \mathrm{dex}\left[5.0792(1.0 - 1.23 \times 10^{-5}(T - 2000)\right]$		27 27
31	$OH + H \rightarrow O + H + H$	$k_{31} = 6.0 \times 10^{-9} \exp\left(-\frac{50900}{T}\right)$		28
32	$HOC^+ + H_2 \rightarrow HCO^+ + H_2$	$k_{32} = 3.8 \times 10^{-10}$		29
33	$HOC^+ + CO \rightarrow HCO^+ + CO$	$k_{33} = 4.0 \times 10^{-10}$		30
34	$C + H_2 \rightarrow CH + H$	$k_{34} = 6.64 \times 10^{-10} \exp\left(-\frac{11700}{T}\right)$		31
35	$CH + H \rightarrow C + H_2$	$k_{35} = 1.31 \times 10^{-10} \exp\left(-\frac{80}{T}\right)$		32

chemical model 2

Table B1.

14	$H^- + H \rightarrow H + H + e^-$	$k_{14} = 2.5634 \times 10^{-9} T_e^{1.78186}$	$T_e \leqslant 0.1$ eV	13

36	$CH + H_2 \rightarrow CH_2 + H$	$k_{36} = 5.46 \times 10^{-10} \exp\left(-\frac{1943}{T}\right)$		33
37	$CH + C \rightarrow C_2 + H$	$k_{37} = 6.59 \times 10^{-11}$		34
38	$CH + O \rightarrow CO + H$	$k_{38} = 6.6 \times 10^{-11}$	$T \leqslant 2000$ K	35
		$= 1.02 \times 10^{-10} \exp\left(-\frac{[illegible]}{T}\right)$	$T > 2000$ K	36
39	[illegible] $\rightarrow CH + H_2$	$k_{39} =$ [illegible] $\times 10^{-11}$		37
40	$CH_2 + O \rightarrow CO + H + H$	$k_{40} = 1.33 \times 10^{-10}$		38
41	$CH_2 + O \rightarrow CO + H_2$	$k_{41} = 8.0 \times 10^{-11}$		39
42	$C_2 + O \rightarrow CO + C$	$k_{42} = 5.0 \times 10^{-11} \left(\frac{T}{300}\right)^{0.5}$	$T \leqslant 300$ K	40
		$= 5.0 \times 10^{-11} \left(\frac{T}{300}\right)^{0.757}$	$T > 300$ K	41
43	$O + H_2 \rightarrow OH + H$	$k_{43} = 3.14 \times 10^{-13} \left(\frac{T}{300}\right)^{2.7} \exp\left(-\frac{3150}{T}\right)$		42
44	$OH + H \rightarrow O + H_2$	$k_{44} = 6.99 \times 10^{-14} \left(\frac{T}{300}\right)^{2.8} \exp\left(-\frac{1950}{T}\right)$		43
45	$OH + H_2 \rightarrow H_2O + H$	$k_{45} = 2.05 \times 10^{-12} \left(\frac{T}{300}\right)^{1.52} \exp\left(-\frac{1736}{T}\right)$		44
46	$OH + C \rightarrow CO + H$	$k_{46} = 1.0 \times 10^{-10}$		34
47	$OH + O \rightarrow O_2 + H$	$k_{47} = 3.50 \times 10^{-11}$	$T \leqslant 261$ K	45
		$= 1.77 \times 10^{-11} \exp\left(\frac{178}{T}\right)$	$T > 261$ K	33
48	$OH + OH \rightarrow H_2O + H$	$k_{48} = 1.65 \times 10^{-12} \left(\frac{T}{300}\right)^{1.14} \exp\left(-\frac{50}{T}\right)$		34
49	$H_2O + H \rightarrow H_2 + OH$	$k_{49} = 1.59 \times 10^{-11} \left(\frac{T}{300}\right)^{1.2} \exp\left(-\frac{9610}{T}\right)$		46
50	$O_2 + H \rightarrow OH + O$	$k_{50} = 2.61 \times 10^{-10} \exp\left(-\frac{8156}{T}\right)$		33
51	$O_2 + H_2 \rightarrow OH + OH$	$k_{51} = 3.16 \times 10^{-10} \exp\left(-\frac{21890}{T}\right)$		47
52	$O_2 + C \rightarrow CO + O$	$k_{52} = 4.7 \times 10^{-11} \left(\frac{T}{300}\right)^{-0.34}$	$T \leqslant 295$ K	34
		$= 2.48 \times 10^{-12} \left(\frac{T}{300}\right)^{1.54} \exp\left(\frac{613}{T}\right)$	$T > 295$ K	33
53	$CO + H \rightarrow C + OH$	$k_{53} = 1.1 \times 10^{-10} \left(\frac{T}{300}\right)^{0.5} \exp\left(-\frac{77700}{T}\right)$		28
54	$H_2^+ + H_2 \rightarrow H_3^+ + H$	$k_{54} = 2.24 \times 10^{-9} \left(\frac{T}{300}\right)^{0.042} \exp\left(-\frac{T}{46600}\right)$		48
55	$H_3^+ + H \rightarrow H_2^+ + H_2$	$k_{55} = 7.7 \times 10^{-9} \exp\left(-\frac{17560}{T}\right)$		49
56	$C + H_2^+ \rightarrow CH^+ + H$	$k_{56} = 2.4 \times 10^{-9}$		28
57	$C + H_3^+ \rightarrow CH^+ + H_2$	$k_{57} = 2.0 \times 10^{-9}$		28
58	$C^+ + H_2 \rightarrow CH^+ + H$	$k_{58} = 1.0 \times 10^{-10} \exp\left(-\frac{4640}{T}\right)$		50
59	$CH^+ + H \rightarrow C^+ + H_2$	$k_{59} = 7.5 \times 10^{-10}$		51
60	$CH^+ + H_2 \rightarrow CH_2^+ + H$	$k_{60} = 1.2 \times 10^{-9}$		51
61	$CH^+ + O \rightarrow CO^+ + H$	$k_{61} = 3.5 \times 10^{-10}$		52
62	$CH_2 + H^+ \rightarrow CH^+ + H_2$	$k_{62} = 1.4 \times 10^{-9}$		28
63	$CH_2^+ + H \rightarrow CH^+ + H_2$	$k_{63} = 1.0 \times 10^{-9} \exp\left(-\frac{7080}{T}\right)$		28
64	$CH_2^+ + H_2 \rightarrow CH_3^+ + H$	$k_{64} = 1.6 \times 10^{-9}$		53
65	$CH_2^+ + O \rightarrow HCO^+ + H$	$k_{65} = 7.5 \times 10^{-10}$		28
66	$CH_3^+ + H \rightarrow CH_2^+ + H_2$	$k_{66} = 7.0 \times 10^{-10} \exp\left(-\frac{10560}{T}\right)$		28
67	$CH_3^+ + O \rightarrow HCO^+ + H_2$	$k_{67} = 4.0 \times 10^{-10}$		54
68	$C_2 + O^+ \rightarrow CO^+ + C$	$k_{68} = 4.8 \times 10^{-10}$		28
69	$O^+ + H_2 \rightarrow OH^+ + H$	$k_{69} = 1.7 \times 10^{-9}$		55
70	$O + H_2^+ \rightarrow OH^+ + H$	$k_{70} = 1.5 \times 10^{-9}$		28
71	$O + H_3^+ \rightarrow OH^+ + H_2$	$k_{71} = 8.4 \times 10^{-10}$		56
72	$OH + H_3^+ \rightarrow H_2O^+ + H_2$	$k_{72} = 1.3 \times 10^{-9}$		28
73	$OH + C^+ \rightarrow CO^+ + H$	$k_{73} = 7.7 \times 10^{-10}$		28
74	$OH^+ + H_2 \rightarrow H_2O^+ + H$	$k_{74} = 1.01 \times 10^{-9}$		57
75	$H_2O^+ + H_2 \rightarrow H_3O^+ + H$	$k_{75} = 6.4 \times 10^{-10}$		58
76	$H_2O + H_3^+ \rightarrow H_3O^+ + H_2$	$k_{76} = 5.9 \times 10^{-9}$		59
77	$H_2O + C^+ \rightarrow HCO^+ + H$	$k_{77} = 9.0 \times 10^{-10}$		60
78	$H_2O + C^+ \rightarrow HOC^+ + H$	$k_{78} = 1.8 \times 10^{-9}$		60
79	$H_3O^+ + C \rightarrow HCO^+ + H_2$	$k_{79} = 1.0 \times 10^{-11}$		28
80	$O_2 + C^+ \rightarrow CO^+ + O$	$k_{80} = 3.8 \times 10^{-10}$		53
81	$O_2 + C^+ \rightarrow CO + O^+$	$k_{81} = 6.2 \times 10^{-10}$		53
82	$O_2 + CH_2^+ \rightarrow HCO^+ + OH$	$k_{82} = 9.1 \times 10^{-10}$		53
83	$O_2^+ + C \rightarrow CO^+ + O$	$k_{83} = 5.2 \times 10^{-11}$		28
84	$CO + H_3^+ \rightarrow HOC^+ + H_2$	$k_{84} = 2.7 \times 10^{-11}$		61
85	$CO + H_3^+ \rightarrow HCO^+ + H_2$	$k_{85} = 1.7 \times 10^{-9}$		61
86	$HCO^+ + C \rightarrow CO + CH^+$	$k_{86} = 1.1 \times 10^{-9}$		28
87	$HCO^+ + H_2O \rightarrow CO + H_3O^+$	$k_{87} = 2.5 \times 10^{-9}$		62

(Glover, Federrath, Mac Low, Klessen, 2010, MNRS, 404, 2)

chemical model 2

(Glover, Federrath, Mac Low, Klessen, 2010, MNRS, 404, 2)

88	$H_2 + He^+ \to He + H_2^+$	$k_{88} = 7.2 \times 10^{-15}$	63
89	$H_2 + He^+ \to He + H + H^+$	$k_{89} = 3.7 \times 10^{-14} \exp\left(\frac{35}{T}\right)$	63
90	$CH + H^+ \to CH^+ + H$	$k_{90} = 1.9 \times 10^{-9}$	28
91	$CH_2 + H^+ \to CH_2^+ + H$	$k_{91} = 1.4 \times 10^{-9}$	28
92	$CH_2 + He^+ \to C^+ + He + H_2$	[illegible]	28
93	$C_2 + He^+ \to C^+ + C + He$	$k_{93} = 1.6 \times 10^{-9}$	28
94	$OH + H^+ \to OH^+ + H$	$k_{94} = 2.1 \times 10^{-9}$	28
95	$OH + He^+ \to O^+ + He + H$	$k_{95} = 1.1 \times 10^{-9}$	28
96	$H_2O + H^+ \to H_2O^+ + H$	$k_{96} = 6.9 \times 10^{-9}$	64
97	$H_2O + He^+ \to OH + He + H^+$	$k_{97} = 2.04 \times 10^{-10}$	65
98	$H_2O + He^+ \to OH^+ + He + H$	$k_{98} = 2.86 \times 10^{-10}$	65
99	$H_2O + He^+ \to H_2O^+ + He$	$k_{99} = 6.05 \times 10^{-11}$	65
100	$O_2 + H^+ \to O_2^+ + H$	$k_{100} = 2.0 \times 10^{-9}$	64
101	$O_2 + He^+ \to O_2^+ + He$	$k_{101} = 3.3 \times 10^{-11}$	66
102	$O_2 + He^+ \to O^+ + O + He$	$k_{102} = 1.1 \times 10^{-9}$	66
103	$O_2^+ + C \to O_2 + C^+$	$k_{103} = 5.2 \times 10^{-11}$	28
104	$CO + He^+ \to C^+ + O + He$	$k_{104} = 1.4 \times 10^{-9} \left(\frac{T}{300}\right)^{-0.5}$	67
105	$CO + He^+ \to C + O^+ + He$	$k_{105} = 1.4 \times 10^{-16} \left(\frac{T}{300}\right)^{-0.5}$	67
106	$CO^+ + H \to CO + H^+$	$k_{106} = 7.5 \times 10^{-10}$	68
107	$C^- + H^+ \to C + H$	$k_{107} = 2.3 \times 10^{-7} \left(\frac{T}{300}\right)^{-0.5}$	28
108	$O^- + H^+ \to O + H$	$k_{108} = 2.3 \times 10^{-7} \left(\frac{T}{300}\right)^{-0.5}$	28
109	$He^+ + H^- \to He + H$	$k_{109} = 2.32 \times 10^{-7} \left(\frac{T}{300}\right)^{-0.52} \exp\left(\frac{T}{22400}\right)$	69
110	$H_3^+ + e^- \to H_2 + H$	$k_{110} = 2.34 \times 10^{-8} \left(\frac{T}{300}\right)^{-0.52}$	70
111	$H_3^+ + e^- \to H + H + H$	$k_{111} = 4.36 \times 10^{-8} \left(\frac{T}{300}\right)^{-0.52}$	70
112	$CH^+ + e^- \to C + H$	$k_{112} = 7.0 \times 10^{-8} \left(\frac{T}{300}\right)^{-0.5}$	71
113	$CH_2^+ + e^- \to CH + H$	$k_{113} = 1.6 \times 10^{-7} \left(\frac{T}{300}\right)^{-0.6}$	72
114	$CH_2^+ + e^- \to C + H + H$	$k_{114} = 4.03 \times 10^{-7} \left(\frac{T}{300}\right)^{-0.6}$	72
115	$CH_2^+ + e^- \to C + H_2$	$k_{115} = 7.68 \times 10^{-8} \left(\frac{T}{300}\right)^{-0.6}$	72
116	$CH_3^+ + e^- \to CH_2 + H$	$k_{116} = 7.75 \times 10^{-8} \left(\frac{T}{300}\right)^{-0.5}$	73
117	$CH_3^+ + e^- \to CH + H_2$	$k_{117} = 1.95 \times 10^{-7} \left(\frac{T}{300}\right)^{-0.5}$	73
118	$CH_3^+ + e^- \to CH + H + H$	$k_{118} = 2.0 \times 10^{-7} \left(\frac{T}{300}\right)^{-0.4}$	28
119	$OH^+ + e^- \to O + H$	$k_{119} = 6.3 \times 10^{-9} \left(\frac{T}{300}\right)^{-0.48}$	74
120	$H_2O^+ + e^- \to O + H + H$	$k_{120} = 3.05 \times 10^{-7} \left(\frac{T}{300}\right)^{-0.5}$	75
121	$H_2O^+ + e^- \to O + H_2$	$k_{121} = 3.9 \times 10^{-8} \left(\frac{T}{300}\right)^{-0.5}$	75
122	$H_2O^+ + e^- \to OH + H$	$k_{122} = 8.6 \times 10^{-8} \left(\frac{T}{300}\right)^{-0.5}$	75
123	$H_3O^+ + e^- \to H + H_2O$	$k_{123} = 1.08 \times 10^{-7} \left(\frac{T}{300}\right)^{-0.5}$	76
124	$H_3O^+ + e^- \to OH + H_2$	$k_{124} = 6.02 \times 10^{-8} \left(\frac{T}{300}\right)^{-0.5}$	76
125	$H_3O^+ + e^- \to OH + H + H$	$k_{125} = 2.58 \times 10^{-7} \left(\frac{T}{300}\right)^{-0.5}$	76
126	$H_3O^+ + e^- \to O + H + H_2$	$k_{126} = 5.6 \times 10^{-9} \left(\frac{T}{300}\right)^{-0.5}$	76
127	$O_2^+ + e^- \to O + O$	$k_{127} = 1.95 \times 10^{-7} \left(\frac{T}{300}\right)^{-0.7}$	77
128	$CO^+ + e^- \to C + O$	$k_{128} = 2.75 \times 10^{-7} \left(\frac{T}{300}\right)^{-0.55}$	78
129	$HCO^+ + e^- \to CO + H$	$k_{129} = 2.76 \times 10^{-7} \left(\frac{T}{300}\right)^{-0.64}$	79
130	$HCO^+ + e^- \to OH + C$	$k_{130} = 2.4 \times 10^{-8} \left(\frac{T}{300}\right)^{-0.64}$	79
131	$HOC^+ + e^- \to CO + H$	$k_{131} = 1.1 \times 10^{-7} \left(\frac{T}{300}\right)^{-1.0}$	28
132	$H^- + C \to CH + e^-$	$k_{132} = 1.0 \times 10^{-9}$	28
133	$H^- + O \to OH + e^-$	$k_{133} = 1.0 \times 10^{-9}$	28
134	$H^- + OH \to H_2O + e^-$	$k_{134} = 1.0 \times 10^{-10}$	28
135	$C^- + H \to CH + e^-$	$k_{135} = 5.0 \times 10^{-10}$	28
136	$C^- + H_2 \to CH_2 + e^-$	$k_{136} = 1.0 \times 10^{-13}$	28
137	$C^- + O \to CO + e^-$	$k_{137} = 5.0 \times 10^{-10}$	28
138	$O^- + H \to OH + e^-$	$k_{138} = 5.0 \times 10^{-10}$	28
139	$O^- + H_2 \to H_2O + e^-$	$k_{139} = 7.0 \times 10^{-10}$	28
140	$O^- + C \to CO + e^-$	$k_{140} = 5.0 \times 10^{-10}$	28

87	$HCO^+ + H_2O \to CO + H_3O^+$	$k_{87} = 2.5 \times 10^{-9}$	62

chemical model 2

(Glover, Federrath, Mac Low, Klessen, 2010, MNRS, 404, 2)

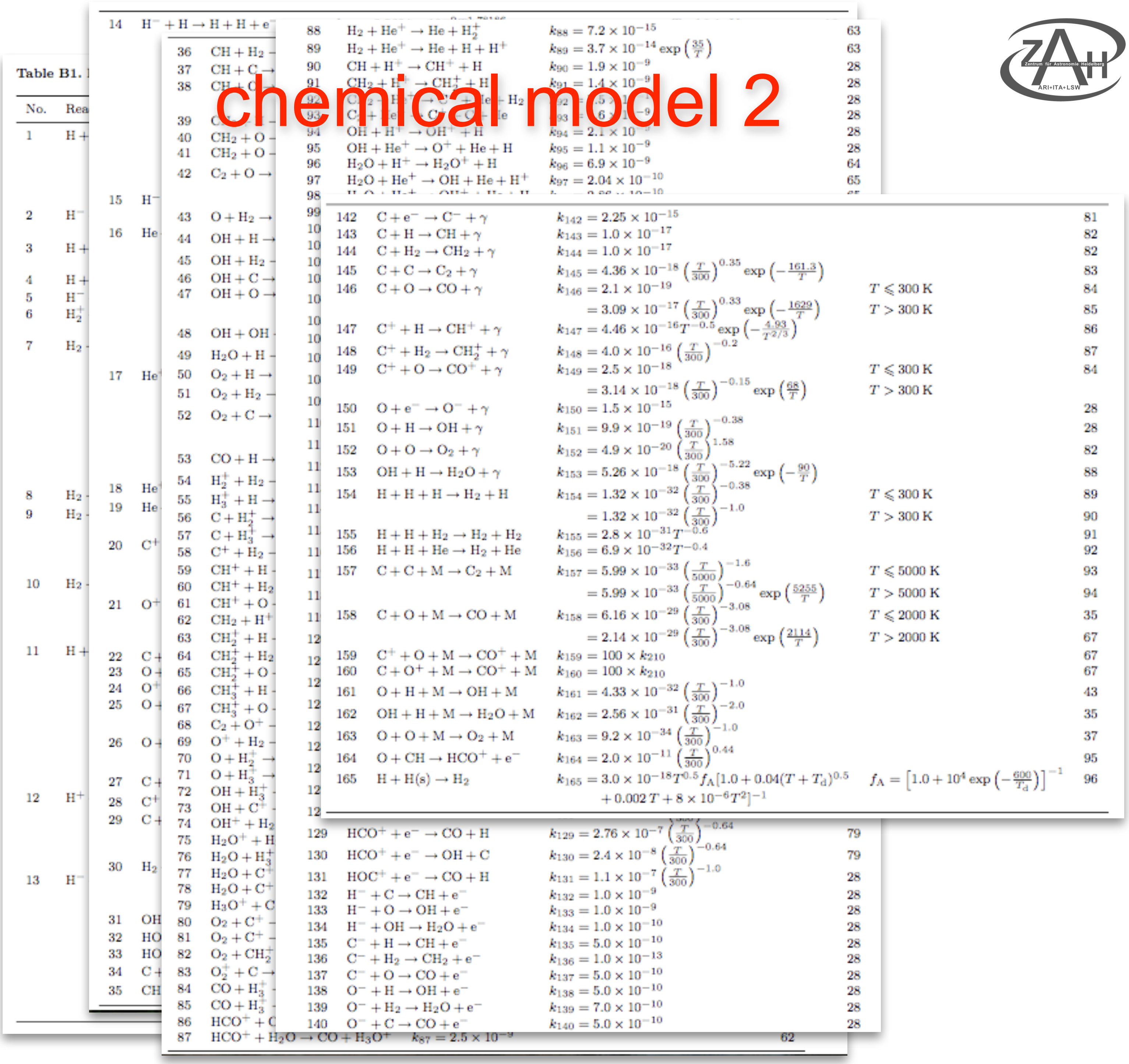

No.	Reaction	Rate coefficient		Ref.
88	$H_2 + He^+ \rightarrow He + H_2^+$	$k_{88} = 7.2 \times 10^{-15}$		63
89	$H_2 + He^+ \rightarrow He + H + H^+$	$k_{89} = 3.7 \times 10^{-14} \exp\left(\frac{35}{T}\right)$		63
90	$CH + H^+ \rightarrow CH^+ + H$	$k_{90} = 1.9 \times 10^{-9}$		28
91	$CH_2 + H^+ \rightarrow CH_2^+ + H$	$k_{91} = 1.4 \times 10^{-9}$		28
92	[illegible]	[illegible]		28
93	[illegible]	[illegible]		28
94	$OH + H^+ \rightarrow OH^+ + H$	$k_{94} = 2.1 \times 10^{-9}$		28
95	$OH + He^+ \rightarrow O^+ + He + H$	$k_{95} = 1.1 \times 10^{-9}$		28
96	$H_2O + H^+ \rightarrow H_2O^+ + H$	$k_{96} = 6.9 \times 10^{-9}$		64
97	$H_2O + He^+ \rightarrow OH + He + H^+$	$k_{97} = 2.04 \times 10^{-10}$		65

No.	Reaction	Rate coefficient		Ref.
142	$C + e^- \rightarrow C^- + \gamma$	$k_{142} = 2.25 \times 10^{-15}$		81
143	$C + H \rightarrow CH + \gamma$	$k_{143} = 1.0 \times 10^{-17}$		82
144	$C + H_2 \rightarrow CH_2 + \gamma$	$k_{144} = 1.0 \times 10^{-17}$		82
145	$C + C \rightarrow C_2 + \gamma$	$k_{145} = 4.36 \times 10^{-18} \left(\frac{T}{300}\right)^{0.35} \exp\left(-\frac{161.3}{T}\right)$		83
146	$C + O \rightarrow CO + \gamma$	$k_{146} = 2.1 \times 10^{-19}$	$T \leqslant 300$ K	84
		$= 3.09 \times 10^{-17} \left(\frac{T}{300}\right)^{0.33} \exp\left(-\frac{1629}{T}\right)$	$T > 300$ K	85
147	$C^+ + H \rightarrow CH^+ + \gamma$	$k_{147} = 4.46 \times 10^{-16} T^{-0.5} \exp\left(-\frac{4.93}{T^{2/3}}\right)$		86
148	$C^+ + H_2 \rightarrow CH_2^+ + \gamma$	$k_{148} = 4.0 \times 10^{-16} \left(\frac{T}{300}\right)^{-0.2}$		87
149	$C^+ + O \rightarrow CO^+ + \gamma$	$k_{149} = 2.5 \times 10^{-18}$	$T \leqslant 300$ K	84
		$= 3.14 \times 10^{-18} \left(\frac{T}{300}\right)^{-0.15} \exp\left(\frac{68}{T}\right)$	$T > 300$ K	84
150	$O + e^- \rightarrow O^- + \gamma$	$k_{150} = 1.5 \times 10^{-15}$		28
151	$O + H \rightarrow OH + \gamma$	$k_{151} = 9.9 \times 10^{-19} \left(\frac{T}{300}\right)^{-0.38}$		28
152	$O + O \rightarrow O_2 + \gamma$	$k_{152} = 4.9 \times 10^{-20} \left(\frac{T}{300}\right)^{1.58}$		82
153	$OH + H \rightarrow H_2O + \gamma$	$k_{153} = 5.26 \times 10^{-18} \left(\frac{T}{300}\right)^{-5.22} \exp\left(-\frac{90}{T}\right)$		88
154	$H + H + H \rightarrow H_2 + H$	$k_{154} = 1.32 \times 10^{-32} \left(\frac{T}{300}\right)^{-0.38}$	$T \leqslant 300$ K	89
		$= 1.32 \times 10^{-32} \left(\frac{T}{300}\right)^{-1.0}$	$T > 300$ K	90
155	$H + H + H_2 \rightarrow H_2 + H_2$	$k_{155} = 2.8 \times 10^{-31} T^{-0.6}$		91
156	$H + H + He \rightarrow H_2 + He$	$k_{156} = 6.9 \times 10^{-32} T^{-0.4}$		92
157	$C + C + M \rightarrow C_2 + M$	$k_{157} = 5.99 \times 10^{-33} \left(\frac{T}{5000}\right)^{-1.6}$	$T \leqslant 5000$ K	93
		$= 5.99 \times 10^{-33} \left(\frac{T}{5000}\right)^{-0.64} \exp\left(\frac{5255}{T}\right)$	$T > 5000$ K	94
158	$C + O + M \rightarrow CO + M$	$k_{158} = 6.16 \times 10^{-29} \left(\frac{T}{300}\right)^{-3.08}$	$T \leqslant 2000$ K	35
		$= 2.14 \times 10^{-29} \left(\frac{T}{300}\right)^{-3.08} \exp\left(\frac{2114}{T}\right)$	$T > 2000$ K	67
159	$C^+ + O + M \rightarrow CO^+ + M$	$k_{159} = 100 \times k_{210}$		67
160	$C + O^+ + M \rightarrow CO^+ + M$	$k_{160} = 100 \times k_{210}$		67
161	$O + H + M \rightarrow OH + M$	$k_{161} = 4.33 \times 10^{-32} \left(\frac{T}{300}\right)^{-1.0}$		43
162	$OH + H + M \rightarrow H_2O + M$	$k_{162} = 2.56 \times 10^{-31} \left(\frac{T}{300}\right)^{-2.0}$		35
163	$O + O + M \rightarrow O_2 + M$	$k_{163} = 9.2 \times 10^{-34} \left(\frac{T}{300}\right)^{-1.0}$		37
164	$O + CH \rightarrow HCO^+ + e^-$	$k_{164} = 2.0 \times 10^{-11} \left(\frac{T}{300}\right)^{0.44}$		95
165	$H + H(s) \rightarrow H_2$	$k_{165} = 3.0 \times 10^{-18} T^{0.5} f_A [1.0 + 0.04 (T + T_d)^{0.5} + 0.002\, T + 8 \times 10^{-6} T^2]^{-1}$	$f_A = \left[1.0 + 10^4 \exp\left(-\frac{600}{T_d}\right)\right]^{-1}$	96

No.	Reaction	Rate coefficient		Ref.
129	$HCO^+ + e^- \rightarrow CO + H$	$k_{129} = 2.76 \times 10^{-7} \left(\frac{T}{300}\right)^{-0.64}$		79
130	$HCO^+ + e^- \rightarrow OH + C$	$k_{130} = 2.4 \times 10^{-8} \left(\frac{T}{300}\right)^{-0.64}$		79
131	$HOC^+ + e^- \rightarrow CO + H$	$k_{131} = 1.1 \times 10^{-7} \left(\frac{T}{300}\right)^{-1.0}$		28
132	$H^- + C \rightarrow CH + e^-$	$k_{132} = 1.0 \times 10^{-9}$		28
133	$H^- + O \rightarrow OH + e^-$	$k_{133} = 1.0 \times 10^{-9}$		28
134	$H^- + OH \rightarrow H_2O + e^-$	$k_{134} = 1.0 \times 10^{-10}$		28
135	$C^- + H \rightarrow CH + e^-$	$k_{135} = 5.0 \times 10^{-10}$		28
136	$C^- + H_2 \rightarrow CH_2 + e^-$	$k_{136} = 1.0 \times 10^{-13}$		28
137	$C^- + O \rightarrow CO + e^-$	$k_{137} = 5.0 \times 10^{-10}$		28
138	$O^- + H \rightarrow OH + e^-$	$k_{138} = 5.0 \times 10^{-10}$		28
139	$O^- + H_2 \rightarrow H_2O + e^-$	$k_{139} = 7.0 \times 10^{-10}$		28
140	$O^- + C \rightarrow CO + e^-$	$k_{140} = 5.0 \times 10^{-10}$		28

chemical model 2

88	$H_2 + He^+ \rightarrow He + H_2^+$	$k_{88} = 7.2 \times 10^{-15}$	63
89	$H_2 + He^+ \rightarrow He + H + H^+$	$k_{89} = 3.7 \times 10^{-14} \exp\left(\frac{35}{T}\right)$	63
90	$CH + H^+ \rightarrow CH^+ + H$	$k_{90} = 1.9 \times 10^{-9}$	28
91	$CH_2 + H^+ \rightarrow CH_2^+ + H$	$k_{91} = 1.4 \times 10^{-9}$	28
94	$OH + H^+ \rightarrow OH^+ + H$	$k_{94} = 2.1 \times 10^{-9}$	28
95	$OH + He^+ \rightarrow O^+ + He + H$	$k_{95} = 1.1 \times 10^{-9}$	28
96	$H_2O + H^+ \rightarrow H_2O^+ + H$	$k_{96} = 6.9 \times 10^{-9}$	64
97	$H_2O + He^+ \rightarrow OH + He + H^+$	$k_{97} = 2.04 \times 10^{-10}$	65

Table B2. List of photochemical reactions included in our chemical model

No.	Reaction	Optically thin rate (s^{-1})	γ	Ref.
166	$H^- + \gamma \rightarrow H + e^-$	$R_{166} = 7.1 \times 10^{-7}$	0.5	1
167	$H_2^+ + \gamma \rightarrow H + H^+$	$R_{167} = 1.1 \times 10^{-9}$	1.9	2
168	$H_2 + \gamma \rightarrow H + H$	$R_{168} = 5.6 \times 10^{-11}$	See §2.2	3
169	$H_3^+ + \gamma \rightarrow H_2 + H^+$	$R_{169} = 4.9 \times 10^{-13}$	1.8	4
170	$H_3^+ + \gamma \rightarrow H_2^+ + H$	$R_{170} = 4.9 \times 10^{-13}$	2.3	4
171	$C + \gamma \rightarrow C^+ + e^-$	$R_{171} = 3.1 \times 10^{-10}$	3.0	5
172	$C^- + \gamma \rightarrow C + e^-$	$R_{172} = 2.4 \times 10^{-7}$	0.9	6
173	$CH + \gamma \rightarrow C + H$	$R_{173} = 8.7 \times 10^{-10}$	1.2	7
174	$CH + \gamma \rightarrow CH^+ + e^-$	$R_{174} = 7.7 \times 10^{-10}$	2.8	8
175	$CH^+ + \gamma \rightarrow C + H^+$	$R_{175} = 2.6 \times 10^{-10}$	2.5	7
176	$CH_2 + \gamma \rightarrow CH + H$	$R_{176} = 7.1 \times 10^{-10}$	1.7	7
177	$CH_2 + \gamma \rightarrow CH_2^+ + e^-$	$R_{177} = 5.9 \times 10^{-10}$	2.3	6
178	$CH_2^+ + \gamma \rightarrow CH^+ + H$	$R_{178} = 4.6 \times 10^{-10}$	1.7	9
179	$CH_3^+ + \gamma \rightarrow CH_2^+ + H$	$R_{179} = 1.0 \times 10^{-9}$	1.7	6
180	$CH_3^+ + \gamma \rightarrow CH^+ + H_2$	$R_{180} = 1.0 \times 10^{-9}$	1.7	6
181	$C_2 + \gamma \rightarrow C + C$	$R_{181} = 1.5 \times 10^{-10}$	2.1	7
182	$O^- + \gamma \rightarrow O + e^-$	$R_{182} = 2.4 \times 10^{-7}$	0.5	6
183	$OH + \gamma \rightarrow O + H$	$R_{183} = 3.7 \times 10^{-10}$	1.7	10
184	$OH + \gamma \rightarrow OH^+ + e^-$	$R_{184} = 1.6 \times 10^{-12}$	3.1	6
185	$OH^+ + \gamma \rightarrow O + H^+$	$R_{185} = 1.0 \times 10^{-12}$	1.8	4
186	$H_2O + \gamma \rightarrow OH + H$	$R_{186} = 6.0 \times 10^{-10}$	1.7	11
187	$H_2O + \gamma \rightarrow H_2O^+ + e^-$	$R_{187} = 3.2 \times 10^{-11}$	3.9	8
188	$H_2O^+ + \gamma \rightarrow H_2^+ + O$	$R_{188} = 5.0 \times 10^{-11}$	See §2.2	12
189	$H_2O^+ + \gamma \rightarrow H^+ + OH$	$R_{189} = 5.0 \times 10^{-11}$	See §2.2	12
190	$H_2O^+ + \gamma \rightarrow O^+ + H_2$	$R_{190} = 5.0 \times 10^{-11}$	See §2.2	12
191	$H_2O^+ + \gamma \rightarrow OH^+ + H$	$R_{191} = 1.5 \times 10^{-10}$	See §2.2	12
192	$H_3O^+ + \gamma \rightarrow H^+ + H_2O$	$R_{192} = 2.5 \times 10^{-11}$	See §2.2	12
193	$H_3O^+ + \gamma \rightarrow H_2^+ + OH$	$R_{193} = 2.5 \times 10^{-11}$	See §2.2	12
194	$H_3O^+ + \gamma \rightarrow H_2O^+ + H$	$R_{194} = 7.5 \times 10^{-12}$	See §2.2	12
195	$H_3O^+ + \gamma \rightarrow OH^+ + H_2$	$R_{195} = 2.5 \times 10^{-11}$	See §2.2	12
196	$O_2 + \gamma \rightarrow O_2^+ + e^-$	$R_{196} = 5.6 \times 10^{-11}$	3.7	7
197	$O_2 + \gamma \rightarrow O + O$	$R_{197} = 7.0 \times 10^{-10}$	1.8	7
198	$CO + \gamma \rightarrow C + O$	$R_{198} = 2.0 \times 10^{-10}$	See §2.2	13

(Glover, Federrath, Mac Low, Klessen, 2010, MNRS, 404, 2)

chemical model 2

88	$H_2 + He^+ \rightarrow He + H_2^+$	$k_{88} = 7.2 \times 10^{-15}$	63
89	$H_2 + He^+ \rightarrow He + H + H^+$	$k_{89} = 3.7 \times 10^{-14} \exp\left(\frac{35}{T}\right)$	63
90	$CH + H^+ \rightarrow CH^+ + H$	$k_{90} = 1.9 \times 10^{-9}$	28
91	$CH_2 + H^+ \rightarrow CH_2^+ + H$	$k_{91} = 1.4 \times 10^{-9}$	28
92	[illegible]	[illegible]	28
93	[illegible]	[illegible]	28
94	$OH + H^+ \rightarrow OH^+ + H$	$k_{94} = 2.1 \times 10^{-9}$	28
95	$OH + He^+ \rightarrow O^+ + He + H$	$k_{95} = 1.1 \times 10^{-9}$	28
96	$H_2O + H^+ \rightarrow H_2O^+ + H$	$k_{96} = 6.9 \times 10^{-9}$	64
97	$H_2O + He^+ \rightarrow OH + He + H^+$	$k_{97} = 2.04 \times 10^{-10}$	65

Table B2. List of photochemical reactions included in our chemical model

No.	Reaction	Optically thin rate (s^{-1})	γ	Ref.
166	$H^- + \gamma \rightarrow H + e^-$	$R_{166} = 7.1 \times 10^{-7}$	0.5	1
167	$H_2^+ + \gamma \rightarrow H + H^+$	$R_{167} = 1.1 \times 10^{-9}$	1.9	2
168	$H_2 + \gamma \rightarrow H + H$	$R_{168} = 5.6 \times 10^{-11}$	See §2.2	3
169	$H_3^+ + \gamma \rightarrow H_2 + H^+$	$R_{169} = 4.9 \times 10^{-13}$	1.8	4
170	$H_3^+ + \gamma \rightarrow H_2^+ + H$	$R_{170} = 4.9 \times 10^{-13}$	2.3	4
171	$C + \gamma \rightarrow C^+ + e^-$	[illegible]	[illegible]	[illegible]
172	$C^- + \gamma \rightarrow$ …			
173	$CH + \gamma \rightarrow$ …			
174	$CH + \gamma \rightarrow$ …			
175	$CH^+ + \gamma$ …			
176	$CH_2 + \gamma$ …			
177	$CH_2 + \gamma$ …			
178	$CH_2^+ + \gamma$ …			
179	$CH_3^+ + \gamma$ …			
180	$CH_3^+ + \gamma$ …			
181	$C_2 + \gamma \rightarrow$ …			
182	$O^- + \gamma \rightarrow$ …			
183	$OH + \gamma \rightarrow$ …			
184	$OH + \gamma \rightarrow$ …			
185	$OH^+ + \gamma$ …			
186	$H_2O + \gamma$ …			
187	$H_2O + \gamma$ …			
188	$H_2O^+ + \gamma$ …			
189	$H_2O^+ + \gamma$ …			
190	$H_2O^+ + \gamma$ …			
191	$H_2O^+ + \gamma$ …			
192	$H_3O^+ + \gamma$ …			
193	$H_3O^+ + \gamma$ …			
194	$H_3O^+ + \gamma$ …			
195	$H_3O^+ + \gamma$ …			
196	$O_2 + \gamma \rightarrow$ …			
197	$O_2 + \gamma \rightarrow O + O$	$R_{197} = 7.0 \times 10^{-10}$	1.8	7
198	$CO + \gamma \rightarrow C + O$	$R_{198} = 2.0 \times 10^{-10}$	See §2.2	13

Table B3. List of reactions included in our chemical model that involve cosmic rays or cosmic-ray induced UV emission

No.	Reaction	Rate ($s^{-1} \zeta_H^{-1}$)	Ref.
199	$H + c.r. \rightarrow H^+ + e^-$	$R_{199} = 1.0$	—
200	$He + c.r. \rightarrow He^+ + e^-$	$R_{200} = 1.1$	1
201	$H_2 + c.r. \rightarrow H^+ + H + e^-$	$R_{201} = 0.037$	1
202	$H_2 + c.r. \rightarrow H + H$	$R_{202} = 0.22$	1
203	$H_2 + c.r. \rightarrow H^+ + H^-$	$R_{203} = 6.5 \times 10^{-4}$	1
204	$H_2 + c.r. \rightarrow H_2^+ + e^-$	$R_{204} = 2.0$	1
205	$C + c.r. \rightarrow C^+ + e^-$	$R_{205} = 3.8$	1
206	$O + c.r. \rightarrow O^+ + e^-$	$R_{206} = 5.7$	1
207	$CO + c.r. \rightarrow CO^+ + e^-$	$R_{207} = 6.5$	1
208	$C + \gamma_{c.r.} \rightarrow C^+ + e^-$	$R_{208} = 2800$	2
209	$CH + \gamma_{c.r.} \rightarrow C + H$	$R_{209} = 4000$	3
210	$CH^+ + \gamma_{c.r.} \rightarrow C^+ + H$	$R_{210} = 960$	3
211	$CH_2 + \gamma_{c.r.} \rightarrow CH_2^+ + e^-$	$R_{211} = 2700$	1
212	$CH_2 + \gamma_{c.r.} \rightarrow CH + H$	$R_{212} = 2700$	1
213	$C_2 + \gamma_{c.r.} \rightarrow C + C$	$R_{213} = 1300$	3
214	$OH + \gamma_{c.r.} \rightarrow O + H$	$R_{214} = 2800$	3
215	$H_2O + \gamma_{c.r.} \rightarrow OH + H$	$R_{215} = 5300$	3
216	$O_2 + \gamma_{c.r.} \rightarrow O + O$	$R_{216} = 4100$	3
217	$O_2 + \gamma_{c.r.} \rightarrow O_2^+ + e^-$	$R_{217} = 640$	3
218	$CO + \gamma_{c.r.} \rightarrow C + O$	$R_{218} = 0.21 T^{1/2} x_{H_2} x_{CO}^{-1/2}$	4

(Glover, Federrath, Mac Low, Klessen, 2010, MNRS, 404, 2)

HI to H2 conversion rate

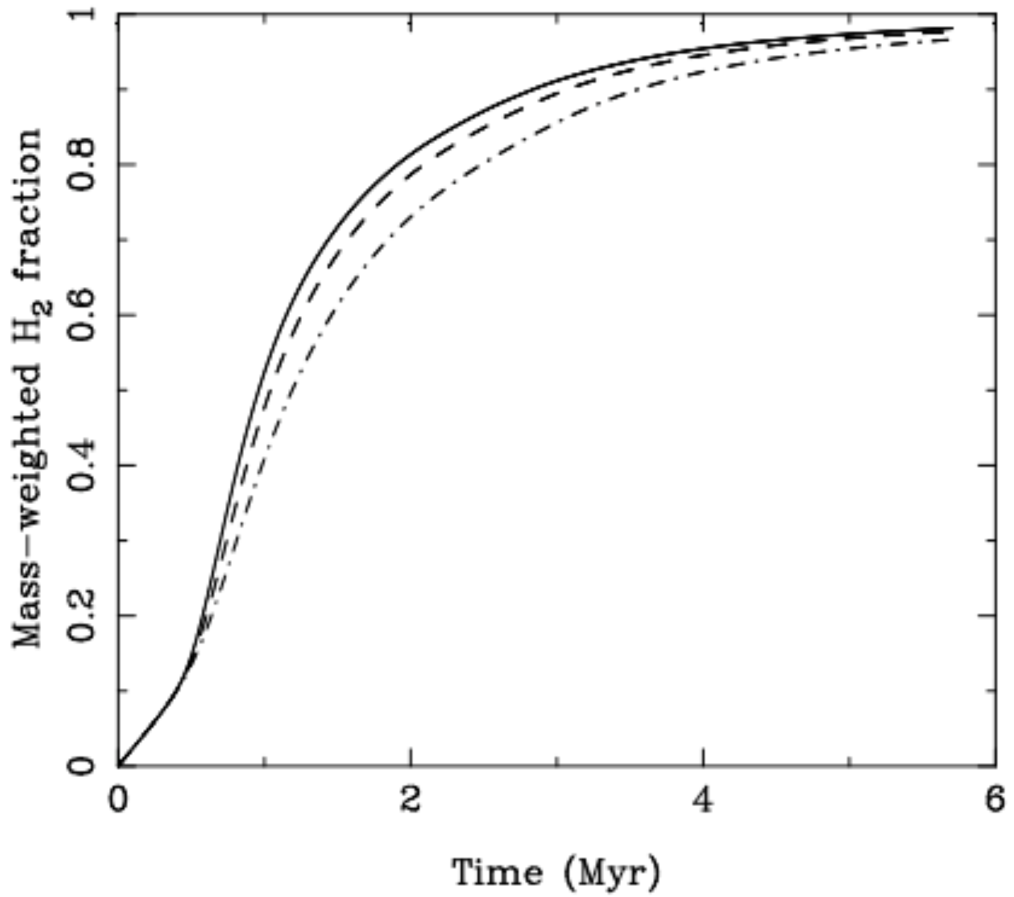

Figure 4. Time evolution of the mass-weighted H_2 abundance in simulations R1, R2 and R3, which have numerical resolutions of 64^3 zones (dot-dashed), 128^3 zones (dashed) and 256^3 zones (solid), respectively.

(Glover, Federrath, Mac Low, Klessen, 2010)

HI to H2 conversion rate

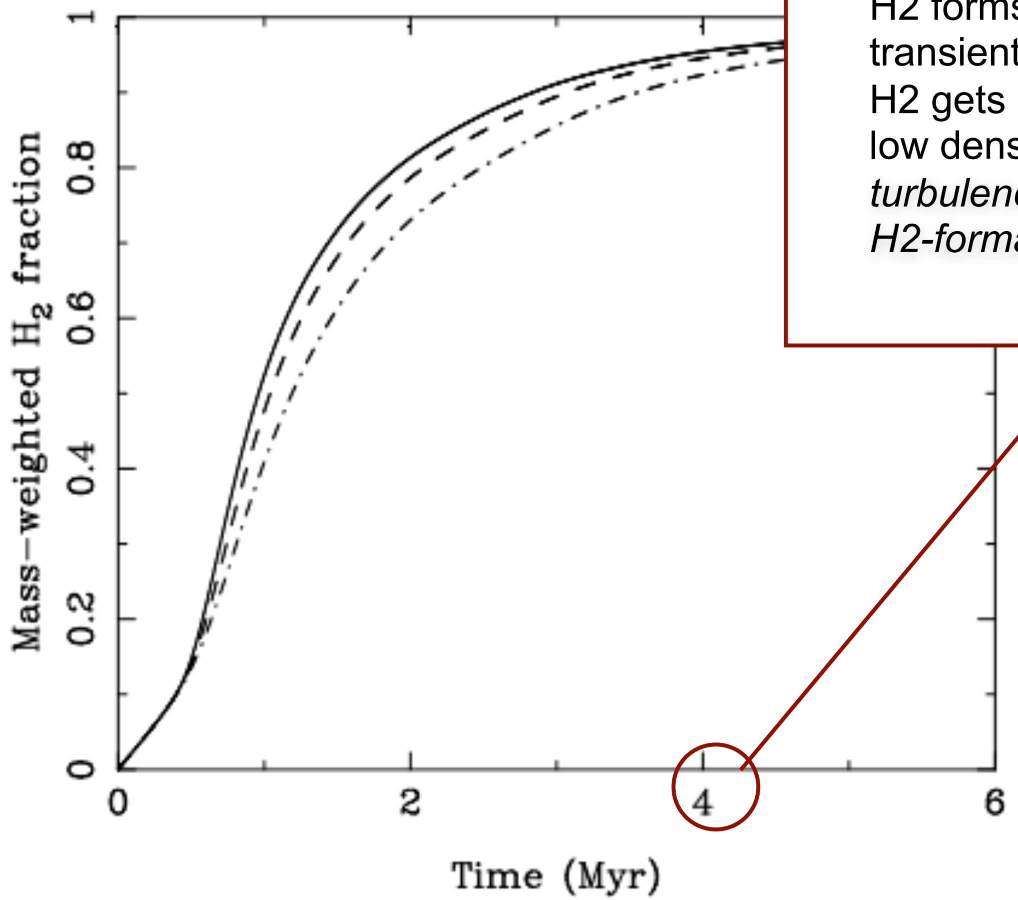

H2 forms rapidly in shocks / transient density fluctuations / H2 gets destroyed slowly in low density regions / *result: turbulence greatly enhances H2-formation rate*

Figure 4. Time evolution of the mass-weighted H_2 abundance in simulations R1, R2 and R3, which have numerical resolutions of 64^3 zones (dot-dashed), 128^3 zones (dashed) and 256^3 zones (solid), respectively.

(Glover, Federrath, Mac Low, Klessen, 2010)

HI to H2 conversion rate

compare to data from
Tamburro et al. (2008) study:

t_{form} ~ few x 10^6 years

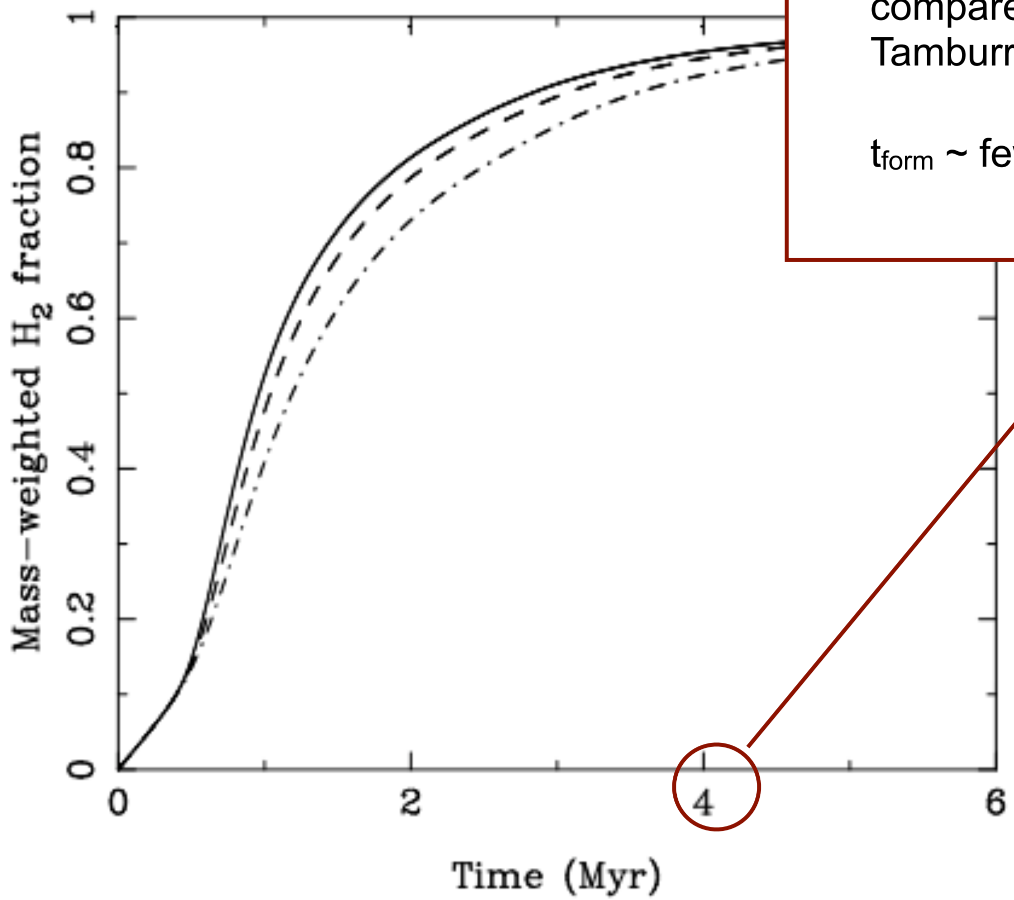

Figure 4. Time evolution of the mass-weighted H_2 abundance in simulations R1, R2 and R3, which have numerical resolutions of 64^3 zones (dot-dashed), 128^3 zones (dashed) and 256^3 zones (solid), respectively.

(Glover, Federrath, Mac Low, Klessen, 2010)

CO, C$^+$ formation rates

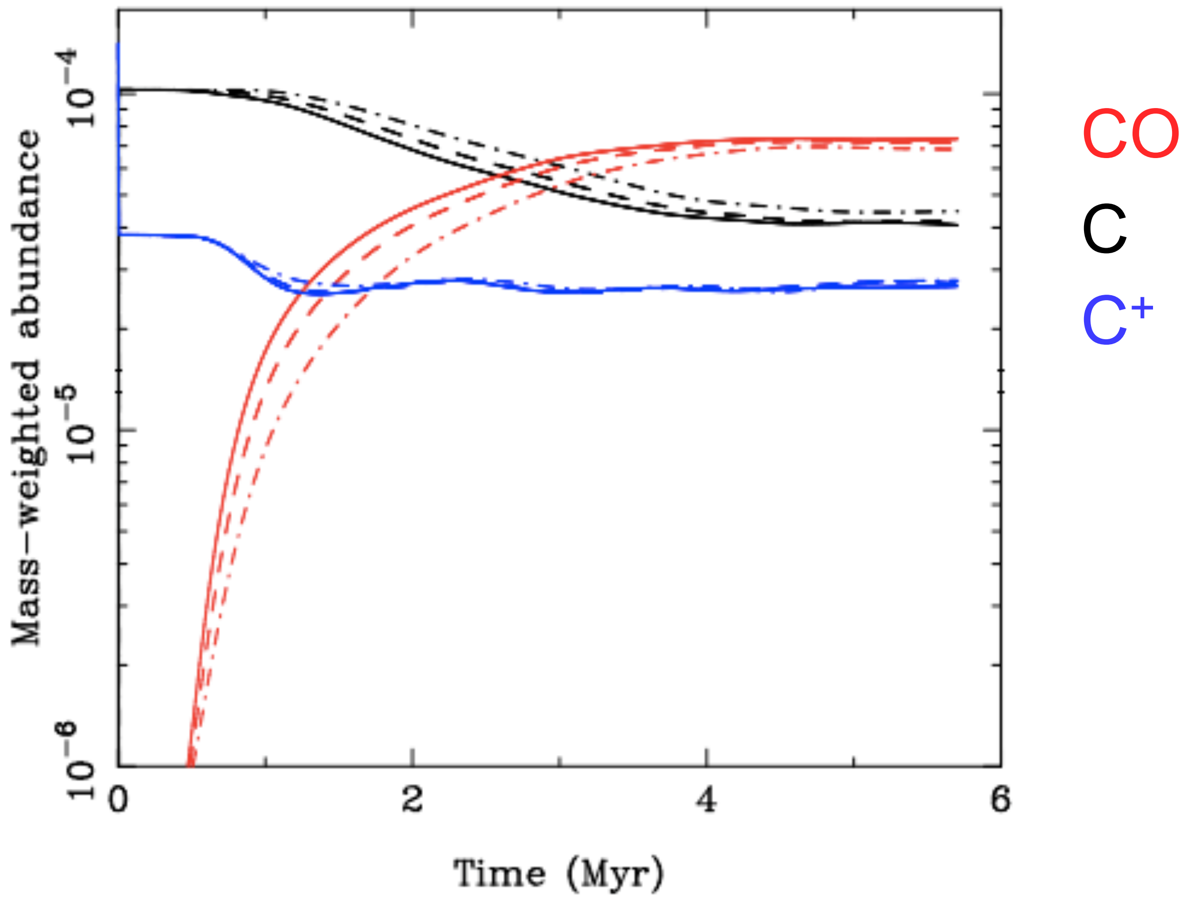

Figure 5. Time evolution of the mass-weighted abundances of atomic carbon (black lines), CO (red lines), and C^+ (blue lines) in simulations with numerical resolutions of 64^3 zones (dot-dashed), 128^3 zones (dashed) and 256^3 zones (solid).

(Glover, Federrath, Mac Low, Klessen, 2010)

effects of chemistry 1

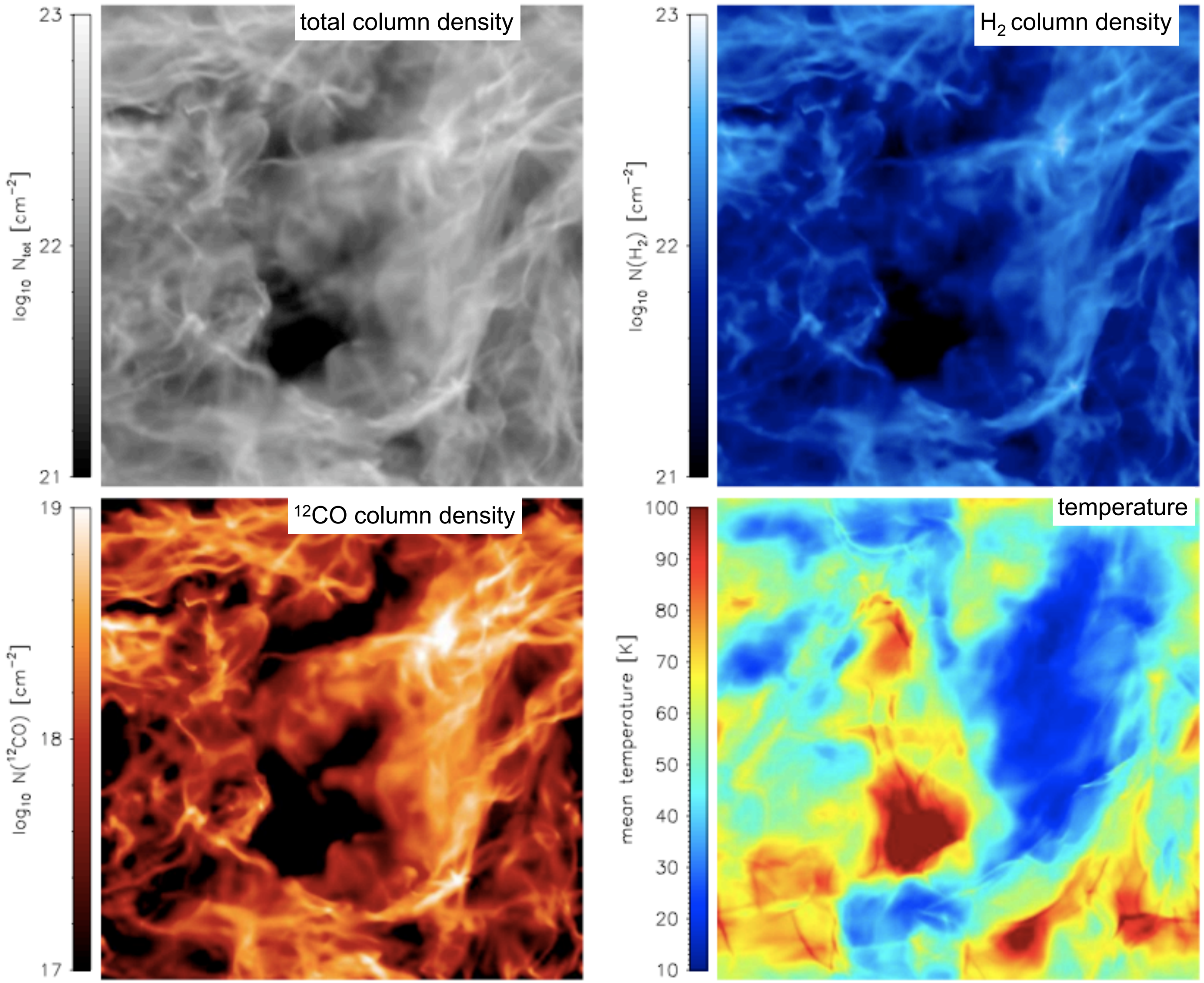

(Glover, Federrath, Mac Low, Klessen, 2010)

effects of chemistry 2

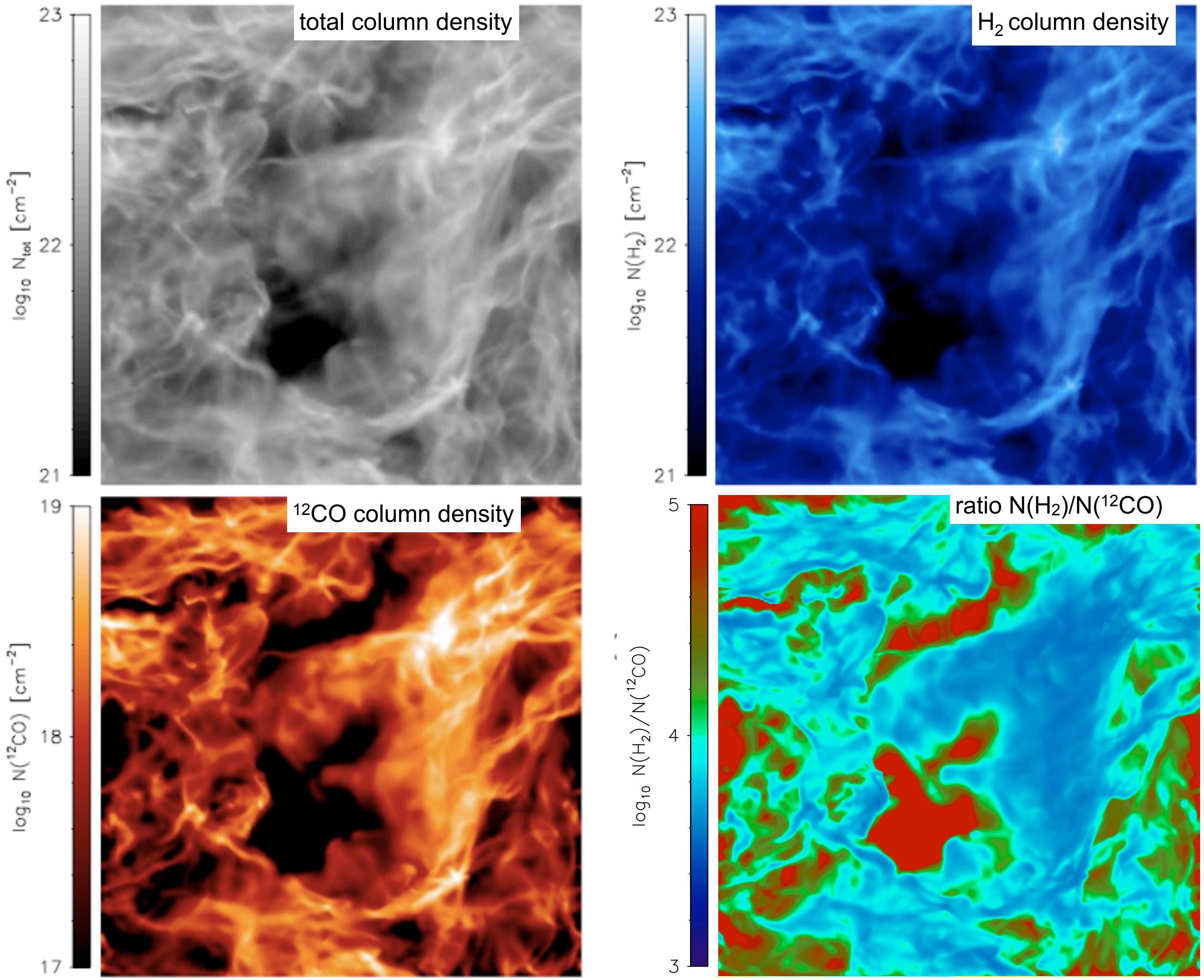

(Glover, Federrath, Mac Low, Klessen, 2010)

effects of chemistry 4

- deliverables / predictions:
  - x-factor estimates (as function of environmental conditions)
  - synthetic line emission maps (in combination with line transfer)
  - pdf's of density, velocity, emissivity / structure functions (to directly connect to observational regime)
  - *COMMENT:* density pdf is *NOT* lognormal!
    --> implications for analytical IMF theories

X-factor

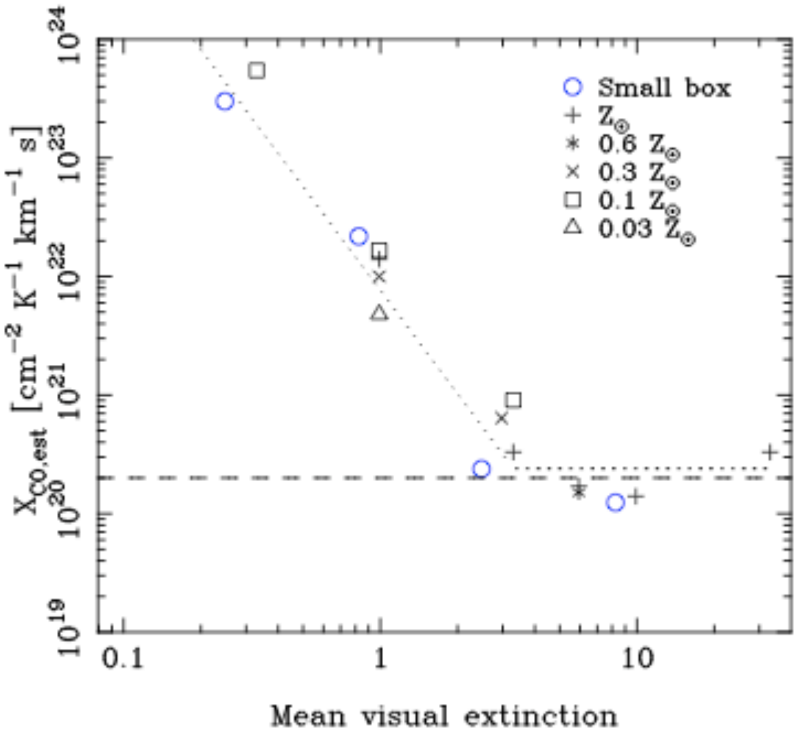

from Glover & Mac Low (2010, ApJ, submitted)

Figure 8. Estimate of the CO-to-H_2 conversion factor $X_{CO,est}$, plotted as a function of the mean visual extinction of the gas, $\langle A_V \rangle$. The simplifications made in our modelling mean that each value of $X_{CO,est}$ is uncertain by at least a factor of two. At $\langle A_V \rangle > 3$, the values we find are consistent with the value of $X_{CO} = 2 \times 10^{20} \mathrm{cm}^{-2}\,\mathrm{K}^{-1}\,\mathrm{km}^{-1}\,\mathrm{s}$ determined observationally for the Milky Way by Dame et al. (2001), indicated in the plot by the horizontal dashed line. At $\langle A_V \rangle < 3$, we find evidence for a strong dependence of $X_{CO,est}$ on $\langle A_V \rangle$. The empirical fit given by Equation 11 is indicated as the dotted line in the Figure, and demonstrates that at low $\langle A_V \rangle$, the CO-to-H_2 conversion factor increases roughly as $X_{CO,est} \propto A_V^{-2.8}$. It should also be noted that at any particular $\langle A_V \rangle$, the dependence of $X_{CO,est}$ on metallicity is relatively small. Previous claims of a strong metallicity dependence likely reflect the fact that there is a strong dependence on the mean extinction, which varies as $\langle A_V \rangle \propto Z$ given fixed mean cloud density and cloud size.

from atomic gas to molecular clouds

- importance of dynamics:
  - how does molecular cloud material form in convergent flows, e.g., as triggered by spiral density waves...?
  - do sequence of idealized numerical experiments
- questions
  - are molecular clouds truly “multi-phase” media?
  - turbulence? dynamical & morphological properties?
  - what is relation to initial & environmental conditions?
  - magnetic field structure?

convergent flows: set-up

numerical set-up

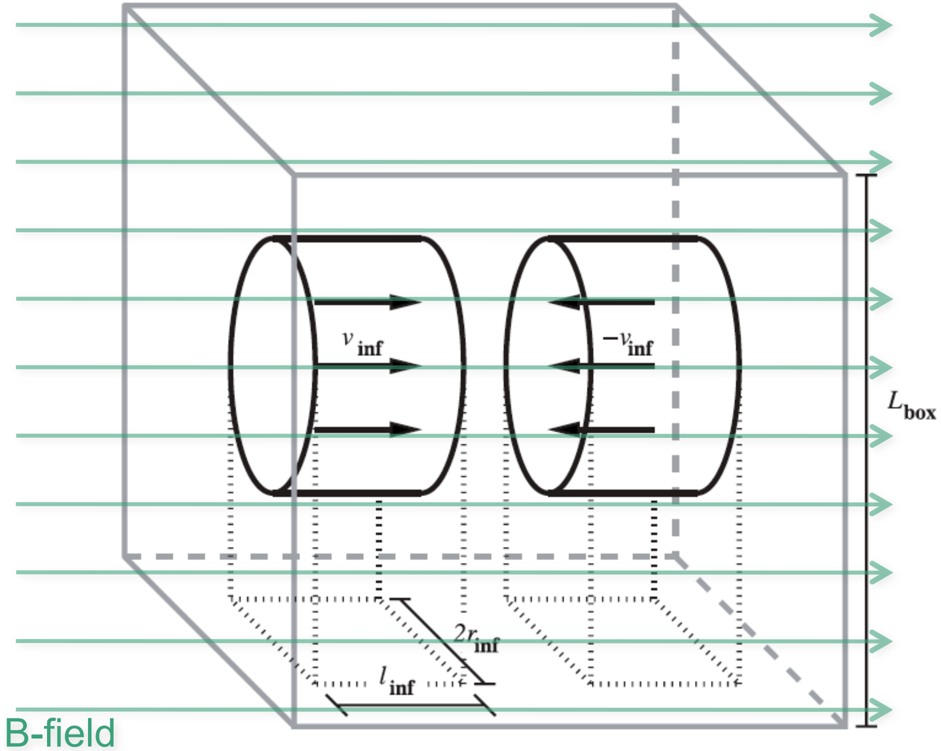

from Vazquez-Semadeni et al. (2007)

- convergent flow studies
  - atomic flows collide
  - cooling curve (soon chemistry)
  - gravity
  - magnetic fields
  - numerics: AMR, BGK, SPH

see studies by Banerjee et al., Heitsch et al., Hennebelle et al., Vazquez-Semadeni et al.

convergent flows: set-up

adopted cooling curve

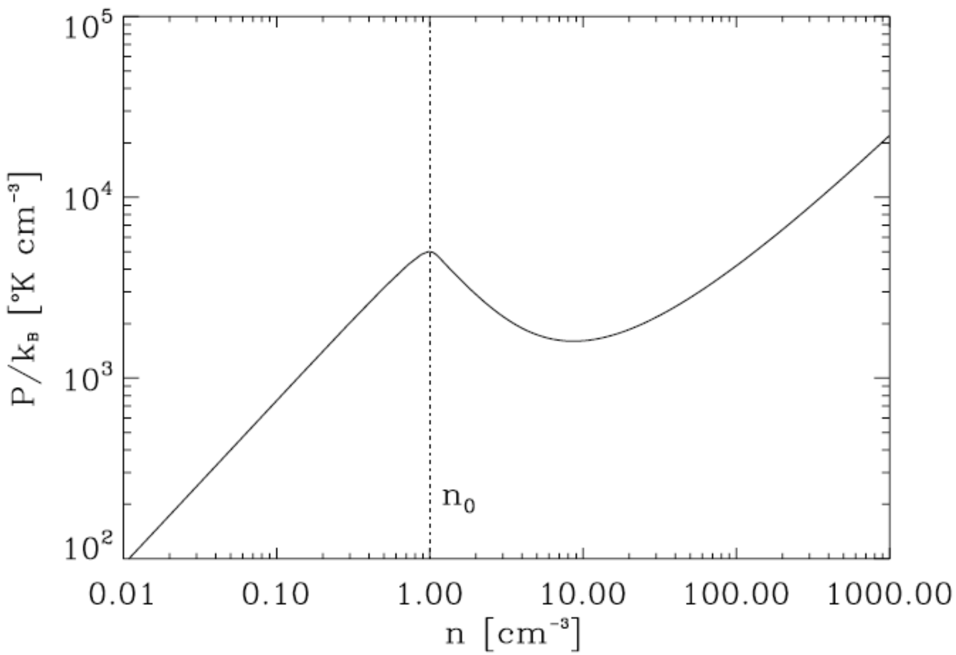

from Vazquez-Semadeni et al. (2007)

- convergent flow studies
  - atomic flows collide
  - cooling curve (soon chemistry)
  - gravity
  - magnetic fields
  - numerics: AMR, BGK, SPH

see studies by Banerjee et al., Heitsch et al., Hennebelle et al., Vazquez-Semadeni et al.

MC formation in convergent flows

thermal instability + gravity creates complex molecular cloud structure:

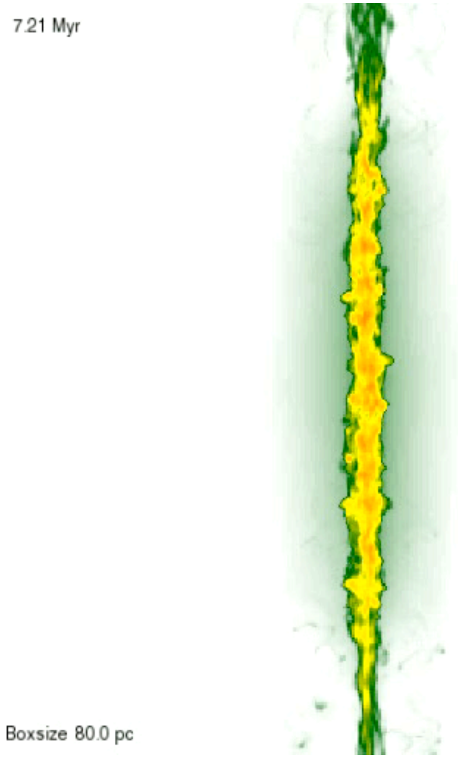

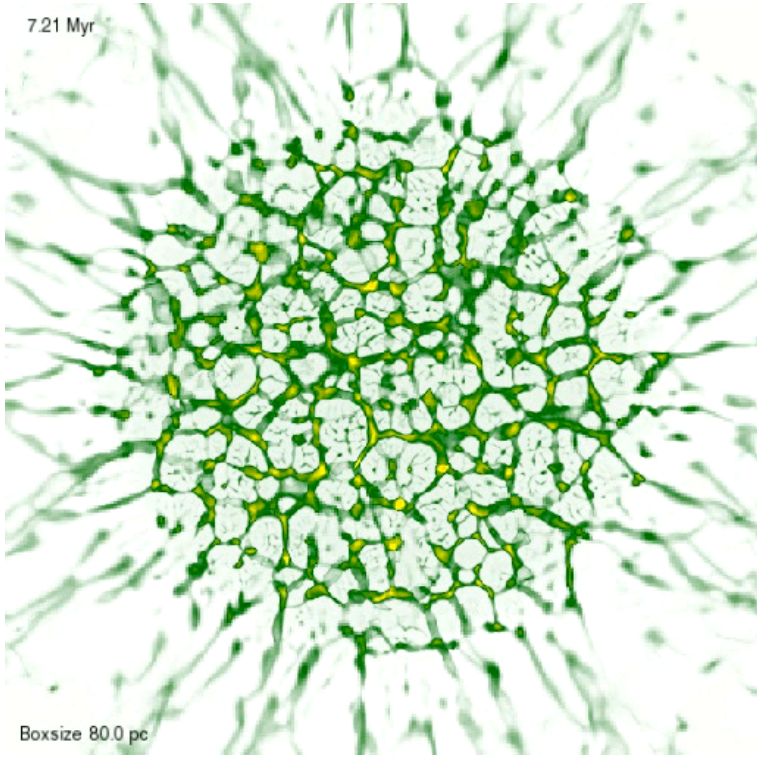

from Banerjee et al. (2008)
(see also studies by Hennebelle et al. and Vazquez-Semadeni et al. and Heitsch et al.)

MC formation in convergent flows

this simple set-up reproduces (and explains!) some of the main properties of MCs:

- highly patchy and clumpy
- high fraction of substructure
- cold dense molecular clumps coexist with warm atomic gas
- not a well bounded entity
- dynamical evolution (different star formation modes: from low mass to high mass SF?)

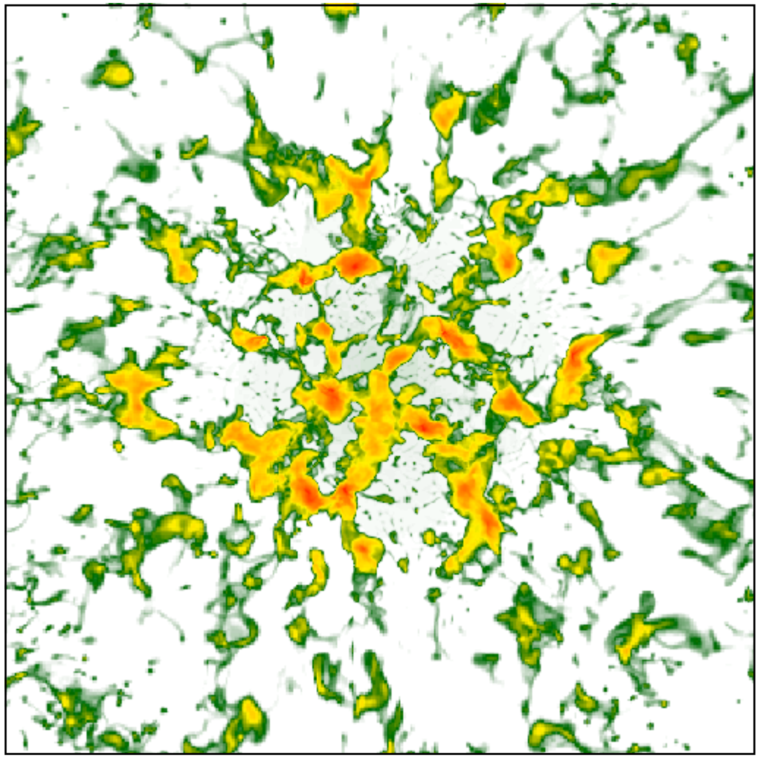

from Banerjee et al. (2008)
(see also studies by Hennebelle et al. and Vazquez-Semadeni et al. and Heitsch et al.)

MC formation in convergent flows

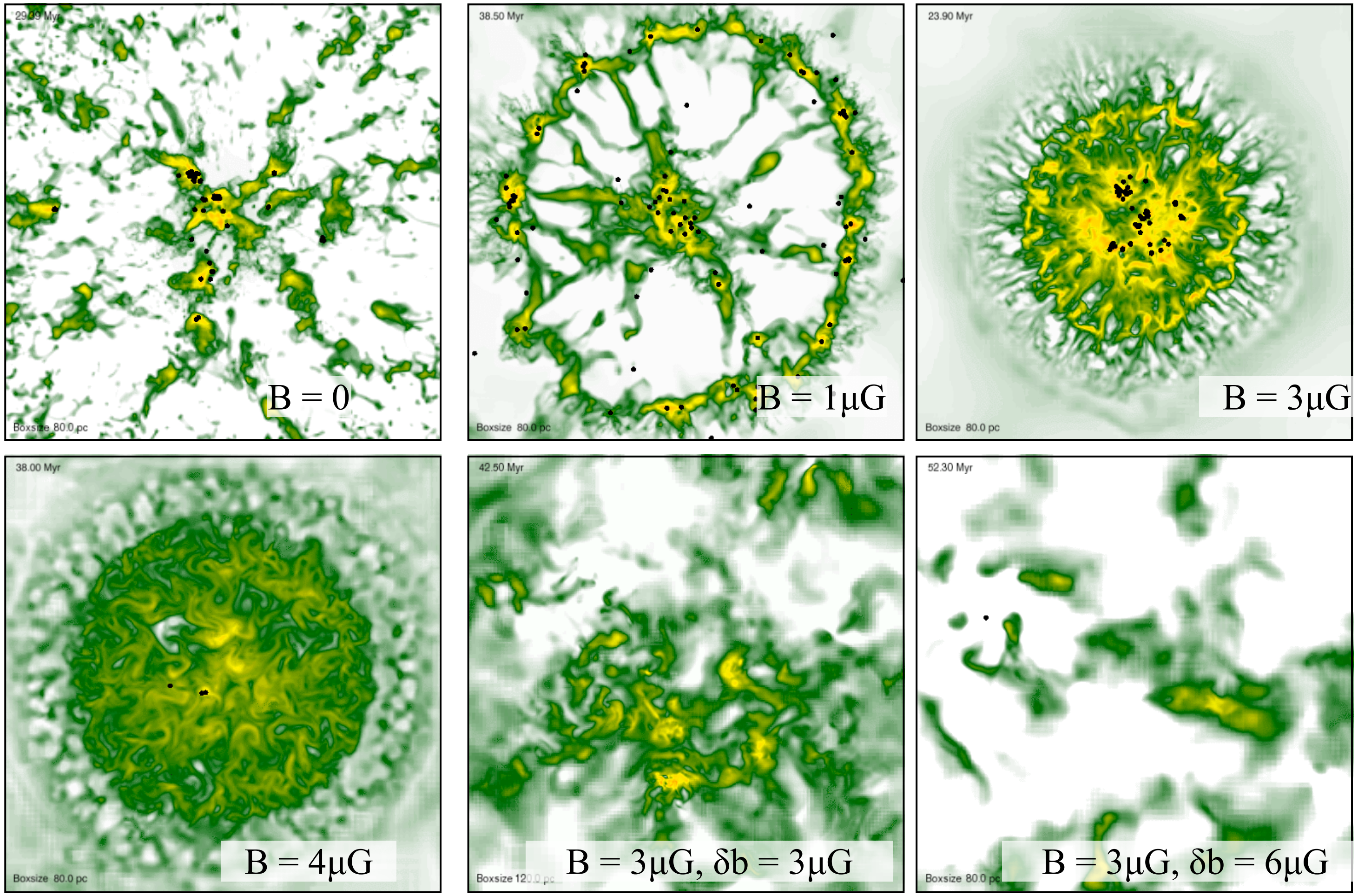

Morphology of the molecular cloud and star formation efficiency depends on the strength of the magnetic field

Banerjee et al. in prep.

MC formation in convergent flows

morphology and clump evolution

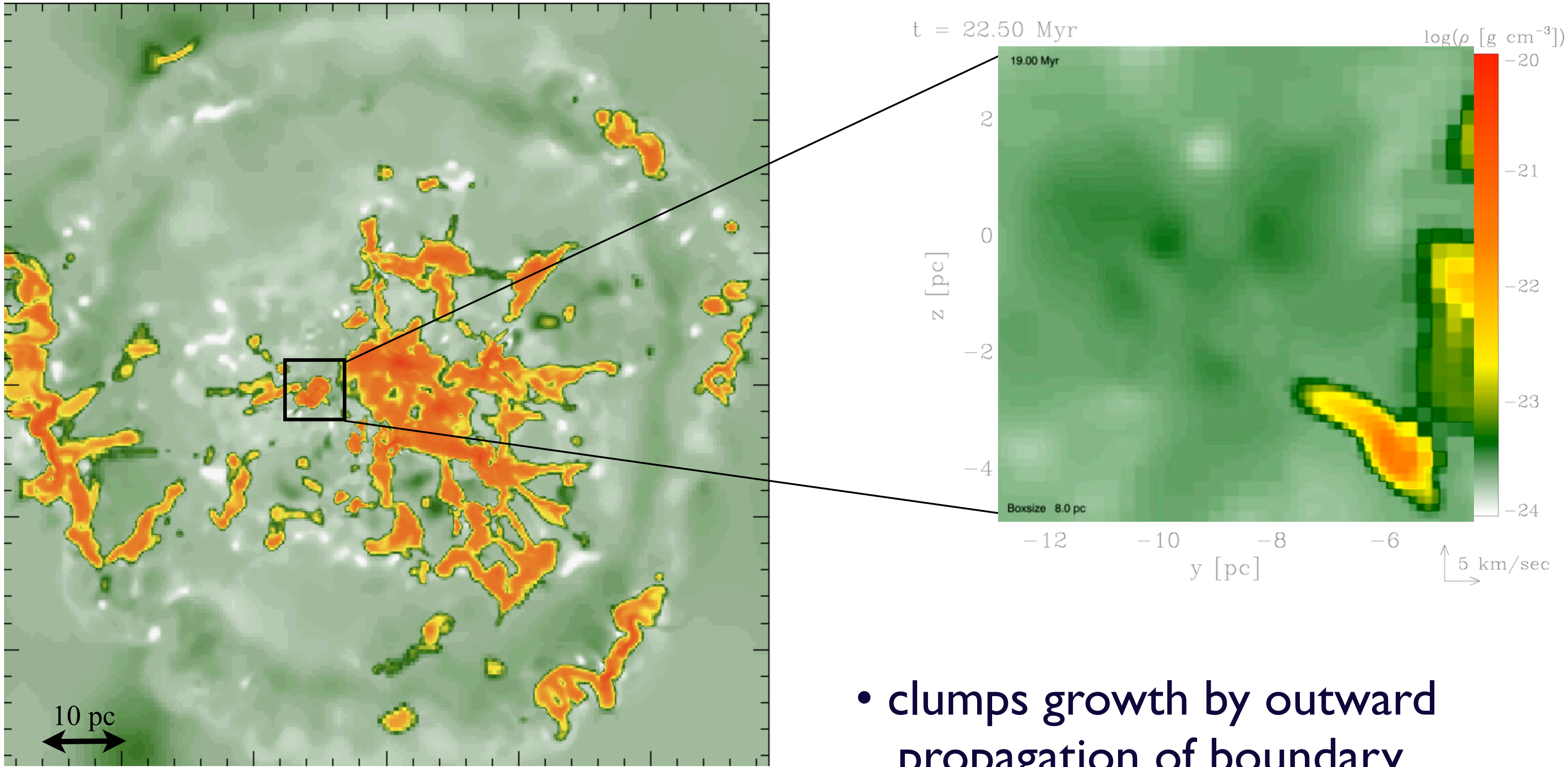

- clumps growth by outward propagation of boundary layers and
- coalescence at later times

- MCs are inhomogeneous
- cold clumps embedded in warm atomic gas

see studies by Banerjee et al., Heitsch et al., Hennebelle et al., Vazquez-Semadeni et al.

some results: growth of cores

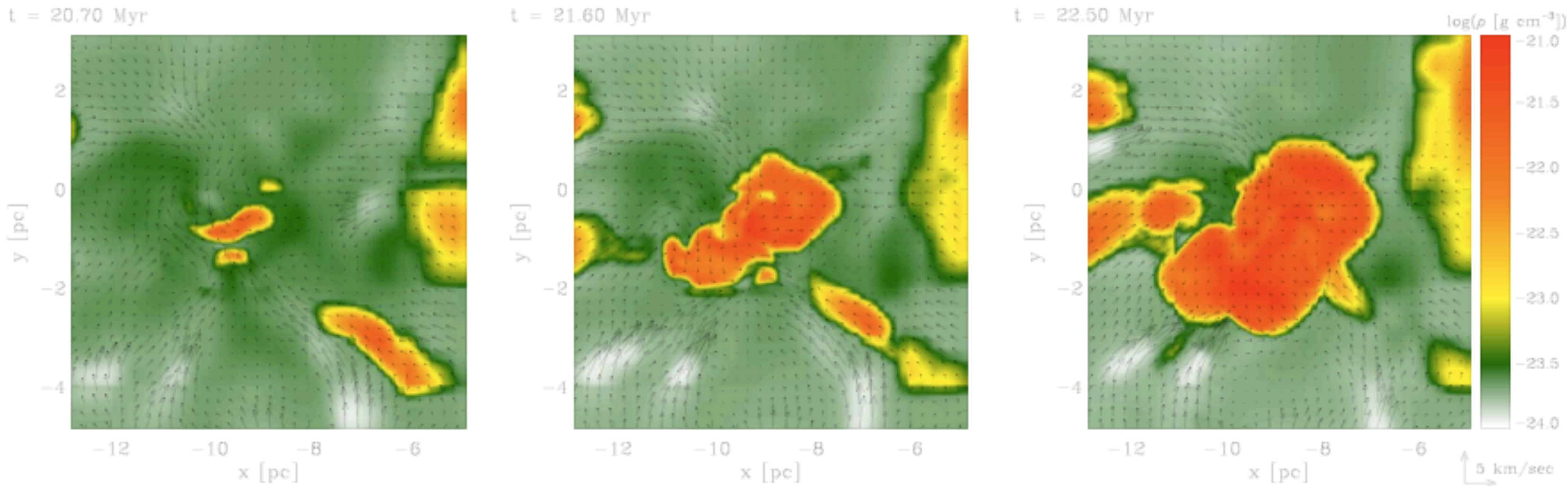

Figure 2. Shows the time evolution of a typical clump which initially develops out of the thermally unstable WNM in shock layers of turbulent flows. A small cold condensate grows by outward propagation of its boundary layer. Coalescence and merging with nearby clumps further increases the size and mass of these clumps. The global gravitational potential of the proto-cloud enhances the merging probability with time. The images show 2D slices of the density (logarithmic colour scale) and the gas velocity (indicated as arrows) in the plane perpendicular to the large scale flows.

two phases of core growth:
(1) by *outward propagation* of *boundary layer* → Jeans sub-critical phase
(2) *core mergers* → super-Jeans → gravitational collapse & star formation
example: *Pipe nebula* ???

from Banerjee et al. (2008)

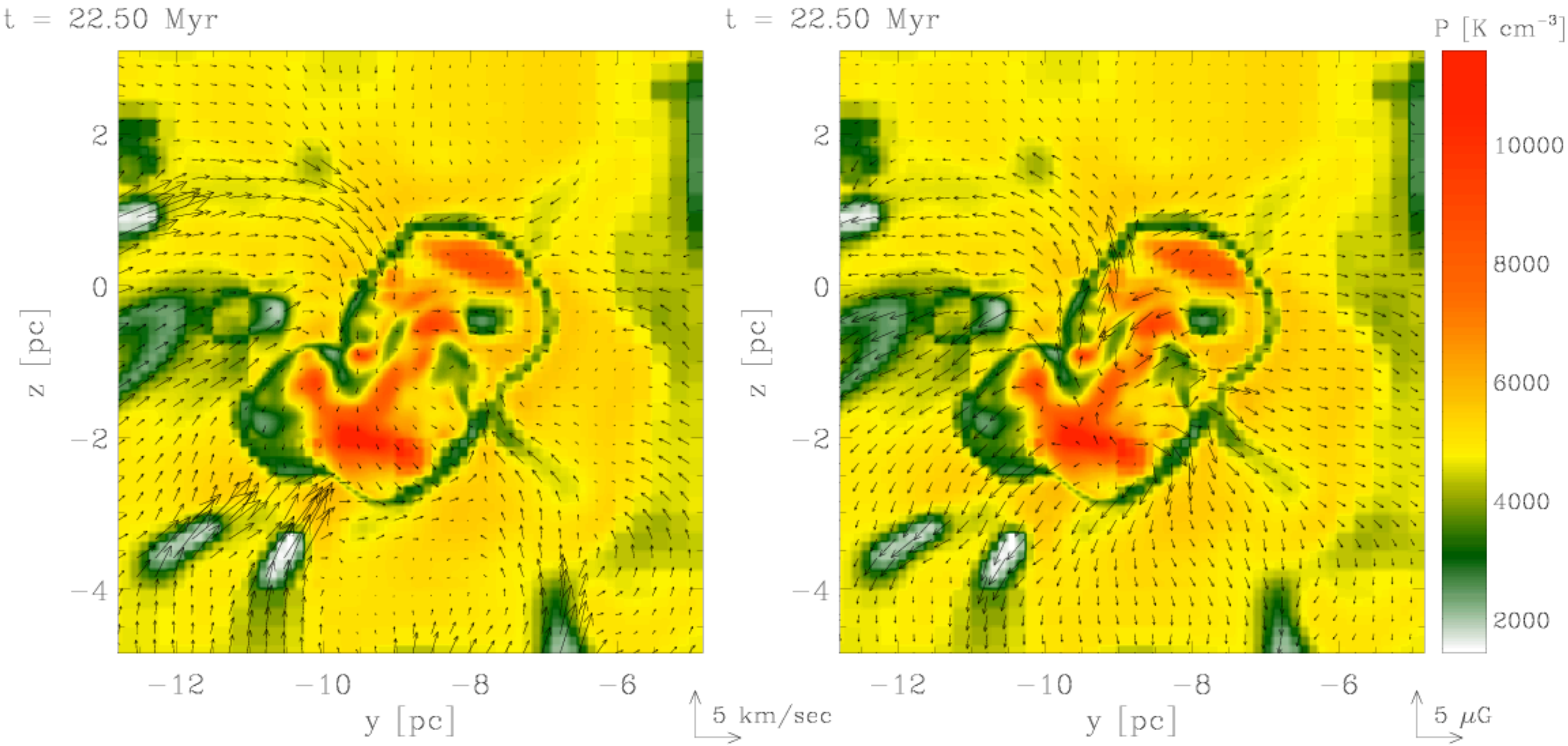

- cores roughly in pressure balance with surroudings
- relation between flow and magnetic field:
  mass flow mostly along field lines

from Banerjee et al. (2008)

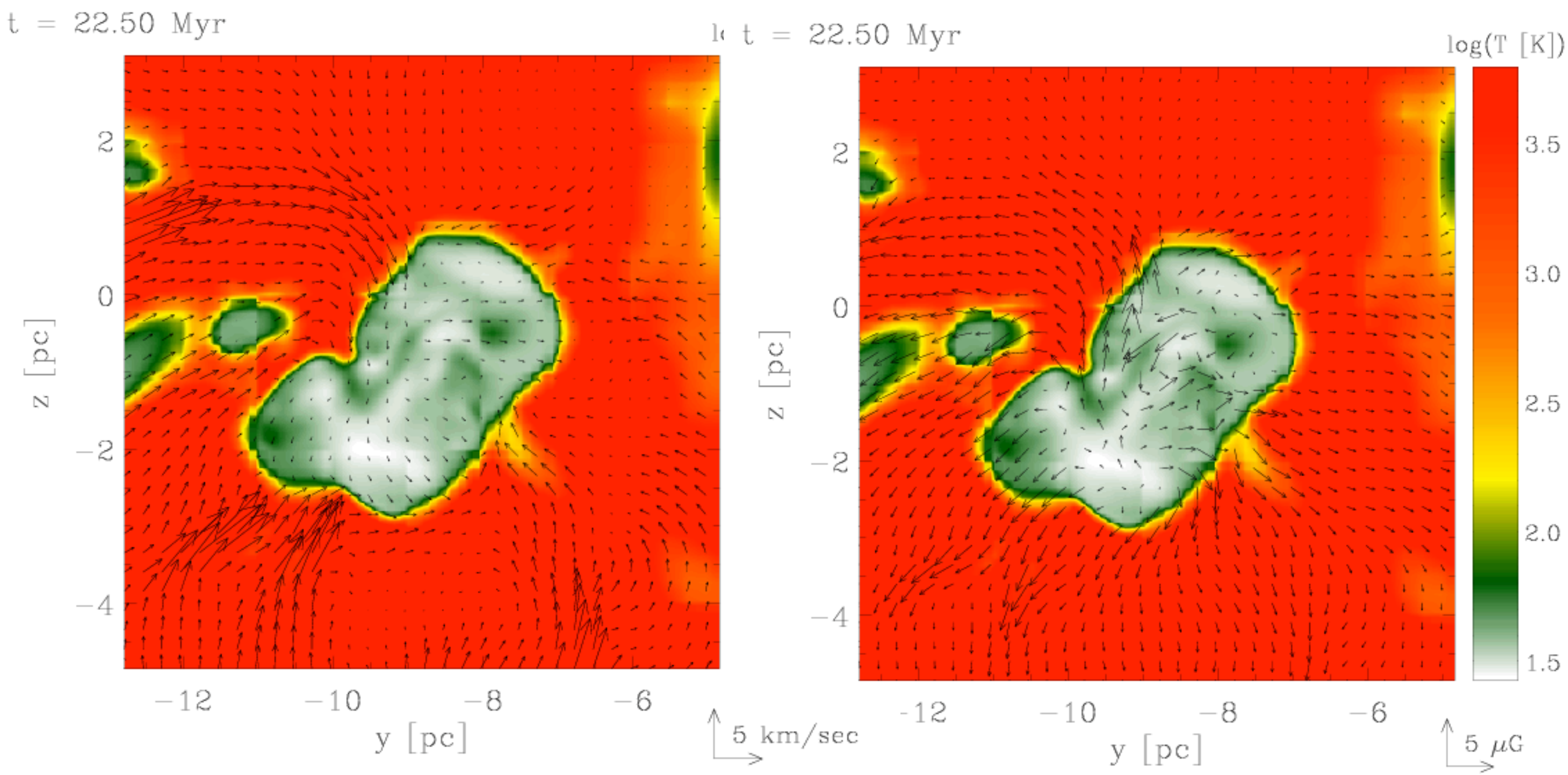

- typical core densities $n \sim 2 – 5 \times 10^3\ cm^{-3}$
- typical core temperatures $T \sim 30 – 50\ K$

from Banerjee et al. (2008)

some results: statistical correlations

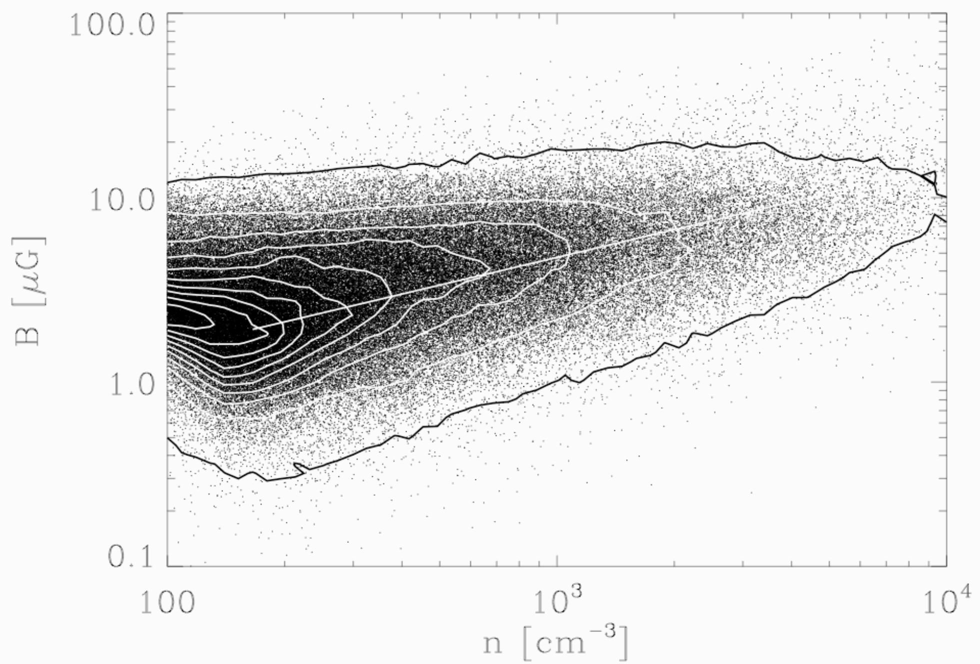

• strong correlation of gas streams and magnetic field lines

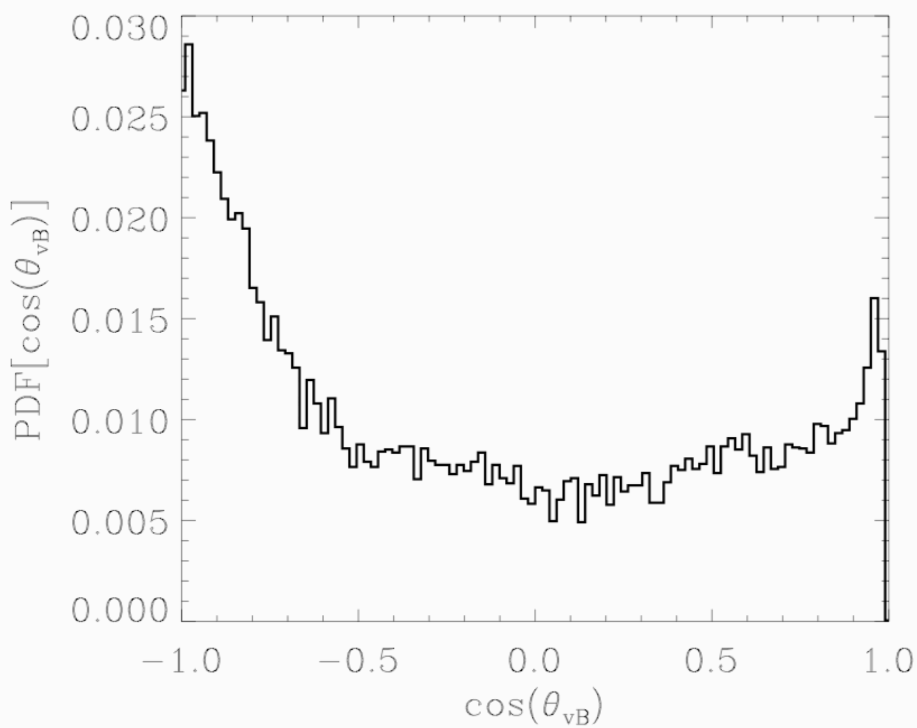

• large scatter of magnetic field strengths:
  sub- and super-critical cores exist
• median slope: $B \propto n^{0.5}$
  (e.g. *Crutcher 1999*)

some results: loci of high-mass stars

global contraction phase

center of the cloud
→ birthplace for **massive stars**?
(eg. Zinnecker & Yorke 2007)

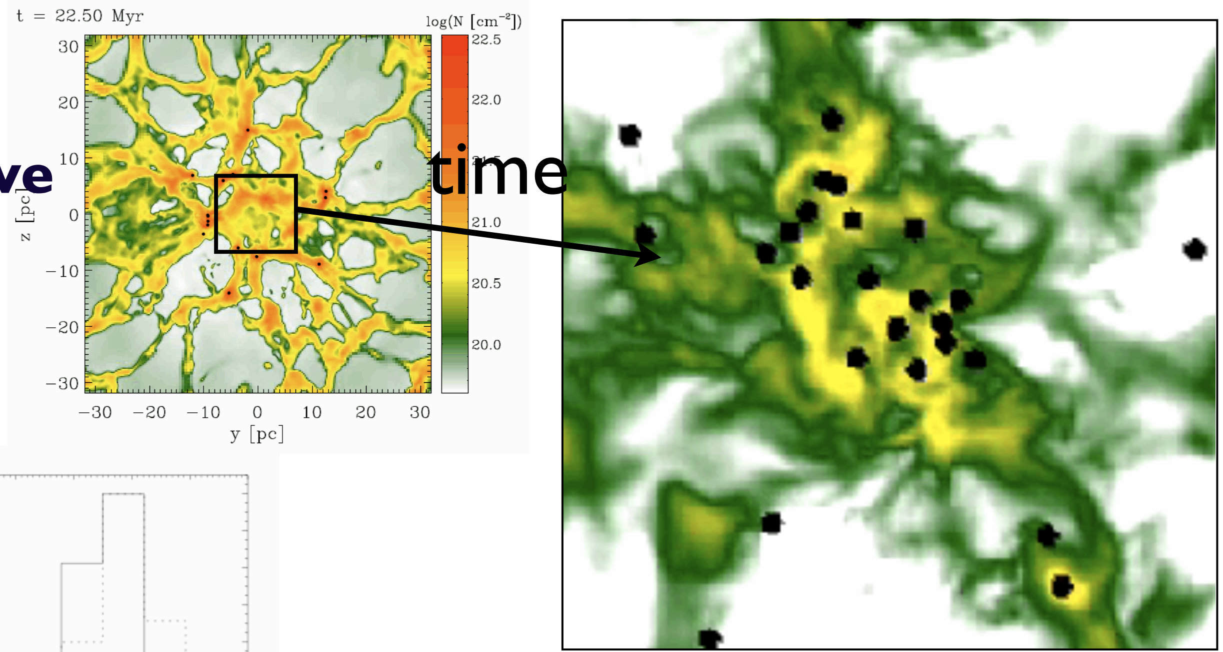

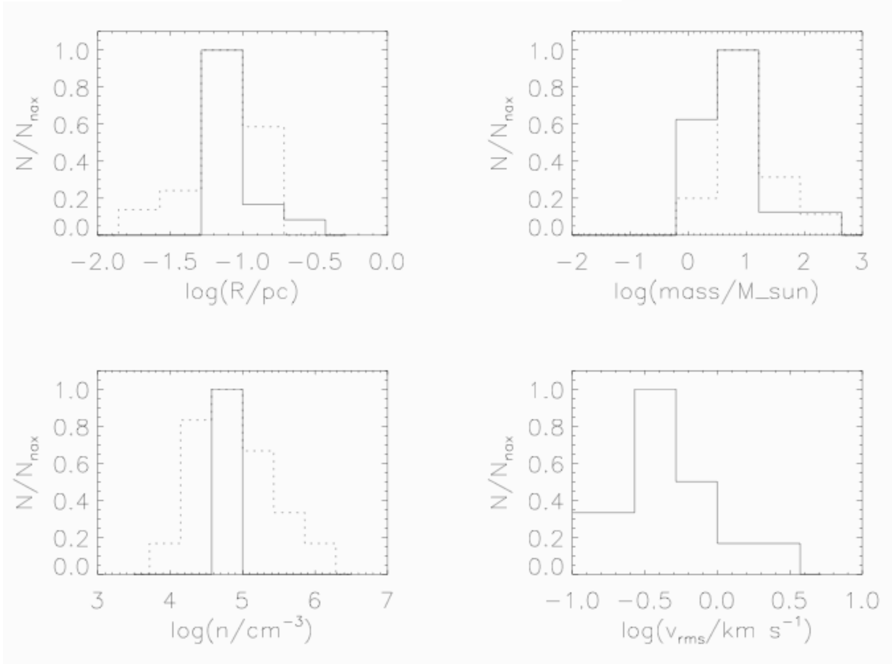

comparison of core properties with observation of Cygnus X by *Motte et al 2007*

Vazquez-Semadeni et al. 2008

dynamical SF in a nutshell

- interstellar gas is highly *inhomogeneous*
  - *gravitational instability*
  - *thermal instability*
  - *turbulent compression* (in shocks $\delta\rho/\rho \propto \mathcal{M}^2$; in atomic gas: $\mathcal{M} \approx 1...3$)

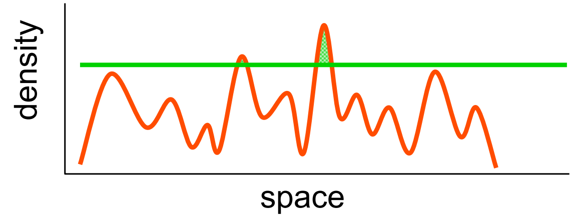

- cold *molecular clouds* can form rapidly in high-density regions at *stagnation points* of *convergent large-scale flows*
  - chemical *phase transition*: atomic → molecular
  - process is *modulated* by large-scale *dynamics* in the galaxy
- inside *cold clouds:* turbulence is highly supersonic ($\mathcal{M} \approx 1...20$)
  → *turbulence* creates large density contrast,
  gravity selects for collapse

  ⟶ **GRAVOTUBULENT FRAGMENTATION**
- *turbulent cascade:* local compression *within* a cloud provokes collapse → formation of individual *stars* and *star clusters*

(e.g. Mac Low & Klessen, 2004, Rev. Mod. Phys., 76, 125-194) turbulence

Turbulent cascade

Kolmogorov (1941) theory
incompressible turbulence

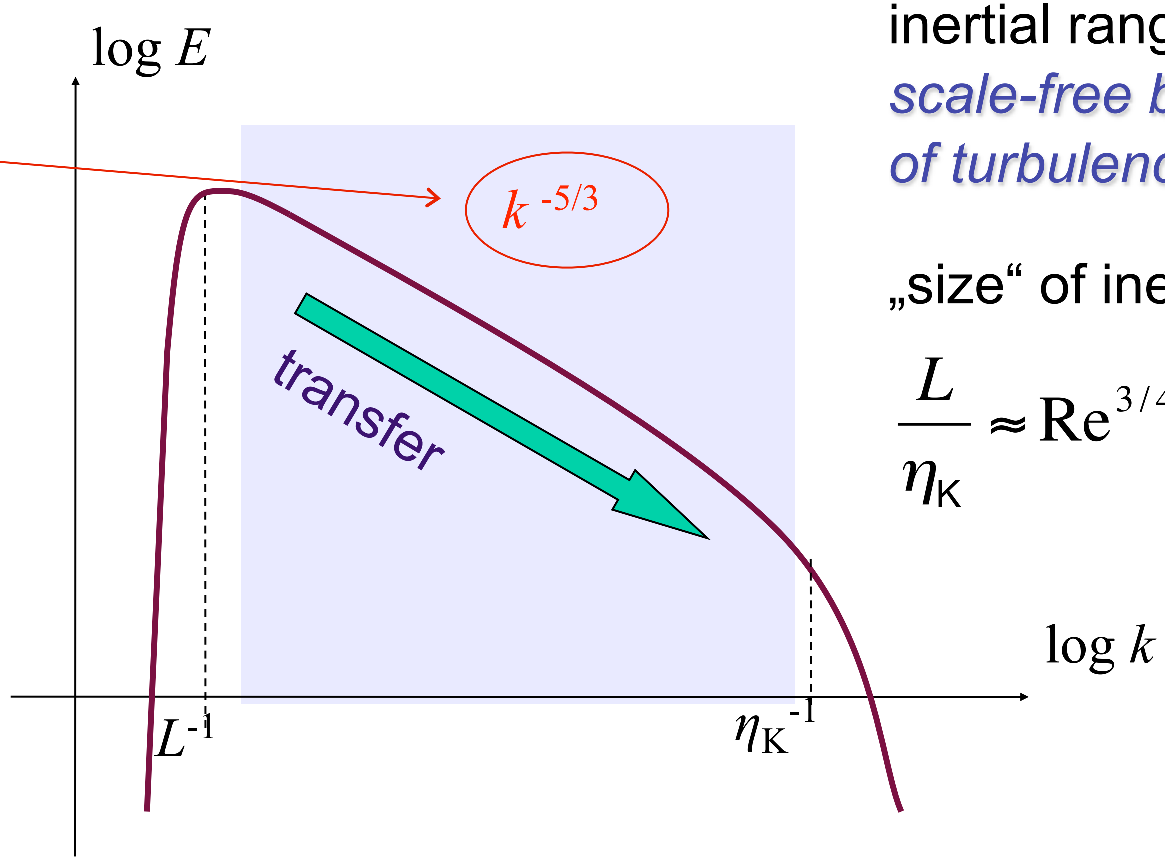

energy
input
scale

energy
dissipation
scale

inertial range:
scale-free behavior of turbulence

„size“ of inertial range:

$$\frac{L}{\eta_K} \approx \mathrm{Re}^{3/4}$$

Turbulent cascade

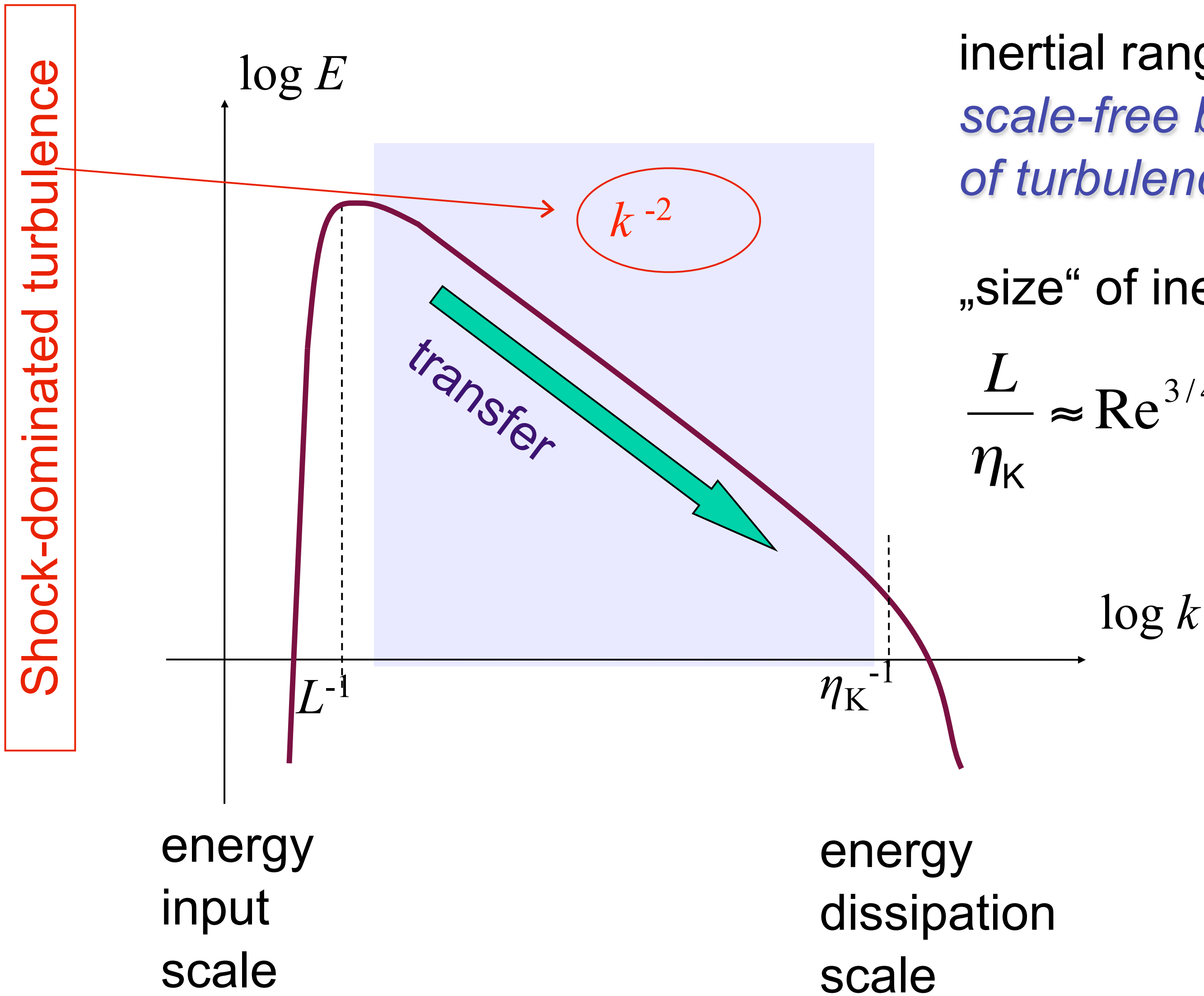

inertial range:

scale-free behavior of turbulence

„size“ of inertial range:

$$\frac{L}{\eta_K} \approx \mathrm{Re}^{3/4}$$

Turbulent cascade in ISM

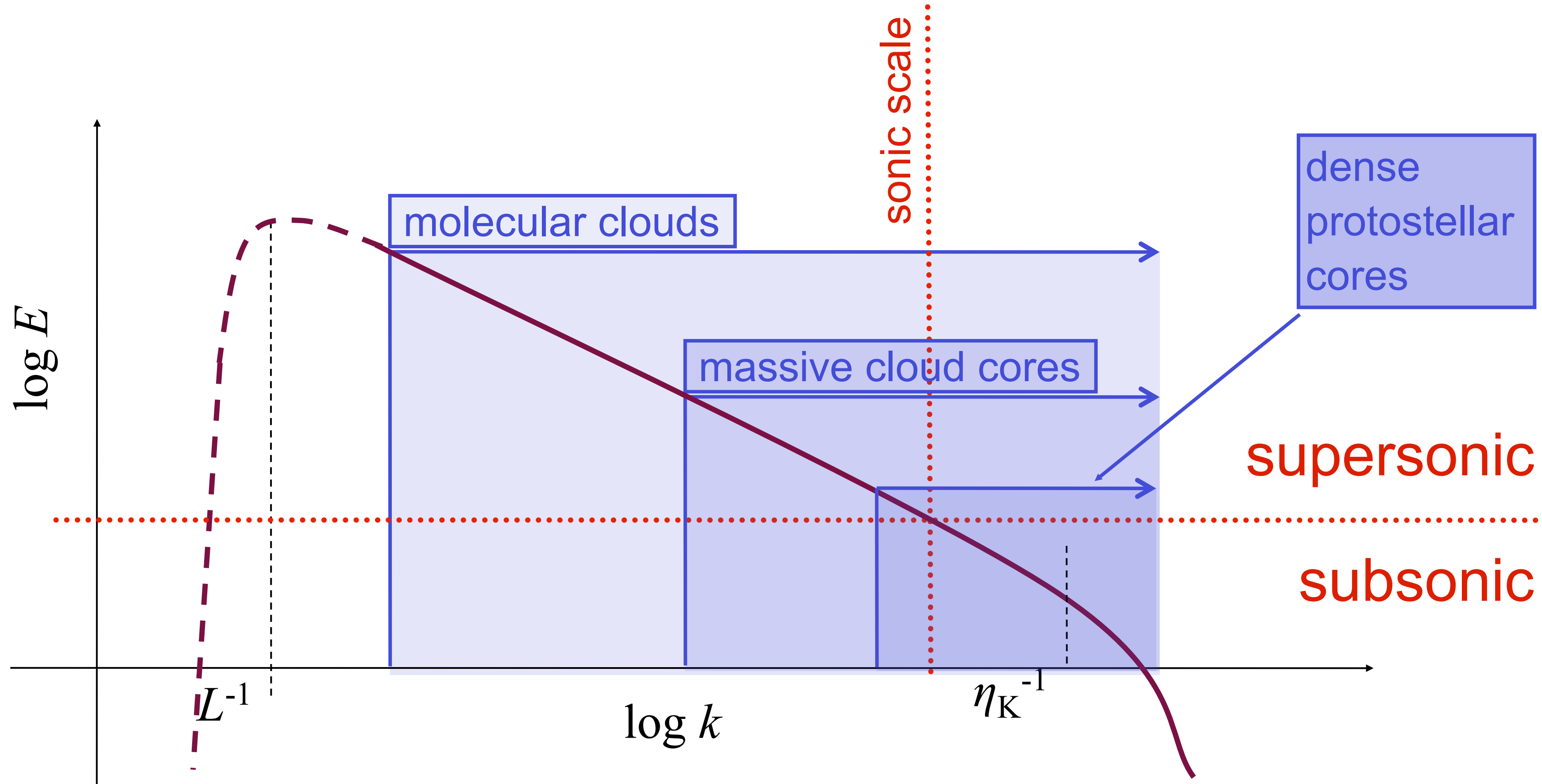

energy source & scale *NOT known* (supernovae, winds, spiral density waves?)

σ_{rms} << 1 km/s
$M_{rms} \leq 1$
$L \approx 0.1$ pc

dissipation scale not known (ambipolar diffusion, molecular diffusion?)

what drives ISM turbulence?

- seems to be driven on large scales, little difference between star-forming and non-SF clouds
  ---> rules out internal sources
- proposals in the literature
  - supernovae
  - expanding HII regions / stellar winds / outflows
  - spiral density waves
  - magneto-rotational instability
  - new idea: accretion onto disk

what drives ISM turbulence?

some energetic arguments...

energy decay by turbulent dissipation:

$$\dot{e} \simeq -(1/2)\rho v_{\mathrm{rms}}^3 / L_{\mathrm{d}}$$

$$= -(3\times 10^{-27}\ \mathrm{erg\,cm^{-3}\,s^{-1}})\left(\frac{n}{1\ \mathrm{cm}^{-3}}\right) \times \left(\frac{v_{\mathrm{rms}}}{10\ \mathrm{km\,s^{-1}}}\right)^3 \left(\frac{L_{\mathrm{d}}}{100\ \mathrm{pc}}\right)^{-1},$$

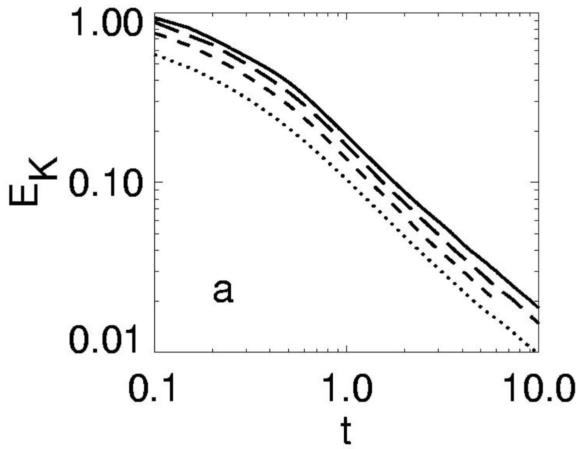

(Mac Low et al. 1999)

decay timescale:

$$\tau_{\mathrm{d}} = e/\dot{e} \simeq L_{\mathrm{d}}/v_{\mathrm{rms}}$$

$$= (9.8\ \mathrm{Myr})\left(\frac{L_{\mathrm{d}}}{100\ \mathrm{pc}}\right)\left(\frac{v_{\mathrm{rms}}}{10\ \mathrm{km\,s^{-1}}}\right)^{-1},$$

(from Mac Low & Klessen, 2004)

what drives ISM turbulence?

magneto-rotational instability:

$$\dot{e} = (3 \times 10^{-29}\ \mathrm{erg\,cm^{-3}\,s^{-1}}) \left(\frac{B}{3\,\mu\mathrm{G}}\right)^2 \left(\frac{\Omega}{(220\ \mathrm{Myr})^{-1}}\right).$$

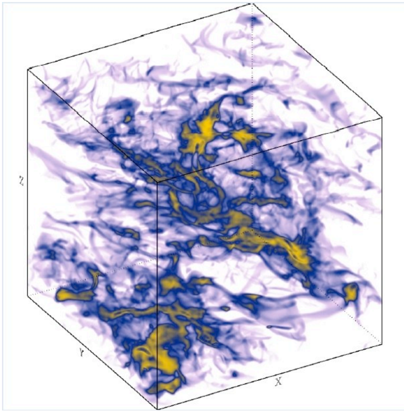

(from Piotek & Ostriker 2005)

gravitational instability (spiral waves)

$$\begin{aligned}\dot{e} &\simeq G(\Sigma_g/H)^2 \lambda^2 \Omega \\ &\simeq (4 \times 10^{-29}\ \mathrm{erg\,cm^{-3}\,s^{-1}}) \\ &\quad \times \left(\frac{\Sigma_g}{10 M_\odot\ \mathrm{pc}^{-2}}\right)^2 \left(\frac{H}{100\ \mathrm{pc}}\right)^{-2} \\ &\quad \times \left(\frac{\lambda}{100\ \mathrm{pc}}\right)^2 \left(\frac{\Omega}{(220\ \mathrm{Myr})^{-1}}\right),\end{aligned}$$

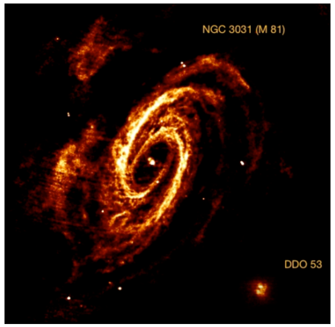

(from Walter et al. 2008)

(from Mac Low & Klessen, 2004)

what drives ISM turbulence?

protostellar outflows

$$\dot{e}=\frac{1}{2}f_{\rm w}\eta_{\rm w}\frac{\dot{\Sigma}_*}{H}v_{\rm w}^2$$
$$\simeq(2\times10^{-28}\ \mathrm{erg\ cm^{-3}\ s^{-1}})\left(\frac{H}{200\ \mathrm{pc}}\right)^{-1}\left(\frac{f_{\rm w}}{0.4}\right)$$
$$\times\left(\frac{v_{\rm w}}{200\ \mathrm{km\ s^{-1}}}\right)\left(\frac{v_{\rm rms}}{10\ \mathrm{km\ s^{-1}}}\right)$$
$$\times\left(\frac{\dot{\Sigma}_*}{4.5\times10^{-9}M_\odot\ \mathrm{pc^{-2}\ yr^{-1}}}\right),$$

(Li & Nakamura 2006 vs. Banerjee et al. 2008)

expanding HII regions

$$\dot{e}=\frac{\langle\delta p\rangle\mathcal{N}(>1)v_i}{Vt_i}$$
$$=(3\times10^{-30}\ \mathrm{erg\ s}\qquad ^{-3})$$
$$\times\left(\frac{N_{\rm H}}{1.5\times10^{22}\ \mathrm{cm^{-2}}}\right)^{-3/14}\left(\frac{M_{cl}}{10^6M_\odot}\right)^{1/14}$$
$$\times\left(\frac{\langle M_*\rangle}{440M_\odot}\right)\left(\frac{\mathcal{N}(>1)}{650}\right)\left(\frac{v_i}{10\ \mathrm{km\ s^{-1}}}\right)$$
$$\times\left(\frac{H_c}{100\ \mathrm{pc}}\right)^{-1}\left(\frac{R_{sf}}{15\ \mathrm{kpc}}\right)^{-2}\left(\frac{t_i}{18.5\ \mathrm{Myr}}\right)^{-1}$$

(note: different numbers by Matzner 2002

(from Mac Low & Klessen, 2004)

what drives ISM turbulence?

supernovae

$$\dot{e} = \frac{\sigma_{SN}\eta_{SN}E_{SN}}{\pi R_{sf}^2 H_c}$$

$$= (3\times10^{-26}\ \mathrm{erg\ s^{-1}\ cm^{-3}})\left(\frac{\eta_{SN}}{0.1}\right)\left(\frac{\sigma_{SN}}{1\ \mathrm{SNu}}\right) \times \left(\frac{H_c}{100\ \mathrm{pc}}\right)^{-1}\left(\frac{R_{sf}}{15\ \mathrm{kpc}}\right)^{-2}\left(\frac{E_{SN}}{10^{51}\ \mathrm{erg}}\right).$$

in star-forming parts of the disk, clearly SN provide enough energy to compensate for the decay of ISM turbulence.
BUT: what is outside the disk?

(from Mac Low & Klessen, 2004)

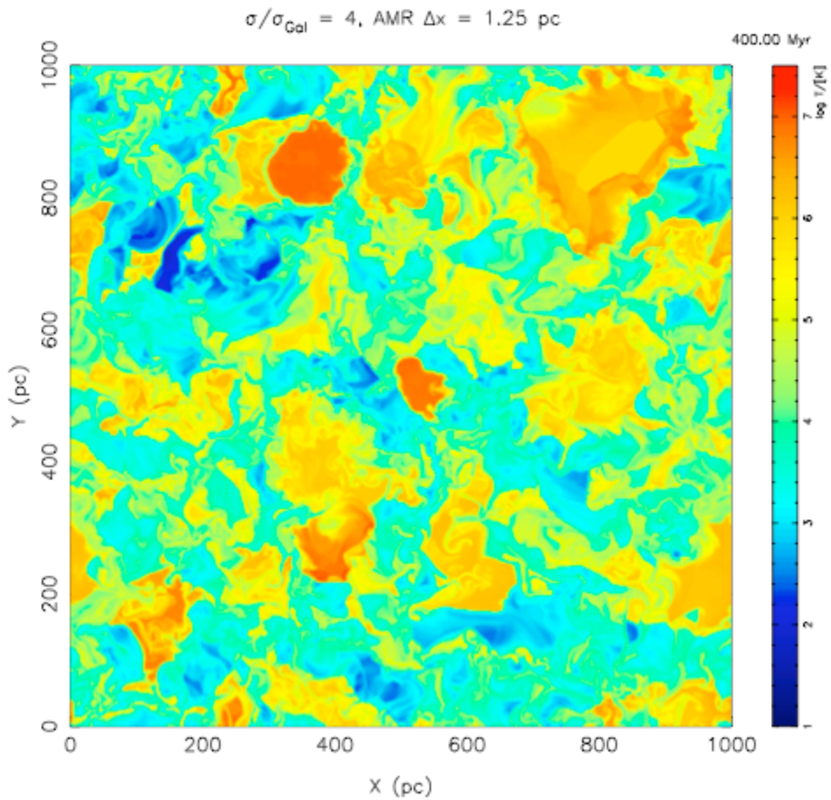

(distribution of temperature in SN driven disk turbulence, by de Avillez & Breitschwerdt 2004)

accretion driven turbulence

- thesis:
  - astrophysical objects *form* by *accretion* of ambient material
  - the *kinetic energy* associated with this process is a key agent *driving internal turbulence*.
  - this works on *ALL* scales:
    - galaxies
    - molecular clouds
    - protostellar accretion disks

Klessen & Hennebelle (2010, A&A, in press)

concept

- turbulence decays on a crossing time

$$\tau_{\rm d} \approx \frac{L_{\rm d}}{\sigma}.$$

- energy decay rate

$$\dot{E}_{\rm decay} \approx \frac{E}{\tau_{\rm d}} = -\frac{1}{2}\frac{M\sigma^3}{L_{\rm d}}$$

- kinetic energy of infalling material

$$\dot{E}_{\rm in} = \frac{1}{2}\dot{M}_{\rm in} v_{\rm in}^2$$

- can both values match, modulo some efficiency?

$$\epsilon = \left|\frac{\dot{E}_{\rm decay}}{\dot{E}_{\rm in}}\right|$$

(Field et al.. 2008, MNRAS, 385, 181, Mac Low & Klessen 2004, RMP, 76, 125)

some estimates from convergent flow studies

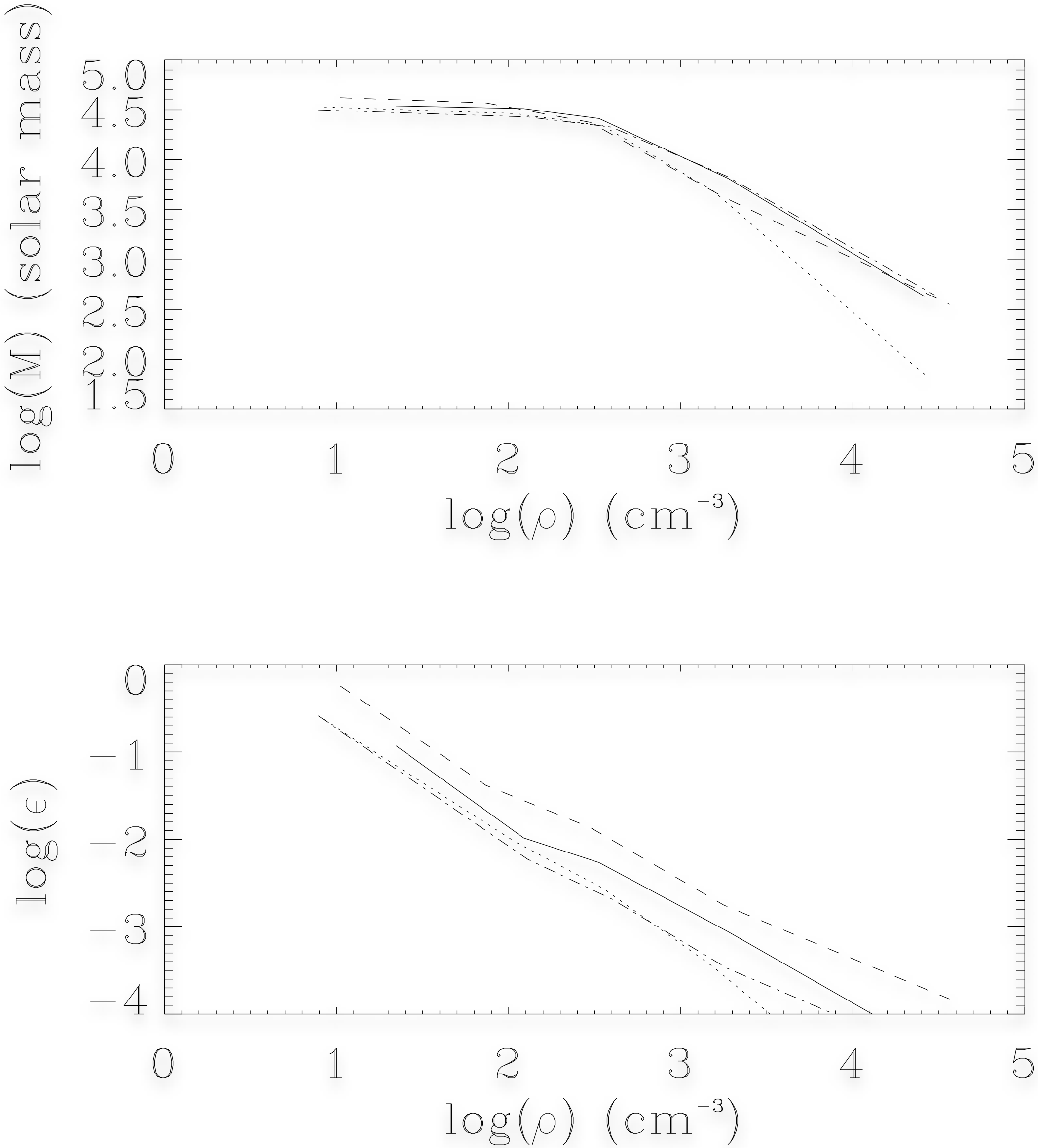

Klessen & Hennebelle (2010)

application to galaxies

- underlying assumption
  - galaxy is in steady state
    ---> accretion rate equals star formation rate
  - what is the required efficiency for the method to work?
- study Milky Way and 11 THINGS
  - excellent observational data in HI:
    velocity dispersion, column density, rotation curve

11 THINGS galaxies

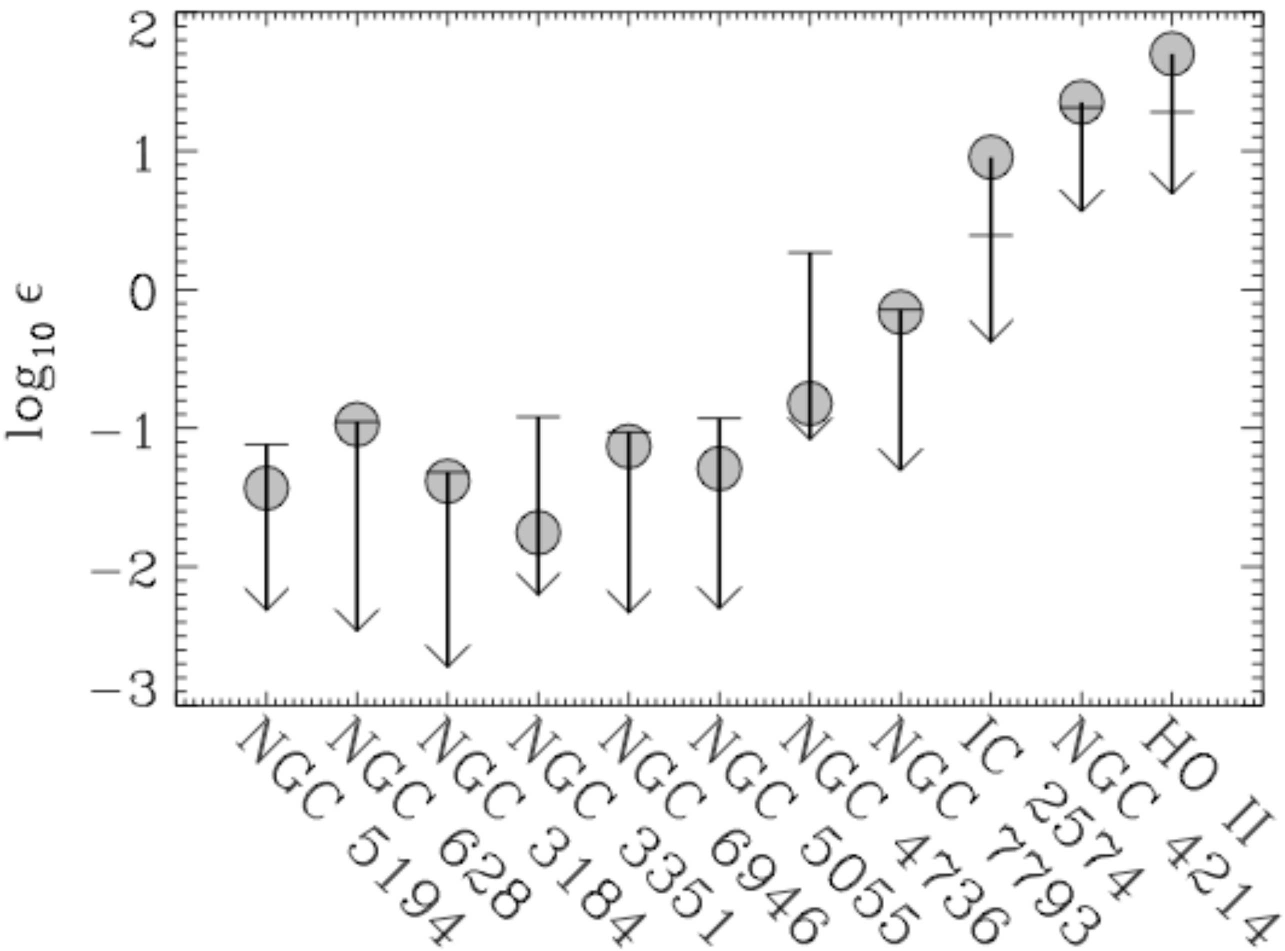

some further thoughts

- method works for Milky Way type galaxies:
  - required efficiencies are ~1% only!
- relevant for outer disks (extended HI disks)
  - there are not other sources of turbulence (certainly not stellar sources, maybe MRI)
- works well for molecular clouds
  - example clouds in the LMC (Fukui et al.)
- potentially interesting for TTS
  - model reproduces dM/dt - M relation (e.g Natta et al. 2006, Muzerolle et al. 2005, Muhanty et al. 2005, Calvet et al. 2004, etc.)

M83

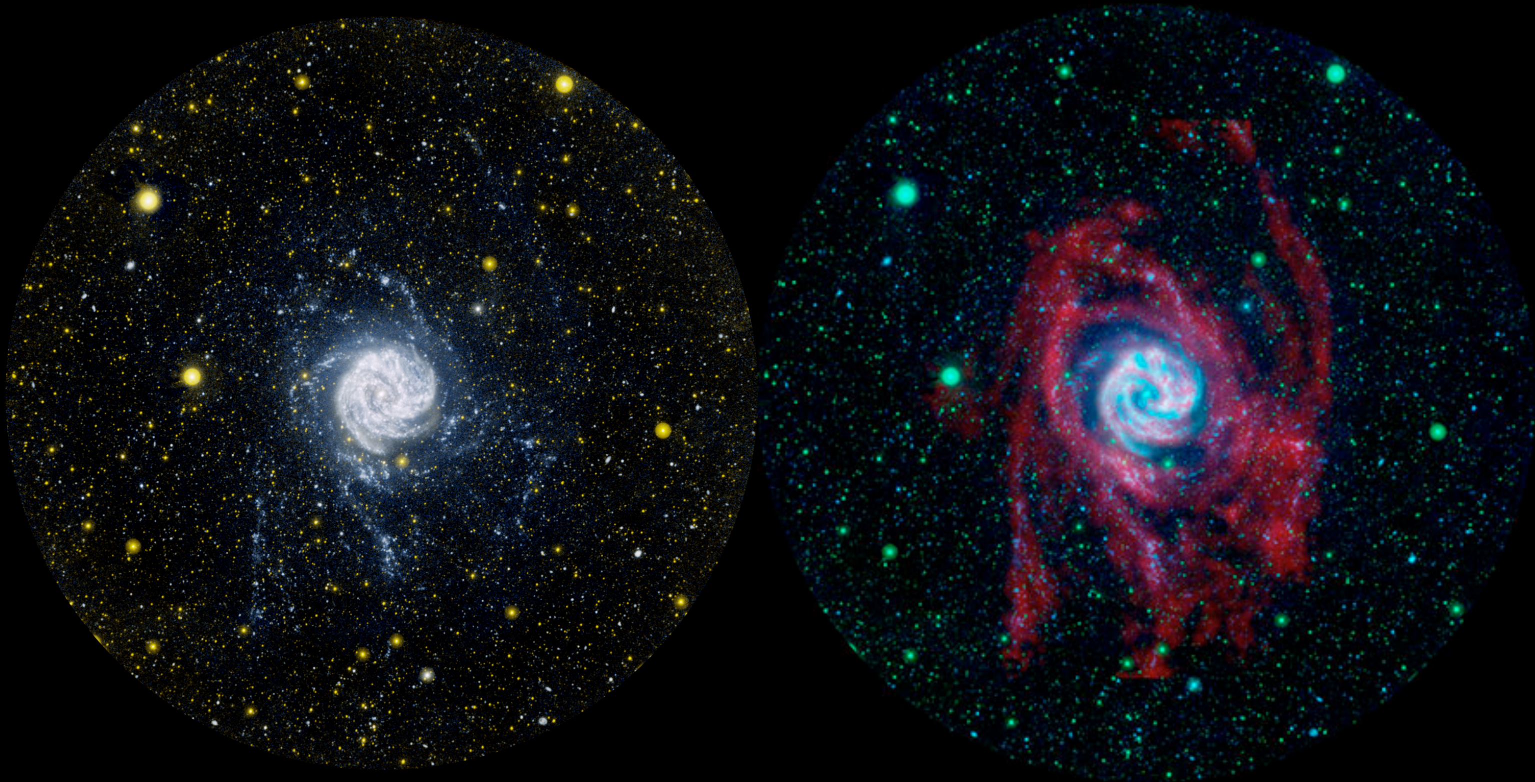

Do we actually see the flow through the disk?
ANSWER: Yes in M83!

M83 HI column

M83 HI velocity dispersion

M83

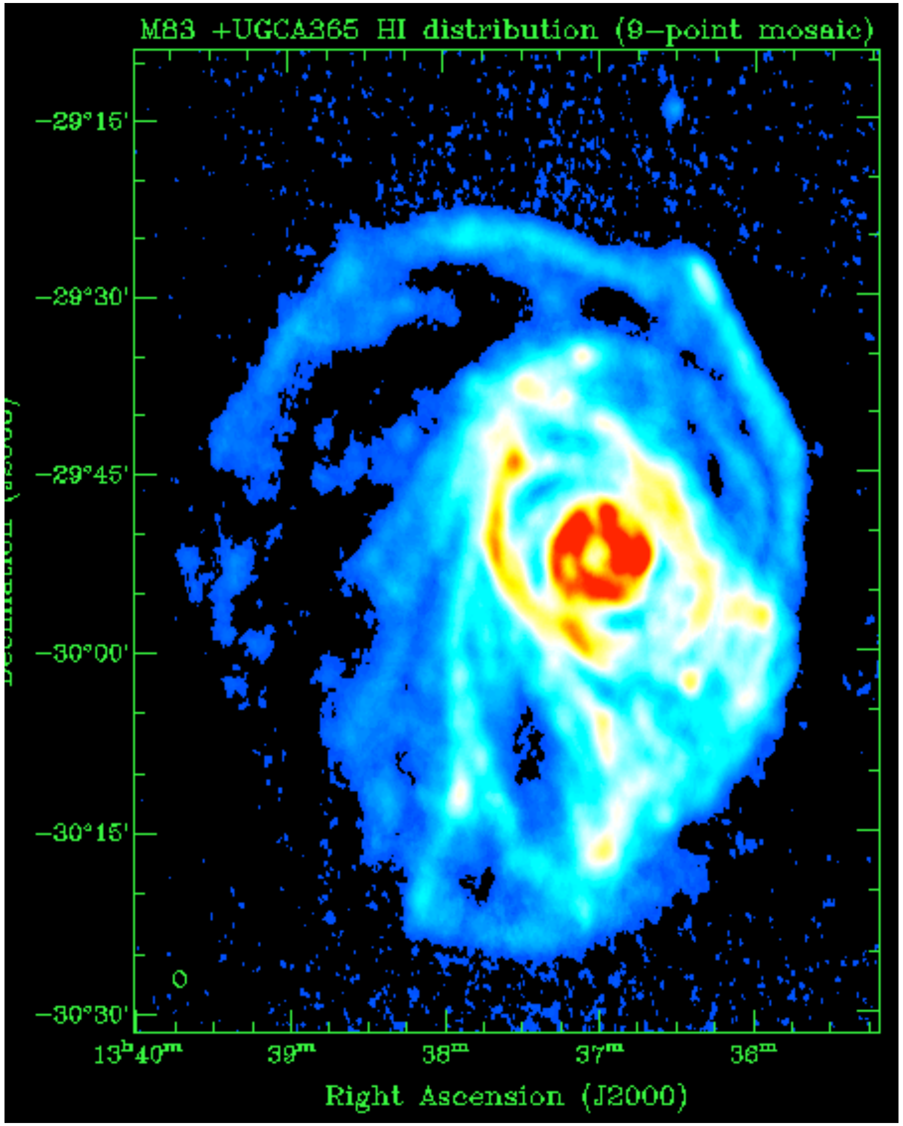

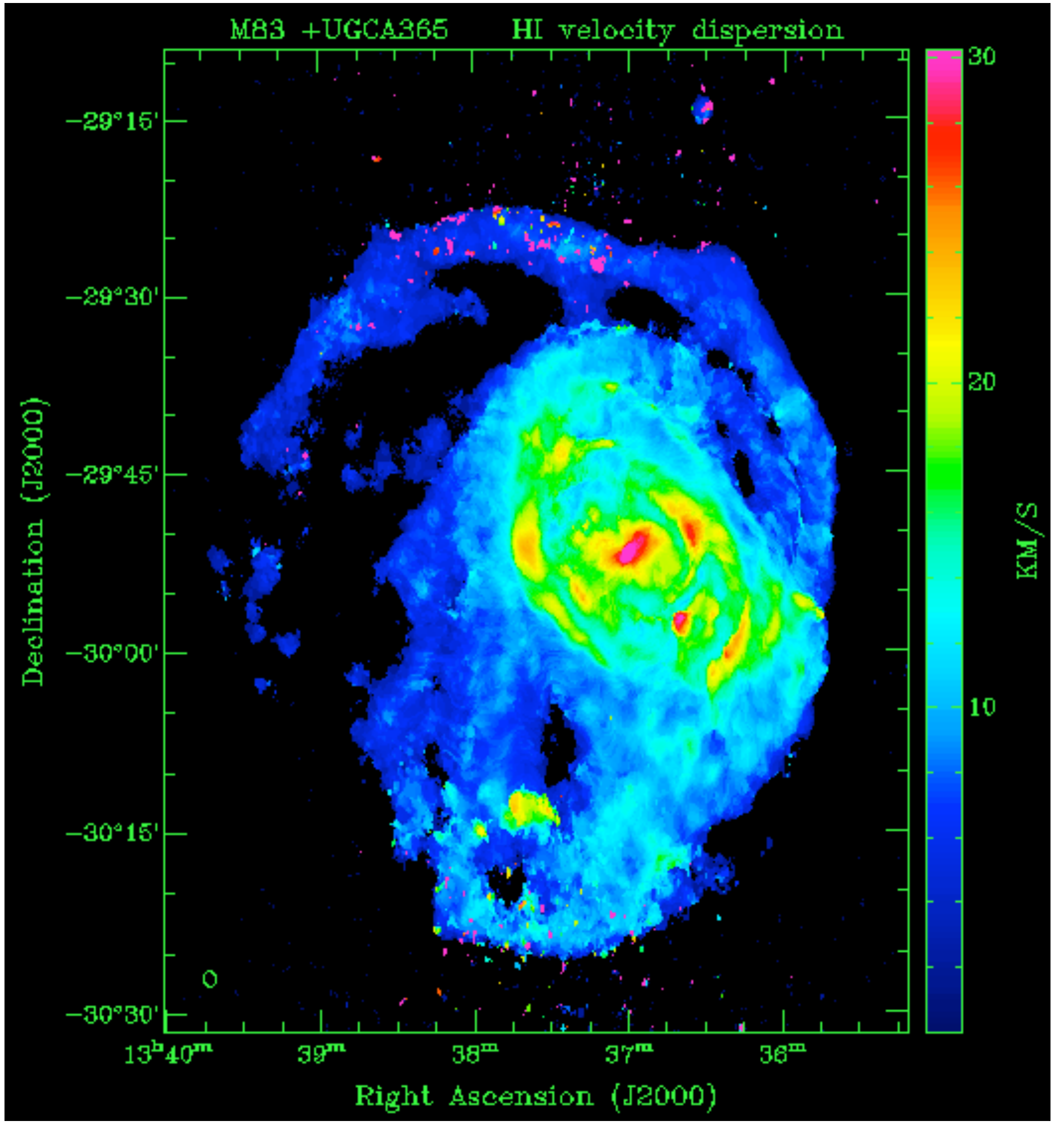

M83

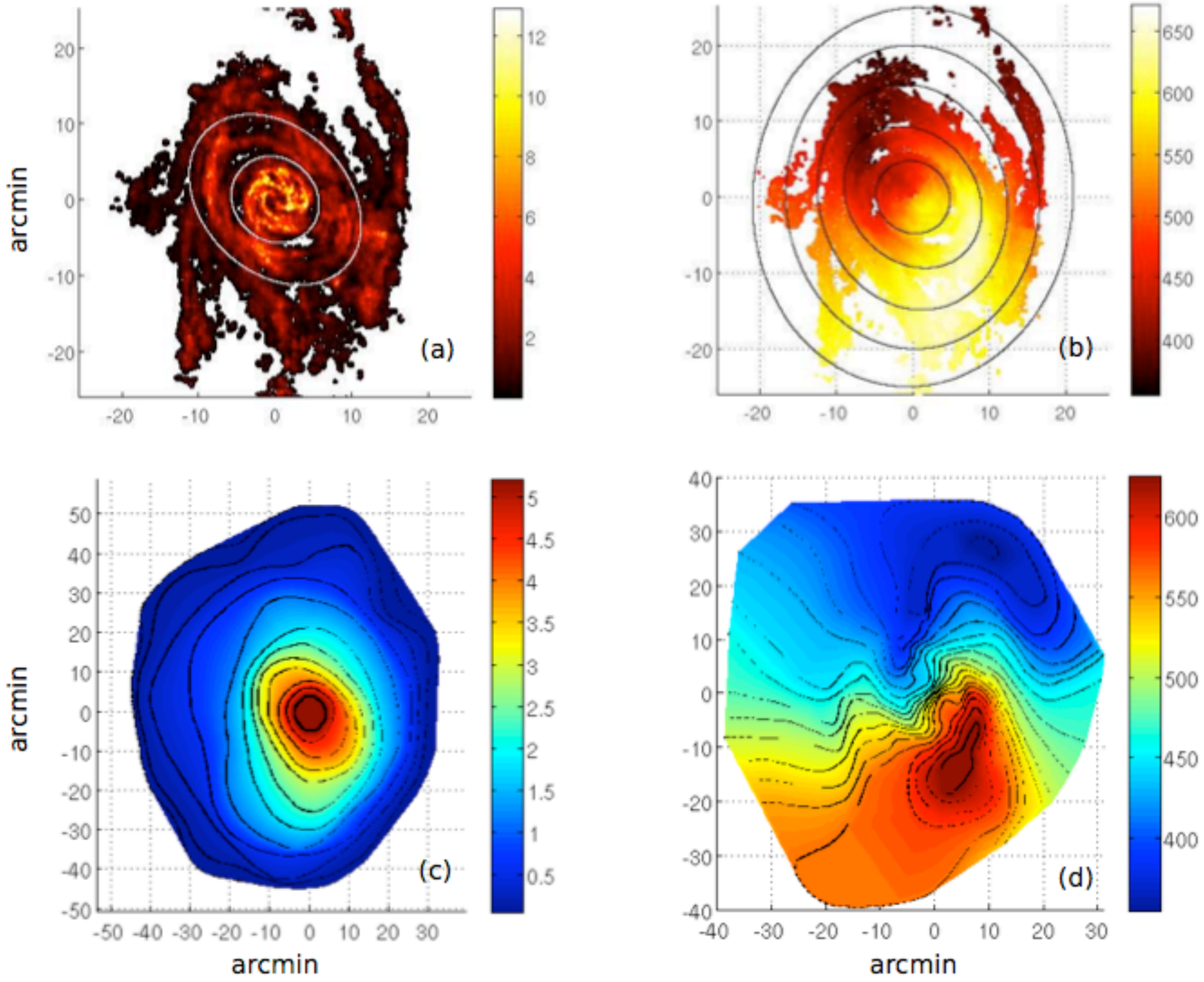

Figure 1. (a) The zeroth moment in units of $M_\odot$ pc^{-2} of the THINGS map. The white ellipses correpond to the black vertical lines ($R = 6', 12.75'$) shown in Fig. 3b, which define the region of the bright HI ring. (b) The first moment in units of km s^{-1} of the THINGS map. Each black ellipse is a result of a tilted circular ring at radii 5′, 10′, 15′, 20′, 25′, with a PA and an inclination extracted from the tilted-ring analysis. To associate structures with the corresponding radii, these ellipses serve as a coordinate system for the fiducial model with $V_{\rm max} = 180$ km s^{-1}. (c) Reconstructed HI intentisty map in units of column density $M_\odot$ pc^{-2} of the Effelsberg map. (d) Reconstructed line-of-sight velocity, $V_{\rm los}$ [km s^{-1}], of the Effelsberg map. The contours shown in (c) and (d) are extracted from HB81 and are used to reconstruct the Effelsberg map.

M83

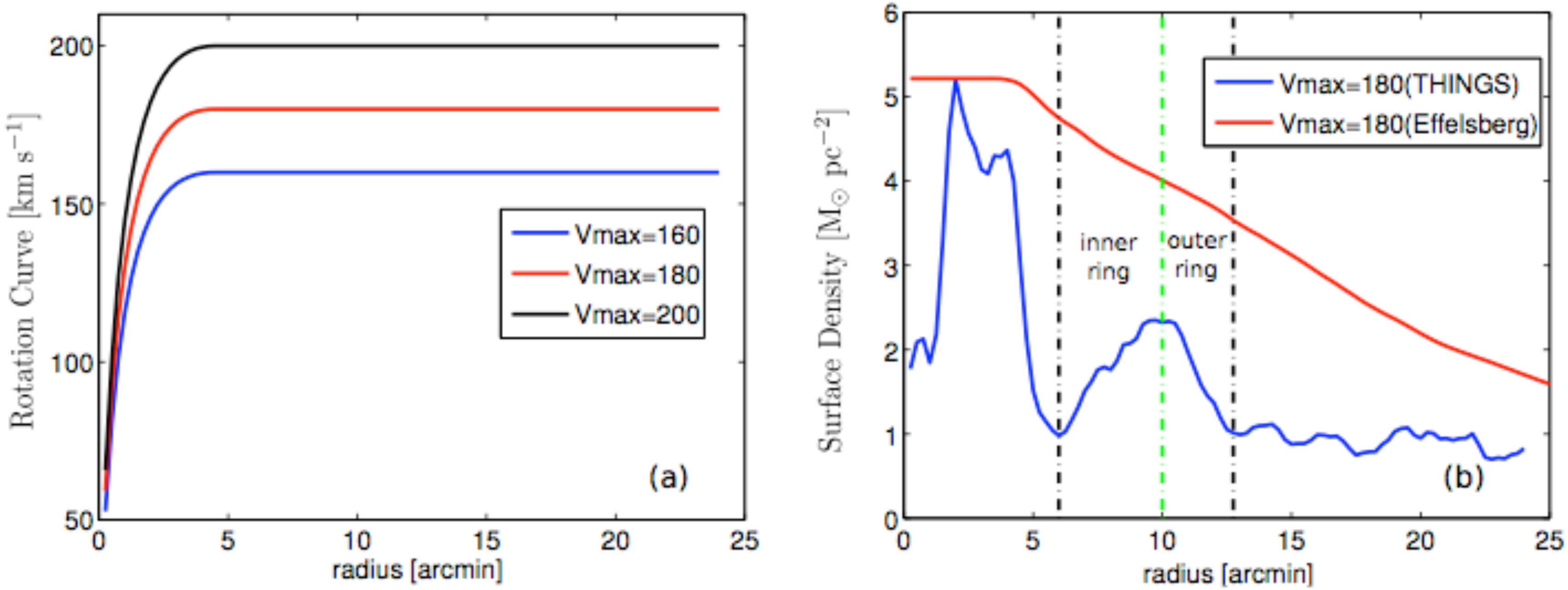

Figure 3. (a) The Brandt-type flat rotation curves as described in Eq. (13). Due to the low inclination of M83, we bracket the real situation with a range of different rotation curves and corresponding fit parameters from the tilted ring model. We assume $n = 0.8$, $R_{\rm max} = 4.5'$, $V_{\rm max} = 160, 180, 200$ km s^{-1}. As suggested in HB81, we take the model with $V_{\rm max} = 180$ as our fiducial case, which will then be justified in § 5. (b) The averaged surface density of the THINGS map (blue curve) and of the Effelsberg map (red curve). They are extracted from the fiducial model. The black vertical lines situated at $6'$ and $12.75'$ define the region of ring structure, which is also shown as the area enclosed by the white ellipses in Fig. 1a and the black ellipses in Fig. 7. The green vertical line marks the location of the density peak and further divides the ring into an inner ring and an outer ring.

M83

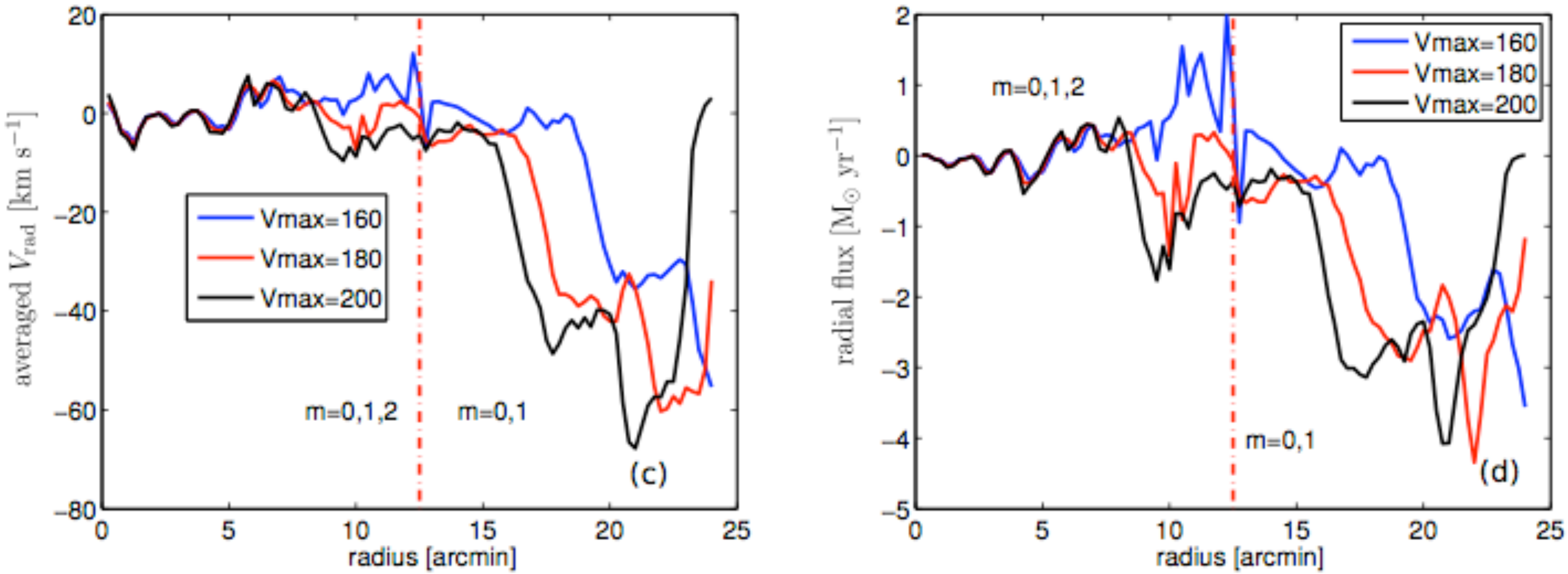

Figure 5. (a) PA and (b) inclination models used to infer radial motion of the gas in the THINGS map. (c) The inferred radial velocity. (d) The inferred radial mass flow. PA and inclination inside the vertical line ($R = 12.5'$) are extracted from the THINGS map, while in the other part we extrapolate these quantities from the Effelsberg map. The Fourier coefficients are fitted for the harmonics $m = 0, 1, 2$ for the radial regime to the left of the vertical line, while only $m = 0, 1$ for the outer parts of the map. In the outer disk, the radial shift is due the different inclinations corresponding to the different models. In all models, the common features are the prominent radial inflow in the outer disk, epicyclic motion in the transition zone (where the HI is organized into a ring like structure, see also Fig. 7 and an indication of moderate radial inflow in the inner disk.

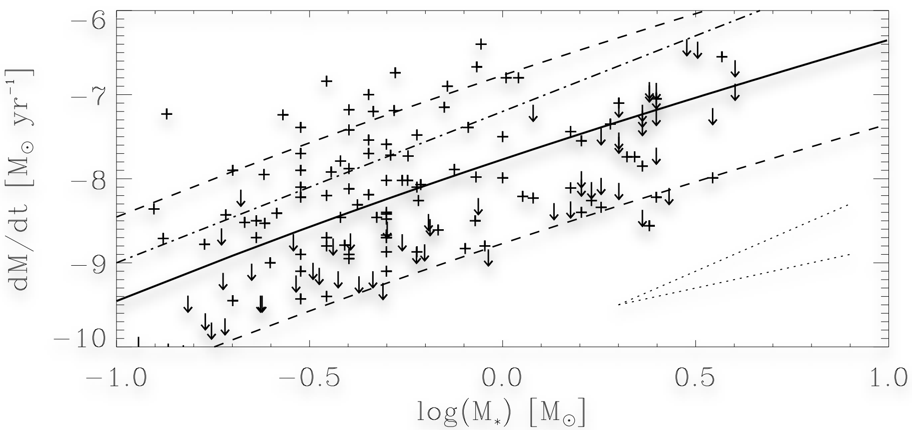

Fig. 7. Prediction of the accretion rate onto the disk as a function of the mass of the star. The solid line corresponds to a mean density of $\bar{n} = 100\,\mathrm{cm}^{-3}$ while the two dashed lines are for $\bar{n} = 1000\ \mathrm{cm}^{-3}$ (upper curve) and $\bar{n} = 10\ \mathrm{cm}^{-3}$ (lower curve). To guide your eye the dotted lines indicate the slope of the relations $\dot{M} \propto M_*^2$ and $\dot{M} \propto M_*$. We compare with data from Calvet et al. (2004), Mohanty et al. (2005), Muzerolle et al. (2005), and Natta et al. (2006) as displayed in Figure 3 of Garcia Lopez et al. (2006), where crosses indicate detections and arrows upper limits. The dot-dashed line is the fit proposed by Natta et al. (2006).

Lecture 3 + 4: star (cluster) formation and the IMF

- ingrediences of star (cluster) formation
  - dynamics in gas and stars
  - importance of thermydynamics
  - effects of magnetic fields
  - radiative feedback
- different IMF models
  - comments on low-mass end
  - comments on high-mass end

theory

Early dynamical theory

- *Jeans (1902):* Interplay between self-gravity and thermal pressure
  - stability of homogeneous spherical density enhancements against gravitational collapse
  - dispersion relation:

$$\boxed{\omega^2 = c_s^2 k^2 - 4\pi G \rho_0}$$

  - instability when $\omega^2 < 0$
  - minimal mass:

$$\boxed{M_J = \tfrac{1}{6}\pi^{-5/2} G^{-3/2} \rho_0^{-1/2} c_s^3 \propto \rho_0^{-1/2} T^{-3/2}}$$

Sir James Jeans, 1877 - 1946

(full detail in Mac Low & Klessen, 2004, Rev. Mod. Phys., 76, 125-194)

First approach to turbulence

- *von Weizsäcker (1943, 1951)* and *Chandrasekhar (1951):* concept of **MICROTURBULENCE**
  - BASIC ASSUMPTION: separation of scales between dynamics and turbulence

    $\ell_{\mathrm{turb}} \ll \ell_{\mathrm{dyn}}$

  - then turbulent velocity dispersion contributes to effective soundspeed:

$$\boxed{c_c^2 \mapsto c_c^2 + \sigma_{rms}^2}$$

  - → Larger effective Jeans masses → more stability
  - BUT: *(1) turbulence depends on k:* $\sigma_{rms}^2(k)$

    (2) supersonic turbulence → $\sigma_{rms}^2(k) >> c_s^2$ *usually*

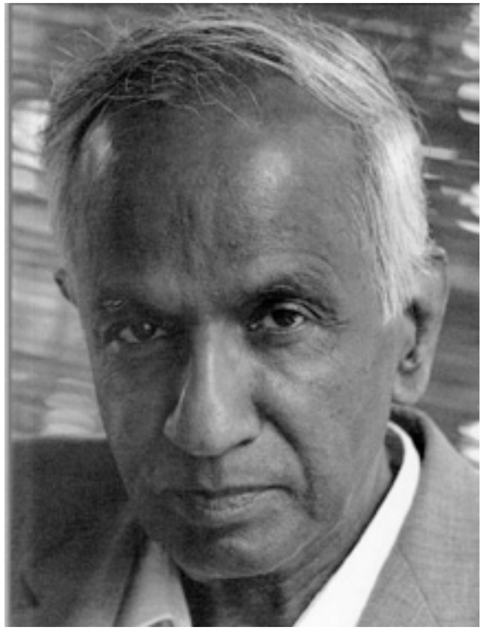

S. Chandrasekhar, 1910 - 1995

(full detail in Mac Low & Klessen, 2004, Rev. Mod. Phys., 76, 125-194)

Problems of early dynamical theory

- Molecular clouds are *highly Jeans-unstable*
  Yet, they do *NOT* form stars at high rate
  and with high efficiency.
  (the observed global SFE in molecular clouds is *~5%*)
  → *something prevents large-scale collapse.*
- All throughout the early 1990's, molecular clouds had been thought to be long-lived quasi-equilitrium entities.
- Molecular clouds are *magnetized.*

(full detail in Mac Low & Klessen, 2004, Rev. Mod. Phys., 76, 125-194)

Magnetic star formation

- *Mestel & Spitzer (1956):* Magnetic fields can prevent collapse*!!!*
  - Critical mass for gravitational collapse in presence of B-field

$$M_{cr} = \frac{5^{3/2}}{48\pi^2} \frac{B^3}{G^{3/2}\rho^2}$$

  - Critical mass-to-flux ratio (Mouschovias & Spitzer 1976)

$$\left[\frac{M}{\Phi}\right]_{cr} = \frac{\zeta}{3\pi}\left[\frac{5}{G}\right]^{1/2}$$

  - Ambipolar diffusion can initiate collapse

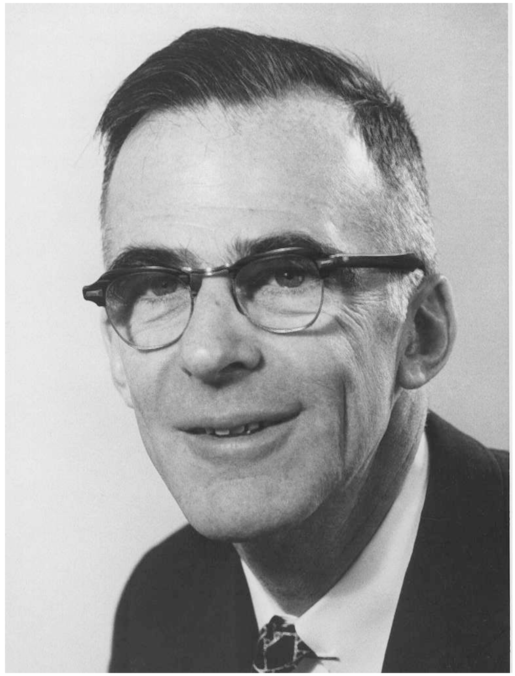

Lyman Spitzer, Jr., 1914 - 1997

(full detail in Mac Low & Klessen, 2004, Rev. Mod. Phys., 76, 125-194)

The "standard theory" of star formation:

- BASIC ASSUMPTION: Stars form from magnetically highly subcritical cores
- Ambipolar diffusion slowly increases (M/Φ): $\tau_{AD} \approx 10\tau_{ff}$
- Once $(M/\Phi) > (M/\Phi)_{crit}$: dynamical collapse of SIS
  - Shu (1977) collapse solution
  - $dM/dt = 0.975\ c_s^3/G$ = const.
- Was (in principle) only intended for isolated, low-mass stars

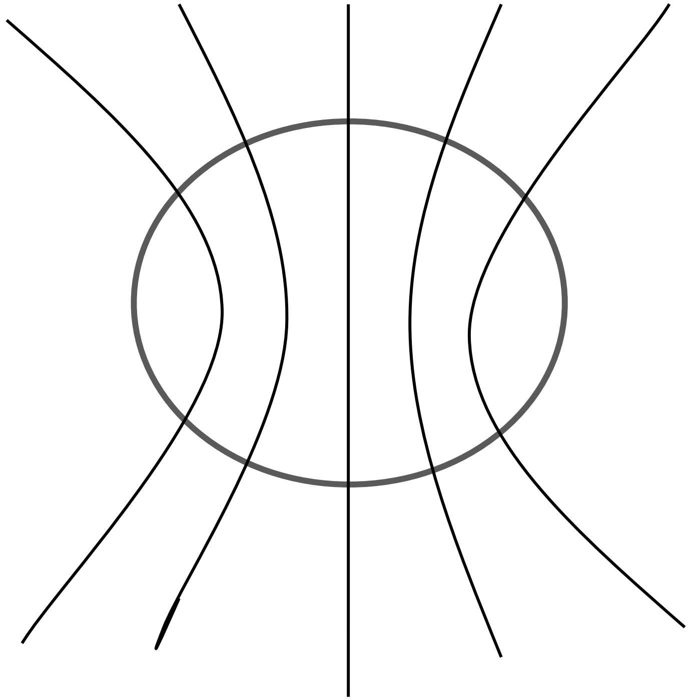

Problems of magnetic SF

- Observed B-fields are weak, at most marginally critical (Crutcher 1999, Bourke et al. 2001)
- Magnetic fields cannot prevent decay of turbulence
  (Mac Low et al. 1998, Stone et al. 1998, Padoan & Nordlund 1999)
- Structure of prestellar cores
  (Bacman et al. 2000, e.g. Barnard 68 from Alves et al. 2001)
- Strongly time varying dM/dt
  (e.g. Hendriksen et al. 1997, André et al. 2000)
- More extended infall motions than predicted by the standard model
  (Williams & Myers 2000, Myers et al. 2000)

Observed B-fields are weak

B versus $N(H_2)$ from *Zeeman measurements*.
(from Bourke et al. 2001)

→ cloud cores are magnetically supercritical***!!!***

$(\Phi/M)_n > 1$ no collapse

$(\Phi/M)_n < 1$ collapse

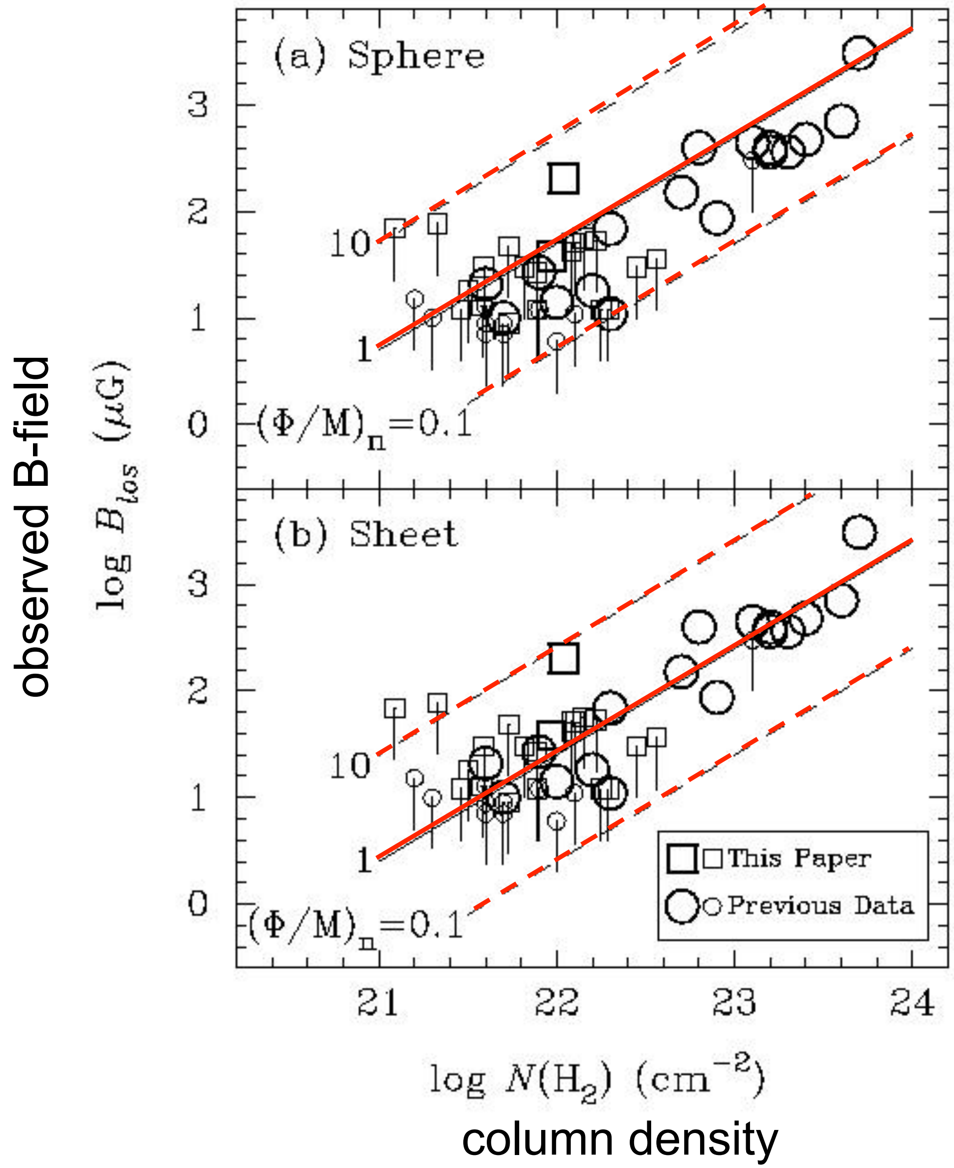

Problems of magnetic SF

- Observed B-fields are weak, at most marginally critical (Crutcher 1999, Bourke et al. 2001)
- Magnetic fields cannot prevent decay of turbulence
  (Mac Low et al. 1998, Stone et al. 1998, Padoan & Nordlund 1999)
- Structure of prestellar cores
  (Bacman et al. 2000, e.g. Barnard 68 from Alves et al. 2001)
- Strongly time varying dM/dt
  (e.g. Hendriksen et al. 1997, André et al. 2000)
- More extended infall motions than predicted by the standard model
  (Williams & Myers 2000, Myers et al. 2000)

Molecular cloud dynamics

- **Timescale problem:** Turbulence *decays* on timescales *comparable to the free-fall time* τ_{ff} ($E \propto t^{-\eta}$ with $\eta \approx 1$).

  (Mac Low et al. 1998,
  Stone et al. 1998,
  Padoan & Nordlund 1999)

- Magnetic fields (static or wave-like) *cannot* prevent loss of energy.

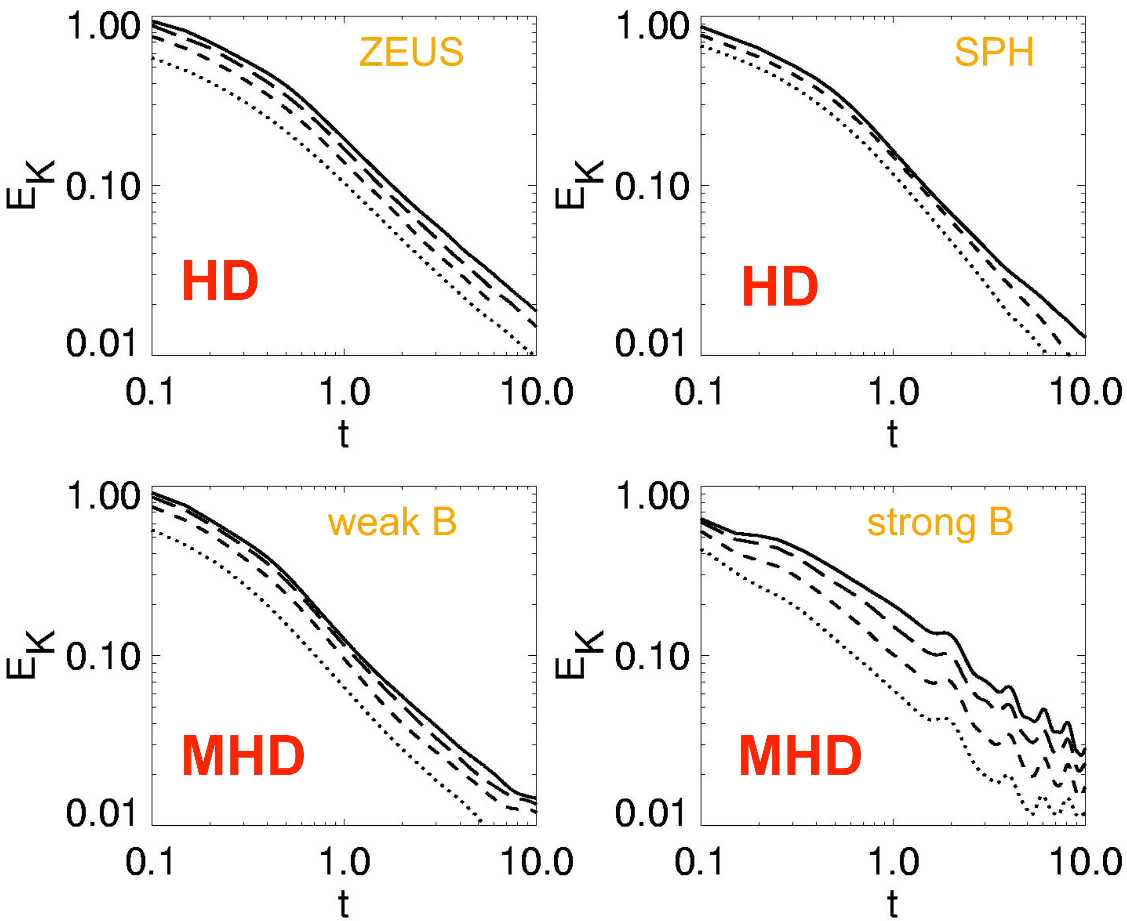

(Mac Low, Klessen, Burkert, & Smith, 1998, PRL)

Problems of magnetic SF

- As many prestellar cores as protostellar cores in SF regions (e.g. André et al 2002)
- Molecular cloud clumps seem to be chemically young
  (Bergin & Langer 1997, Pratap et al 1997, Aikawa et al 2001)
- Stellar age distribution small ($\tau_{ff} << \tau_{AD}$)
  (Ballesteros-Paredes et al. 1999, Elmegreen 2000, Hartmann 2001)
- Strong theoretical criticism of the SIS as starting condition for gravitational collapse
  (e.g. Whitworth et al 1996, Nakano 1998, as summarized in Klessen & Mac Low 2004)
- Most stars form as binaries

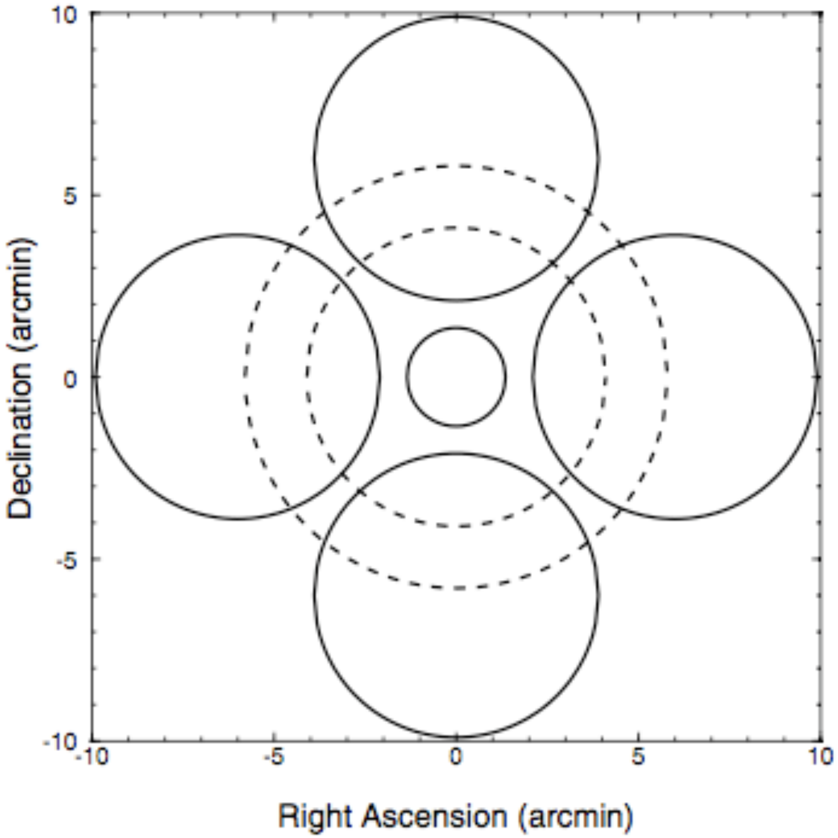

Fig. 1.— The Arecibo telescope primary beam (small circle centered at 0,0) and the four GBT telescope primary beams (large circles centered 6′ north, south, east, and west of 0,0. The dotted circles show the first sidelobe of the Arecibo telescope beam. All circles are at the half-power points.

Crutcher et al. (2008)

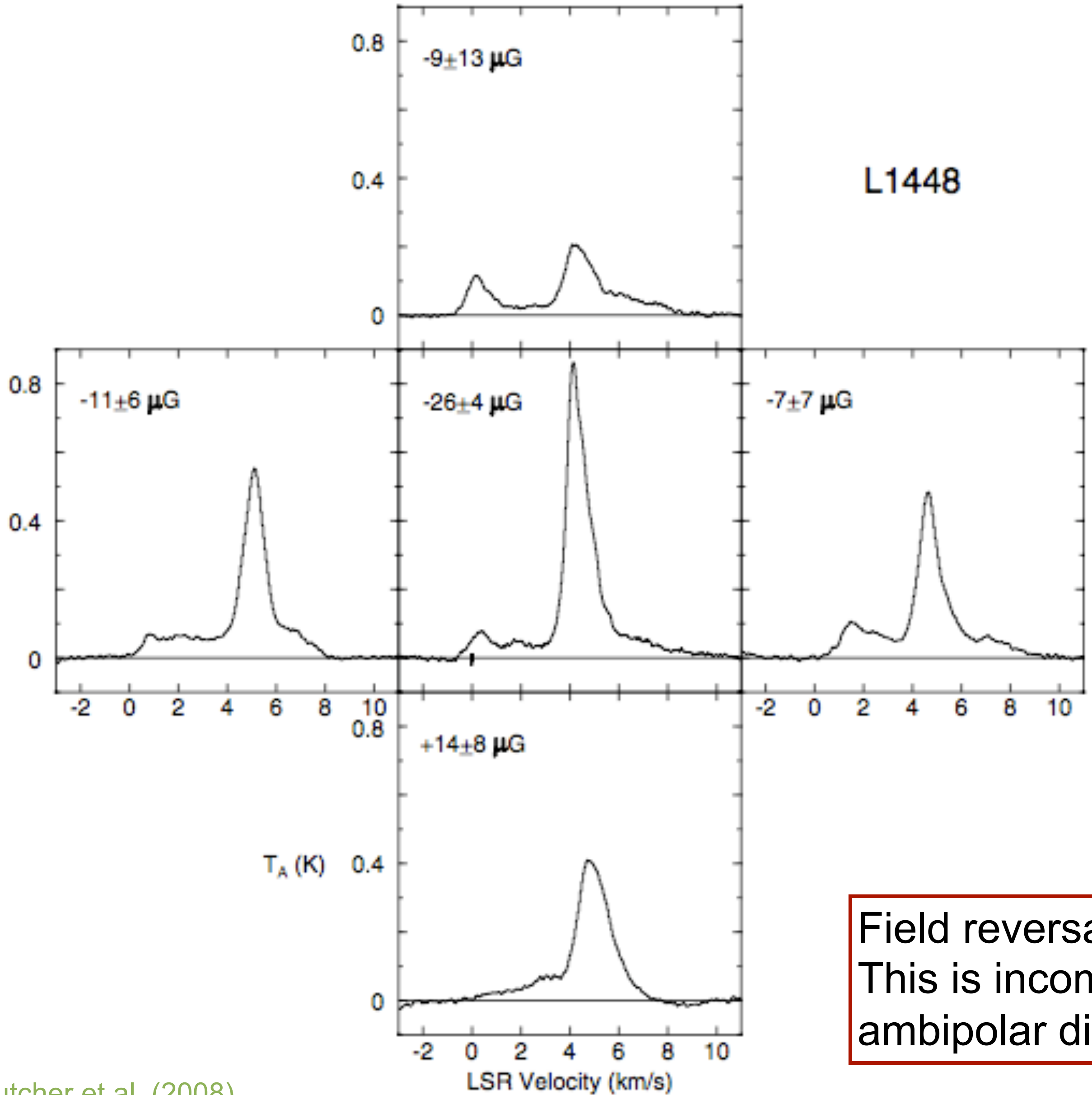

Field reversal in the outer parts.
This is incompatible with "standard" ambipolar diffusion theory!

Crutcher et al. (2008)

Fig. 2.— OH 1667 MHz spectra toward the core of L1448CO obtained with the Arecibo telescope (center panel) and toward each of the envelope positions 6′ north, south, east, and west of the core, obtained with the GBT. In the upper left of each panel is the inferred B_{LOS} and its 1σ uncertainty at that position. A negative B_{LOS} means the magnetic field points toward the observer, and vice versa for a positive B_{LOS}.

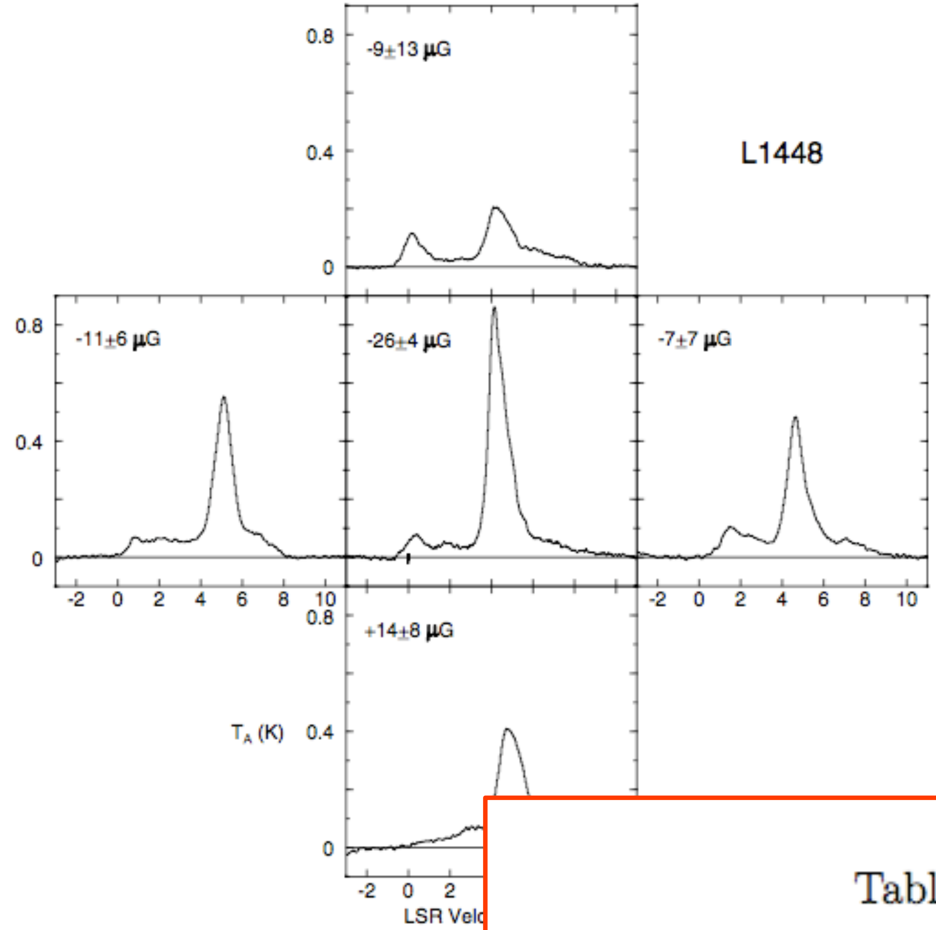

Fig. 2.— OH 1667 MHz spectra toward the
telescope (center panel) and toward each of the
west of the core, obtained with the GBT. In the
and its 1σ uncertainty at that position. A neg
toward the observer, and vice versa for a posit

example: L1448

Table 2. Relative Mass/Flux

Cloud	$\mathcal{R}$	$\mathcal{R}'$	Probability $\mathcal{R}$ or $\mathcal{R}' > 1$
L1448CO	0.02 ± 0.36	0.07 ± 0.34	0.005
B217-2	0.15 ± 0.43	0.19 ± 0.41	0.05
L1544	0.42 ± 0.46	0.46 ± 0.43	0.11
B1	0.41 ± 0.20	0.44 ± 0.19	0.010

Crutcher et al. (2008)

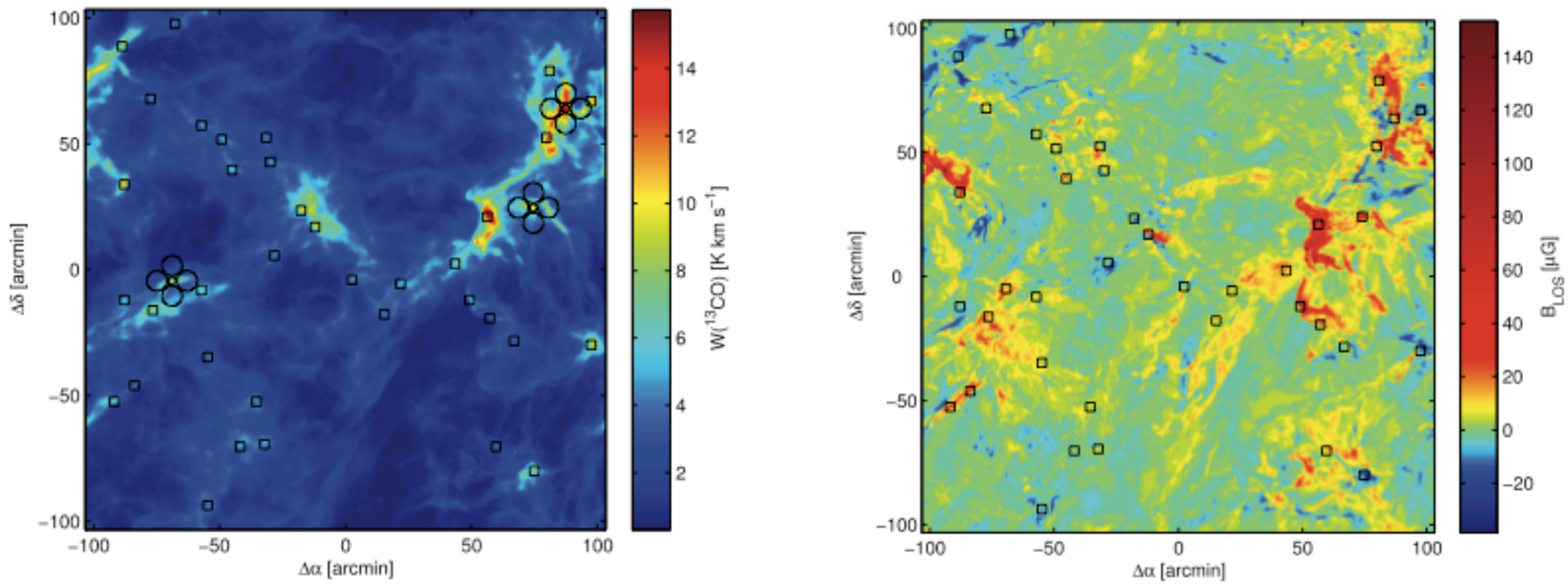

FIG. 1.—*Left*: Simulated [13]CO (1–0) map of the model in the *z*-axis direction. The locations of the cloud cores are shown with squares. The circles indicate the locations of telescope beams used in the synthetic observations of three cores. *Right*: Line-of-sight magnetic field strength as calculated from Zeeman splitting.

Lunttila et al. (2008)

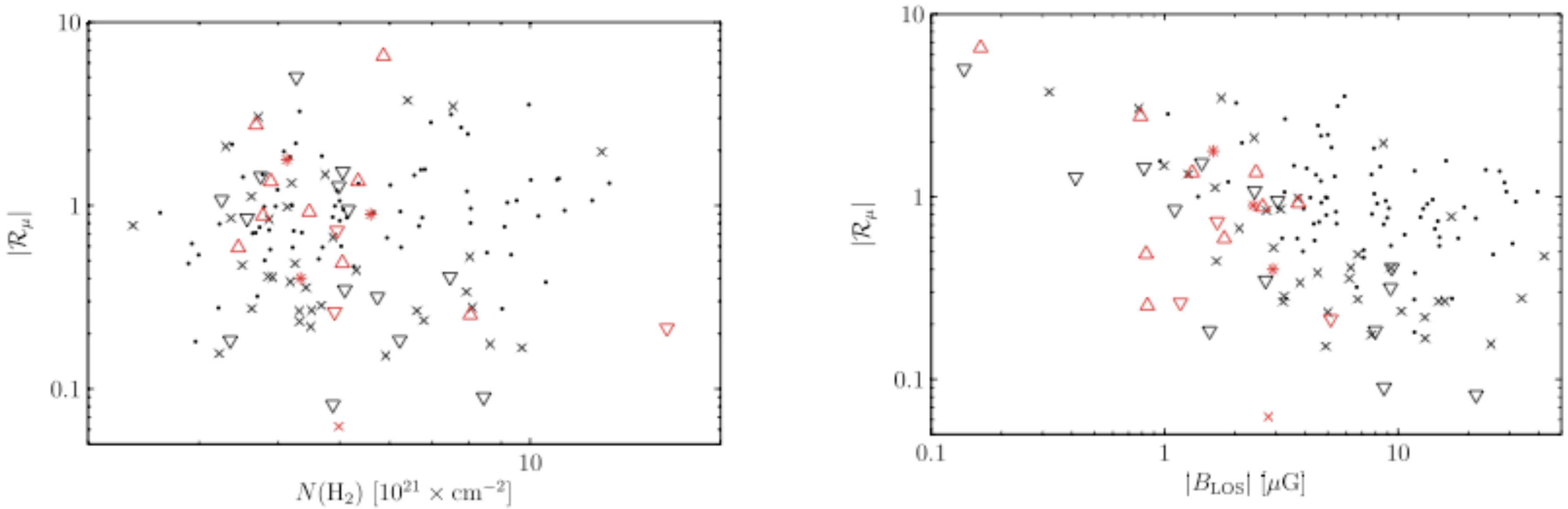

FIG. 3.—*Left*: Relative mass-to-flux ratio for the selected cores as a function of column density. Red symbols indicate the cores with $\mathcal{R}_\mu < 0$. Dots, crosses, triangles pointing down, triangles pointing up, and asterisks denote zero, one, two, three, or four field reversals in the envelopes relative to the core center. *Right*: Relative mass-to-flux ratio as a function of inferred magnetic field strength in the central beam. The symbols have the same meaning as in the left panel.

Lunttila et al. (2008)

current view

gravoturbulent star formation

- idea:

Star formation is controlled by interplay between gravity and supersonic turbulence!

- dual role of turbulence:
  - *stability on large scales*
  - *initiating collapse on small scales*

(e.g., Larson, 2003, Rep. Prog. Phys, 66, 1651;
or Mac Low & Klessen, 2004, Rev. Mod. Phys., 76, 125)

gravoturbulent star formation

- idea:

Star formation is controlled by interplay between gravity and supersonic turbulence!

- validity:

This hold on *all* scales and applies to build-up of stars and star clusters within molecular clouds as well as to the formation of molecular clouds in galactic disk.

(e.g., Larson, 2003, Rep. Prog. Phys, 66, 1651;
or Mac Low & Klessen, 2004, Rev. Mod. Phys., 76, 125)

gravotturbulent star formation

- interstellar gas is highly *inhomogeneous*
  - *gravitational instability*
  - *thermal instability*
  - *turbulent compression* (in shocks $\delta\rho/\rho \propto \mathcal{M}^2$; in atomic gas: $\mathcal{M} \approx 1...3$)

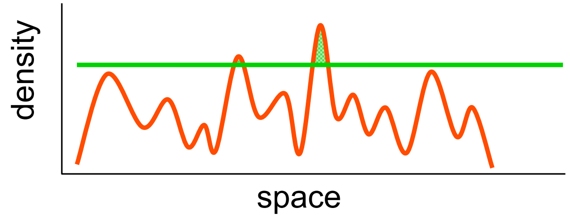

- cold *molecular clouds* can form rapidly in high-density regions at *stagnation points* of *convergent large-scale flows*
  - chemical *phase transition*: atomic → molecular
  - process is *modulated* by large-scale *dynamics* in the galaxy
- inside *cold clouds:* turbulence is highly supersonic ($\mathcal{M} \approx 1...20$)
  → *turbulence* creates large density contrast,
  gravity selects for collapse

  ⟶ ***GRAVOTUBULENT FRAGMENTATION***

- *turbulent cascade:* local compression *within* a cloud provokes collapse → formation of individual *stars* and *star clusters*

different statistical approaches

- there are different quantitative IMF based on turbulence
  - Padoan & Nordlund (2002, 2007)
  - Hennebelle & Chabrier (2008, 2009)
  - both relate the mass spectrum to statistical characteristics of the turbulent velocity fields

The Astrophysical Journal, 684:395–410, 2008 September 1

ANALYTICAL THEORY FOR THE INITIAL MASS FUNCTION: CO CLUMPS AND PRESTELLAR CORES

Patrick Hennebelle
Laboratoire de Radioastronomie, UMR CNRS 8112, École Normale Supérieure et Observatoire de Paris,
24 rue Lhomond, 75231 Paris Cedex 05, France

and

Gilles Chabrier[1]
École Normale Supérieure de Lyon, CRAL, UMR CNRS 5574, Université de Lyon, 69364 Lyon Cedex 07, France
Received 2008 February 12; accepted 2008 May 4

different statistical approaches

- there are different quantitative IMF based on turbulence
  - Padoan & Nordlund (2002, 2007)
  - Hennebelle & Chabrier (2008, 2009)
  - both relate the mass spectrum to statistical characteristics of the turbulent velocity fields

THE ASTROPHYSICAL JOURNAL, 684:395–410, 2008 September 1

ANALYTICAL THEORY FOR THE INITIAL MASS FUNCTION: CO CLUMPS AND PRESTELLAR CORES

THE ASTROPHYSICAL JOURNAL, 702:1428–1442, 2009 September 10 doi:10.1088/0004-637X/702/2/1428

ANALYTICAL THEORY FOR THE INITIAL MASS FUNCTION. II. PROPERTIES OF THE FLOW

PATRICK HENNEBELLE[1] AND GILLES CHABRIER[2]
[1] Laboratoire de radioastronomie, UMR CNRS 8112, École normale supérieure et Observatoire de Paris, 24 rue Lhomond, 75231 Paris cedex 05, France
[2] École normale supérieure de Lyon, CRAL, UMR CNRS 5574, Université de Lyon, 69364 Lyon Cedex 07, France
Received 2009 April 1; accepted 2009 July 17; published 2009 August 21

different statistical approaches

- there are different quantitative IMF based on turbulence
  - Padoan & Nordlund (2002, 2007)
  - Hennebelle & Chabrier (2008, 2009)

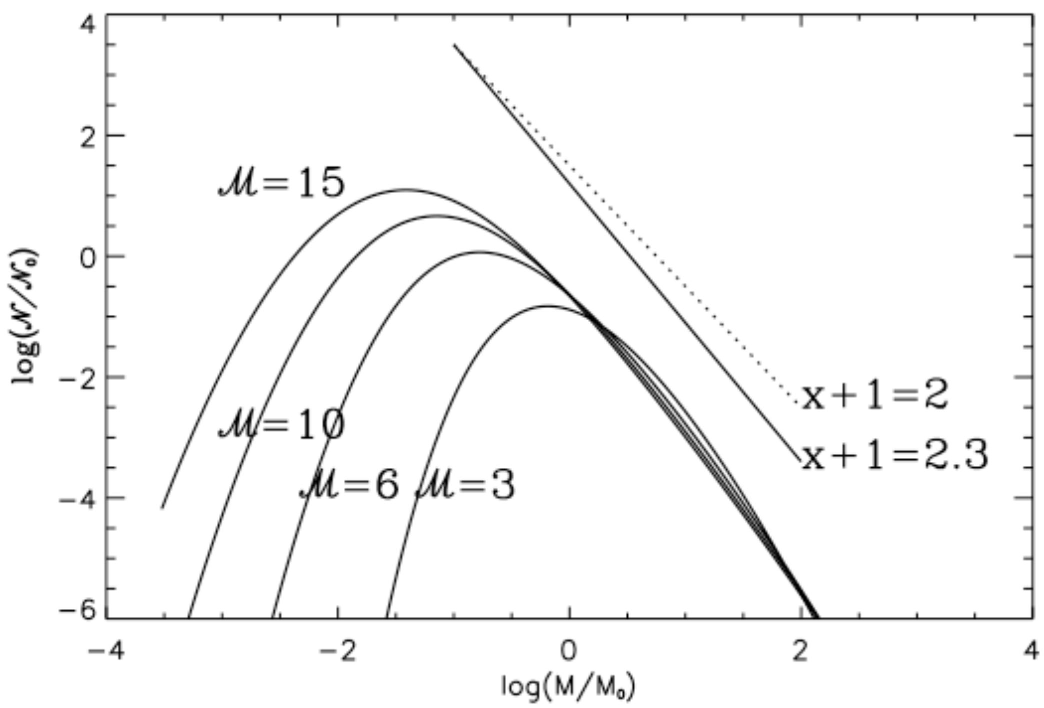

FIG. 2.—Mass spectrum for $\mathcal{M}_*^2 = 2$ and various values of $\mathcal{M}$.

different statistical approaches

- there are different quantitative IMF based on turbulence
  - Padoan & Nordlund (2002, 2007)
  - Hennebelle & Chabrier (2008, 2009)
  - both relate the mass spectrum to statistical characteristics of the turbulent velocity fields
- there are alternative approaches
  - IMF as closest packing problem / *sampling* problem in *fractal* clouds (Larson 1992, 1995, Elmegreen 1997ab, 2000ab, 2002)
  - IMF as purely *statistical* problem (Larson 1973, Zinnecker 1984, 1990, Adams & Fatuzzo 1996)
  - IMF from (proto)stellar *feedback* (Silk 1995, Adams & Fatuzzo 1996)
  - IMF from competitive *coagulation* (Murray & Lin 1995, Bonnell et al. 2001ab, etc.)

caveat: everybody gets the IMF!

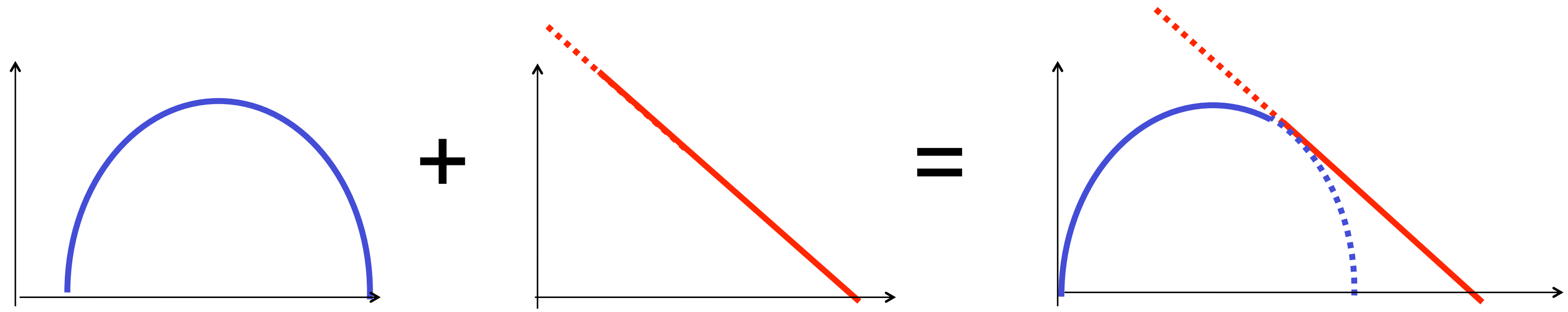

- combine scale free process → *POWER LAW BEHAVIOR*
  - turbulence (Padoan & Nordlund 2002, Hennebelle & Chabrier 2008)
  - gravity in dense clusters (Bonnell & Bate 2006, Klessen 2001)
  - universality: dust-induced EOS kink insensitive to radiation field (Elmegreen et al. 2008)
- with highly stochastic processes → central limit theorem
  → *GAUSSIAN DISTRIBUTION*
  - basically mean thermal Jeans length (or feedback)
  - universality: insensitive to metallicity (Clark et al. 2009, submitted)

caveat: everybody gets the IMF!

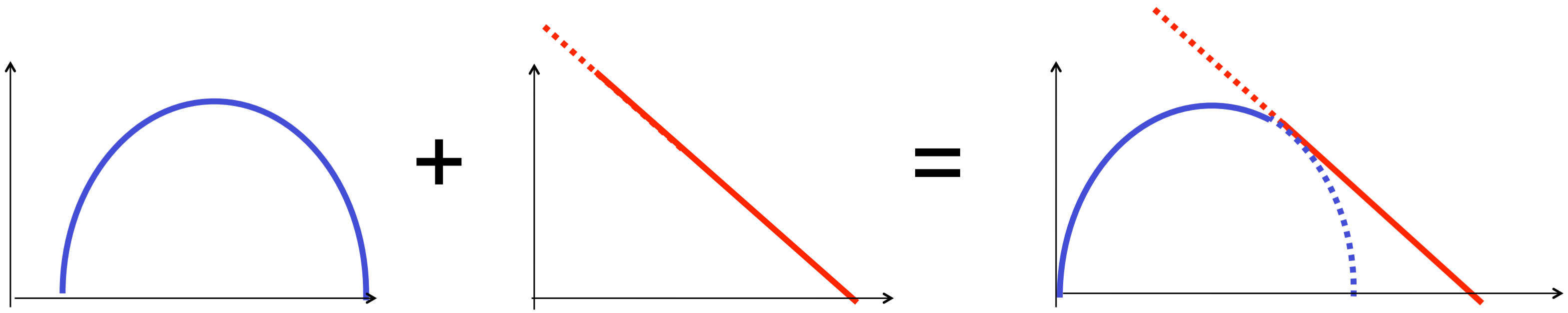

"everyone" gets the right IMF
→ better look for secondary indicators

- *stellar multiplicity*
- protostellar *spin* (including disk)
- *spatial distribution* + *kinematics* in young clusters
- *magnetic field strength* and *orientation*

dynamical
approach

Turbulent cascade

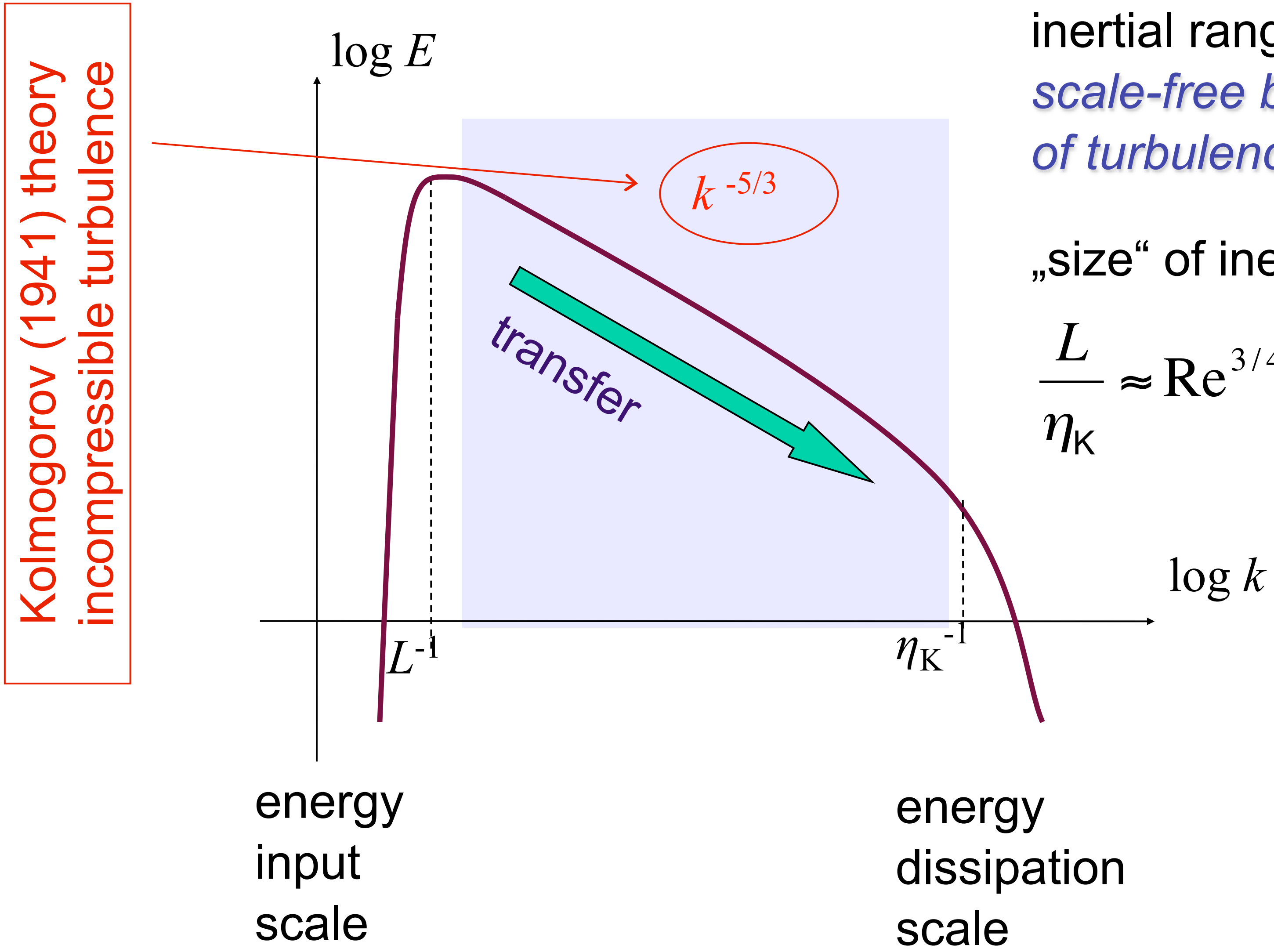

inertial range:

scale-free behavior
of turbulence

„size“ of inertial range:

$$\frac{L}{\eta_K} \approx \mathrm{Re}^{3/4}$$

Turbulent cascade

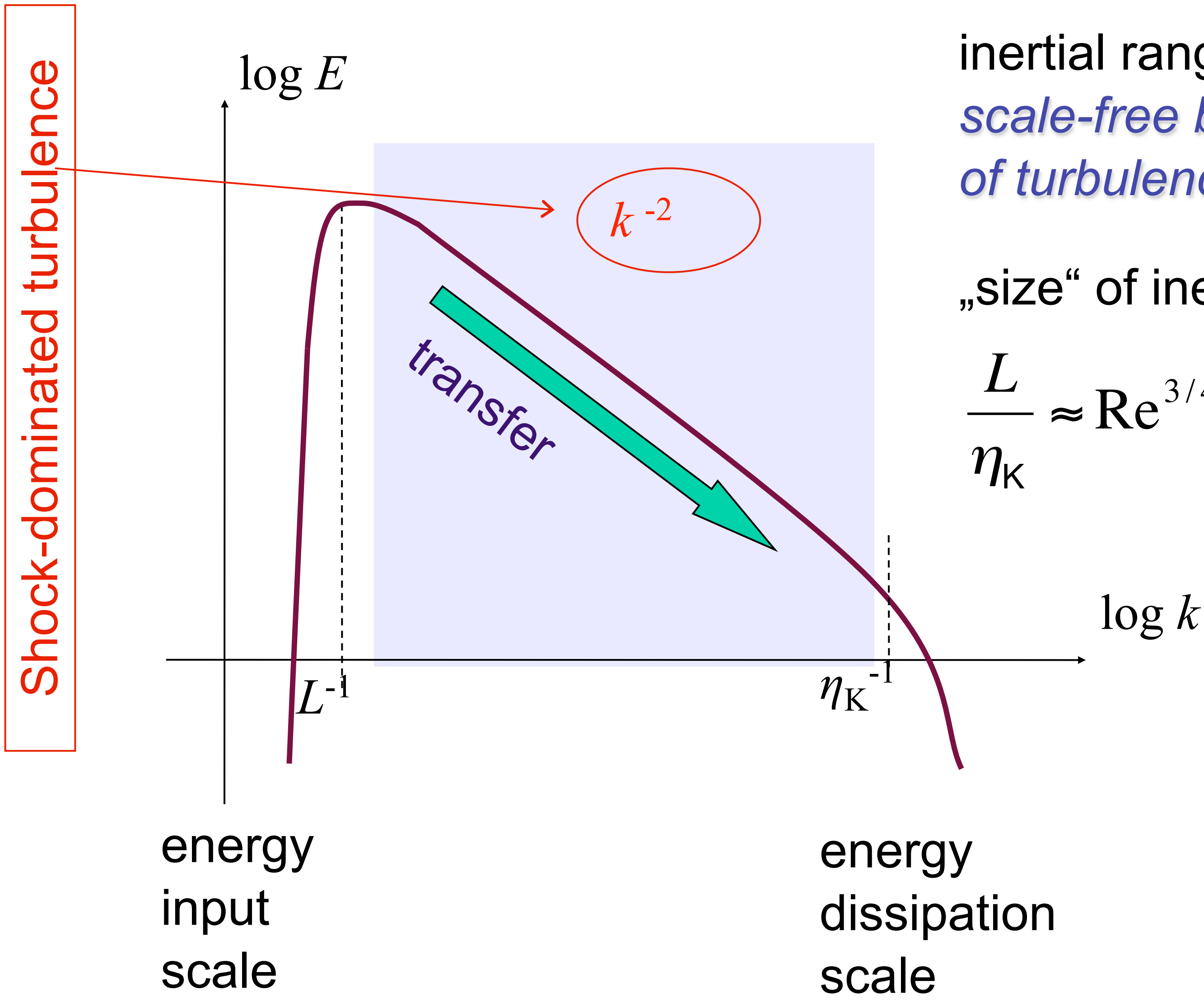

inertial range:
scale-free behavior of turbulence

„size" of inertial range:

$$\frac{L}{\eta_K} \approx \mathrm{Re}^{3/4}$$

Turbulent cascade in ISM

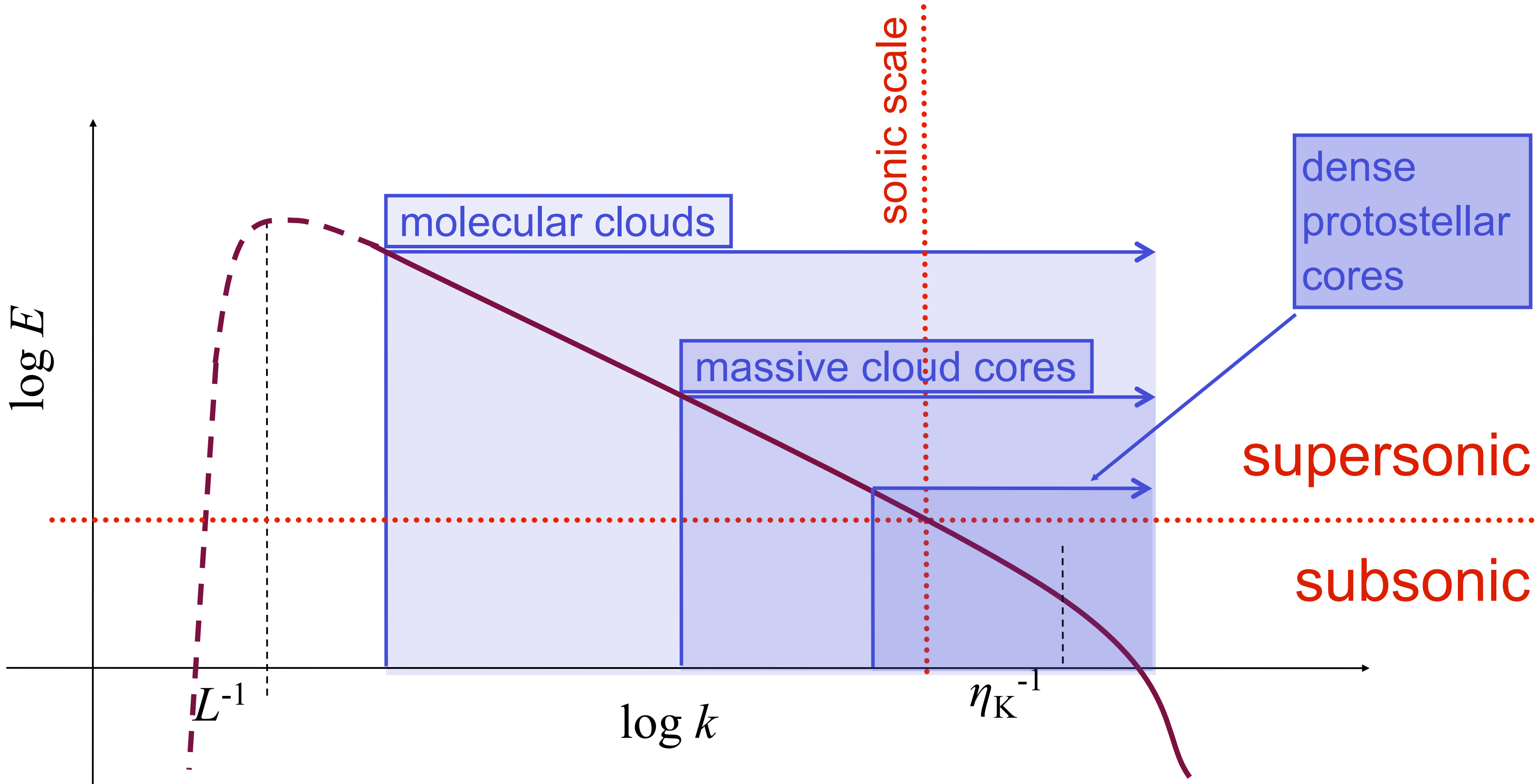

energy source & scale
NOT known
(supernovae, winds,
spiral density waves?)

σ_{rms} << 1 km/s
$M_{rms} \leq 1$
L ≈ 0.1 pc

dissipation scale not known
(ambipolar diffusion,
molecular diffusion?)

Density structure of MC's

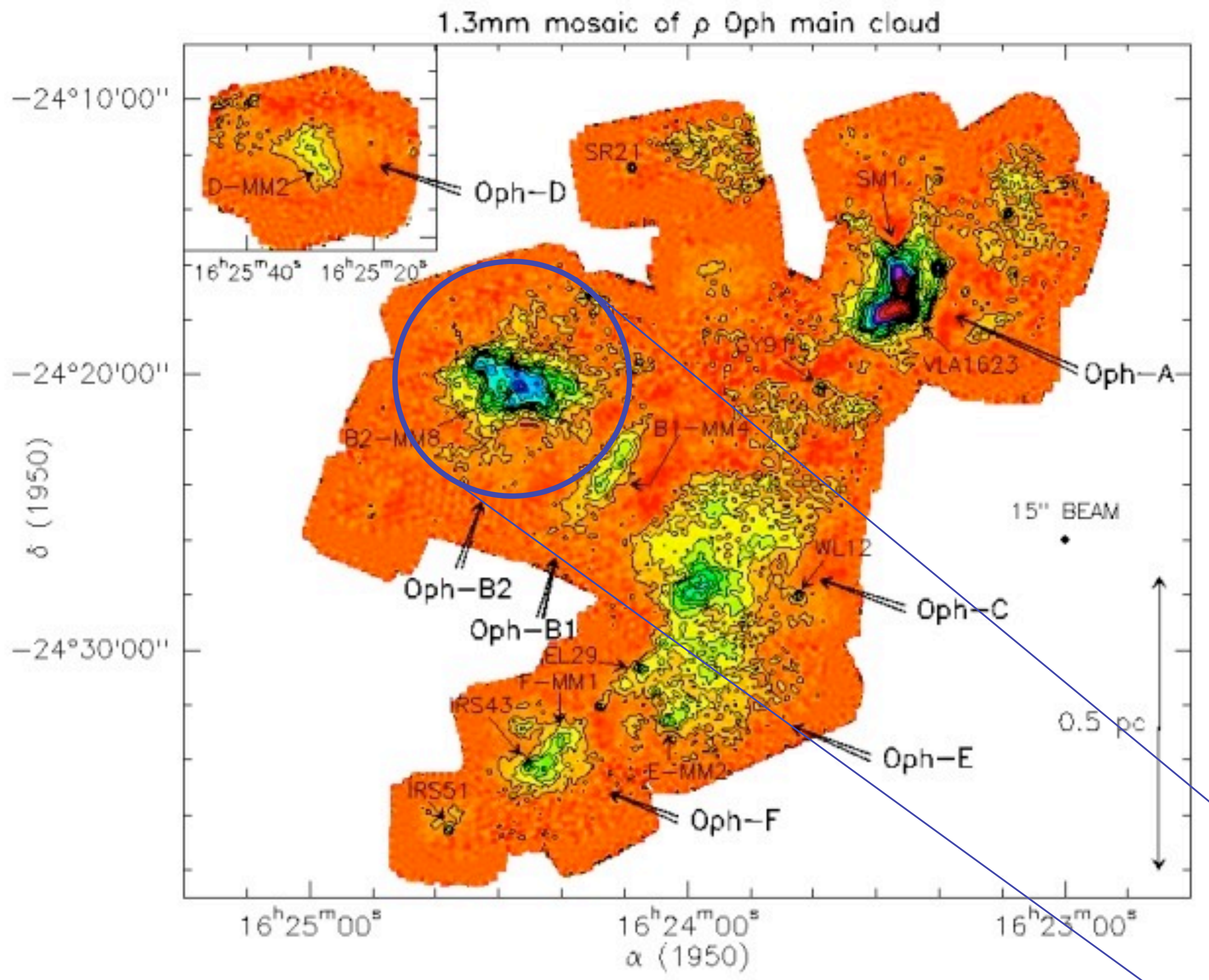

(Motte, André, & Neri 1998)

molecular clouds are highly inhomogeneous

stars form in the densest and coldest parts of the cloud

ρ-Ophiuchus cloud seen in dust emission

let's focus on a cloud core like this one

Evolution of cloud cores

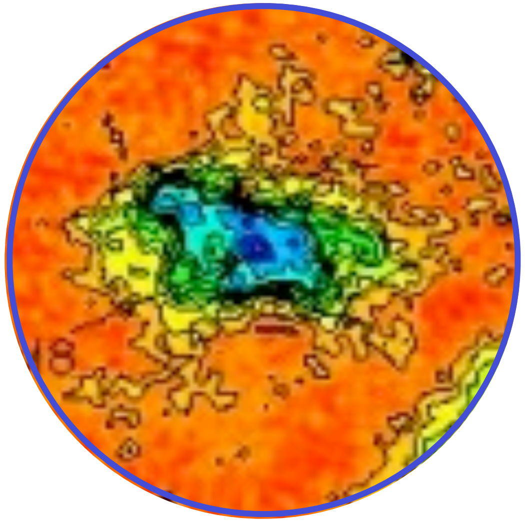

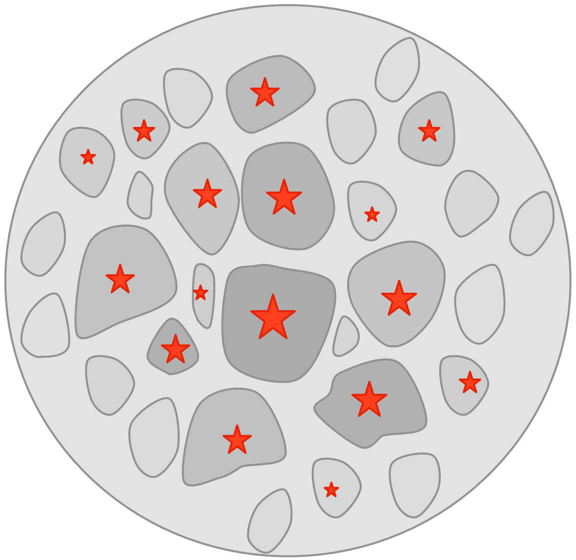

- How does this core evolve?
  Does it form one single massive star or cluster with mass distribution?

- Turbulent cascade „goes through“ cloud core
  --> NO *scale separation* possible
  --> NO *effective sound speed*
- Turbulence is supersonic!
  --> produces strong density contrasts:
  $\delta\rho/\rho \approx M^2$
  --> with typical $M \approx 10$ --> $\delta\rho/\rho \approx 100$!
- many of the shock-generated fluctuations are Jeans unstable and go into collapse
- --> expectation: *core breaks up and forms a cluster of stars*

Evolution of cloud cores

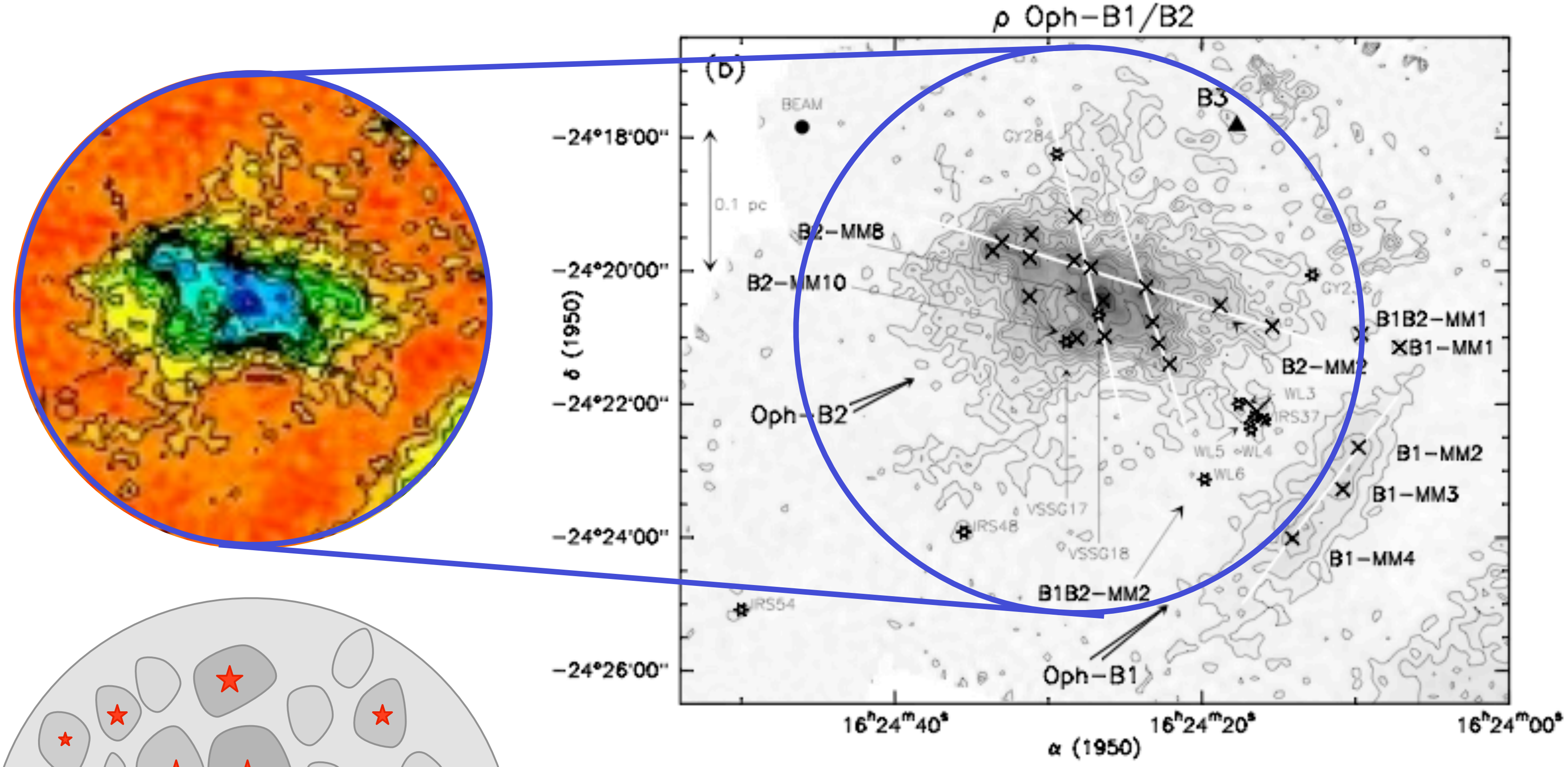

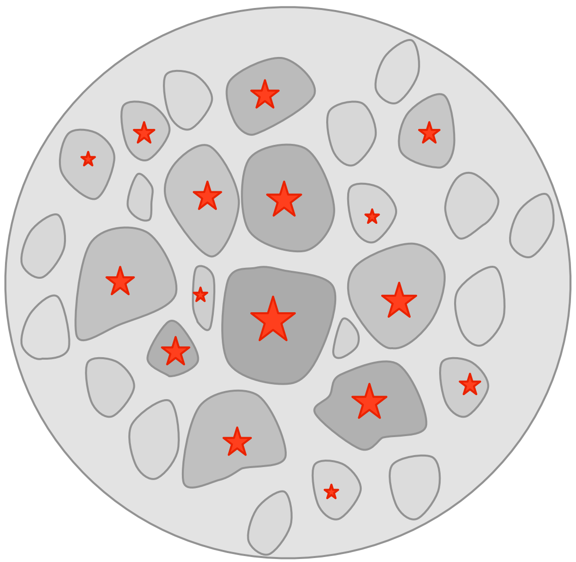

indeed ρ-Oph B1/2 contains several cores ("starless" cores are denoted by ×, cores with embedded protostars by ☆)

(Motte, André, & Neri 1998)

Formation and evolution of cores

What happens to distribution of cloud cores?

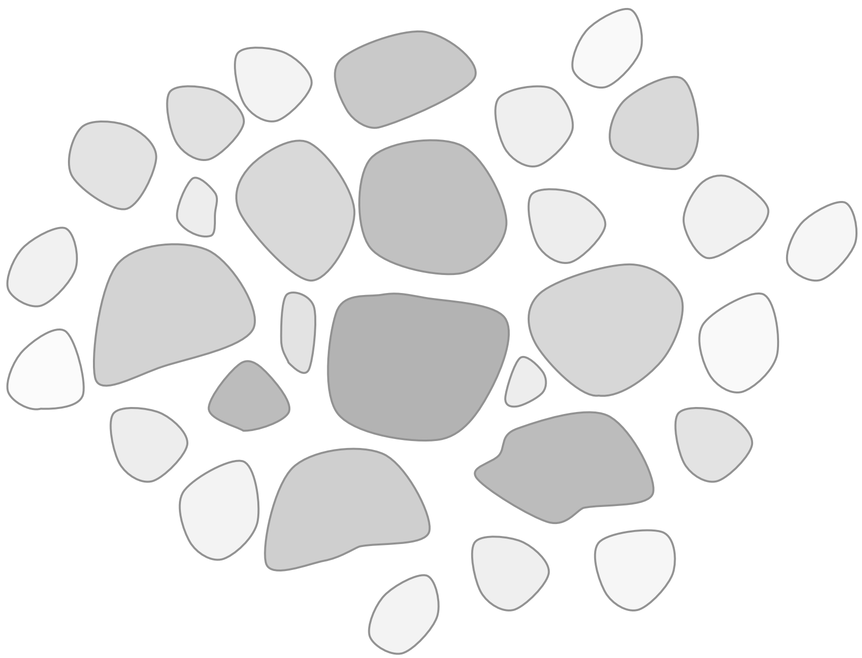

Two exteme cases:

(1) turbulence dominates energy budget:

$\alpha = E_{kin}/|E_{pot}| > 1$

--> individual cores do *not* interact

--> *collapse* of *individual* cores dominates *stellar mass growth*

--> *loose cluster of low-mass stars*

(2) turbulence decays, i.e. gravity dominates:

$\alpha = E_{kin}/|E_{pot}| < 1$

--> *global contraction*

--> core do *interact* while collapsing

--> *competition* influences *mass growth*

--> *dense cluster with high-mass stars*

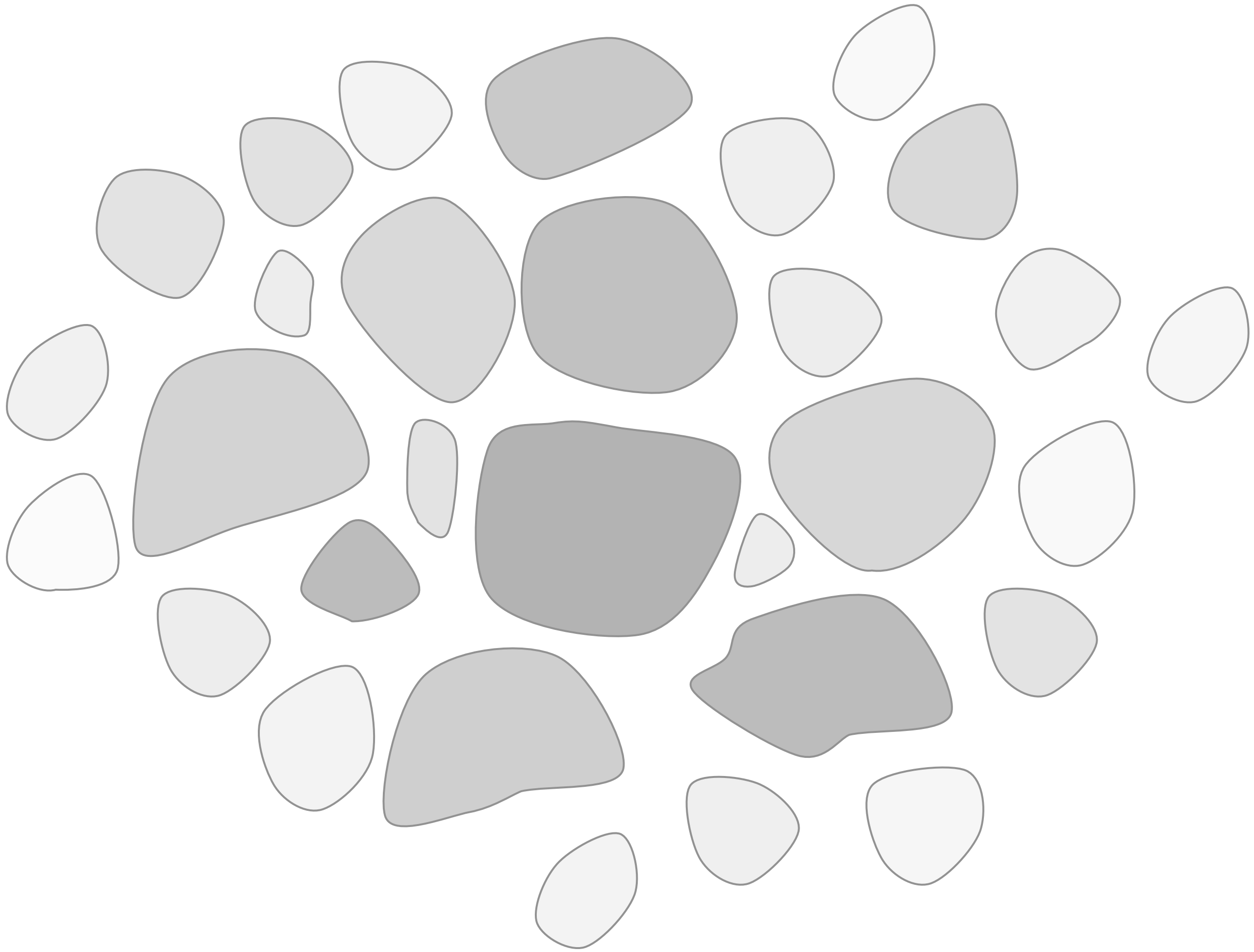

turbulence creates a hierarchy of clumps

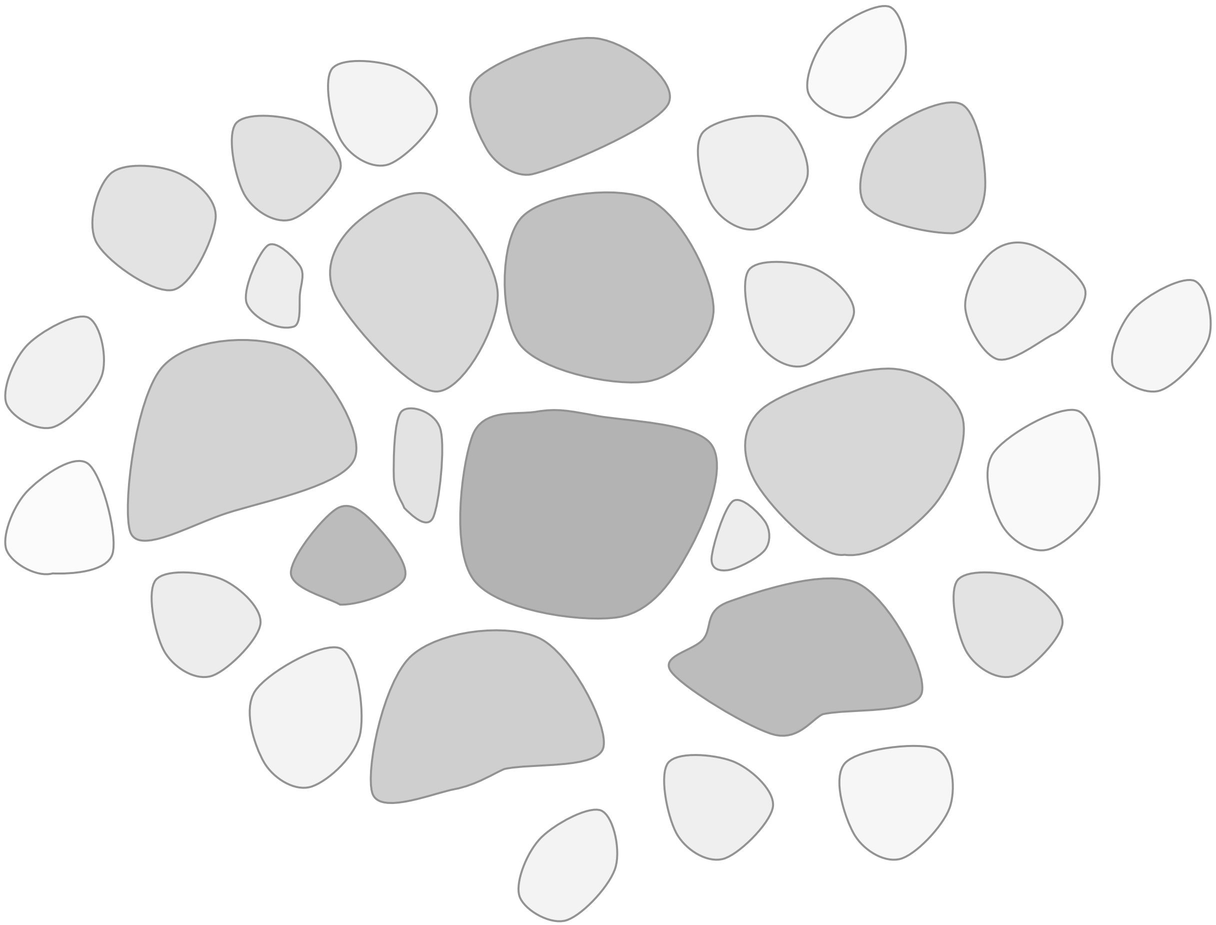

as turbulence decays locally, contraction sets in

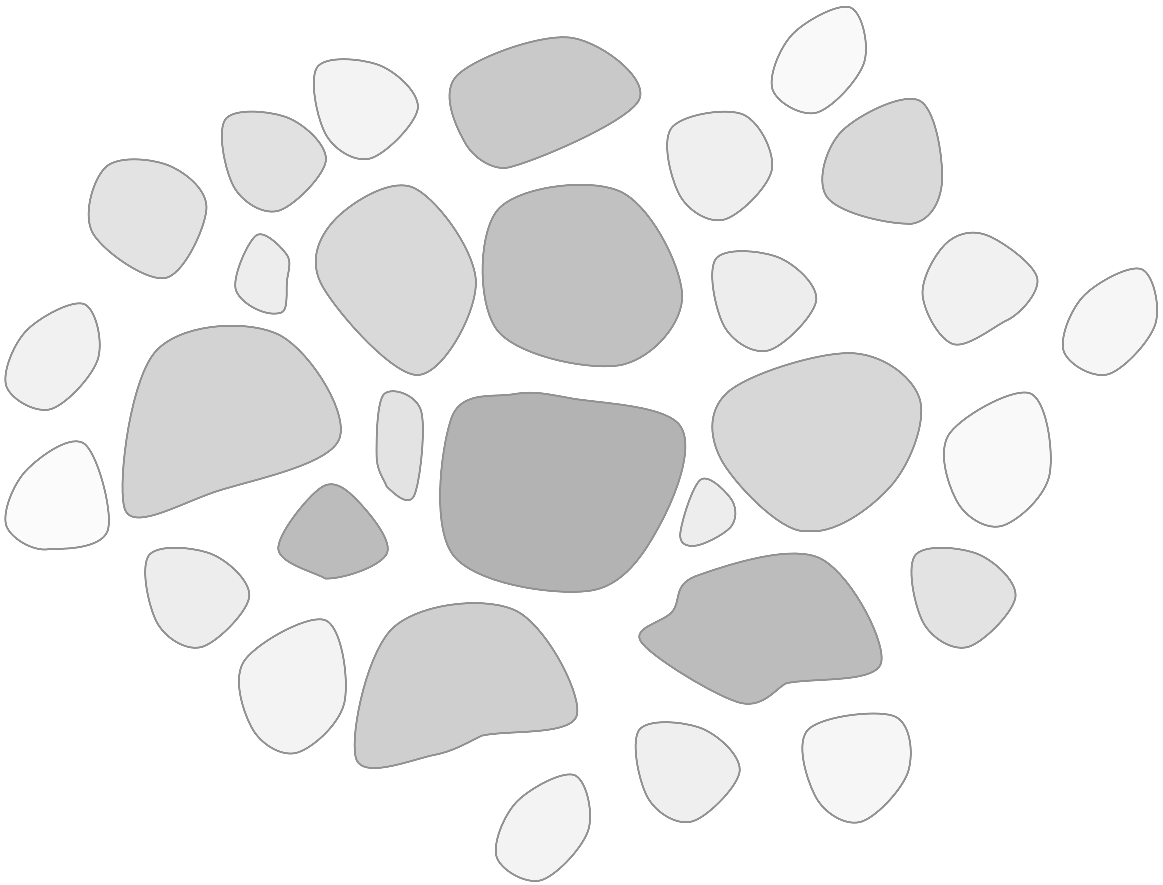

as turbulence decays locally, contraction sets in

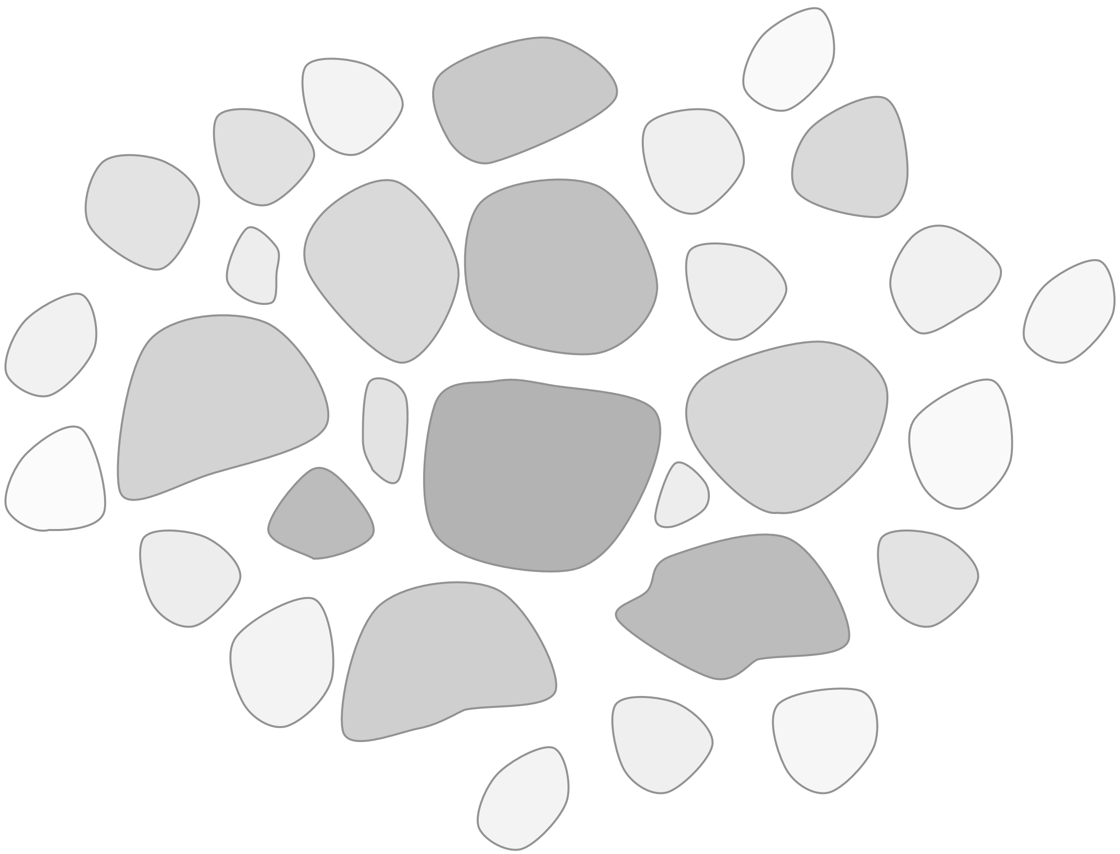

while region contracts, individual clumps collapse to form stars

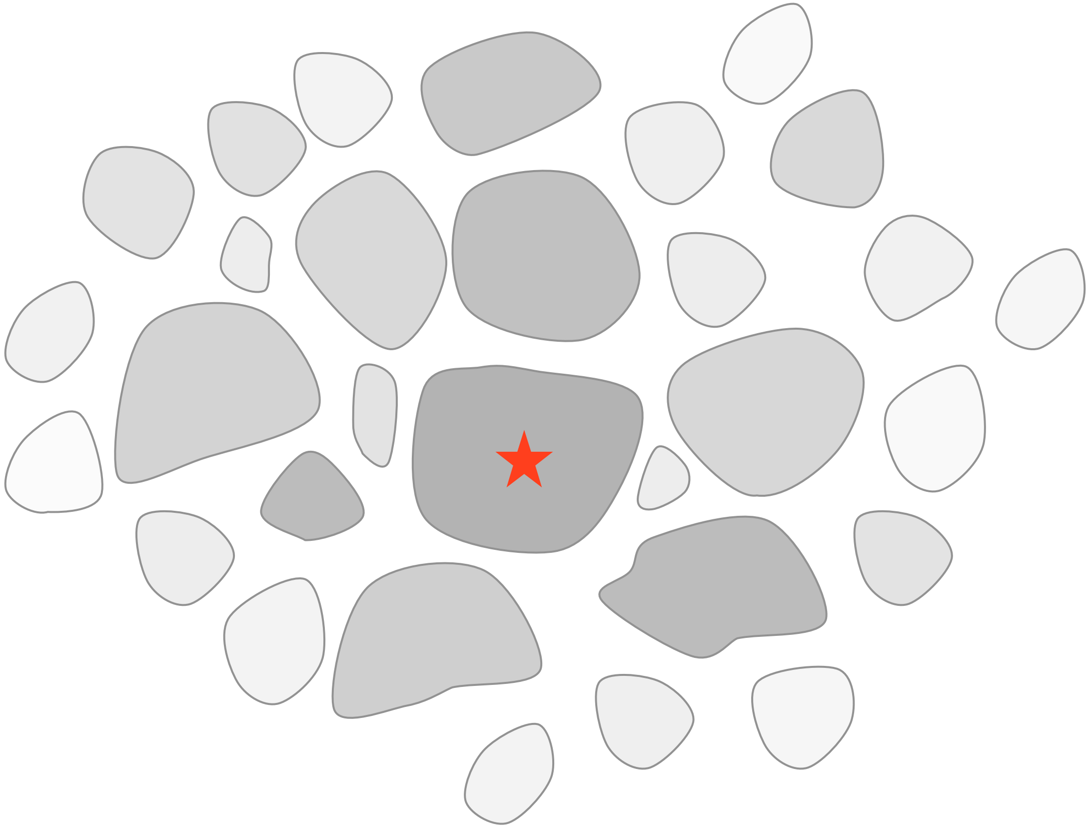

while region contracts, individual clumps collapse to form stars

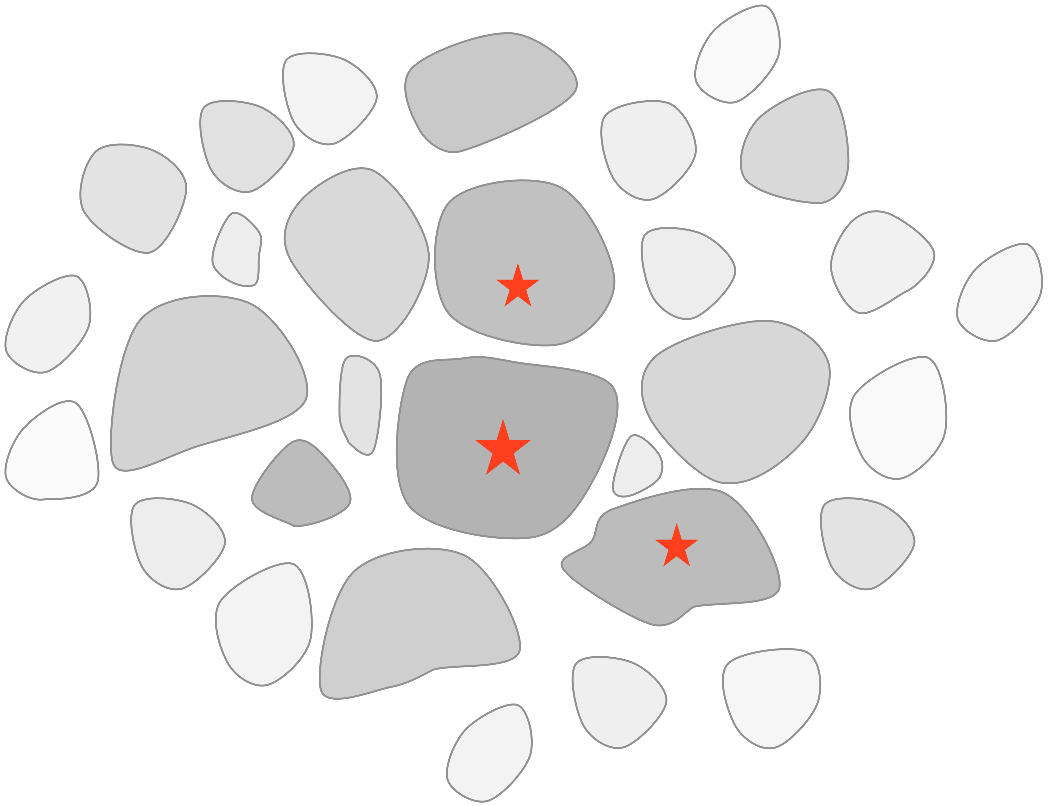

individual clumps collapse to form stars

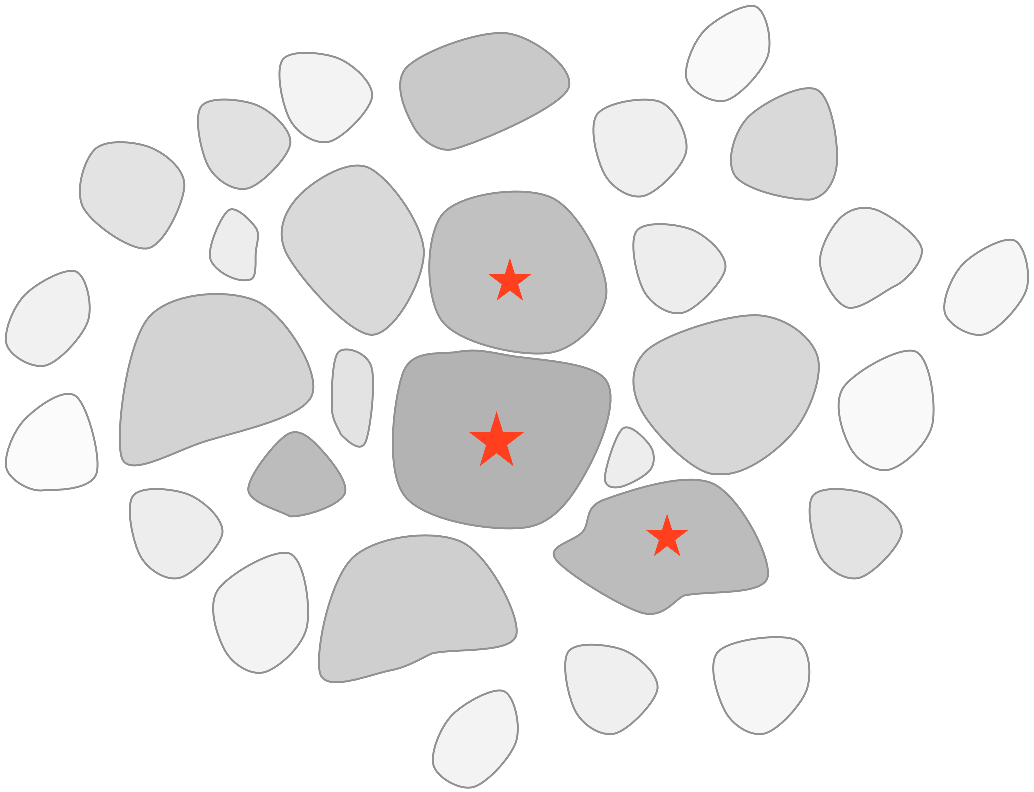

individual clumps collapse to form stars

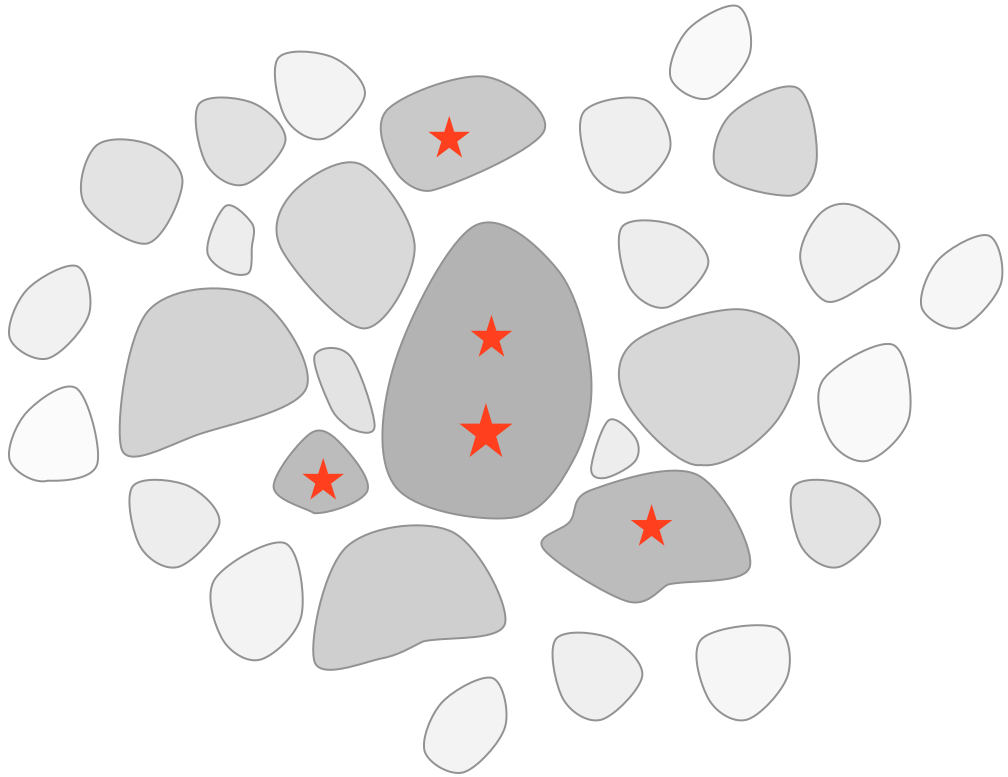

$\alpha = E_{kin}/|E_{pot}| < 1$

in *dense clusters*, clumps may merge while collapsing
--> then contain multiple protostars

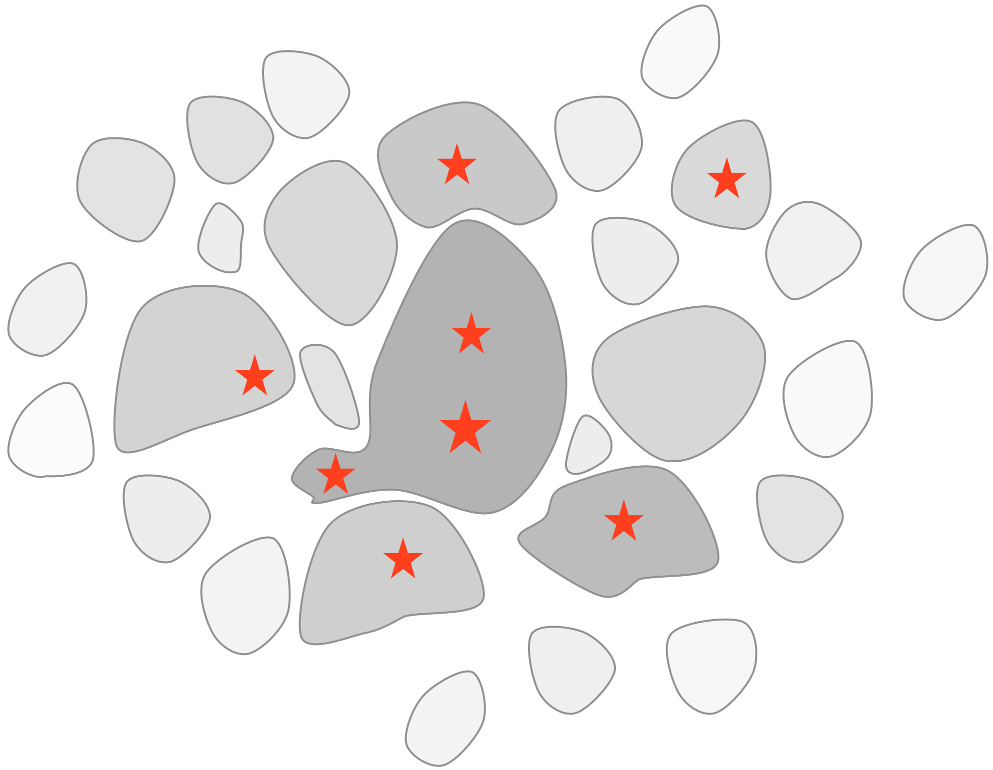

in *dense clusters*, clumps may merge while collapsing
--> then contain multiple protostars

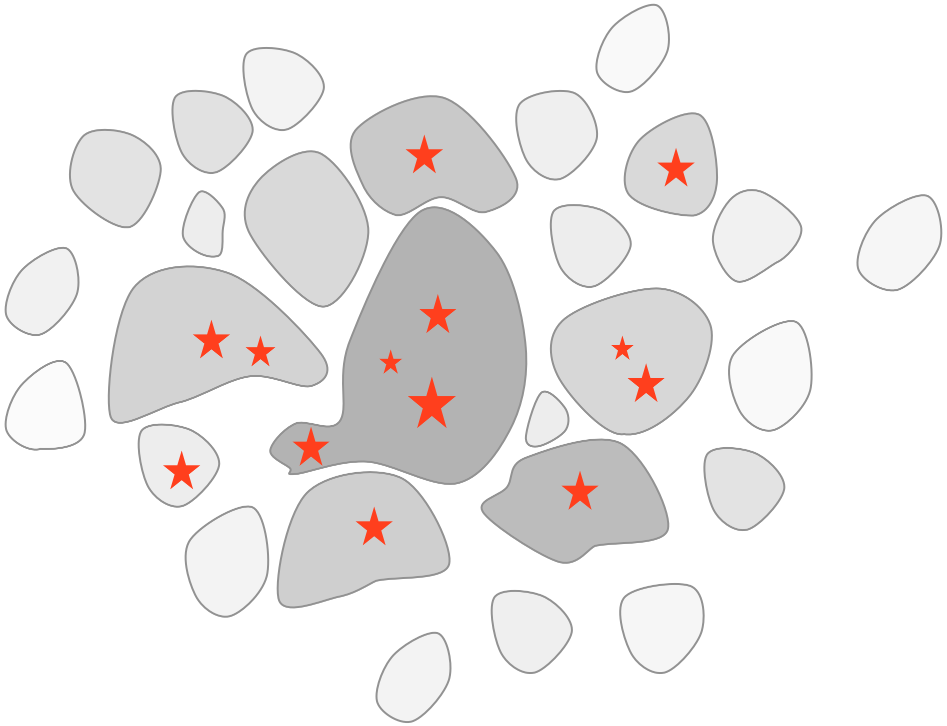

in *dense clusters*, clumps may merge while collapsing
--> then contain multiple protostars

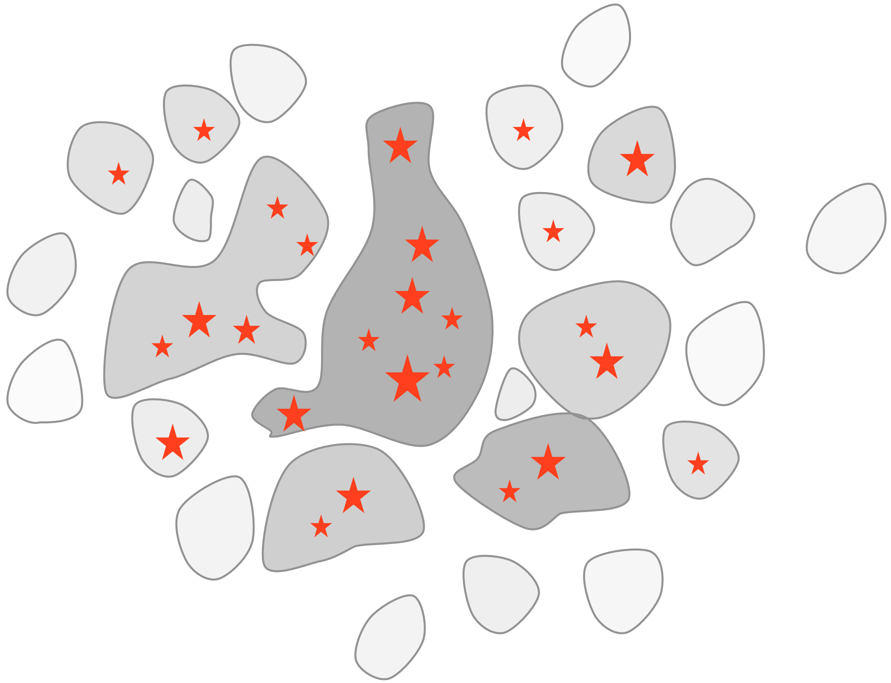

in *dense clusters*, competitive mass growth
becomes important

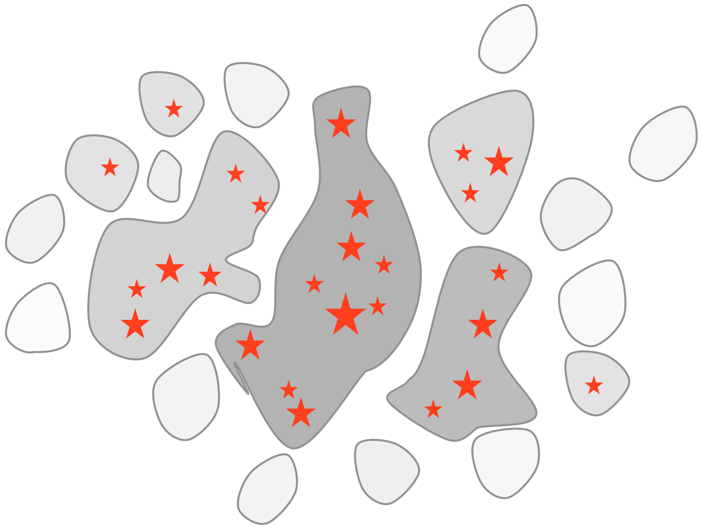

in *dense clusters*, competitive mass growth
becomes important

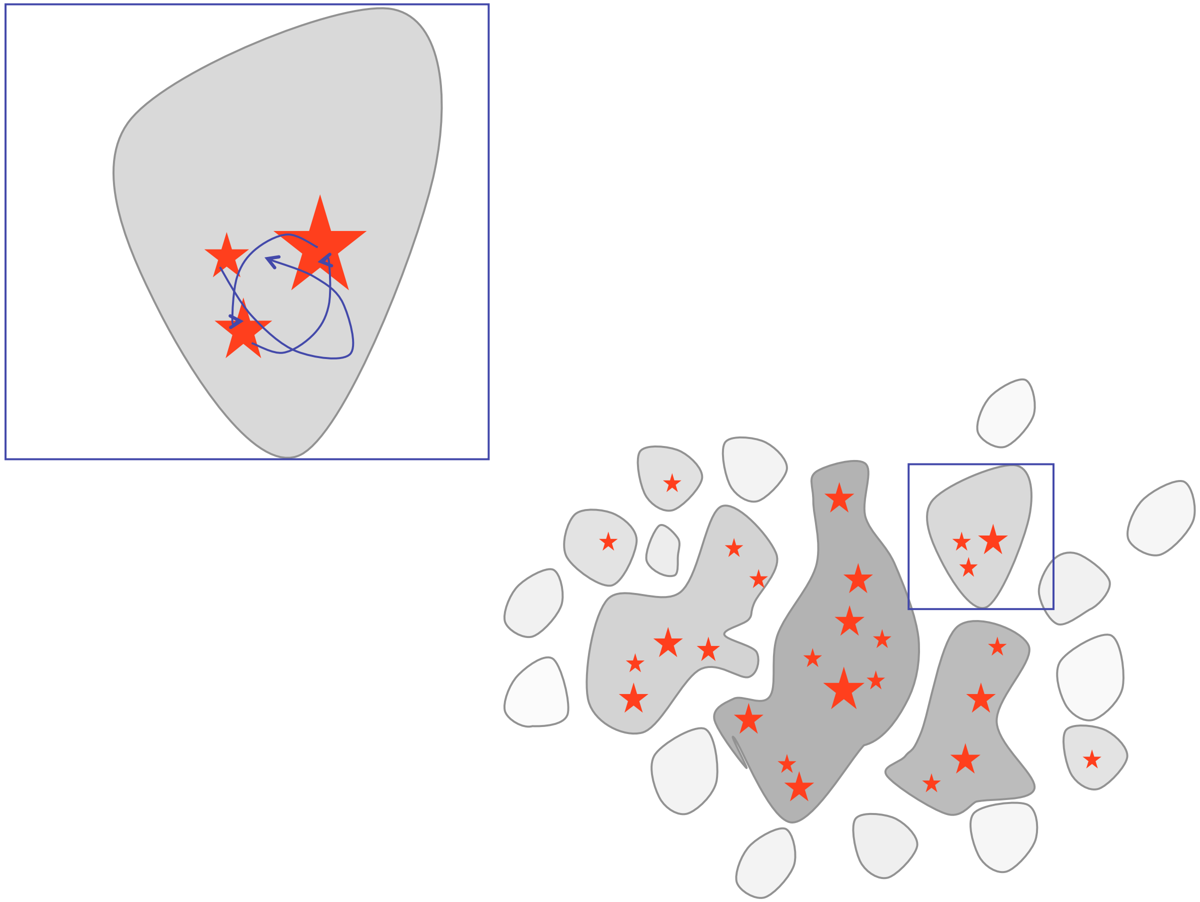

in *dense clusters*, *N*-body effects influence mass growth

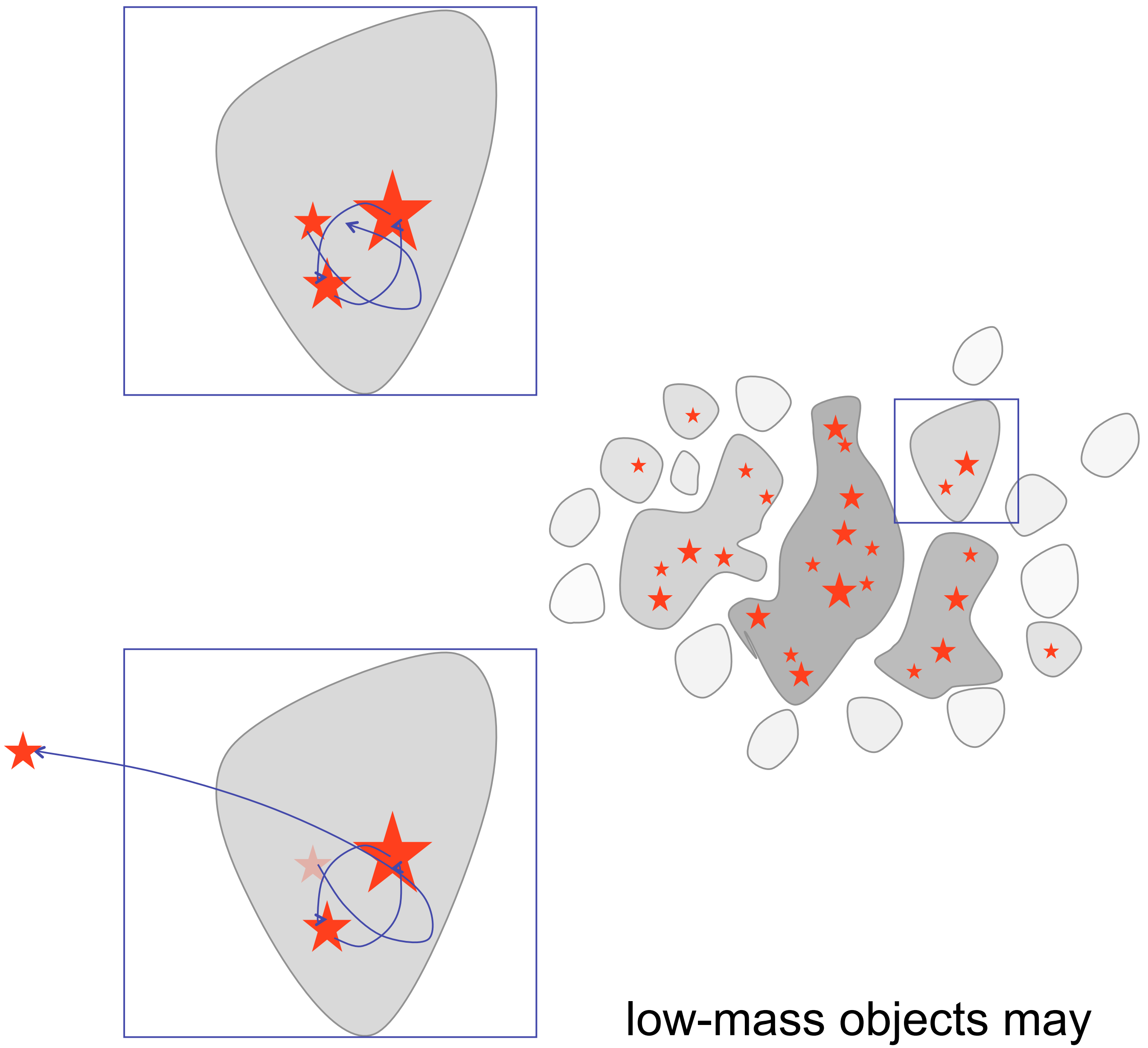

low-mass objects may
become ejected --> accretion stops

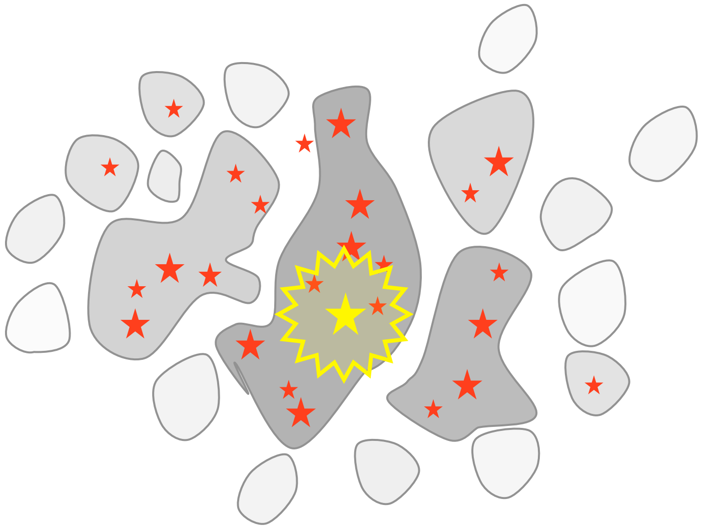

feedback terminates star formation

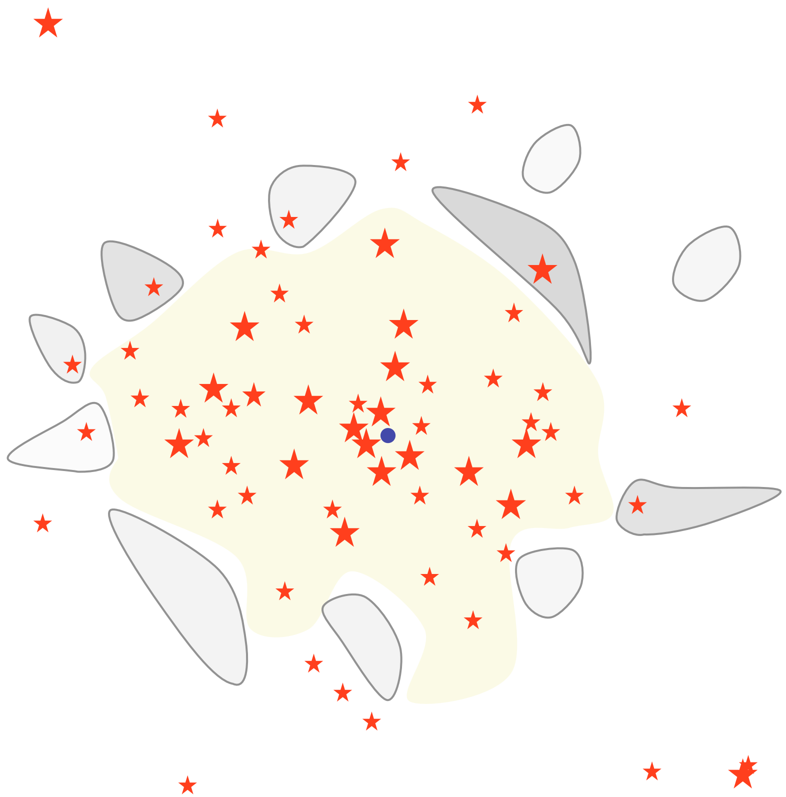

result: *star cluster*, possibly with HII region

NGC 602 in the LMC: Hubble Heritage Image

result: *star cluster* with H_{II} region

initial mass function

IMF

- distribution of stellar masses depends on
  - turbulent initial conditions
    --> mass spectrum of prestellar cloud cores
  - collapse and interaction of prestellar cores
    --> competitive accretion and *N*-body effects
  - thermodynamic properties of gas
    --> balance between heating and cooling
    --> EOS (determines which cores go into collapse)
  - (proto) stellar feedback terminates star formation
    ionizing radiation, bipolar outflows, winds, SN

(e.g. Larson 2003, Prog. Rep. Phys.; Mac Low & Klessen, 2004, Rev. Mod. Phys, 76, 125 - 194)

IMF

- distribution of stellar masses depends on
  - *turbulent initial conditions*
    --> mass spectrum of prestellar cloud cores ???
  - collapse and interaction of prestellar cores
    --> competitive accretion and *N*-body effects
  - thermodynamic properties of gas
    --> balance between heating and cooling
    --> EOS (determines which cores go into collapse)
  - (proto) stellar feedback terminates star formation
    ionizing radiation, bipolar outflows, winds, SN

(e.g. Larson 2003, Prog. Rep. Phys.; Mac Low & Klessen, 2004, Rev. Mod. Phys, 76, 125 - 194)

compressive vs. rotational driving

- statistical characteristics of turbulence depend strongly on „type“ of driving
- example: dilatational vs. solenoidal driving
- question: what drives ISM turbulence on different scales?

dilatational vs. solenoidal

density as function of time / cut through 1024^3 cube simulation (FLASH)

compressive
larger structures, higher ρ-contrast

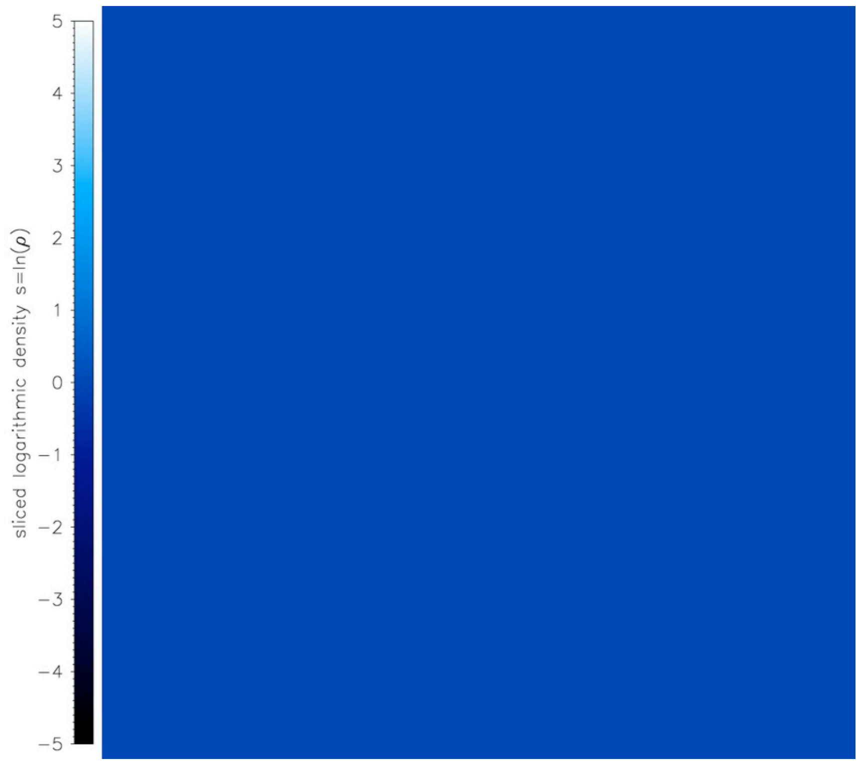

rotational
smaller structures, small ρ-pdf

Federrath, Klessen, Schmidt (2008a,b)

dilatational vs. solenoidal

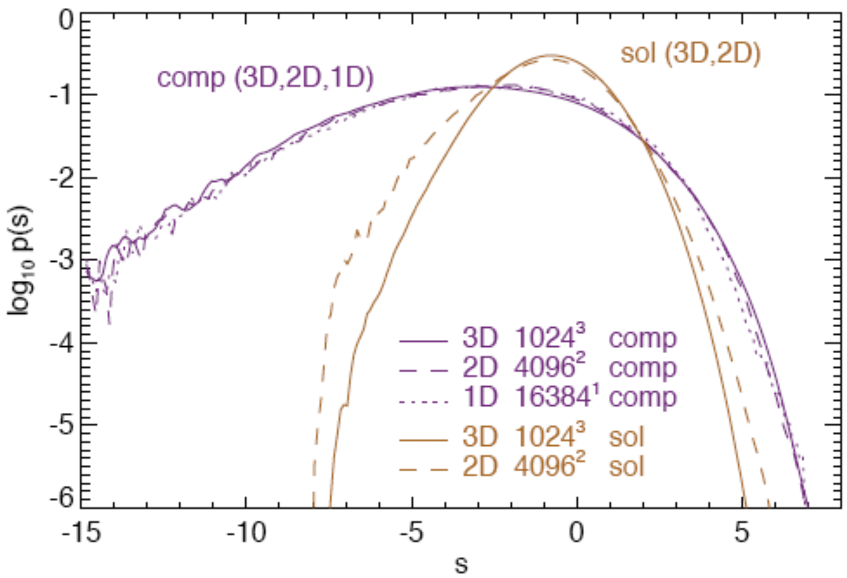

FIG. 3.— Volume-weighted density PDFs $p(s)$ obtained from 3D, 2D and 1D simulations with compressive forcing and from 3D and 2D simulations using solenoidal forcing. Note that in 1D, only compressive forcing is possible as in the study by Passot & Vázquez-Semadeni (1998). As suggested by eq. (5), compressive forcing yields almost identical density PDFs in 1D, 2D and 3D with $b\sim1$, whereas solenoidal forcing leads to a density PDF with $b\sim1/2$ in 2D and with $b\sim1/3$ in 3D.

Federrath, Klessen, Schmidt (2008a)

- density pdf depends on "dimensionality" of driving
  - relation between width of pdf and Mach number

$$\boxed{\sigma_\rho/\rho_0 = b\mathcal{M}}$$

  - with b depending on ζ via

$$\boxed{b = 1 + \left[\frac{1}{D} - 1\right]\zeta = \begin{cases} 1 - \frac{2}{3}\zeta & , \text{for } D = 3 \\ 1 - \frac{1}{2}\zeta & , \text{for } D = 2 \\ 1 & , \text{for } D = 1 \end{cases}}$$

  - with ζ being the ratio of dilatational vs. solenoidal modes:

$$\mathcal{P}_{ij}^{\zeta} = \zeta\mathcal{P}_{ij}^{\perp} + (1-\zeta)\mathcal{P}_{ij}^{||} = \zeta\delta_{ij} + (1-2\zeta)\frac{k_i k_j}{|k|^2}$$

dilatational vs. solenoidal

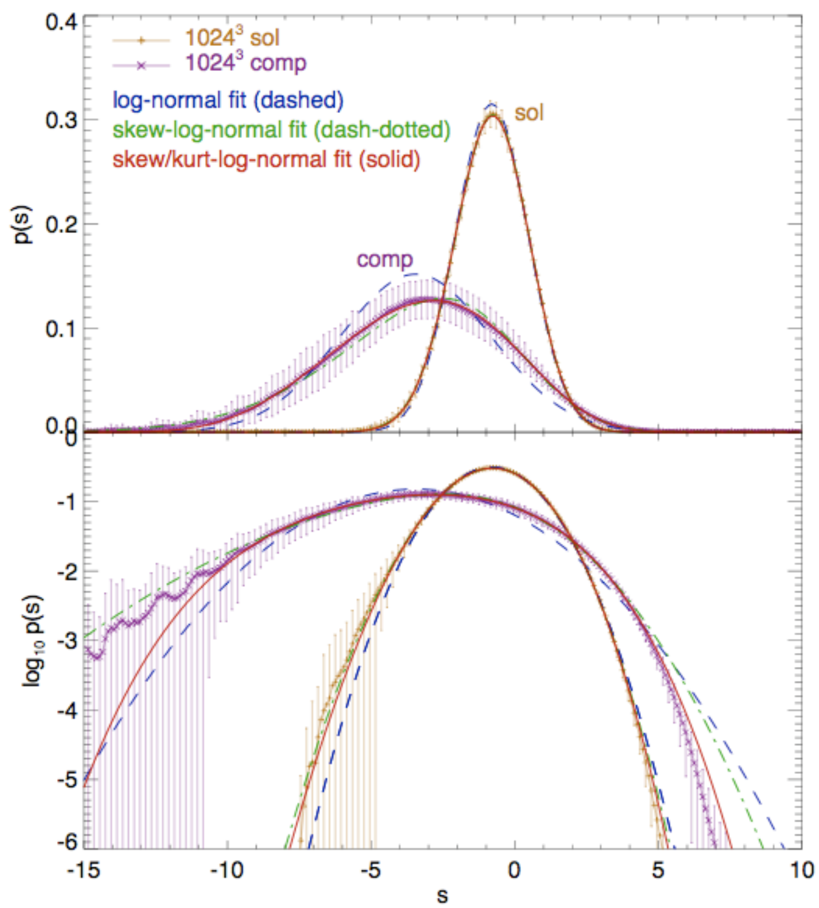

good fit needs 3rd and 4th moment of distribution!

Federrath, Klessen, Schmidt (2008b)

- density pdf depends on "dimensionality" of driving
  → is that a problem for the Krumholz & McKee model of the SF efficiency?
- density pdf of compressive driving is *NOT log-normal*
  → is that a problem for the Padoan & Nordlund, or Hennebelle & Chabrier IMF model?
- most "physical" sources should be *compressive* (convergent flows from spiral shocks or SN)

dilatational vs. solenoidal

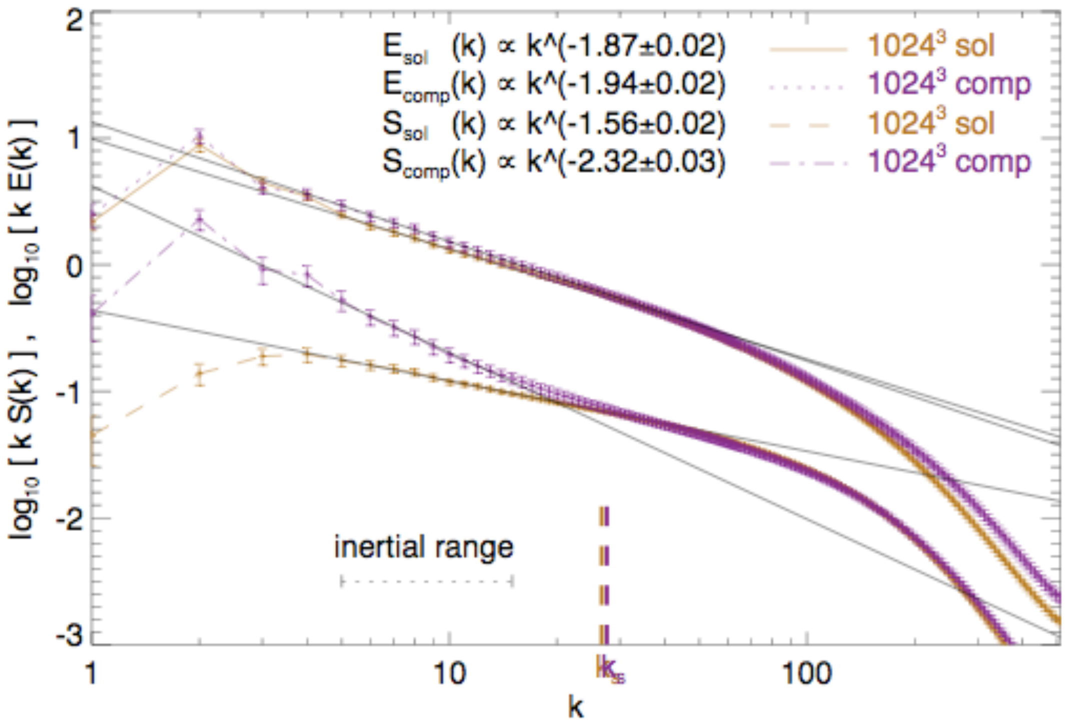

compensated density spectrum kS(k) shows clear break at sonic scale. below that shock compression no longer is important in shaping the power spectrum ...

- density power spectrum differs between dilatational and solenoidal driving!

→ dilatational driving leads to break at sonic scale!

- can we use that to determine driving sources from observations ?

Federrath, Klessen, Schmidt (2008b)

IMF

- distribution of stellar masses depends on
  - turbulent initial conditions
    --> mass spectrum of prestellar cloud cores
  - collapse and interaction of prestellar cores
    --> competitive mass growth and *N*-body effects
  - thermodynamic properties of gas
    --> balance between heating and cooling
    --> EOS (determines which cores go into collapse)
  - (proto) stellar feedback terminates star formation
    ionizing radiation, bipolar outflows, winds, SN

(e.g. Larson 2003, Prog. Rep. Phys.; Mac Low & Klessen, 2004, Rev. Mod. Phys, 76, 125 - 194)

example: model of Orion cloud

„model“ of Orion cloud:
15.000.000 SPH particles,
10^4 M_{sun} in 10 pc, mass resolution
0,02 M_{sun}, forms ~2.500
„stars“ (sink particles)

isothermal EOS, top bound, bottom unbound

has clustered as well as distributed „star“ formation

efficiency varies from 1% to 20%

develops full IMF
(distribution of sink particle masses)

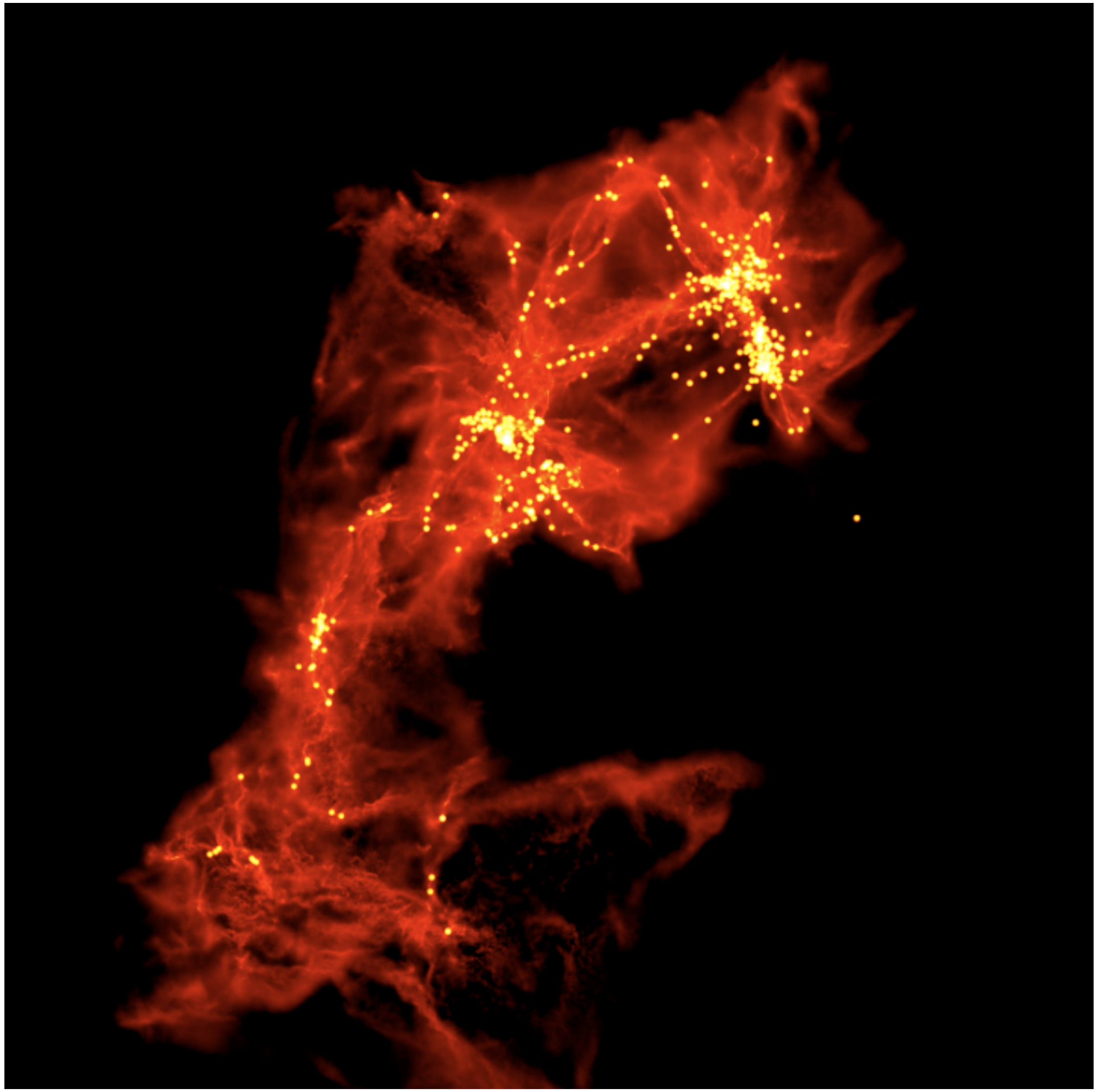

(Bonnell & Clark 2008)

example: model of Orion cloud

„model“ of Orion cloud:
15.000.000 SPH particles,
10^4 M_{sun} in 10 pc, mass resolution
0,02 M_{sun}, forms ~2.500
„stars“ (sink particles)

MASSIVE STARS
- form early in high-density gas clumps (cluster center)
- high accretion rates, maintained for a long time

LOW-MASS STARS
- form later as gas falls into potential well
- high relative velocities
- little subsequent accretion

Bonnell & Clark 2008

example: model of Orion cloud

„model“ of Orion cloud:
15.000.000 SPH particles,
10^4 M_{sun} in 10 pc, mass resolution
0,02 M_{sun}, forms ~2.500
„stars“ (sink particles)

isothermal EOS, top bound, bottom unbound

has clustered as well as distributed „star“ formation

efficiency varies from 1% to 20%

develops full IMF
(distribution of sink particle masses)

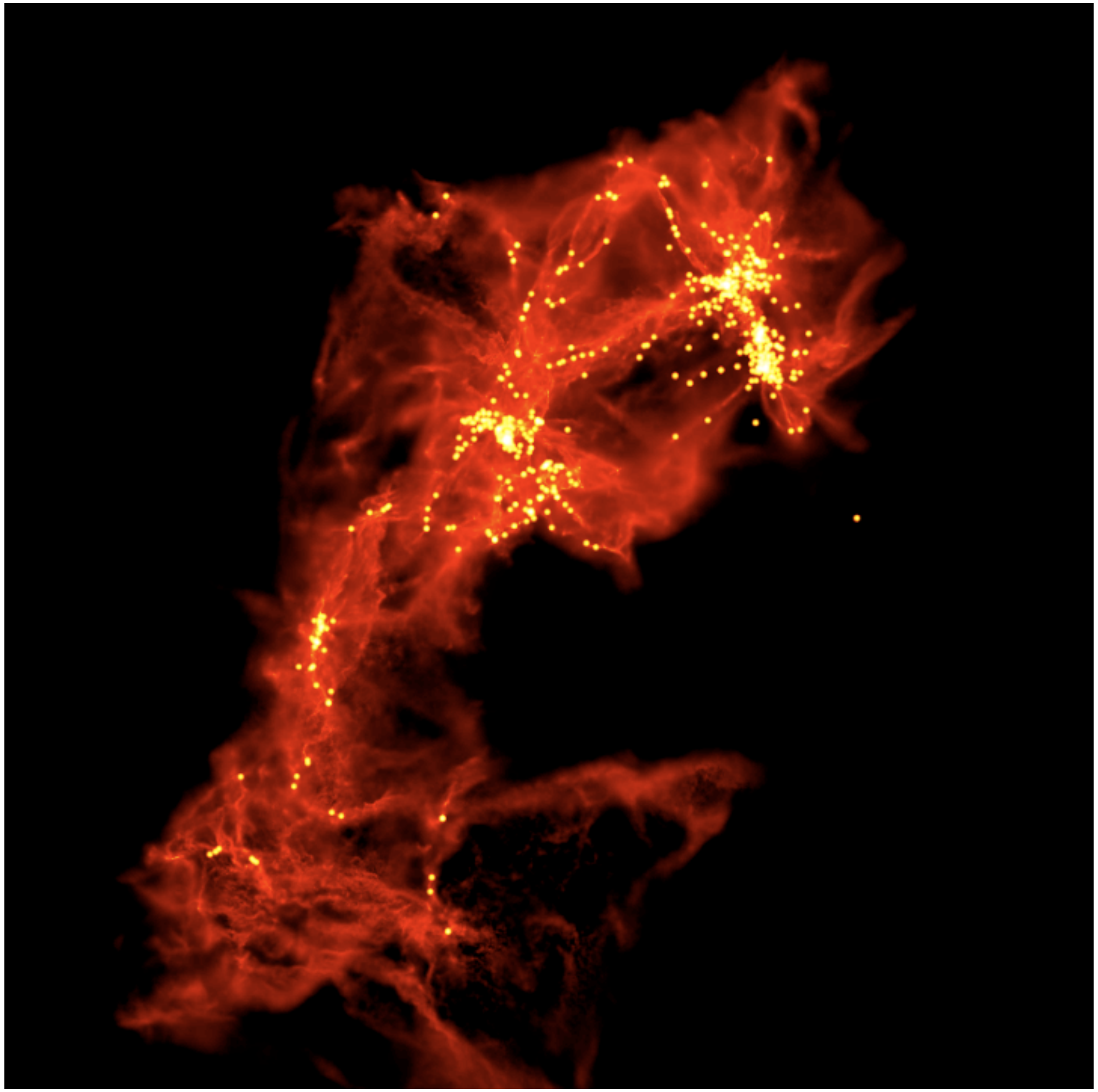

(Bonnell & Clark 2008)

Dynamics of nascent star cluster

in dense clusters protostellar interaction may be come important!

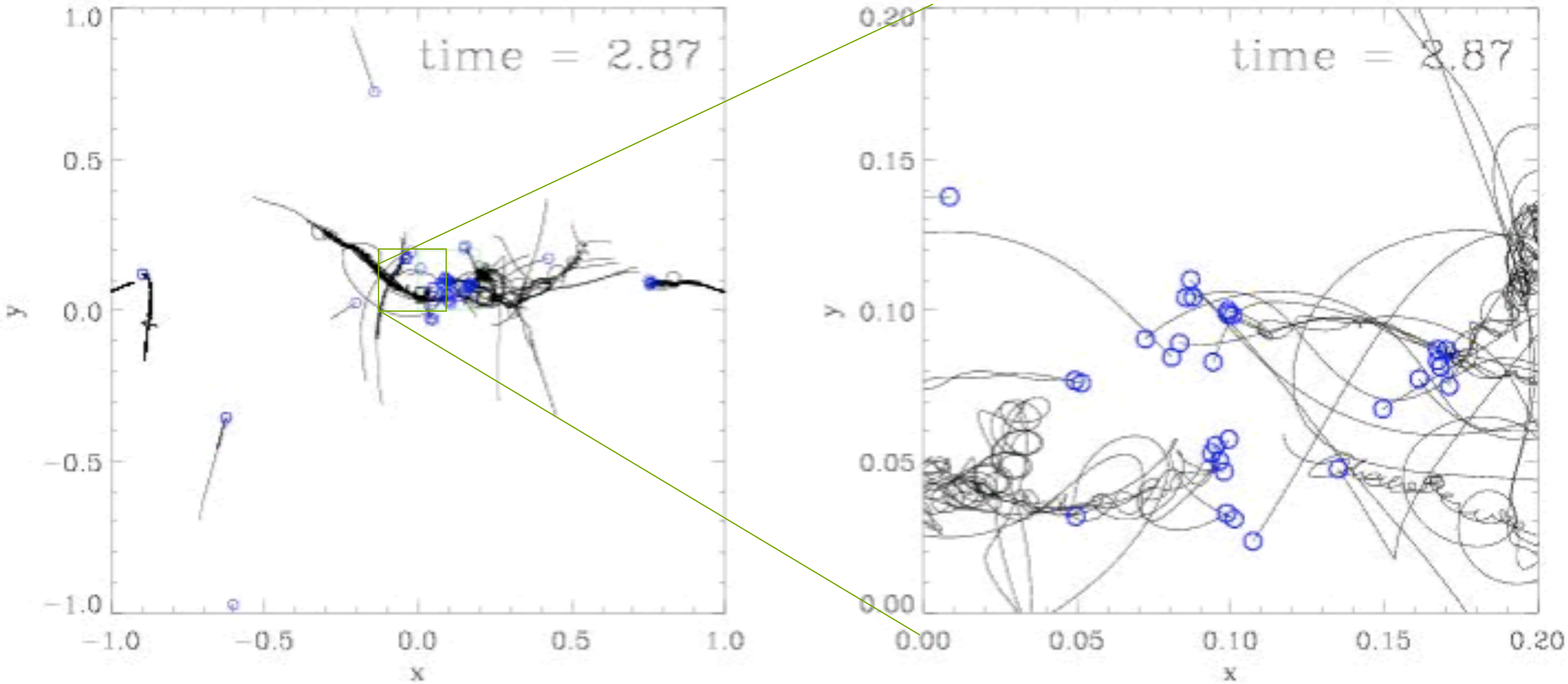

Trajectories of protostars in a nascent dense cluster created by gravoturbulent fragmentation
(from Klessen & Burkert 2000, ApJS, 128, 287)

accretion rates in clust

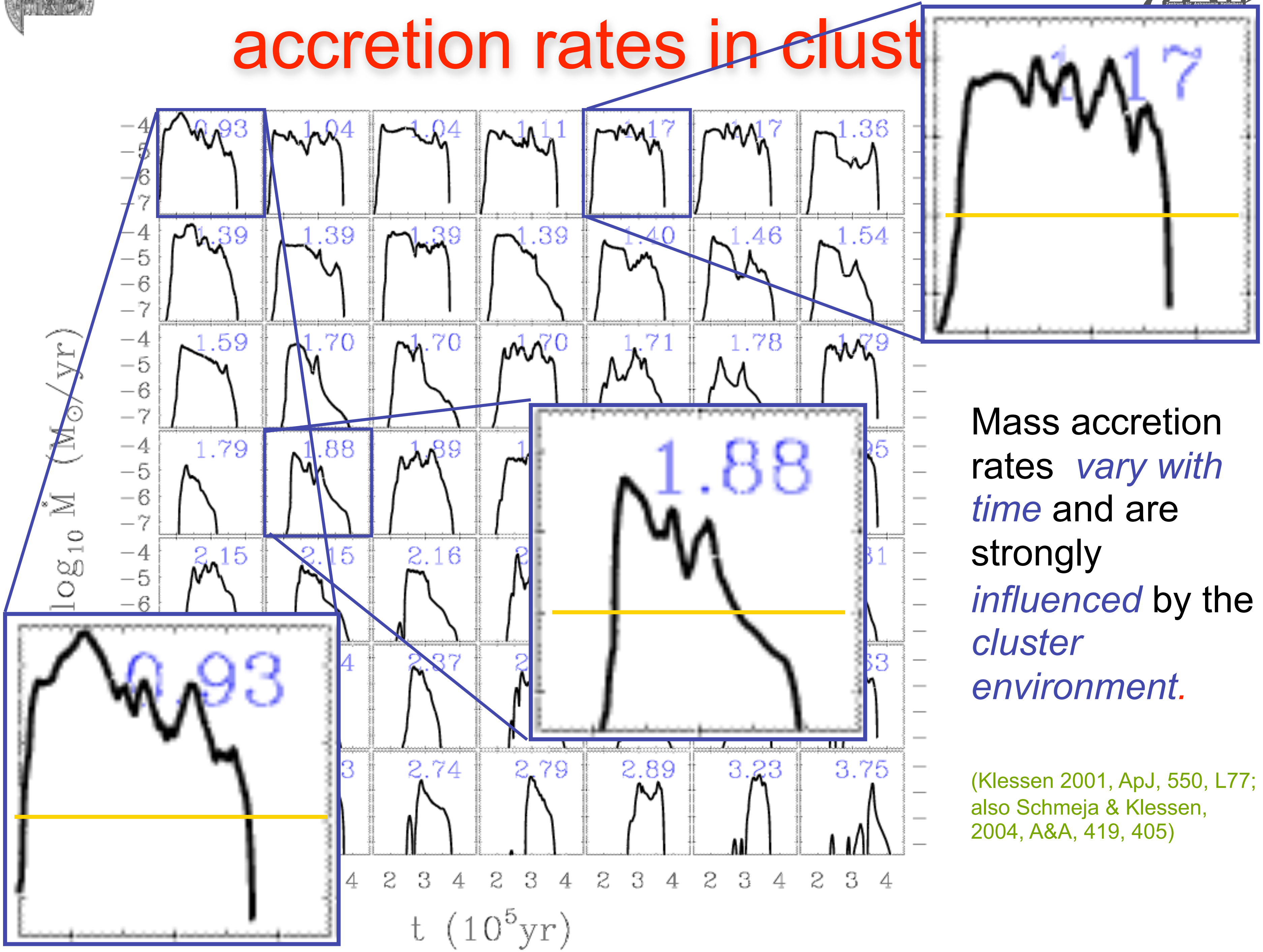

Mass accretion rates *vary with time* and are strongly *influenced* by the *cluster environment*.

(Klessen 2001, ApJ, 550, L77; also Schmeja & Klessen, 2004, A&A, 419, 405)

IMF

- distribution of stellar masses depends on
  - turbulent initial conditions
    --> mass spectrum of prestellar cloud cores
  - collapse and interaction of prestellar cores
    --> competitive accretion and *N*-body effects
  - *thermodynamic properties of gas*
    --> balance between heating and cooling
    --> EOS (determines which cores go into collapse)
  - (proto) stellar feedback terminates star formation
    ionizing radiation, bipolar outflows, winds, SN

(e.g. Larson 2003, Prog. Rep. Phys.; Mac Low & Klessen, 2004, Rev. Mod. Phys, 76, 125 - 194)

dependency on EOS

- degree of fragmentation depends on *EOS!*

- polytropic EOS: **p** $\propto \rho^{\gamma}$
- $\gamma<1$: dense cluster of low-mass stars
- $\gamma>1$: isolated high-mass stars
- (see Li, Klessen, & Mac Low 2003, ApJ, 592, 975; also Kawachi & Hanawa 1998, Larson 2003)

dependency on EOS

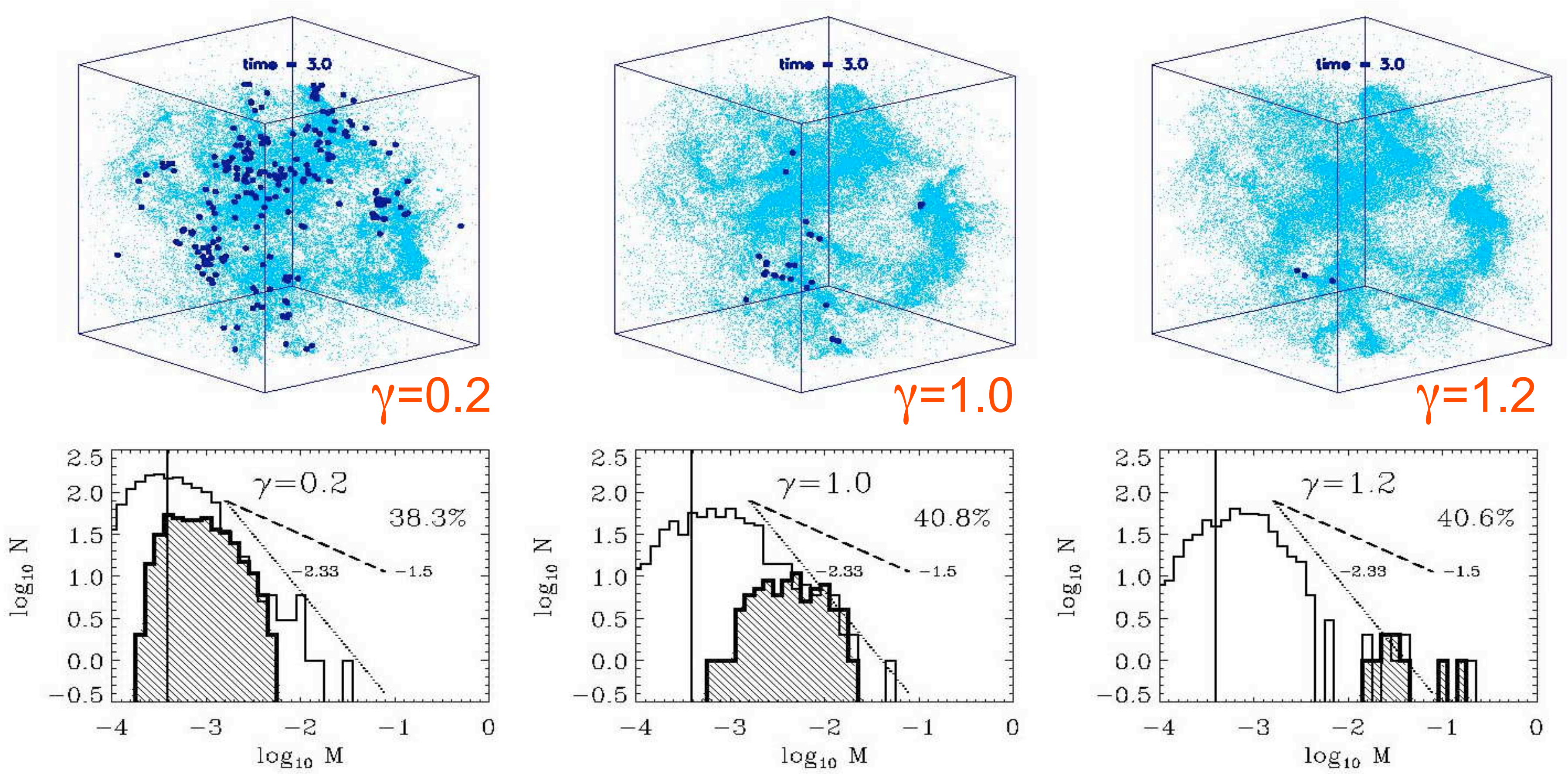

for $\gamma<1$ fragmentation is enhanced → *cluster of low-mass stars*

for $\gamma>1$ it is suppressed → formation of *isolated massive stars*

(from Li, Klessen, & Mac Low 2003, ApJ, 592, 975)

how does that work?

(1) $\mathbf{p} \propto \rho^{\gamma} \rightarrow \rho \propto \mathbf{p}^{1/\gamma}$

(2) $\mathbf{M_{jeans}} \propto \gamma^{3/2} \rho^{(3\gamma-4)/2}$

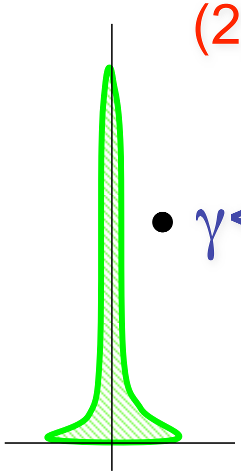

- $\gamma<1$: → *large* density excursion for given pressure
  → $\langle M_{jeans} \rangle$ becomes small
  → number of fluctuations with $M > M_{jeans}$ is large

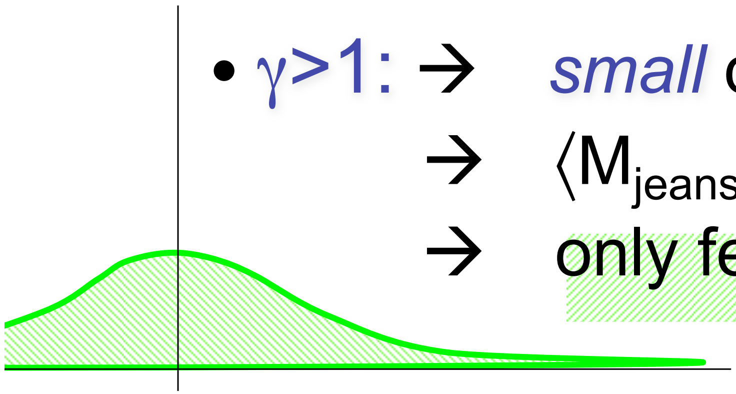

- $\gamma>1$: → *small* density excursion for given pressure
  → $\langle M_{jeans} \rangle$ is large
  → only few and massive clumps exceed M_{jeans}

EOS in different environments

EOS as function of metallicity

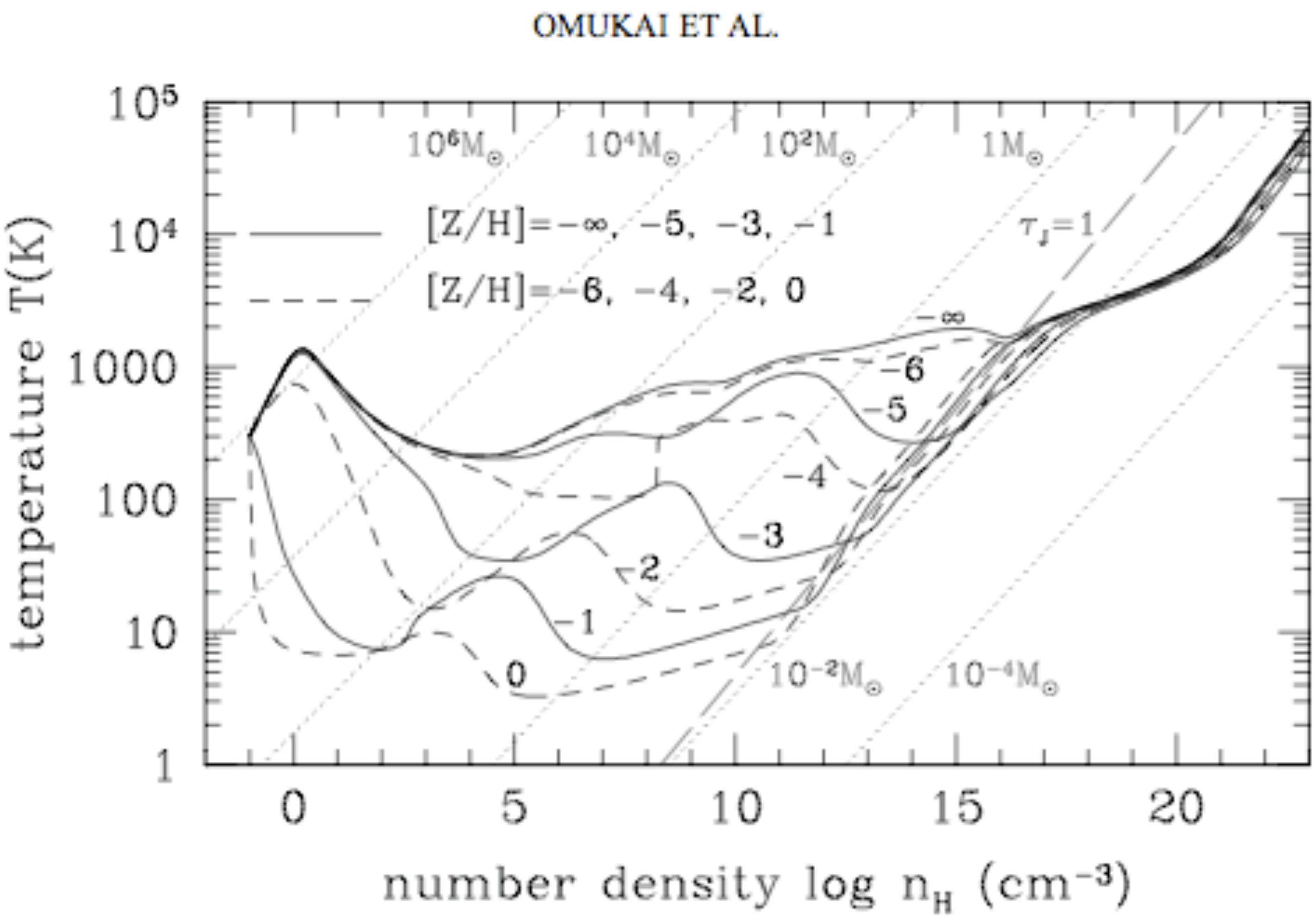

(Omukai et al. 2005)

EOS as function of metallicity

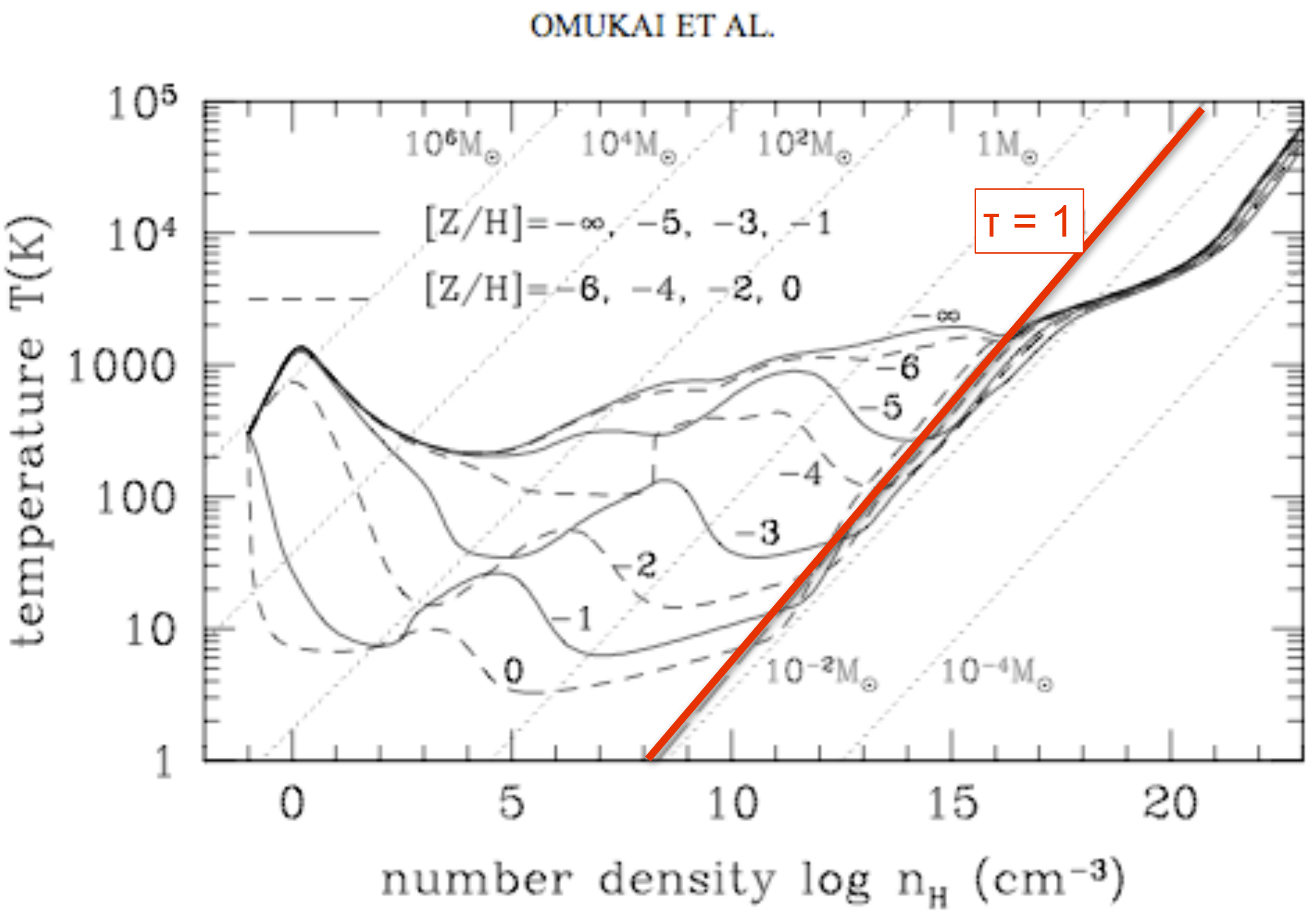

(Omukai et al. 2005)

EOS as function of metallicity

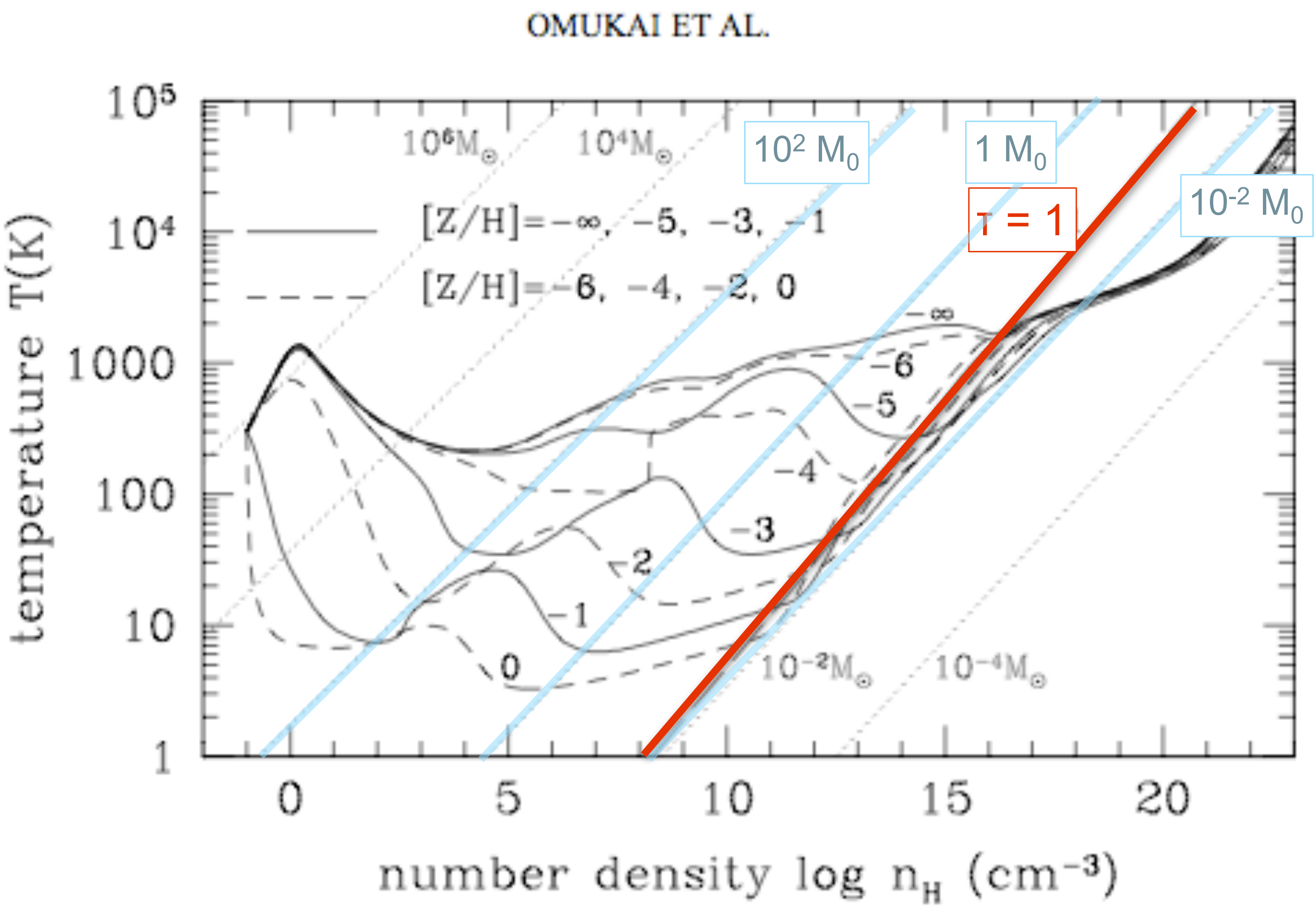

(Omukai et al. 2005)

present-day star formation

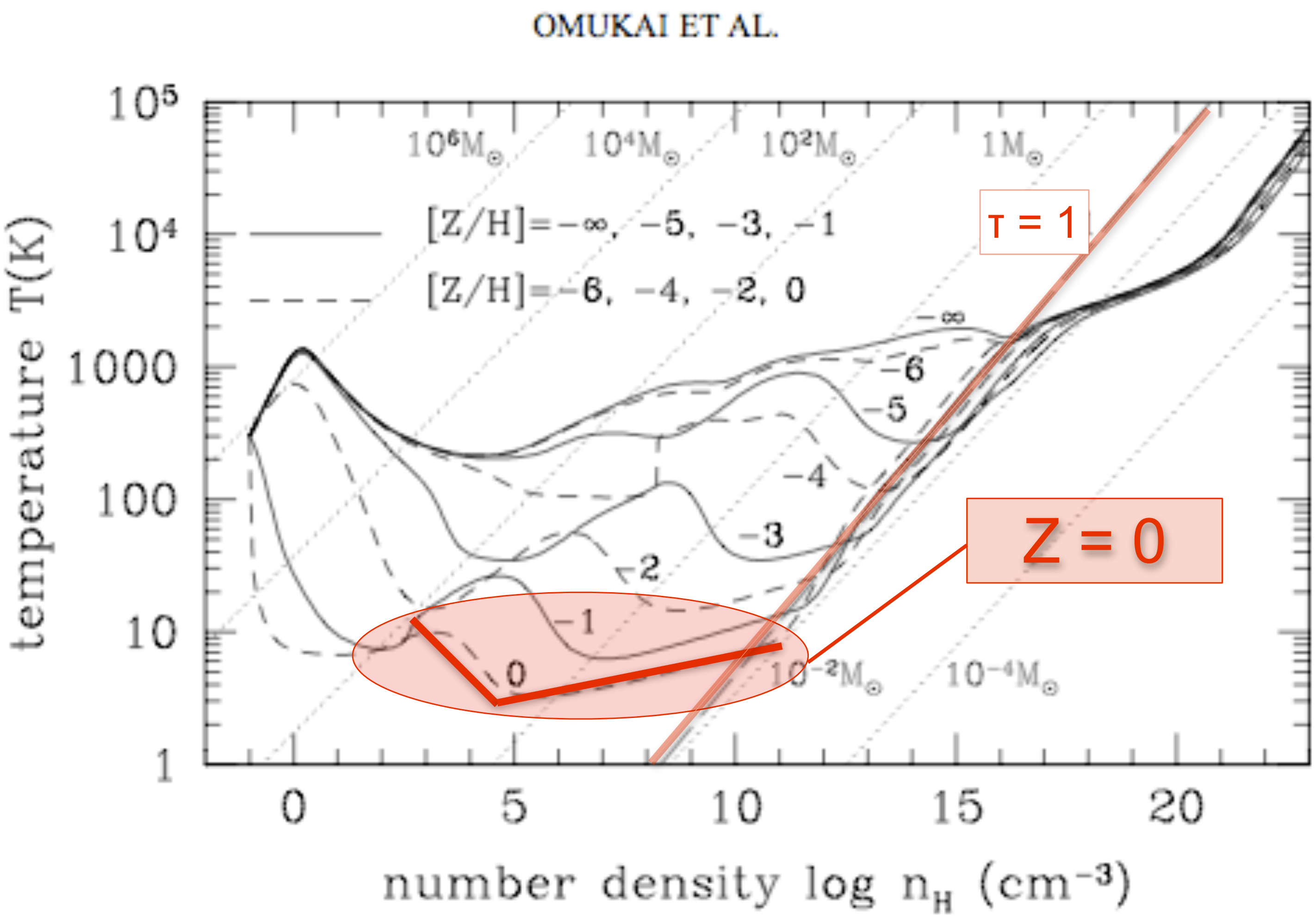

(Omukai et al. 2005, Jappsen et al. 2005, Larson 2005)

present-day star formation

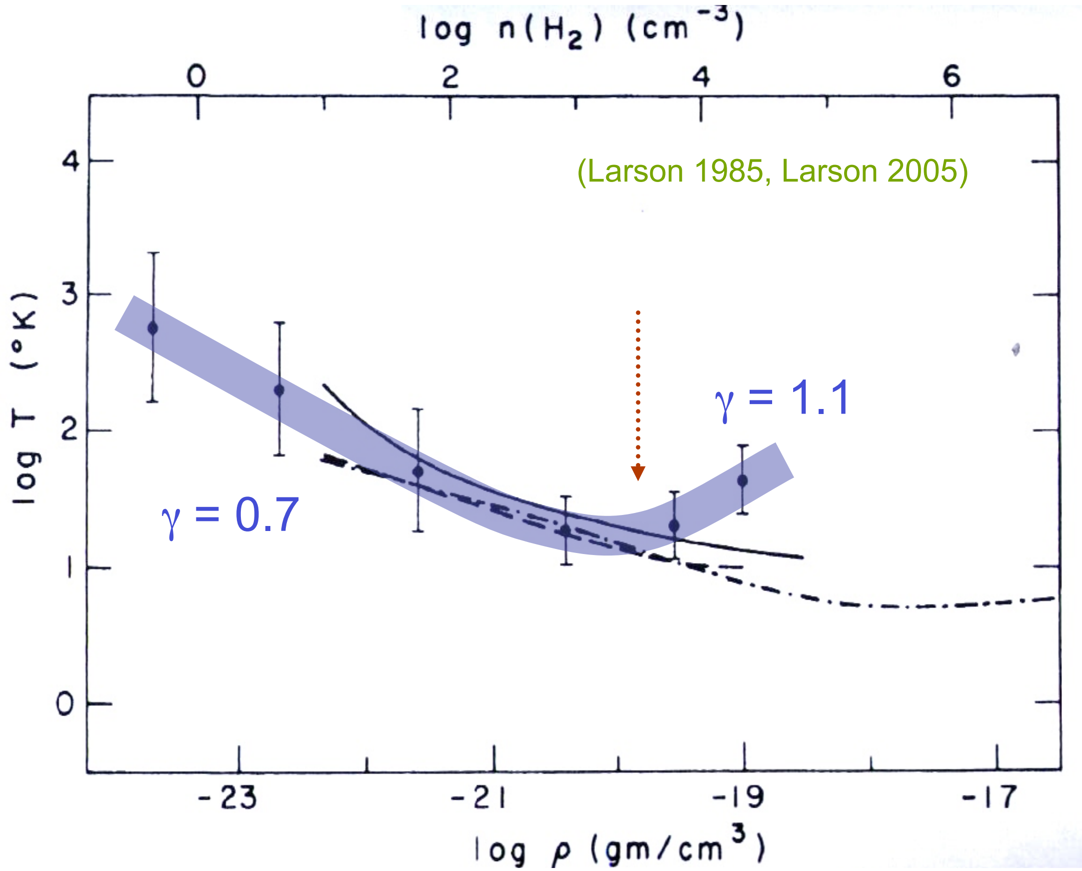

present-day star formation

This kink in EOS is very insensitive to environmental conditions such as ambient radiation field
--> reason for universal for of the IMF? (Elmegreen et al. 2008)

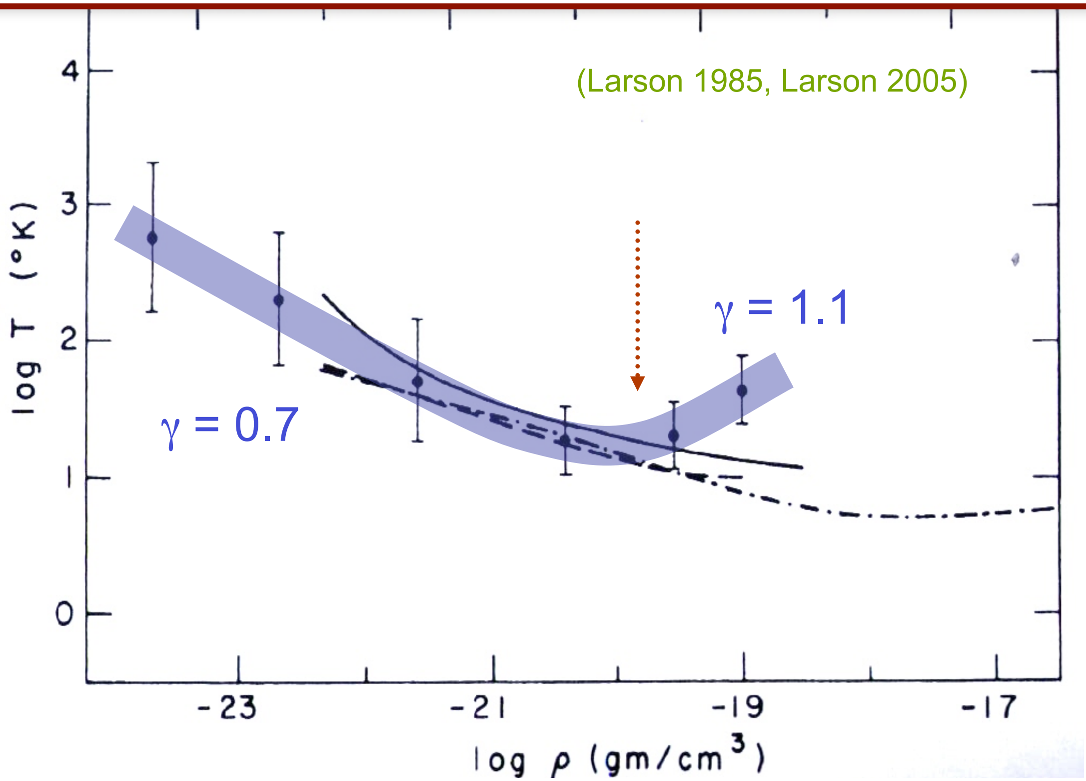

IMF from simple piece-wise polytropic EOS

$\gamma_1 = 0.7$

$\gamma_2 = 1.1$

$$\boxed{T \sim \rho^{\gamma-1}}$$

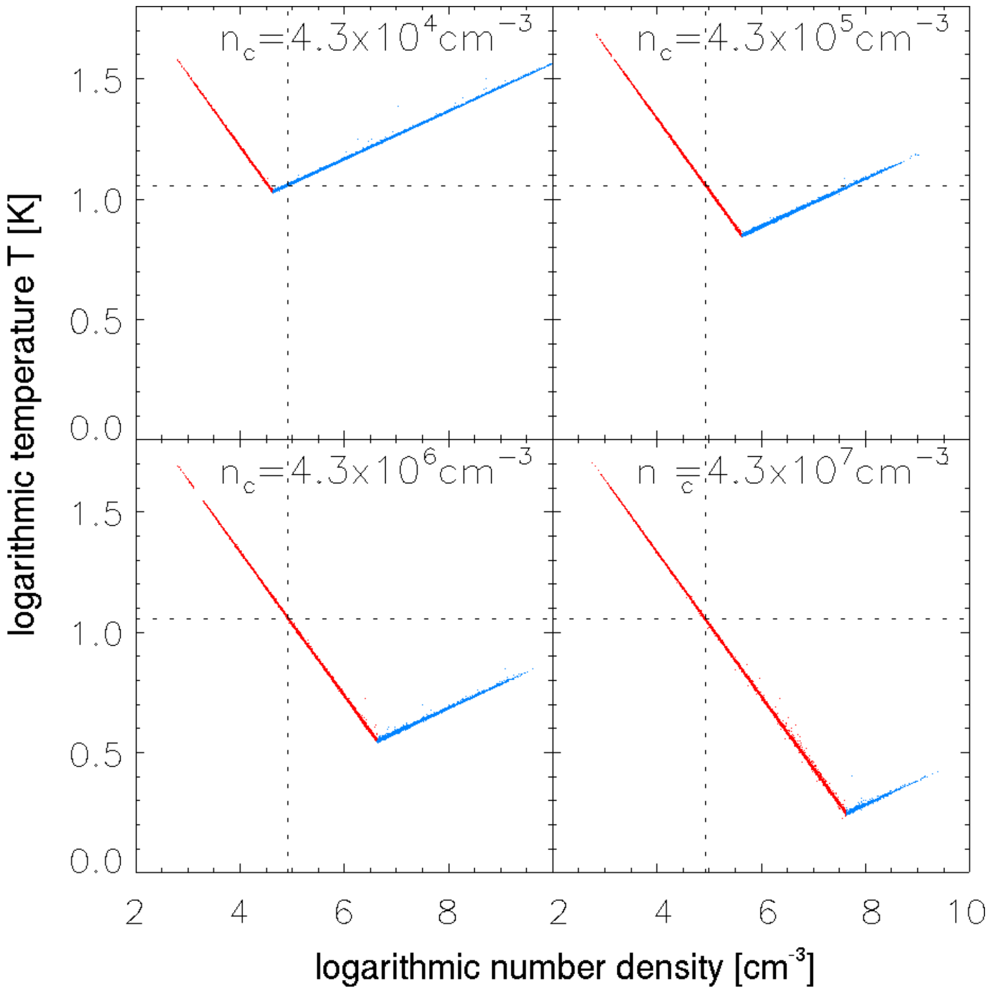

EOS and Jeans Mass:

$\mathbf{p} \propto \rho^{\gamma} \;\rightarrow\; \rho \propto \mathbf{p}^{1/\gamma}$

$\mathbf{M_{jeans}} \propto \gamma^{3/2}\,\rho^{(3\gamma-4)/2}$

(Jappsen et al. 2005)

IMF from simple piece-wise EOS

critical density ⬆ ⇨ median mass ⬇

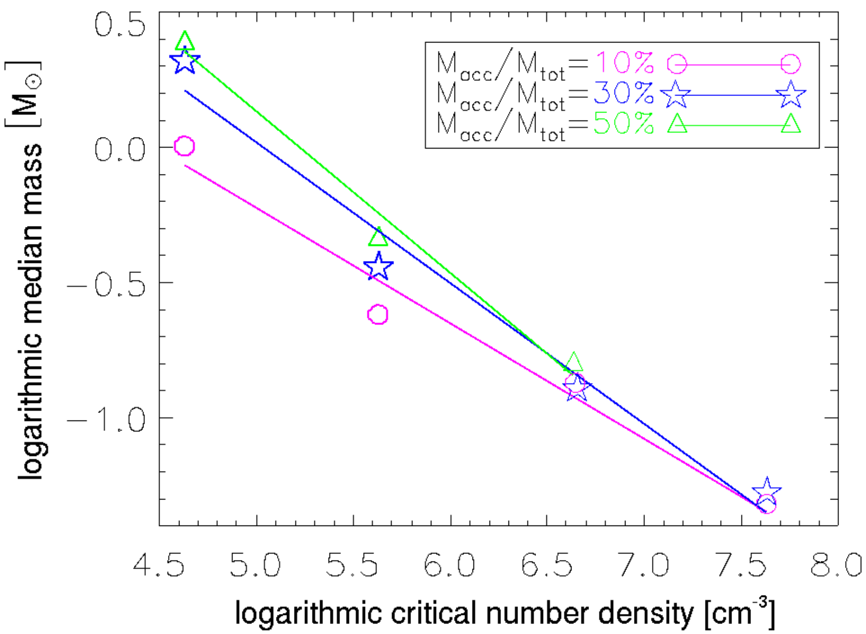

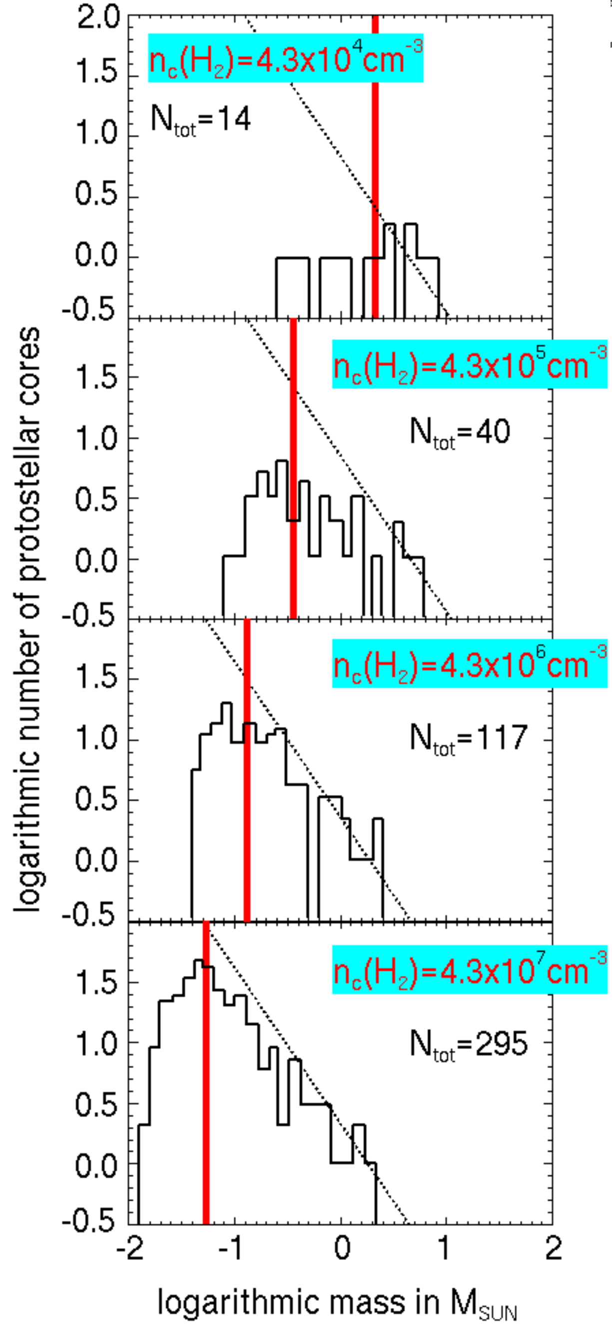

(Jappsen et al. 2005)

IMF in nearby molecular clouds

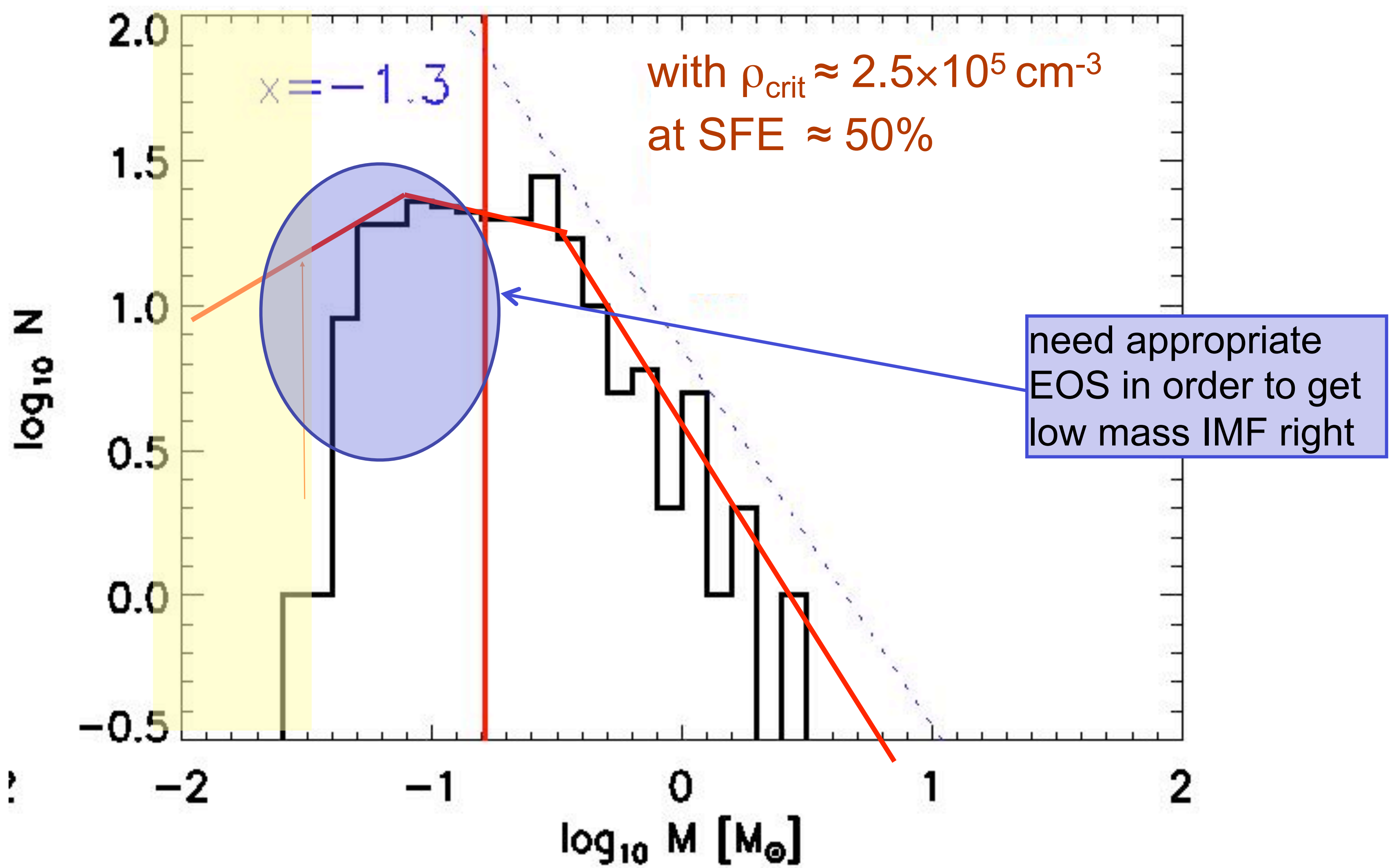

(Jappsen et al. 2005, A&A, 435, 611)

dependence on Z at low density

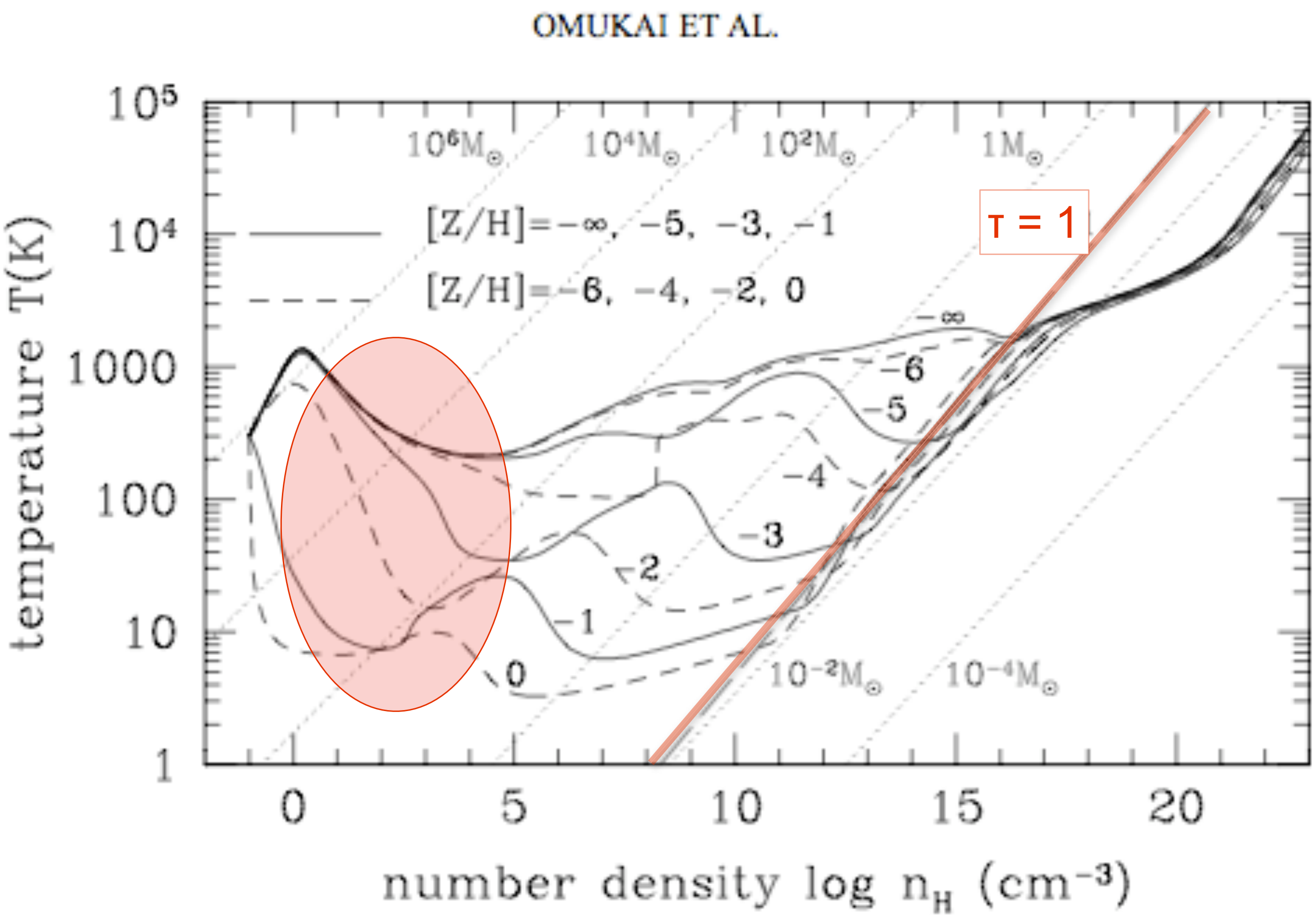

(Omukai et al. 2005)

dependence on Z at low density

- at densities $n < 10^2$ cm^{-3} and metallicities $Z < 10^{-2}$ *H_2 cooling* dominates behavior.
  (Jappsen et al. 2007)
- fragmentation depends on *initial conditions*
  - example 1: *solid-body rotating top-hat* initial conditions with dark matter fluctuations (a la Bromm et al. 1999) fragment no matter what metallicity you take (in regime $n \leq 10^6$ cm^{-3})
    because *unstable disk* builds up
    (Jappsen et al. 2009a)
  - example 2: *centrally concentrated halo* does *not* fragment up to densities of $n \approx 10^6$ cm^{-3} up to metallicities $Z \approx -1$ (Jappsen et al. 2009b)

implications for Pop III

- star formation will depend on *degree of turbulence* in protogalactic halo
- speculation: *differences in stellar mass function*?
- speculation:
  - low-mass halos → low level of turbulence → relatively massive stars
  - high-mass halos (atomic cooling halos) → high degree of turbulence → wider mass spectrum with peak at lower-masses?

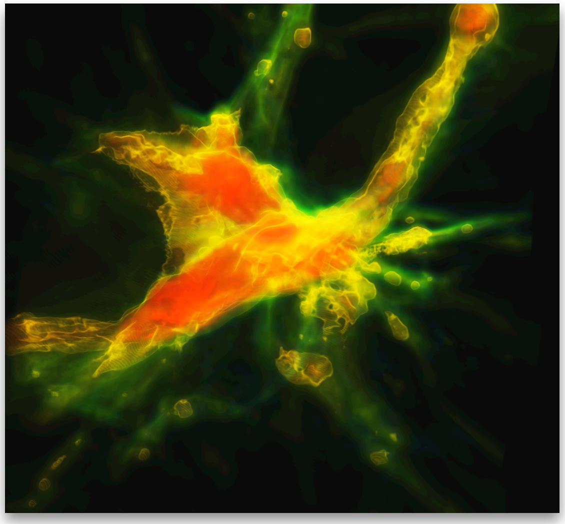

(Greif et al. 2008)

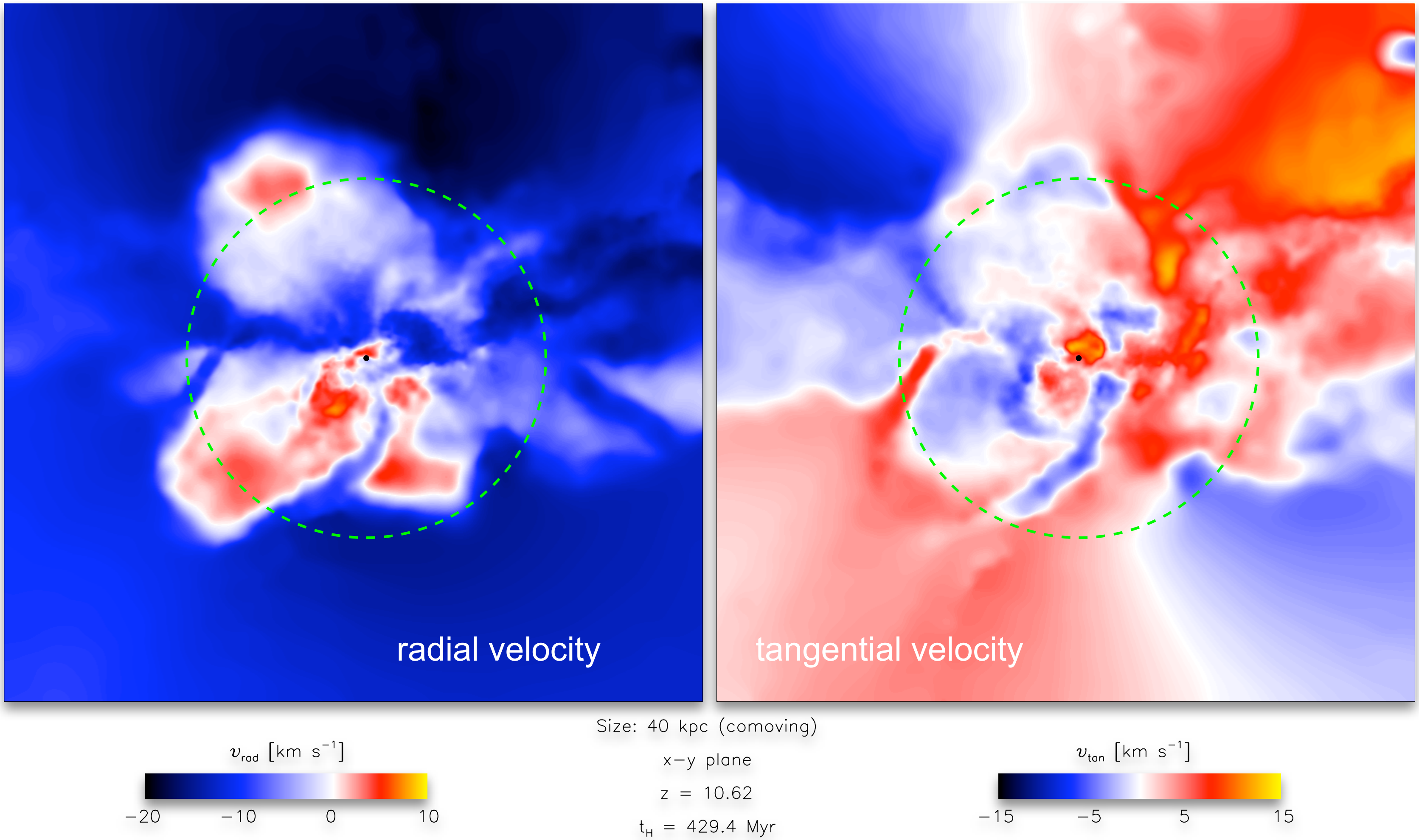

turbulence developing in an atomic cooling halo

(Greif et al. 2008)

Pop III.1

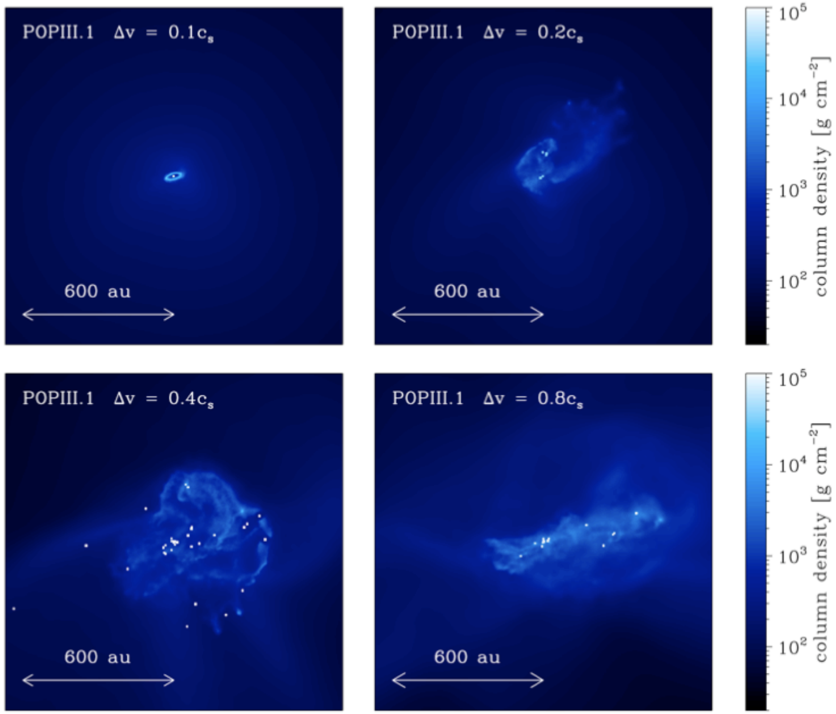

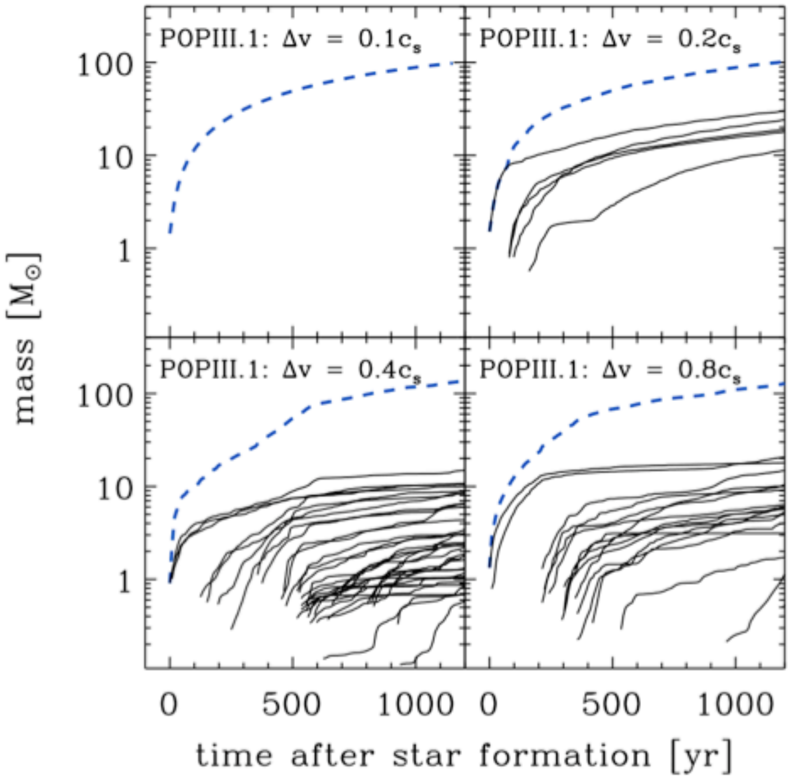

(Clark et al, submitted)

Pop III.2

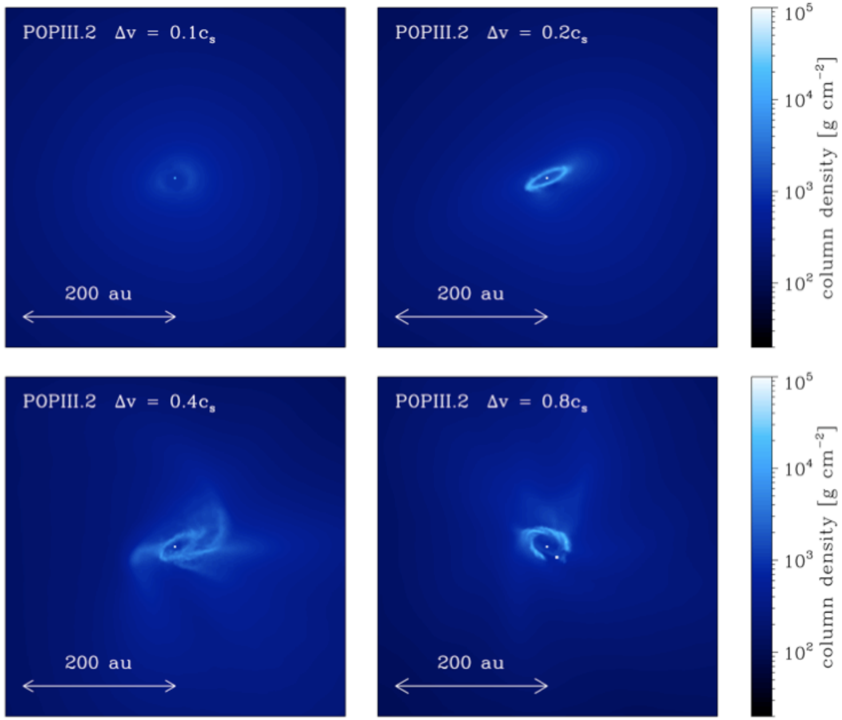

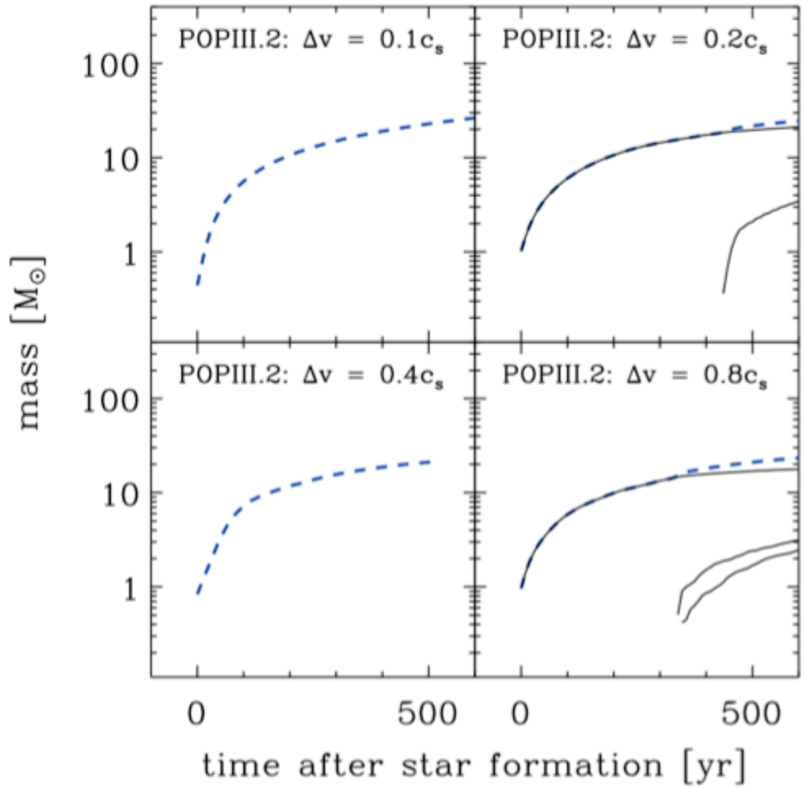

(Clark et al, submitted)

once again: thermodynamics

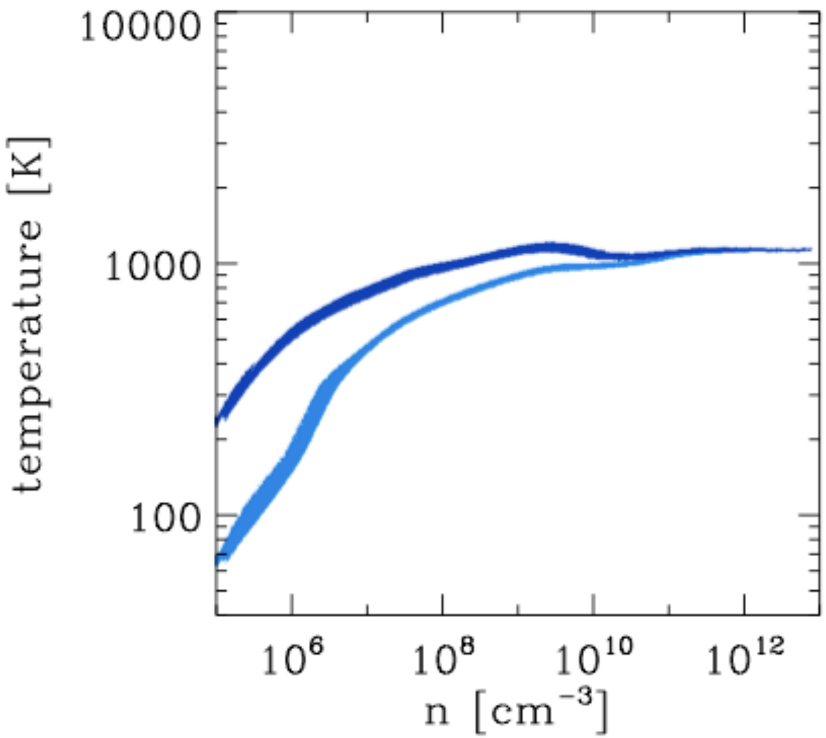

FIG. 6.— Temperature as a function of number density for the Pop. III.1 (dark blue) and Pop. III.2 (light blue) $\Delta v_{\rm turb} = 0.1\, c_s$ simulations. In both cases, the curves denote the state of the cloud at the point just before the formation of the sink particle.

also Pop III.2 gas heats up above the CMB

--> weaker fragmentation!

once again: thermodynamics

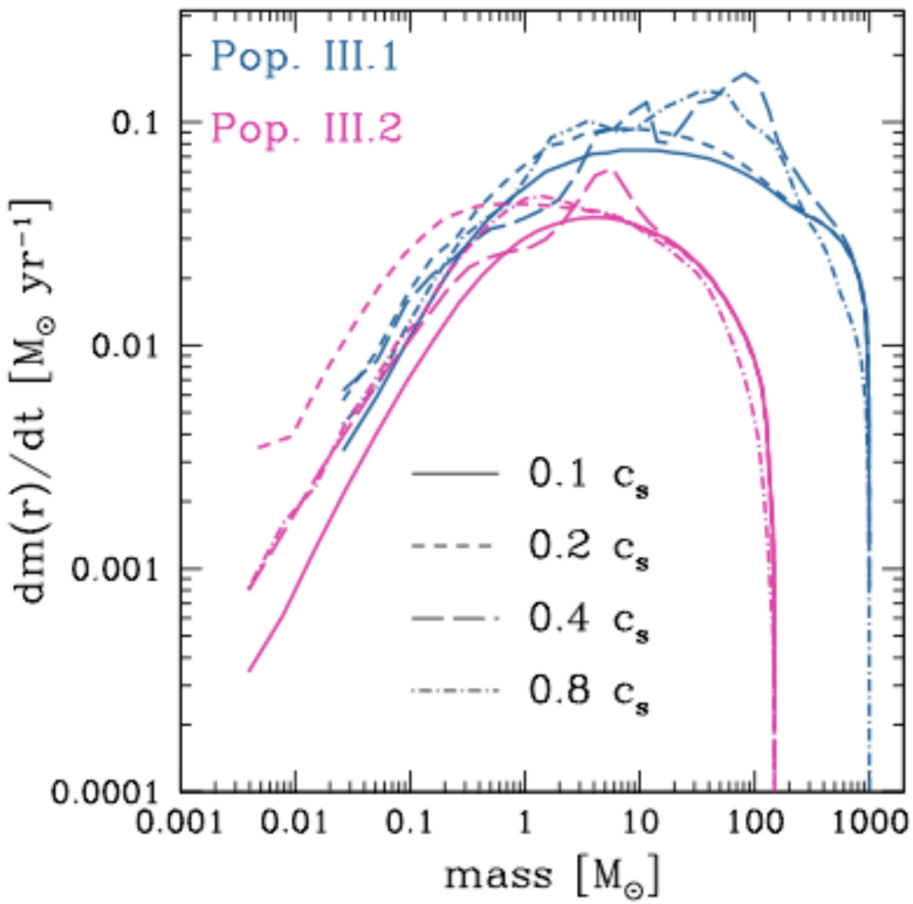

FIG. 8.— Accretion rates as a function of enclosed gas mass in the Pop. III.1 (upper lines; blue) and Pop. III.2 (lower lines; magenta) simulations, estimated as described in Section 4.1. Note that the sharp decline in the accretion rates for enclosed masses close to the initial cloud mass is an artifact of our problem setup; we would not expect to see this in a realistic Pop. III halo.

comparison of accretion rates...

transition: Pop III to Pop II.5

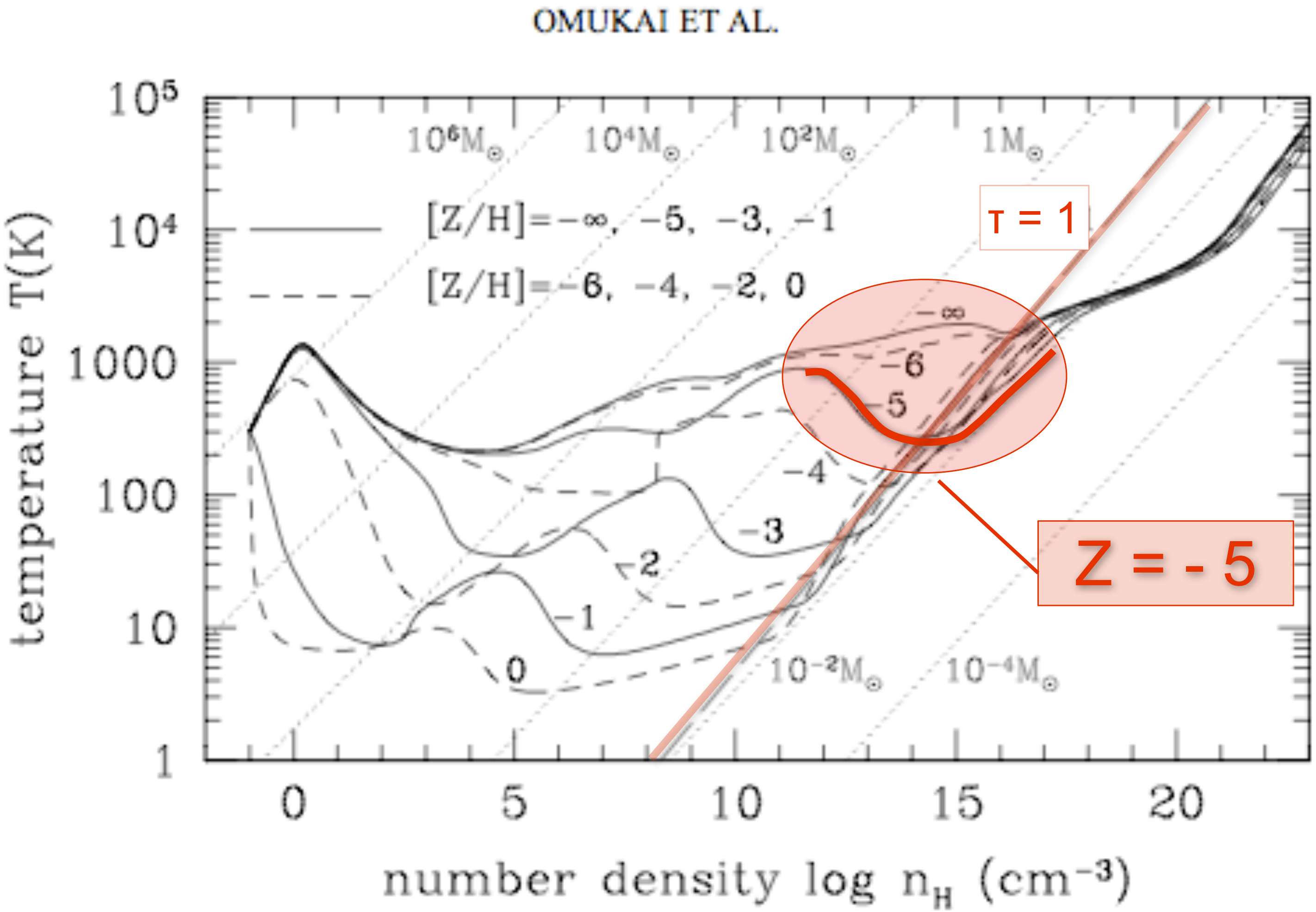

(Omukai et al. 2005)

transition: Pop III to Pop II.5

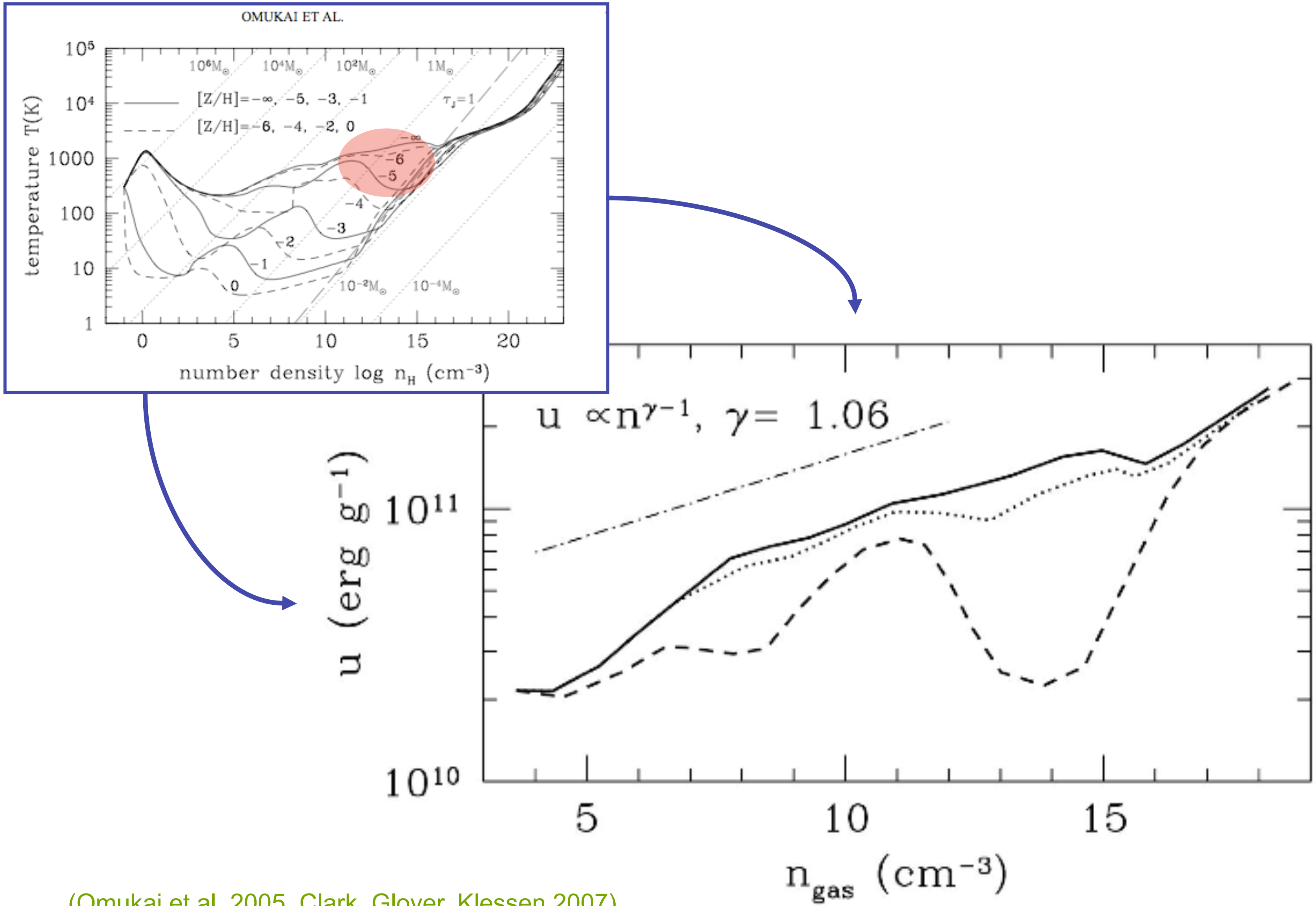

(Omukai et al. 2005, Clark, Glover, Klessen 2007)

dust induced fragmentation at $Z=10^{-5}$

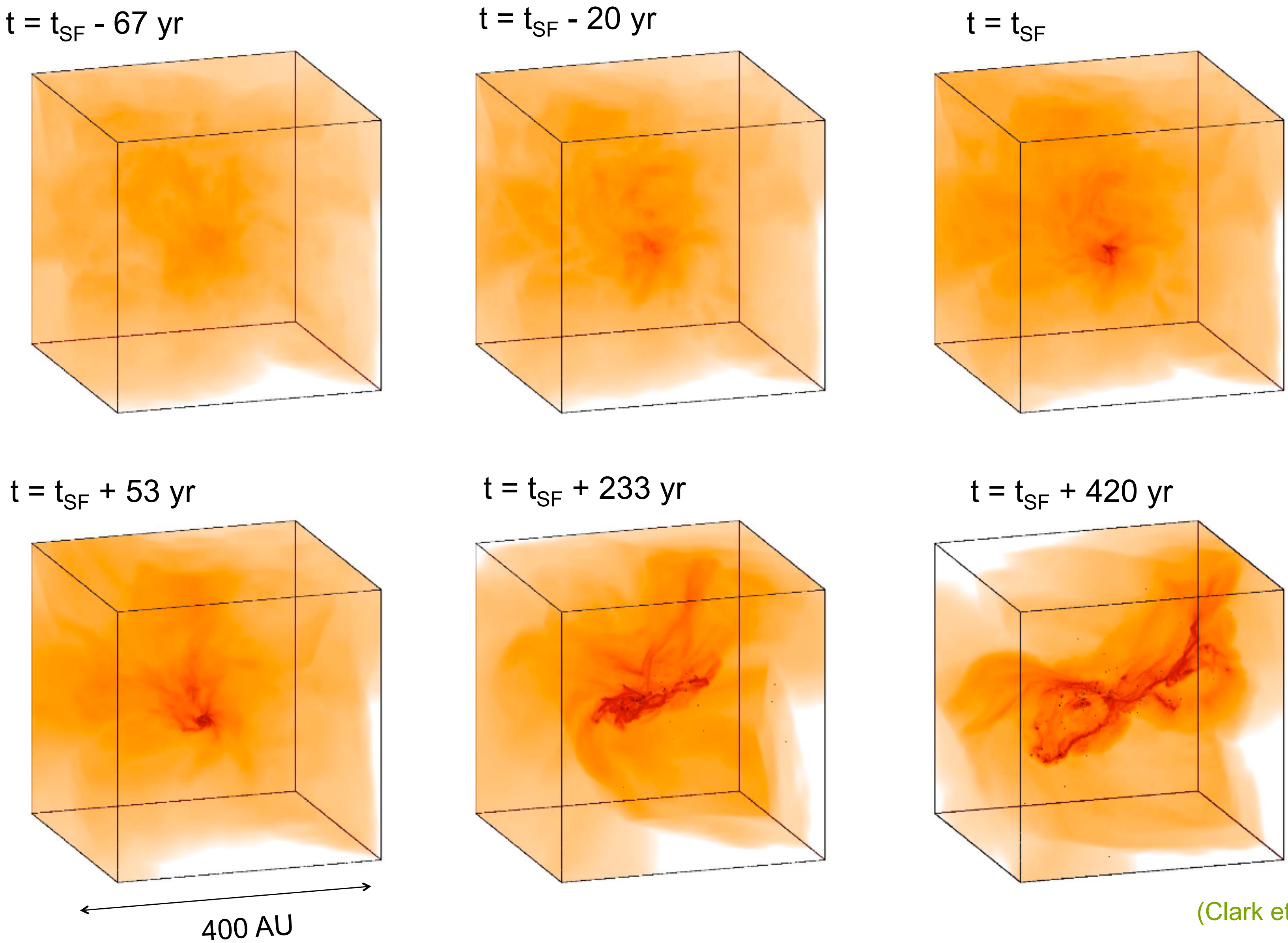

(Clark et al. 2007)

dust induced fragmentation at $Z=10^{-5}$

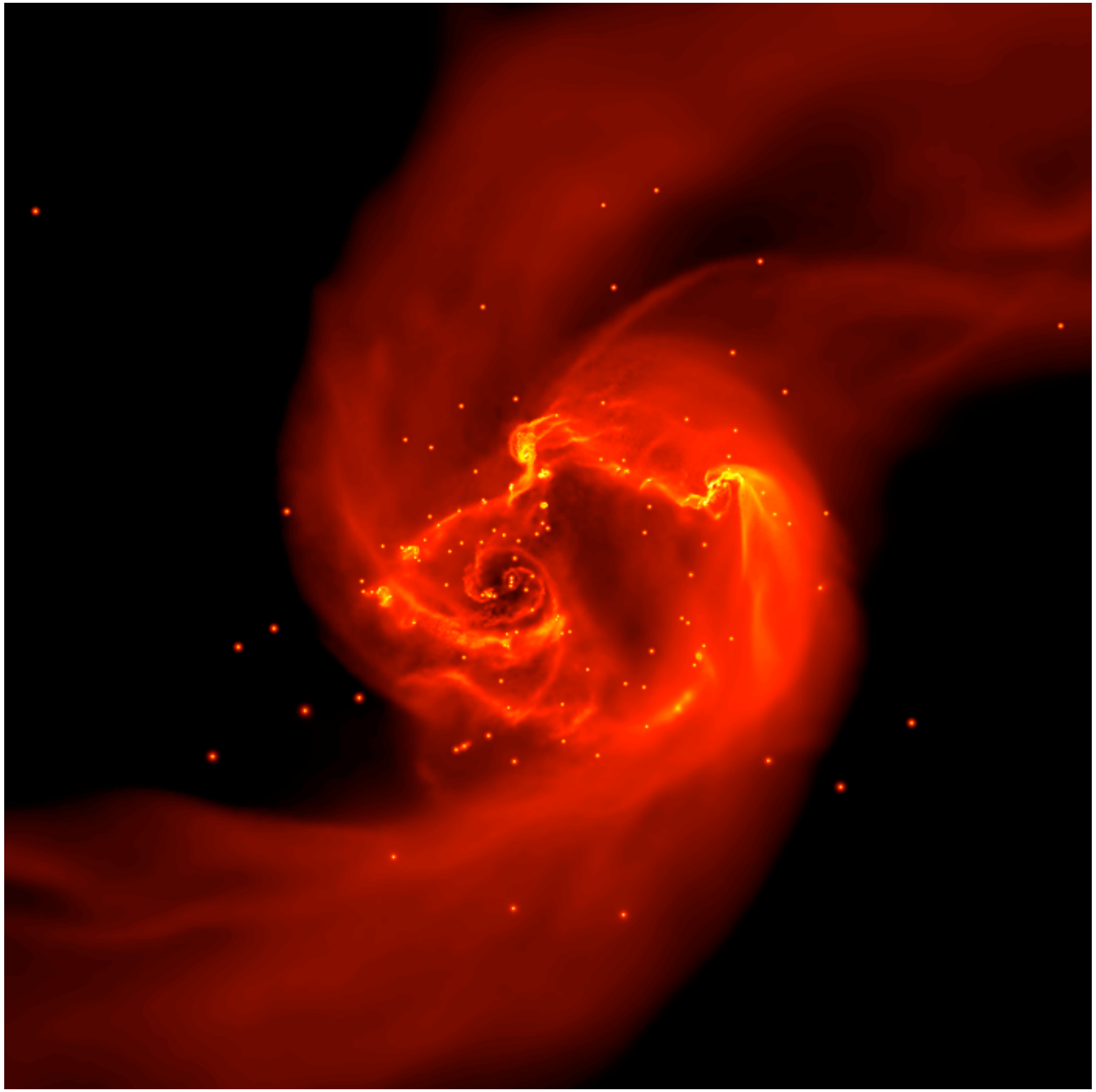

dense cluster of low-mass protostars builds up:

- mass spectrum peaks *below* $1\ M_{sun}$
- cluster VERY dense $n_{stars} = 2.5 \times 10^{9}\ pc^{-3}$
- fragmentation at density $n_{gas} = 10^{12} - 10^{13}\ cm^{-3}$

(Clark et al. 2008, ApJ 672, 757)

cluster build-up

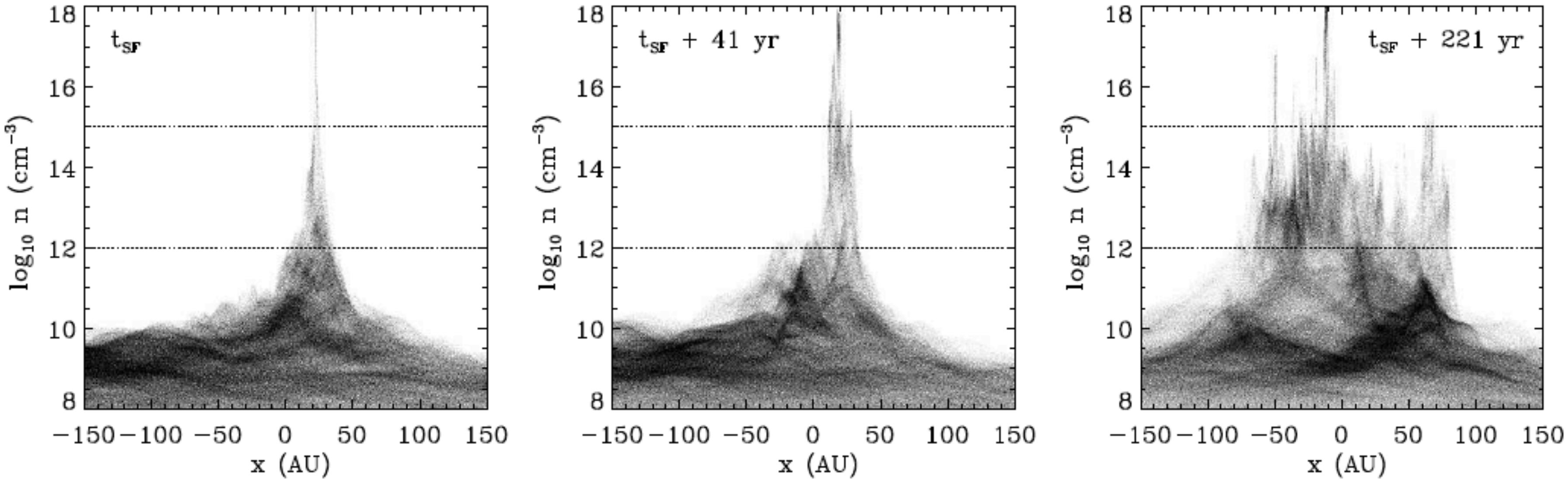

FIG. 3.— We illustrate the onset of the fragmentation process in the high resolution $Z = 10^{-5}\,Z_{\odot}$ simulation. The graphs show the densities of the particles, plotted as a function of their x-position. Note that for each plot, the particle data has been centered on the region of interest. We show here results at three different output times, ranging from the time that the first star forms (t_{sf}) to 221 years afterwards. The densities lying between the two horizontal dashed lines denote the range over which dust cooling lowers the gas temperature.

(Clark et al. 2007)

cluster build-up

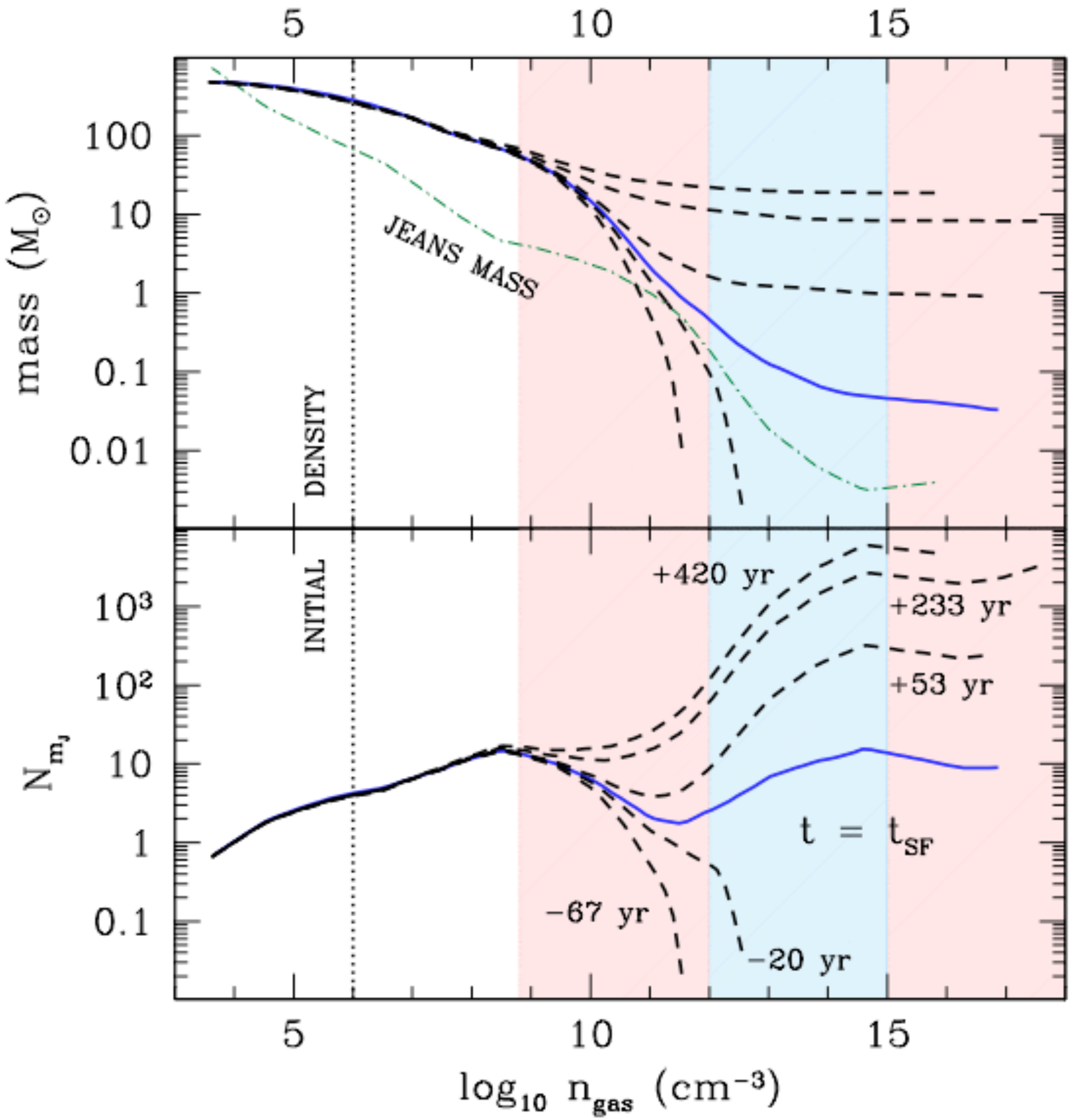

$\gamma > 1$
(heating)

$\gamma < 1$
(cooling)

(Clark et al. 2007)

gas properties

gas properties at time when first star forms

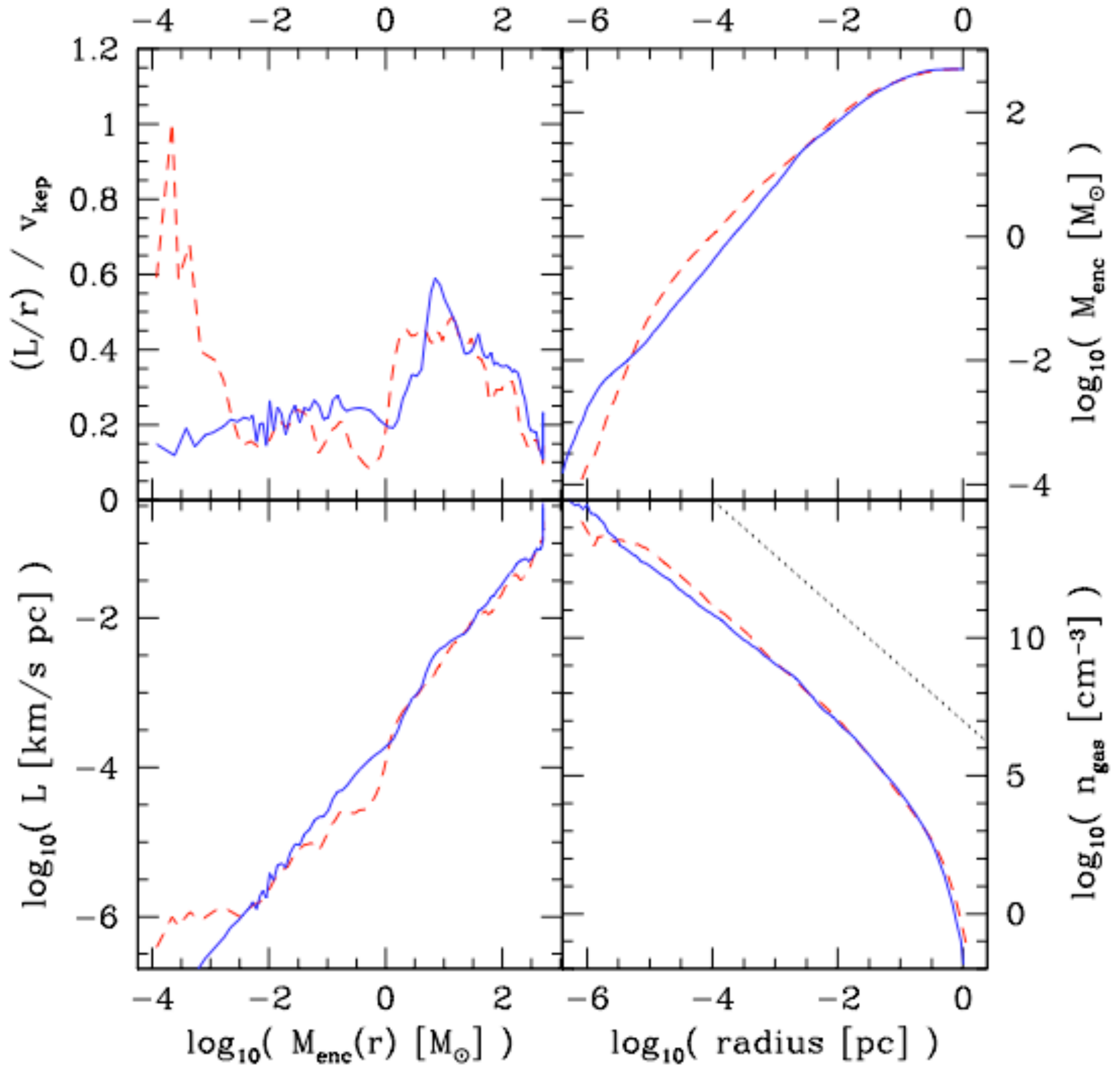

(Clark et al. 2007)

dust induced fragmentation at $Z=10^{-5}$

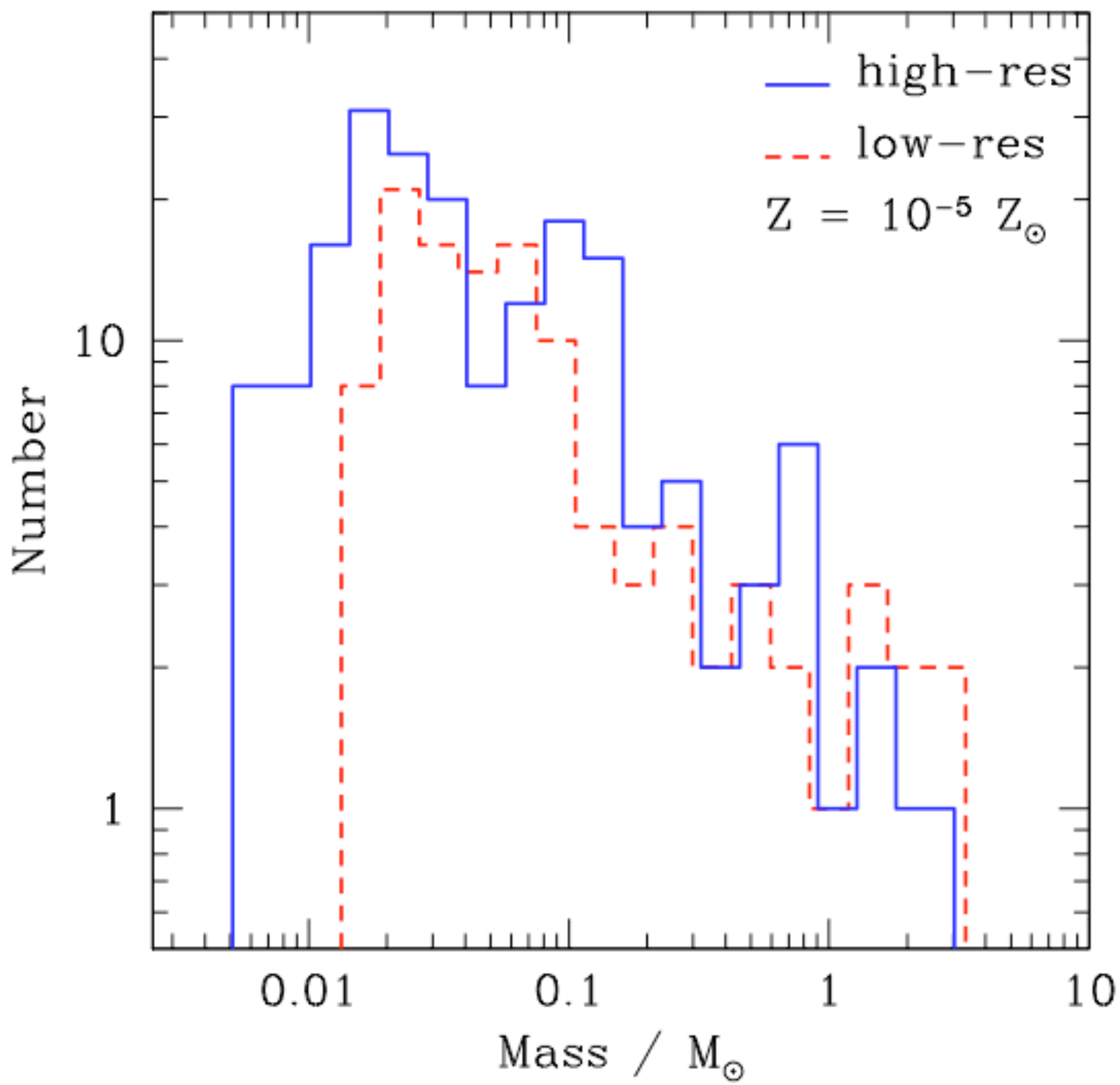

dense cluster of low-mass protostars builds up:

- mass spectrum peaks below 1 M_{sun}
- cluster VERY dense $n_{stars} = 2.5 \times 10^9 \, pc^{-3}$

- *predictions:*
  * low-mass stars with [Fe/H] ~ 10^{-5}
  * high binary fraction

(Clark et al. 2008)

dust induced fragmentation at $Z=10^{-5}$

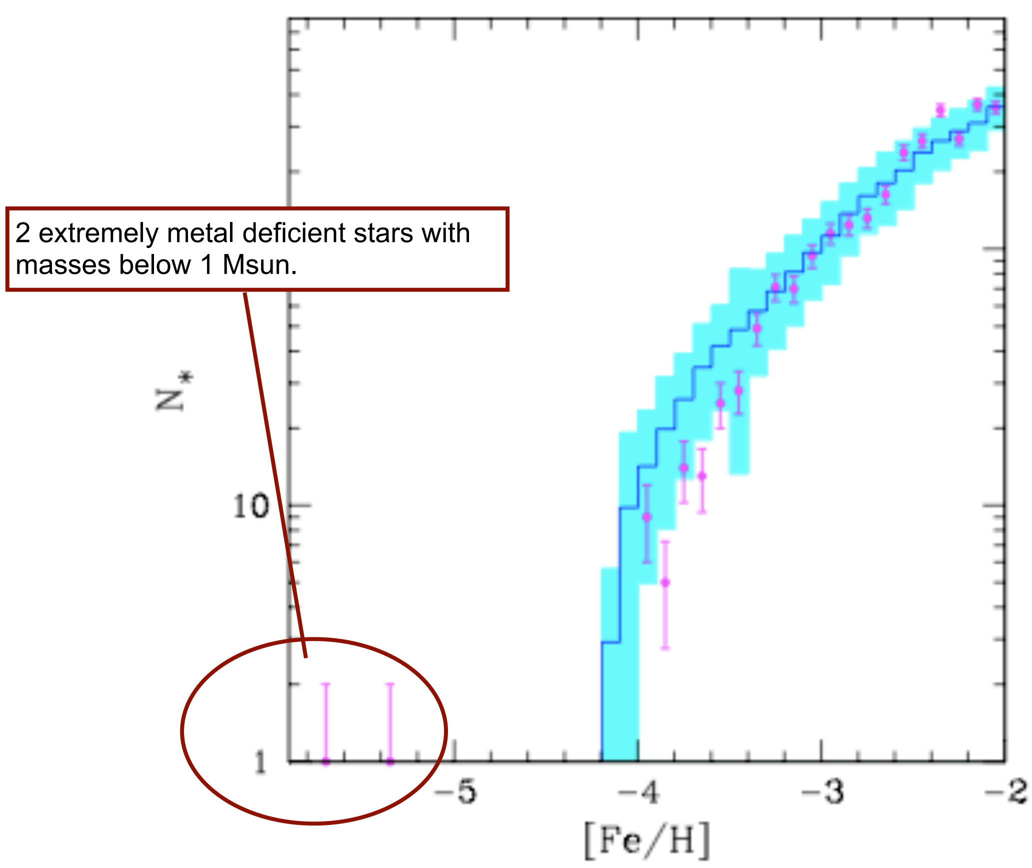

(plot from Salvadori et al. 2006, data from Frebel et al. 2005)

dense cluster of low-mass protostars builds up:

- mass spectrum peaks below 1 M_{sun}
- cluster VERY dense $n_{stars} = 2.5 \times 10^9\ pc^{-3}$
- *predictions:*
  * low-mass stars with [Fe/H] ~ 10^{-5}
  * high binary fraction

(Clark et al. 2008)

metal-free star formation

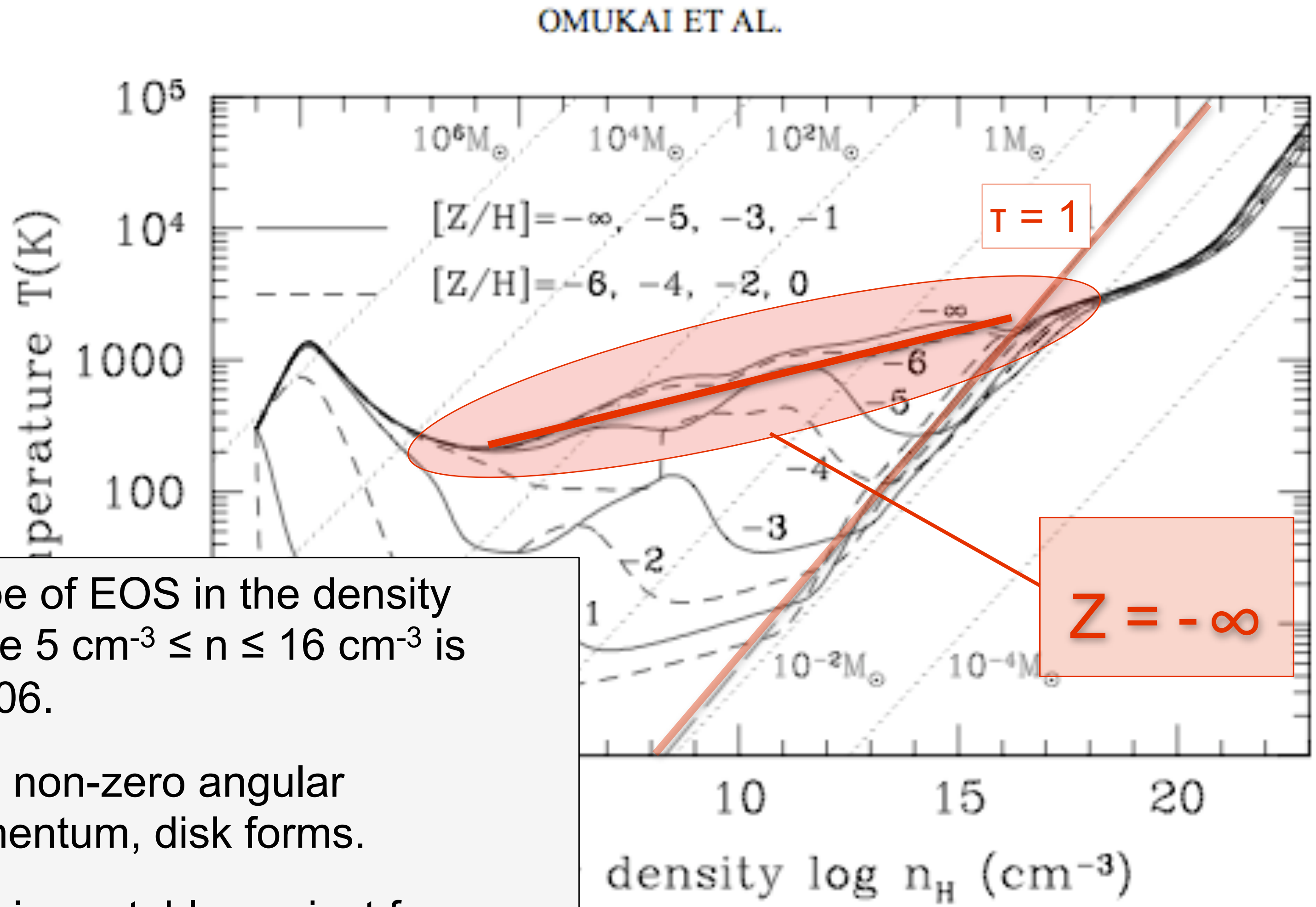

- slope of EOS in the density range 5 cm^{-3} ≤ n ≤ 16 cm^{-3} is γ≈1.06.
- with non-zero angular momentum, disk forms.
- disk is unstable against fragmentation at high density

more on Z=0 star formation

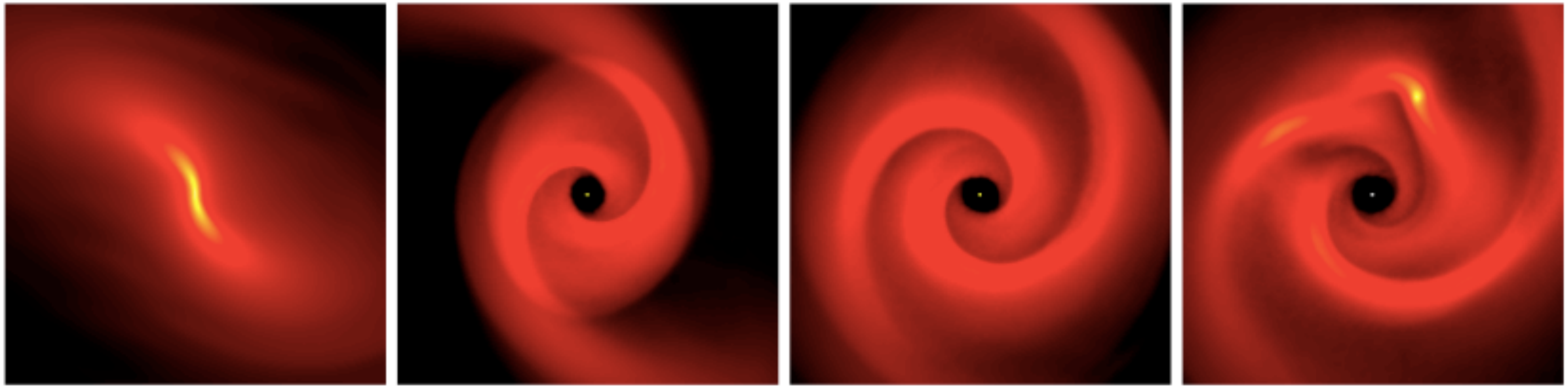

FIGURE 1. Column density images of the inner 66 au of the simulation, following the formation of the first protostar (sink particle) and the subsequent build-up of the protostellar disc and its eventual fragmentation. Starting from left-hand panel, which shows the gas at 1 yr before the protostar forms (t_{SF}), the next 3 panels show the evolution at times $t_{SF}+76$ yr, $t_{SF}+152$ yr and $t_{SF}+228$ yr. The colour table is stretched from 10^3 g cm^{-2} to 10^6 g cm^{-2}.

more on Z=0 star formation

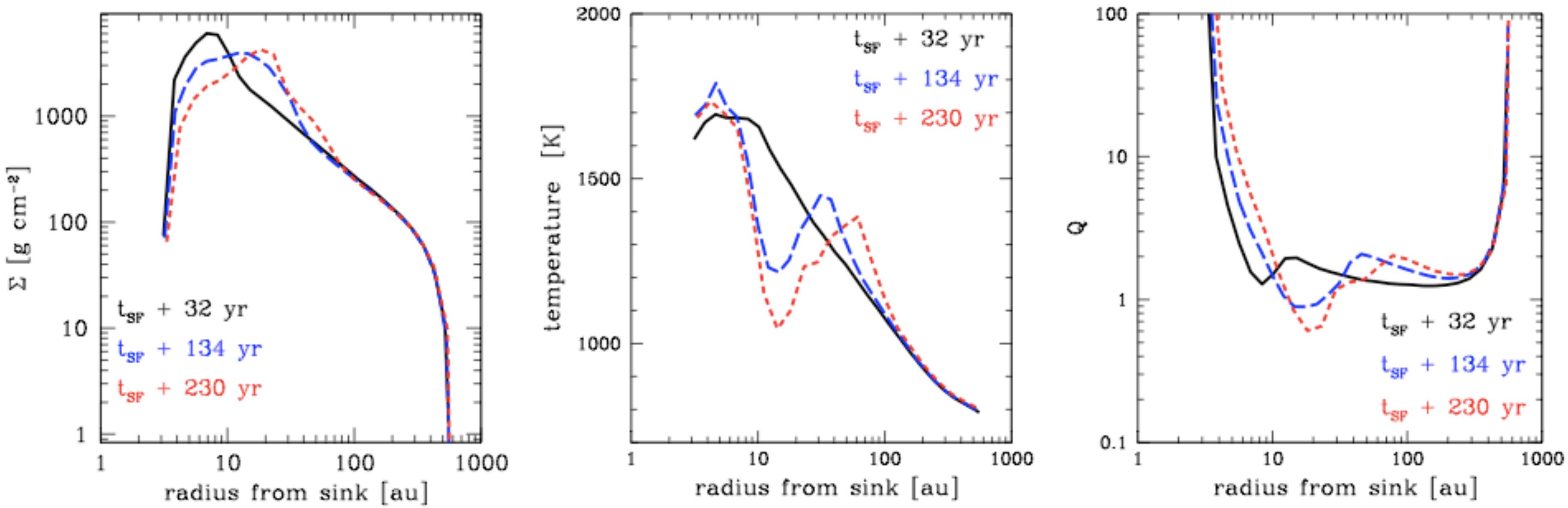

FIGURE 2. In the left-hand and central plots we show the radial profiles of the disc's surface density and gas temperature, centred on the first protostellar core to form in the simulation. The quantities are mass-weighted and taken from a slice through the midplane of the disc. In the right-hand plot we show the radial distribution of the corresponding Toomre parameter, $Q = c_s \kappa / \pi G \Sigma$, where c_s is the sound speed and κ is the epicyclic frequency. We adopt the standard simplification, and replace κ with the orbital frequency.

more on Z=0 star formation

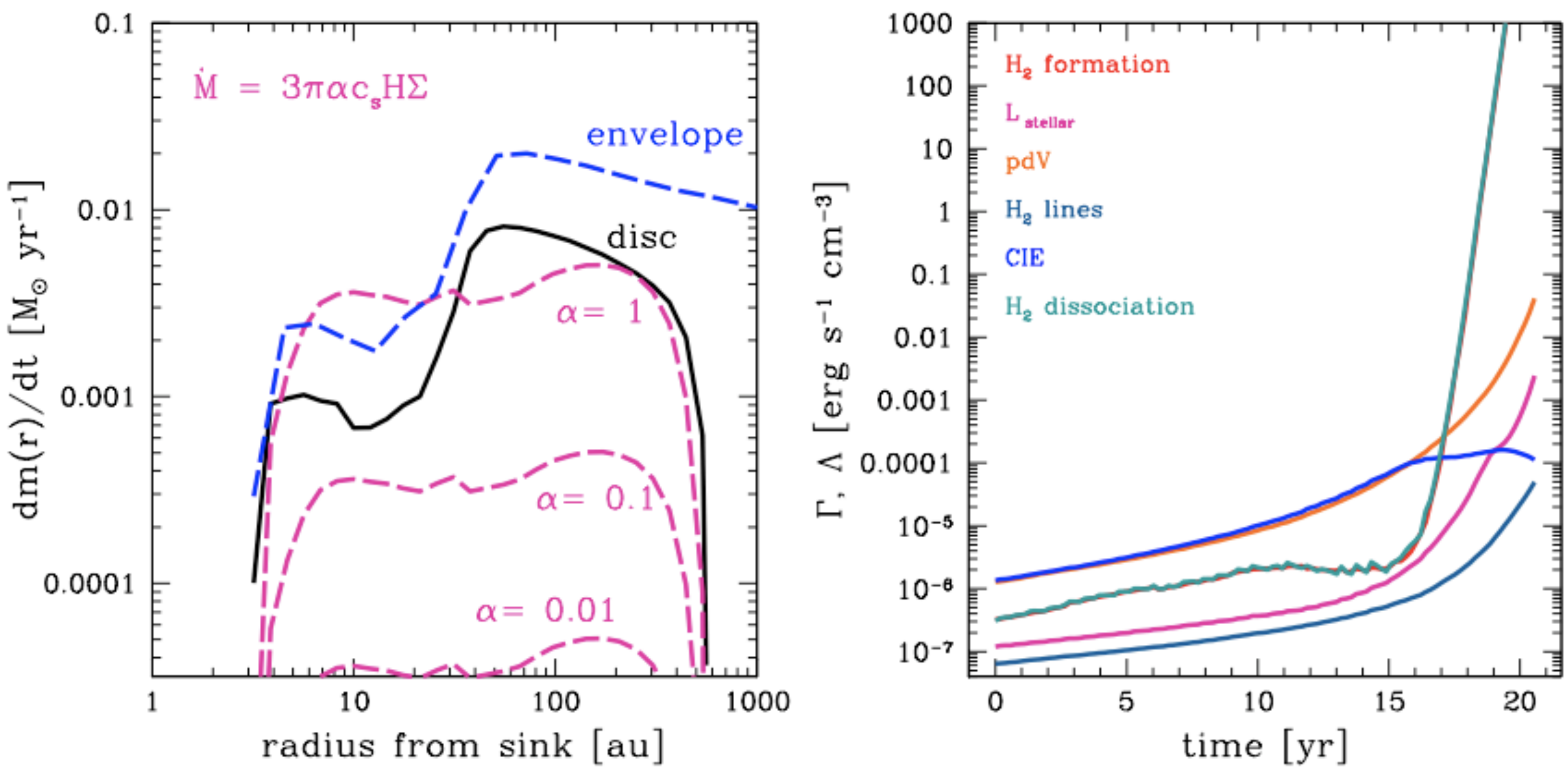

FIGURE 3. The left-hand plot shows the mass transfer through the disc. The solid black line shows the amount of mass moving inwards through each radial annulus in the disc per unit time. The dashed blue line shows the same quantity for the full spherical infalling envelope. The pink dashed lines show the accretion rates expected from an 'alpha' (thin) disc model, with three values of alpha. The right-hand plot shows the main heating and cooling processes that control the temperature evolution in the collapsing clump in the run-up to its eventual collapse.

primordial star formation

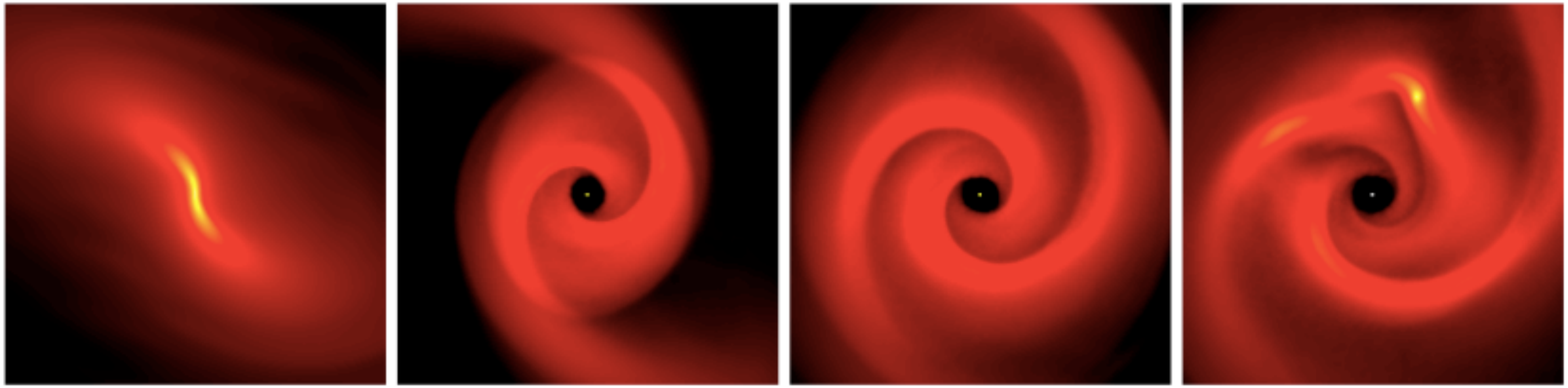

- first star formation is not less complex than present-day star formation
- brave claim: *all* Pop III stars form in multiple systems
- even braver claim: some Pop III stars fall in the mass range < 0.5 $M_\odot$ ---> they should still *be around*!!!!

IMF

- distribution of stellar masses depends on
  - turbulent initial conditions
    --> mass spectrum of prestellar cloud cores
  - collapse and interaction of prestellar cores
    --> competitive accretion and *N*-body effects
  - *thermodynamic properties of gas*
    --> balance between heating and cooling
    --> EOS (determines which cores go into collapse)
  - (proto) stellar feedback terminates star formation
    ionizing radiation, bipolar outflows, winds, SN

Introduction

We want to address the following questions:

- What determines the upper stellar mass limit?
- What is the physics behind the observed HII regions?

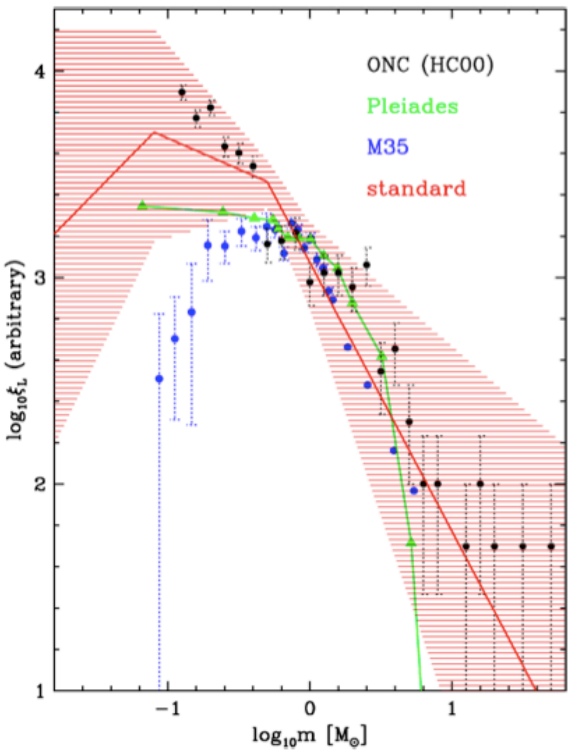

IMF (Kroupa 2002)

Rosetta nebula (NGC 2237)

Feedback Processes

- radiation pressure on dust particles
- ionizing radiation
- stellar wind
- jets and outflows

Feedback Processes

- radiation pressure on dust particles
- ionizing radiation
- stellar wind
- jets and outflows

Radiation Pressure

has gained the most attention in the literature, most recent simulations by Krumholz et al. 2009

Ionization

only a few numerical studies so far (eg. Dale et al. 2007, Gritschneder et al. 2009), but H II regions around massive protostars can be observed!
$\longrightarrow$ direct comparison with observations possible

high-mass star formation

- focus on collapse of individual high-mass cores...
  - massive core with 1,000 $M_\odot$
  - Bonnor-Ebert type density profile
    (flat inner core with 0.5 pc and rho ~ $r^{-3/2}$ further out)
  - initial m=2 perturbation, rotation with $\beta = 0.05$
  - sink particle with radius 600 AU and threshold density of 7×10^{-16} g cm^{-3}
  - cell size 100 AU

Peters et al. (2010a, ApJ, 711, 1017), Peters et al. (2010b, arXiv:1003.4998), Peters et al. (2010c,1005.3271)

high-mass star formation

- method:
  - FLASH with ionizing and non-ionizing radiation using raytracing based on hybrid-characteristics
  - protostellar model from Hosokawa & Omukai
  - rate equation for ionization fraction
  - relevant heating and cooling processes

  - *first 3D calculations that consistently treat both ionizing and non-ionizing radiation in the context of high-mass star formation*

Peters et al. (2010a,b,c)

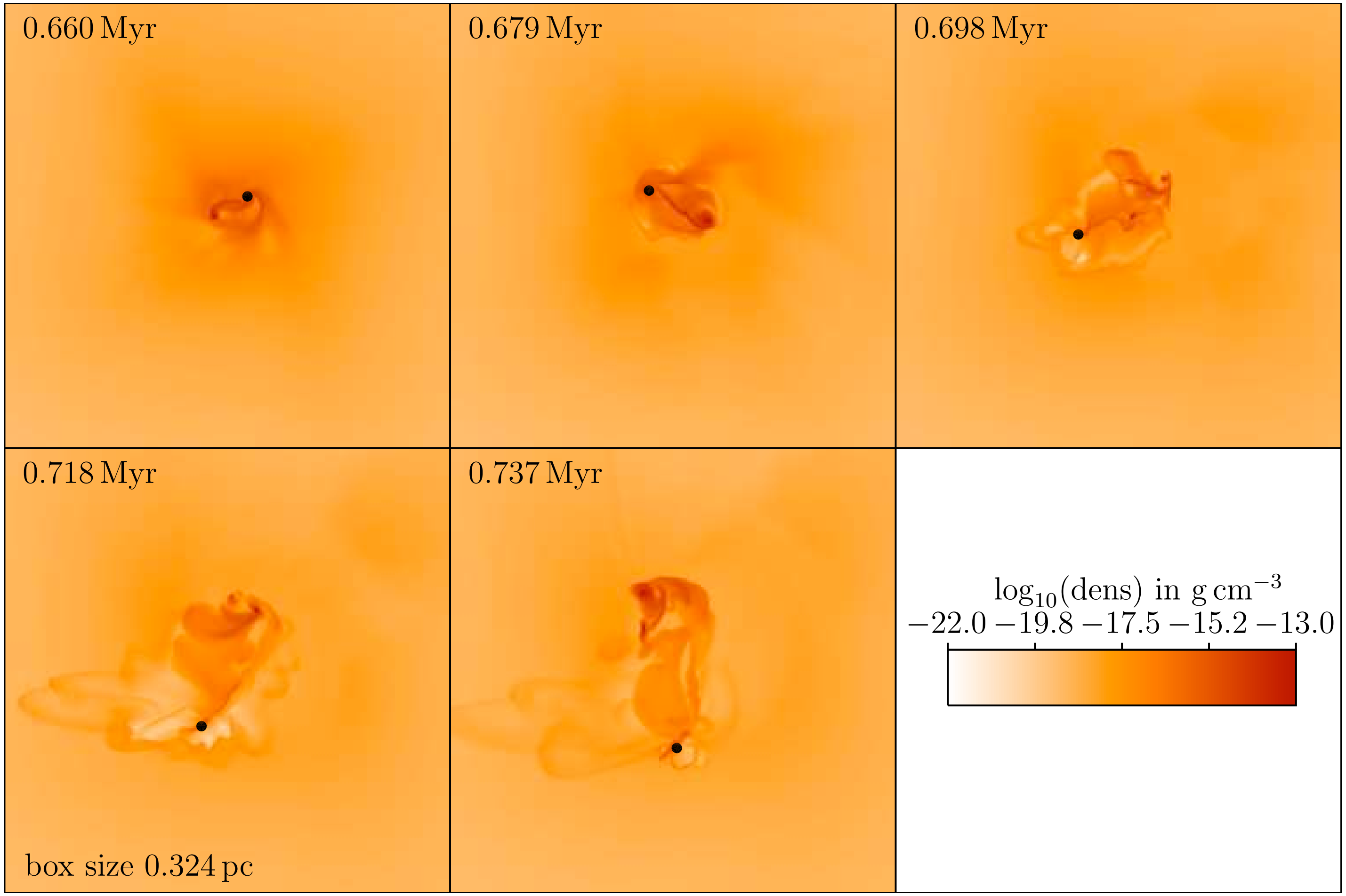

- disk is gravitationally unstable and fragments
- we suppress secondary sink formation by "Jeans heating"
- H II region is shielded effectively by dense filaments
- ionization feedback does not cut off accretion!

Peters et al. (2010a,b,c)

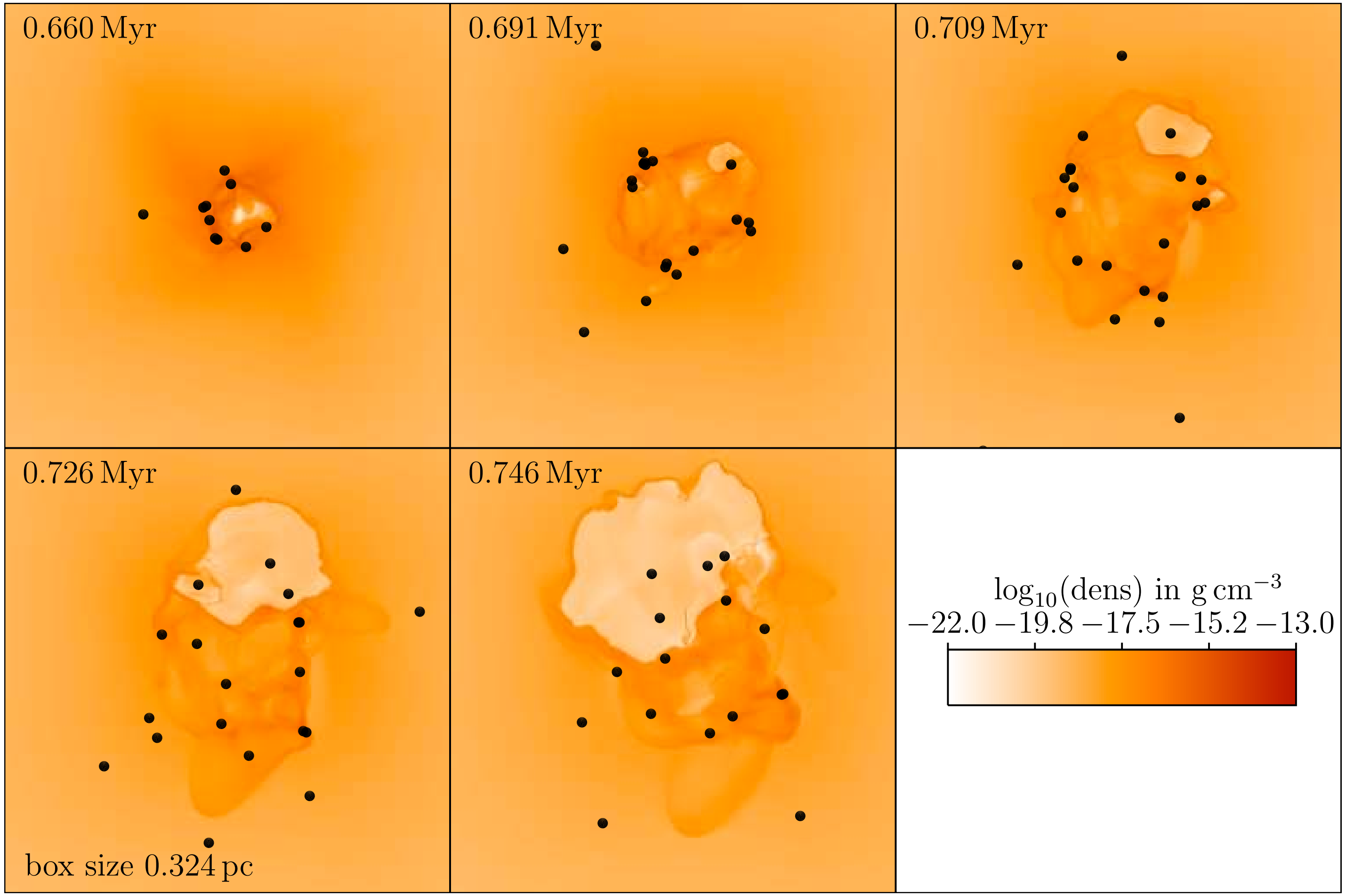

- all protostars accrete from common gas reservoir
- accretion flow suppresses expansion of ionized bubble
- cluster shows “fragmentation-induced starvation”
- halting of accretion flow allows bubble to expand

Peters et al. (2010a,b,c)

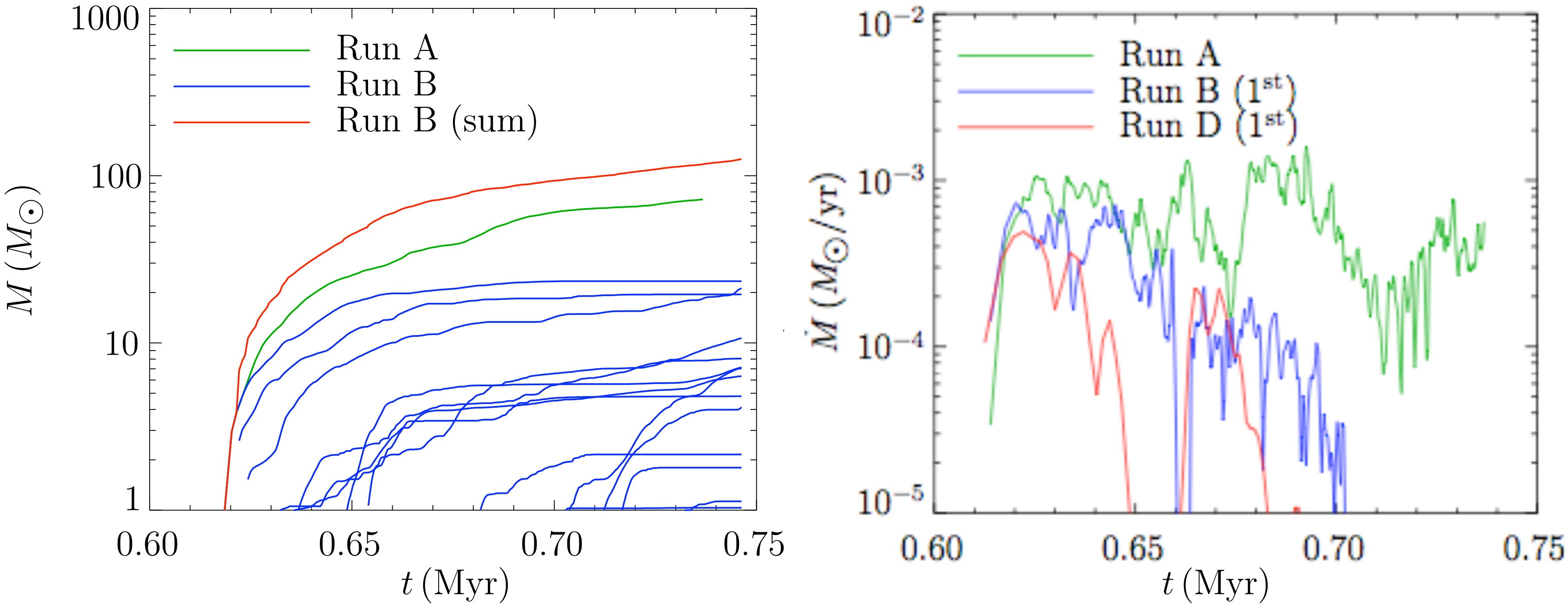

- single protostar accretes $72M_\odot$ in $120\,\mathrm{kyr}$ (Run A)
- ionization feedback alone is unable to stop accretion
- accretion is limited when multiple protostars can form (Run B)
- no star in multi sink simulation reaches more than $30M_\odot$

Peters et al. (2010a,b,c)

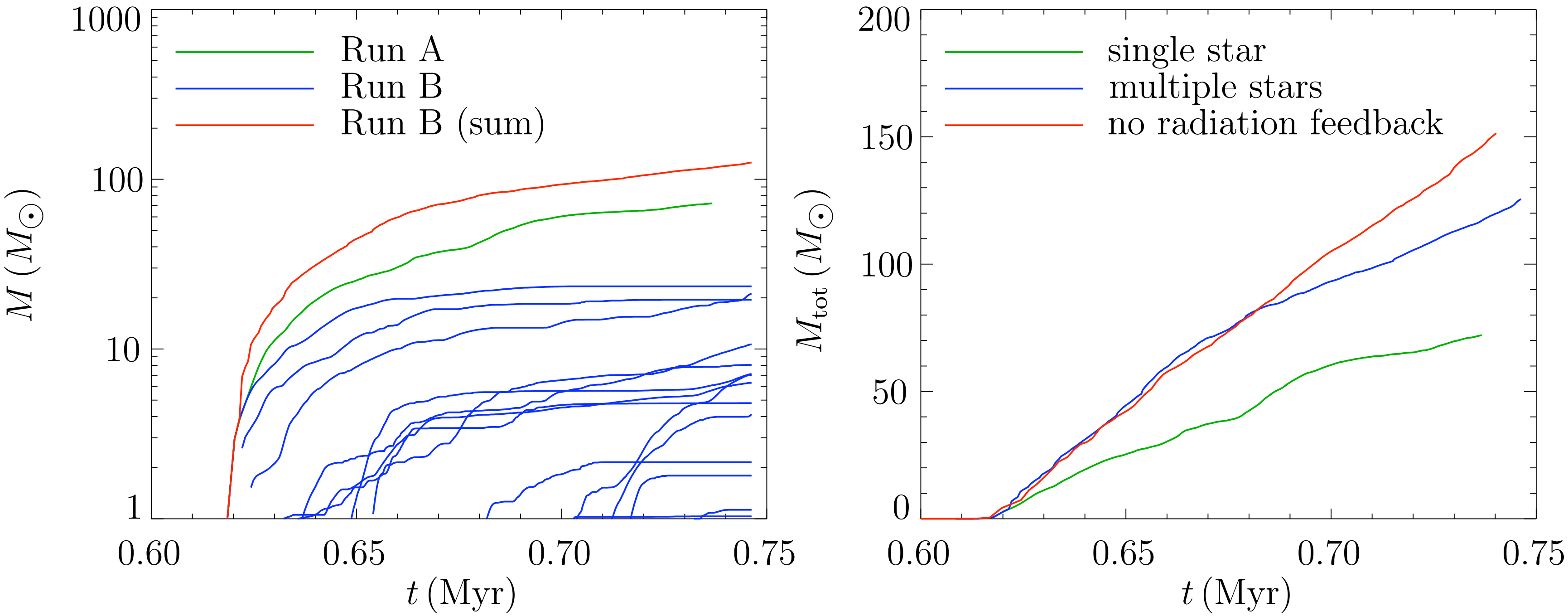

- compare with control run without radiation feedback
- total accretion rate does not change with accretion heating
- expansion of ionized bubble causes turn-off
- no triggered star formation by expanding bubble

Peters et al. (2010a,b,c)

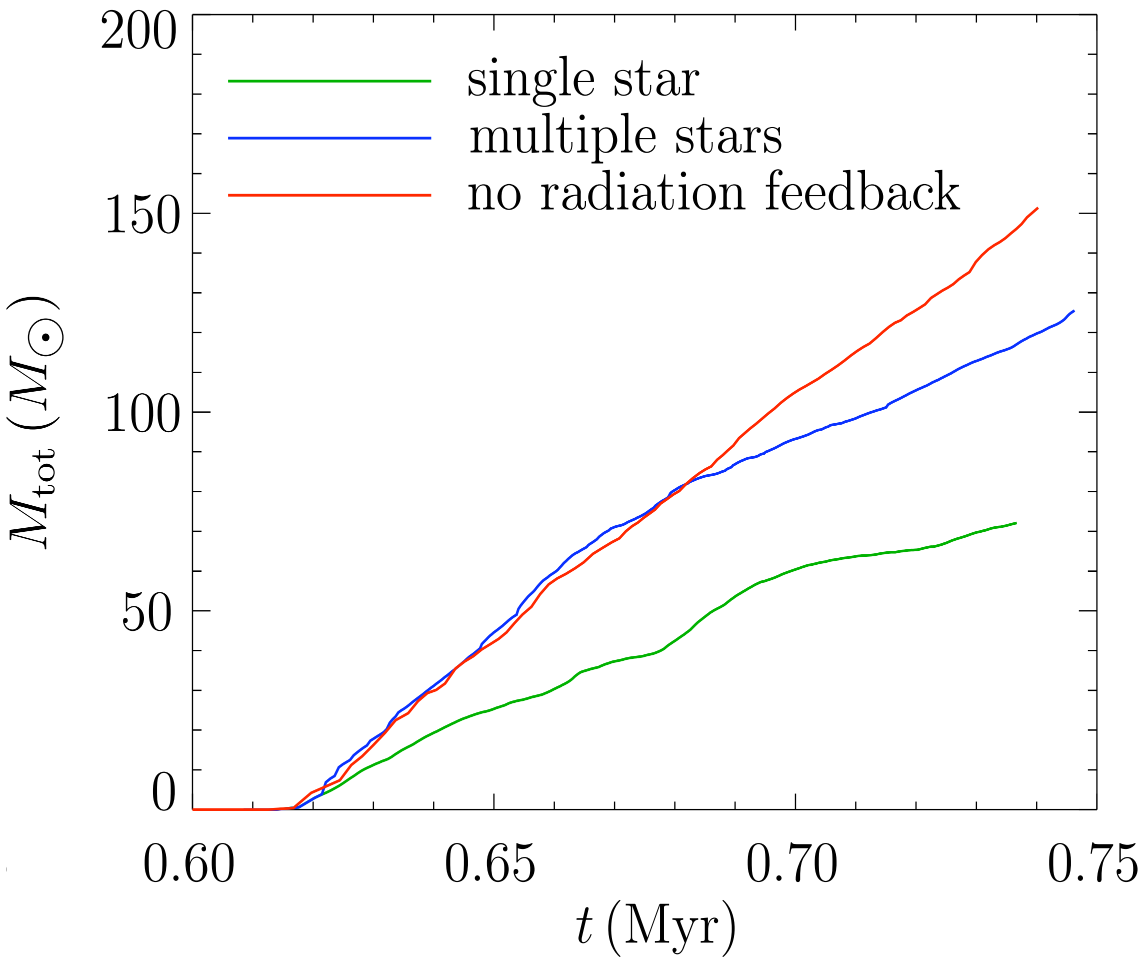

OVERVIEW OF COLLAPSE SIMULATIONS.

Name	Resolution	Radiative Feedback	Multiple Sinks	M_{sinks} ($M_\odot$)	N_{sinks}	M_{max} ($M_\odot$)
Run A	98 AU	yes	no	72.13	1	72.13
Run B	98 AU	yes	yes	125.56	25	23.39
Run D	98 AU	no	yes	151.43	37	14.64

Peters et al. (2010a,b,c)

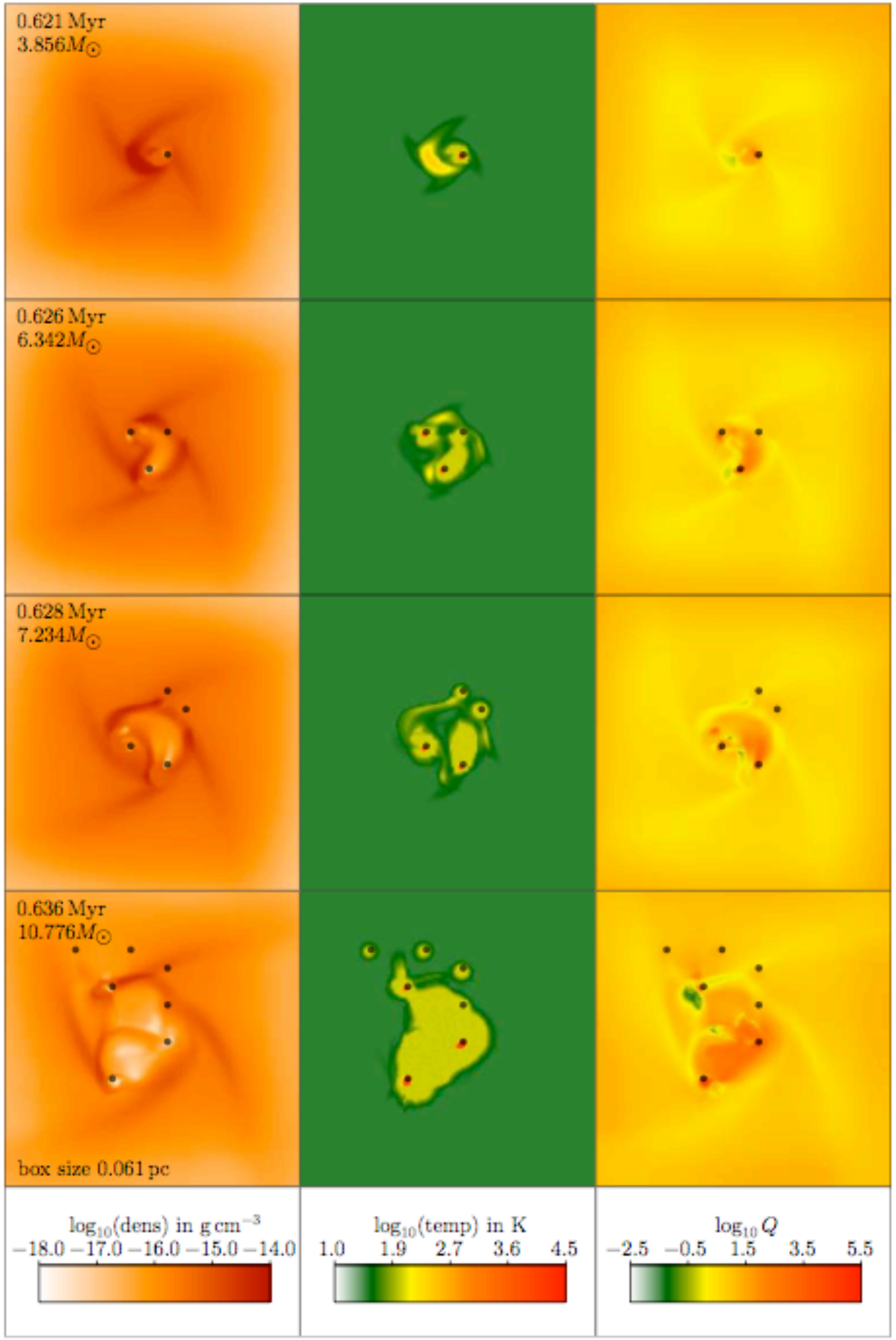

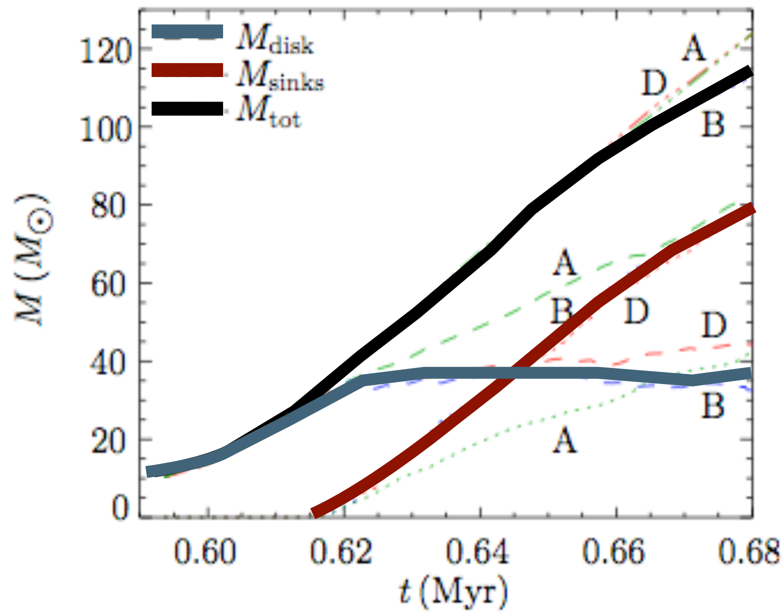

mass load onto the disk exceeds inward transport --> becomes gravitationally unstable (see also Kratter & Matzner 2006, Kratter et al. 2010)

fragments to form multiple stars --> explains why high-mass stars are seen in clusters

Peters et al. (2010a,b,c)

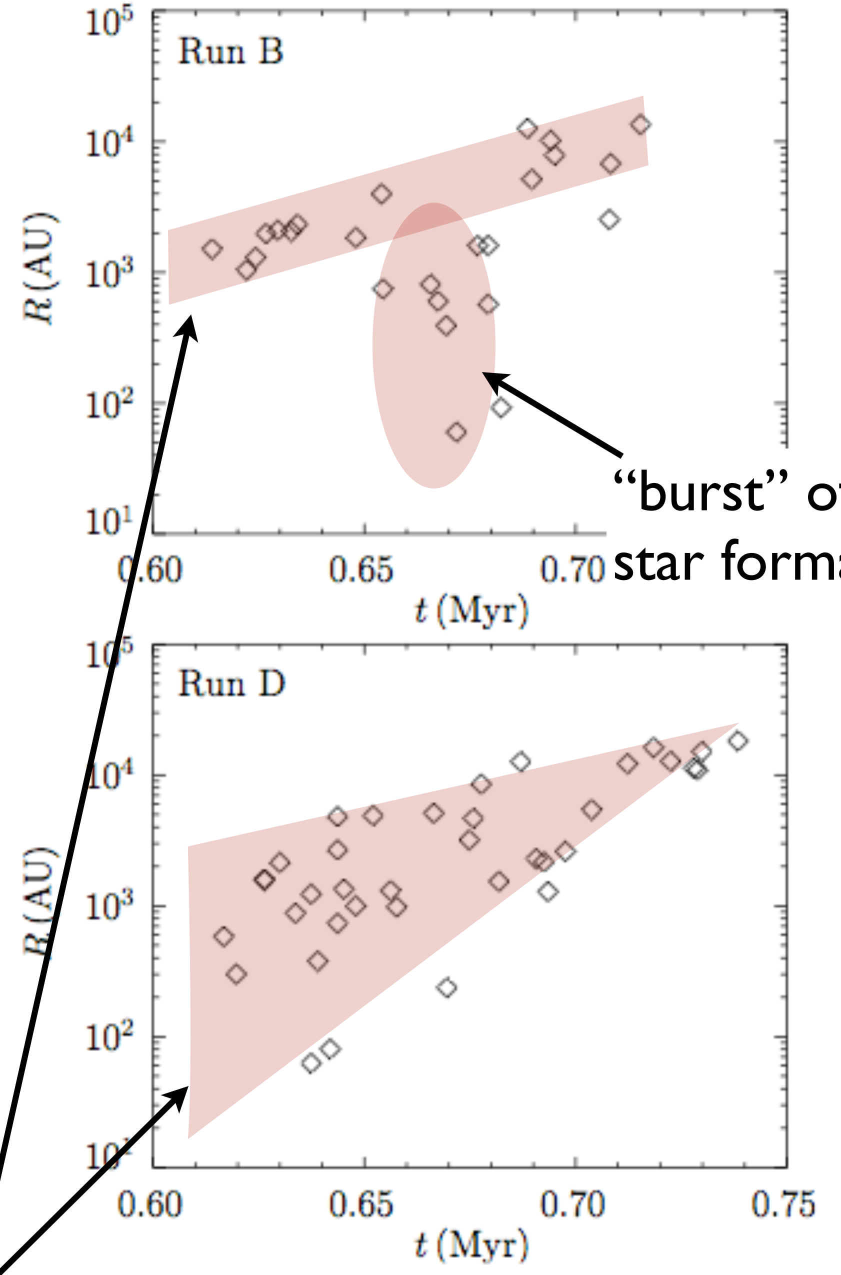

"burst" of star formation

younger protostars form at larger radii

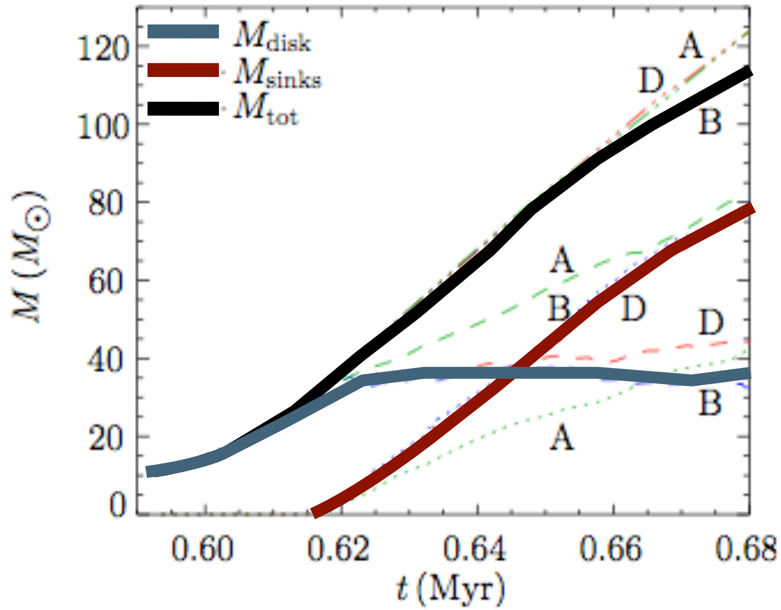

mass load onto the disk exceeds inward transport --> becomes gravitationally unstable (see also Kratter & Matzner 2006, Kratter et al. 2010)

fragments to form multiple stars --> explains why high-mass stars are seen in clusters

Peters et al. (2010a,b,c)

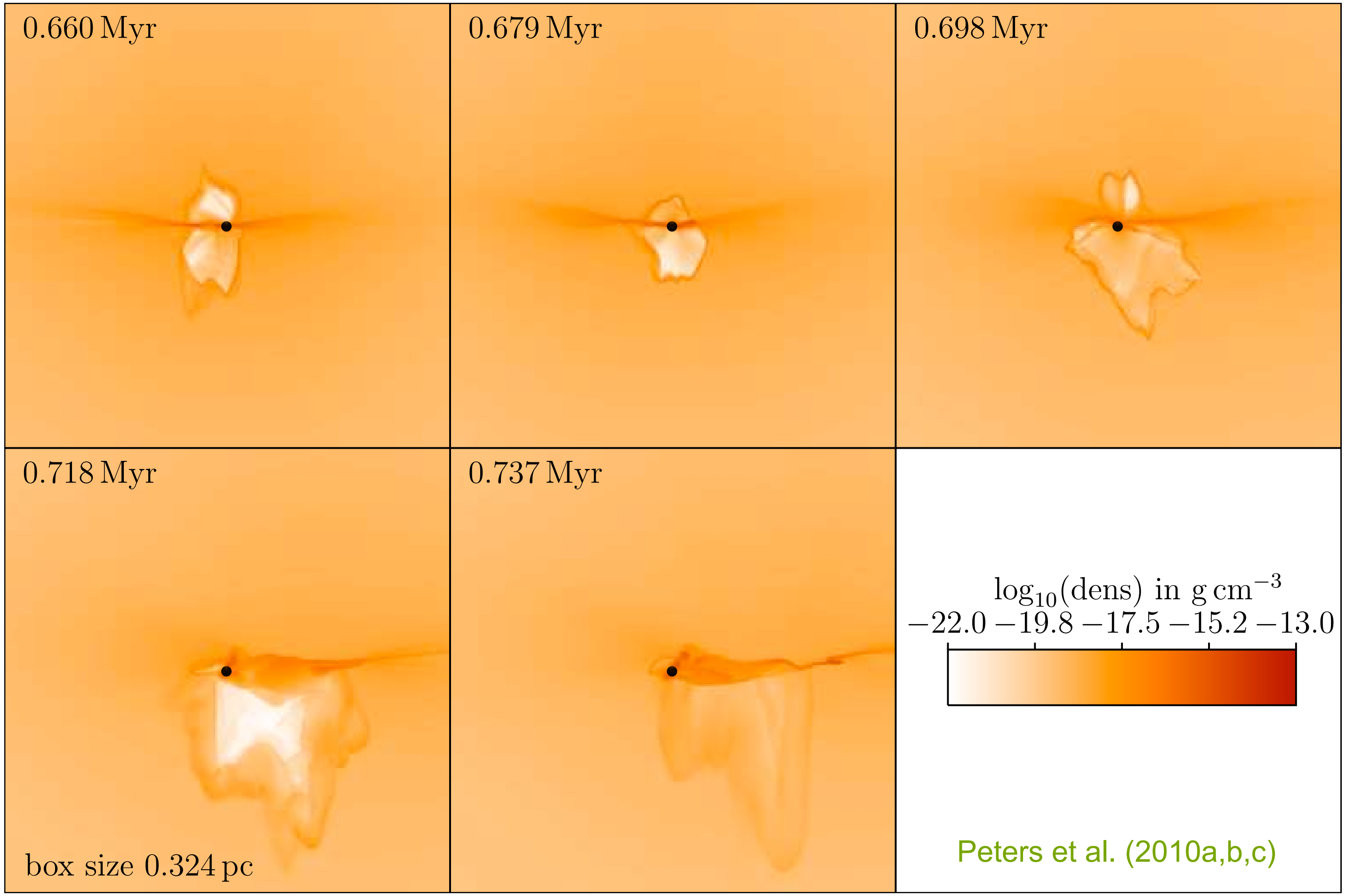

- thermal pressure drives bipolar outflow
- filaments can effectively shield ionizing radiation
- when thermal support gets lost, outflow gets quenched again
- no direct relation between mass of star and size of outflow

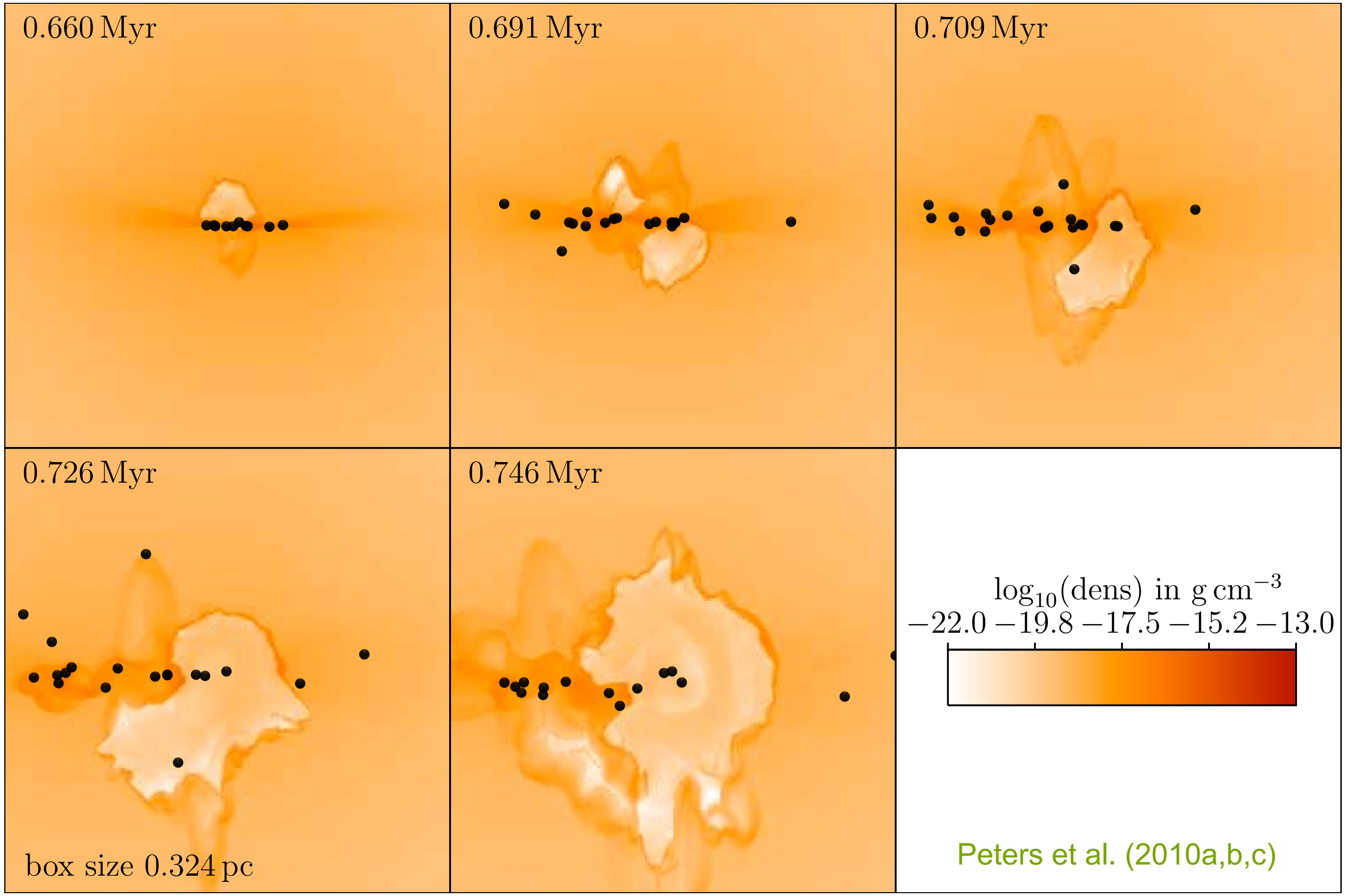

- bipolar outflow during accretion phase
- when accretion flow stops, ionized bubble can expand
- expansion is highly anisotropic
- bubbles around most massive stars merge

- numerical data can be used to generate continuum maps
- calculate free-free absorption coefficient for every cell
- integrate radiative transfer equation (neglecting scattering)
- convolve resulting image with beam width
- VLA parameters:
    - distance $2.65\,\mathrm{kpc}$
    - wavelength $2\,\mathrm{cm}$
    - FWHM $0\overset{\prime\prime}{.}14$
    - noise $10^{-3}\,\mathrm{Jy}$

Peters et al. (2010a,b,c)

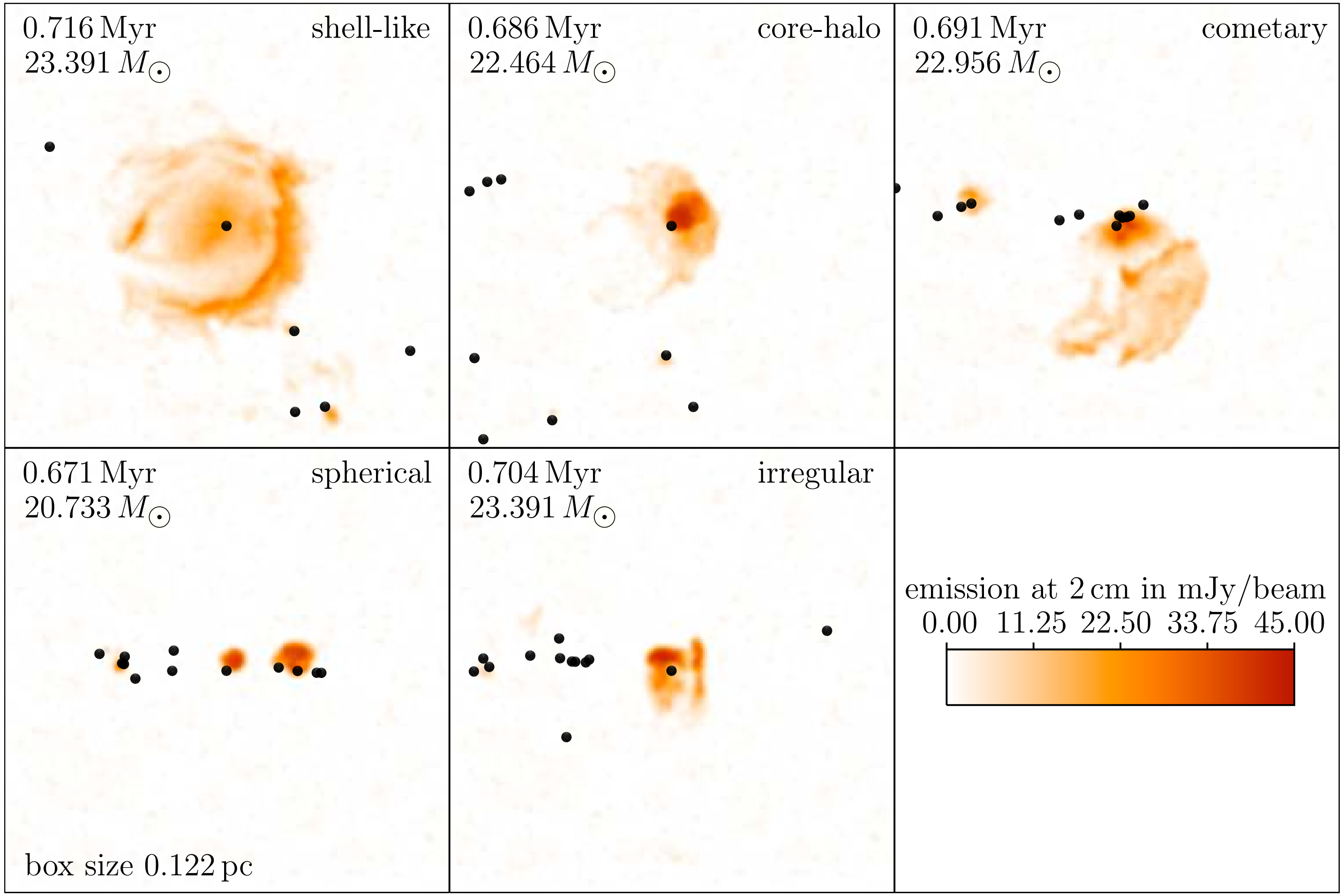

- synthetic VLA observations at $2\,\mathrm{cm}$ of simulation data
- interaction of ionizing radiation with accretion flow creates high variability in time and shape
- flickering resolves the lifetime paradox!

Peters et al. (2010a,b,c)

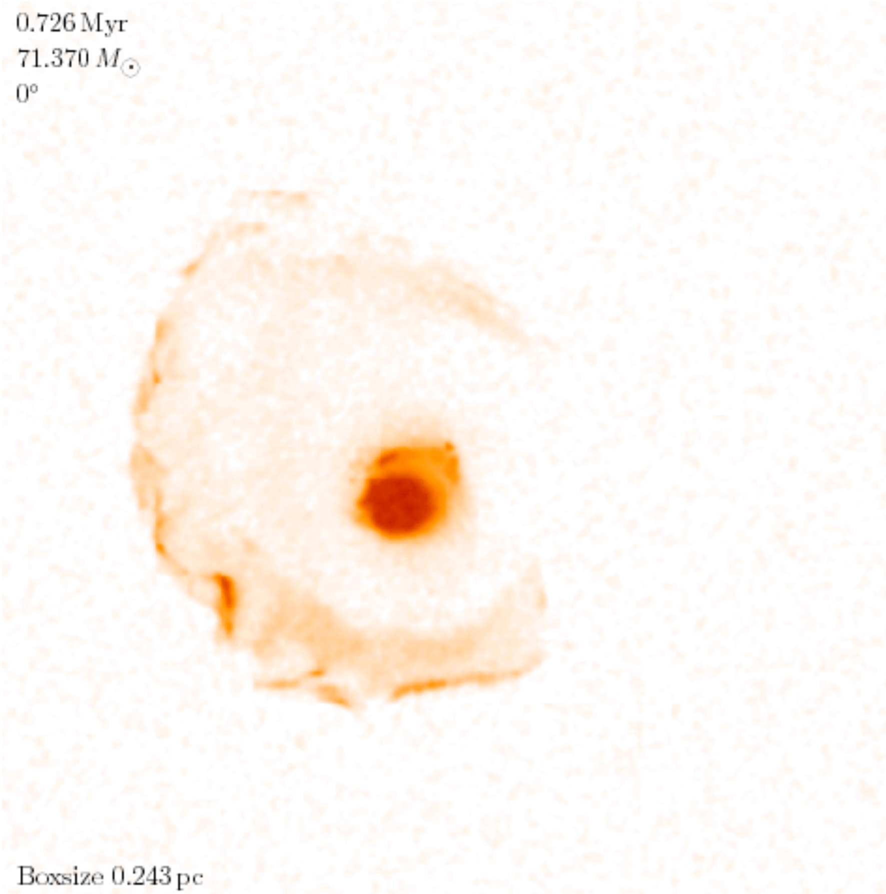

Morphology of HII region depends on viewing angle

Peters et al. (2010a,b,c)

H II Region Morphologies

Type	WC89	K94	single	multiple
Spherical/Unresolved	43	55	19	60 ± 5
Cometary	20	16	7	10 ± 5
Core-halo	16	9	15	4 ± 2
Shell-like	4	1	3	5 ± 1
Irregular	17	19	57	21 ± 5

WC89: Wood & Churchwell 1989, K94: Kurtz et al. 1994

- statistics over 25 simulation snapshots and 20 viewing angles
- statistics can be used to distinguish between different models
- single sink simulation does not reproduce lifetime problem

Peters et al. (2010a,b,c)

Conclusions and Outlook

Conclusions

- Ionization feedback cannot stop accretion
- Ionization drives bipolar outflow
- H II region shows high variability in time and shape
- All classified morphologies can be observed in one run
- Lifetime of H II region determined by accretion time scale
- Rapid accretion through dense, unstable flows
- Fragmentation-induced mass limits of massive stars

star formation

- stars form in clusters (at all cosmic ages!)
- star formation is a highly complex process, involving multiple scales and multiple physical processes
- initial conditions matter big time
- first star formation is not less complex than present-day star formation
- IMF is result of many processes (turbulence, *N*-body dynamics, thermodynamics, feedback, etc.)
- IMF is “easy” to get, look for secondary statistics